Axial-Radial Numerical Modeling of Annular Seals by Mimetic FDM

A dissertation

presented to

the faculty of the Department of Mechanical & Aerospace Engineering

of the School of Engineering and Applied Science

University of Virginia

In partial fulfillment

of the requirements for the degree

Doctor of Philosophy (Mechanical and Aerospace Engineering)

by

Neal Robert Morgan

May 2022

Annular pressure seals are critical components used in turbomachinery. The annular seal is a thin annular clearance region “sealing” between a high-pressure region and a low-pressure region of a rotating machine by limiting the leakage of the working fluid. The working fluid leakage is limited by the cross-sectional area allowed to the flow, and frequently further limited by axisymmetric grooves machined into the rotor or stator within which the fluid expands, contracts, and recirculates. Modern analysis techniques of such seals tend to fall into two categories. Either the seal model is greatly simplified through assumptions and application of empirical factors, or the seal is modeled using 3-D CFD techniques in generalized fluid dynamics codes. The method of simplification is referred to as “Bulk Flow” analysis due to the use of radially averaged “bulk” values for flow variables. This model takes those radially averaged values and assumes a circumferential solution based on small orbit circular whirling motion. The 3-D momentum equations are thus reduced to a series of 1-D equations in the axial direction with shear forces modeled empirically through Blasius type friction factors. These 1-D equations can be solved rapidly at the expense of accuracy and flexibility in seal geometry types. Comparatively, 3-D CFD codes require large 3-D meshes and the solution of the full 3-D Navier-Stokes equations accompanied by turbulence model. The CFD solutions are accurate within the precision of the boundary conditions used at the expense of much greater computational cost and engineer expertise requirements.

A 2-D seal code is developed with an axial-radial grid to strike a balance between the 1-D bulk flow method and 3-D generalized CFD. This 2-D seal code distinguishes itself through rigorous application of modern numerical and code techniques. The code allows the 0th and 1st order solution of the geometrically perturbed and incompressible cylindrical Reynolds Averaged Navier-Stokes equations to model the seal’s eccentric annular region with an assumed small and circular whirl orbit. Currently a single one-equation turbulence model is included to model the transport of turbulent kinetic energy for high Reynolds number flows. The 0th order solution provides the user with leakage results, wall shear stress, and initial pressure differential estimates. The 1st order solution refines the pressure differential estimate and models the circumferential variation to obtain rotordynamic coefficients from multiple whirl speed cases.

Approval Sheet

This dissertation is submitted in partial fulfillment of the requirements for the degree of

Doctor of Philosophy (Mechanical and Aerospace Engineering)

Neal Robert Morgan

Neal Robert Morgan

This dissertation has been read and approved by the Examining Committee:

Dr. Houston Wood, Adviser (MAE)

Dr. Christopher Goyne, Committee Chair (MAE)

Dr. Haibo Dong, (MAE)

Dr. Zongli Lin, (ECE)

Dr. Sarah Sun, (MAE & ECE)

Accepted for the School of Engineering and Applied Science:

Dr. Jennifer L. West, Dean, School of Engineering and Applied Science

May 2022

To my wife for taking care of me, and to the professors and students of the Mechanical & Aerospace Engineering department who accompanied me through my studies and research.

Contents

Chapter 1

Introduction and Motivation

1.1 Annular Pressure Seals in Turbomachinery

The Study of turbomachinery is built on the foundation of fluid dynamics, thermodynamics, and vibrational dynamics. The safe and efficient operation of these machines, and their performance, is reliant on rigorous analysis and manipulation of the working fluid in the rotating system. Growing the market for turbomachinery often requires improvements to existing designs to gain performance in a smaller or more efficient system. These performance requirements must be met by new designs with more pressure stages, higher rotor speeds, narrower clearances, and optimization. It is impractical to rely on analysis methods that require physical experimentation to obtain empirical coefficients for testing of uncommon designs or design optimization studies. However, computational resources do not yet exist to make large 3-D computational fluid dynamics (CFD) studies practical on a corporate time scale for most applications. There exists a gap in commonly applied analysis techniques between 1-D approximations based on many assumptions and 3-D CFD relying only on the Navier-Stokes equations and a turbulence model. This work focuses on introducing alternative analysis methods for the secondary flow paths between pressure stages in turbomachinery, typically designed as annular pressure seals.

Sealing between high and low pressure regions has long been a complication in turbomachinery. Mechanical seals provide the best performance from a leakage perspective, however they wear over time, distributing debris through the flow passages and requiring frequent maintenance to clean and replace seals. Instead, non-contacting annular seals are commonly employed in turbomachinery

as secondary flow paths that limit leakage between regions with large pressure differences, while avoiding much of the wear or rub of rotor and stator associated with a contacting seal. Annular pressure seals consist of a stationary outer surface (stator) and a rotating inner surface along the shaft (rotor) of the machine, separated by a radially narrow clearance. Many seal geometry designs consist of additional geometry such as circumferential or helical grooves or teeth added to either rotor or stator surfaces. The leakage of working fluid from high pressure to low pressure regions is restricted by the cross-sectional area of the seal passage, with clearances on the order of 0.003-0.005 times the rotor radius,[1] and further reduced by additional flow direction changes and recirculation caused by macro roughness geometries which convert kinetic energy to thermal energy. As a smooth annular seal's geometry is similar to that of a plain journal bearing, direct (radial) and cross-coupled (tangential) stiffness and damping forces are generated by the converging/diverging wedge formed by the fluid being pulled circumferentially into the smaller clearance, caused when the shaft position becomes eccentric due to vibration.[2] These forces increase with the reduction of clearance, which also has the largest effect on reducing leakage. Because of the cross-coupled stiffness response of annular pressure seals, their design must balance the leakage of working fluid between pressure zones and their destabilizing effect on the machine's rotordynamic behavior. To design a seal that effectively reduces leakage, improving machine efficiency, it is necessary to accurately model the flow to predict the rotordynamic response forces generated.

Initially, annular seals were "straight seals" or "smooth seals" with smooth-walled annularly cylindrical flow passages. This was advantageous because of the simplicity of analysis of the flow behavior. Such a seal can be modeled analytically as a superposition of pressure driven flow through a non-rotating annular passage and axisymmetric Couette flow between an inner rotating wall and a stationary outer wall prior to the onset of turbulence. Over time seal designs became increasingly complex geometrically and higher rotor speeds and pressure differentials frequently drive the flow into the turbulent regime. Various design applications for annular pressure seals typically have a wide range of Reynolds numbers from 100[3] to 100,000,[4] or higher, depending on the working fluid and application of the machine. The onset of turbulence in an annular pressure seal with a turbulence model based on a Reynolds number, obtained using twice the clearance and the rotor surface speed, can begin as early as a Reynolds number around 1,800[5] which can be compared to the critical Reynolds number for pipe flow of 2,300.[6] Note this turbulence may not

become fully developed even up to Reynolds numbers around 12,000.[7] This variability in turbulent behavior causes seal flows to be difficult to predict with high numerical accuracy. Seal analysis methods thus require either physical experimentation or complex numerical models to accurately determine leakage, power loss, and forces on the rotor. Traditionally, annular seals have been modeled using Darcy-Weisbach type friction factors[8–10] since the early 20th century[11–16] and later a 1-D approximation method known as ”bulk-flow”.[1,2,17–19] This method is fast and order of magnitude accurate, but relies on empirical factors that require physical experimentation or more complex numerical analysis to predict. As a 1-D method bulk-flow is also inherently unable to handle various geometries flexibly. Seal researchers are increasingly looking to CFD analysis tools to calculate the fluid flow within the seal domain with increased accuracy compared to more traditional bulk-flow methods.

1.2 Literature Review

1.2.1 Bulk-Flow and Empirical Factors

bulk-flow analysis is so named because the primary assumption is that the radial pressure variation is negligible, thus a “bulk” velocity is assumed for the flow as a radial average across the cearance gap, and further averaged over a particular axial and circumferential control volume. The neglect of radial velocity gradients necessitates the assumption of an empirical friction factor to estimate the wall shear stresses in the seal. The radius of the seal is then assumed to be much larger than the clearance allowing the circumferential curvature to be neglected. The fluid flow is assumed to turbulent and, when the rotor is non-eccentric, steady state and fully developed. This allows for the rapid numerical solution of the concentric annular flow through a seal with a non-vibrating rotor from the non-dimensionalized Navier-Stokes (N-S) momentum equations simplified with the above assumptions. The rotor’s actual eccentricity is then assumed to be much less than the radial clearance and a perturbation model is developed by assuming a periodic circular function for radial clearance as a function of whirl speed.

Bulk-flow methods for analysis of annular seals are available in 1, 2 and 3 control volume (CV) methods to model straight, hole-pattern, labyrinth, and helical seals.[19–25] Models for two and three

CVs are similar to the single CV model except for the need to include interaction between the clearance region and the groove cavities. The only distinction between the two and three CV models is the addition of a simple CV, typically with the same equations as a single CV model to account for the regions between grooves. Scharrer writes the continuity equations in terms of mass flow rate and uses a Pradtl mixing length hypothesis to determine free shear stress and couple two CV's.[19,26] The Prandtl mixing length is employed as a measure of how far from the boundary between control volumes the recirculation begins to dominate the flow in a labyrinth groove. Scharrer also takes the novel approach of modeling the recirculating flow inside the groove cavity, his second CV. The flow is modeled with a half-infinite turbulent jet, simulating flow entering the cavity with one direction and diffusing into multiple directions. Childs also models the connections between the first and second CV's of a two CV model with mass transfer rates and Prandtl's mixing length hyptothesis, however he uses a more typical black box approach to the third control volume instead of assuming a special flow field.[1] Ha's three CV model writes the continuity equation as in the single CV model, with the addition of the Prandtl mixing length hypothesis terms and a radial velocity at the boundary between second and third control volumes.[24] Each of the approaches applying Prandtl's mixing length employed approximately the same values in an annular labyrinth seal as found by Rhode.[27] Nordmann's three CV model does not appear to employ the mixing length.[28] Otherwise this method is very similar to both the work of Childs and Ha. All four models employed an additional empirical coefficient to estimate pressure losses as the flow accelerates out of a groove cavity, in the case of a two CV model, or from region 2 to 1 in a three CV model. The control volume equations' repetition between grooves serves to imply that the flow can be modeled with the same patterns in each groove section. Han[29] created an early analytical model for leakage prediction through labyrinth seals and discussed the flow character of the groove filled vortices. The rectangular grooves under consideration were assumed to have an "inviscid core of uniform vorticity" within the groove cavity enveloped by boundary layer regions between this core and the walls and jet flow region. This assumes no flow between the jet region and the groove cavity, with the two regions interacting only with fluid-fluid shear forces. Flow streamlines similar to those described by Han's theory can be seen in CFD simulation results presented by Morgan *et. al.*[30–33]

All of these bulk-flow models employ friction factor models to replace the shear stress terms in the momentum equations and use empirical coefficients for entrance and exit losses. Brighton[34]

effectively summarizes the analytical development of empirical friction factors for pipe flow and applies this to concentric annular cross-sections. Empirical friction factors are given for a wide range of annulus diameters and fluid Reynolds numbers, along with characterization of pressure driven flow profiles through annular regions. Elrod[35] tested annular seal entrance and exit lengths and friction factors experimentally to develop empirical relationships. Smooth and honeycomb seals were tested experimentally to determine the length of the entrance and exit zones and the differences in empirical friction factors used to describe these regions when compared to the developed flow of the seal. The key feature of all of these empirical coefficients is that they require large amounts of experimental data, or CFD simulations, to model and validate for each new seal geometry and operating conditions investigated. This is prohibitively expensive for large scale optimization studies.

1.2.2 CFD Applied to Annular Pressure Seals

The primary alternative analysis method to bulk-flow analysis, is the use of CFD for solving the complete Navier-Stokes equations in conjunction with an appropriate turbulence model. Unlike the bulk-flow models, computational fluid dynamics simulations make no simplifying assumptions based on the seal geometry, shear stress at the wall, relationship between wall shear stress and mean fluid velocity, or characterization of interfaces between control volumes through empirical friction factors. There are still some simplifying assumptions in the RANS equations and turbulence models, but not individual seal specific ones. The annular seal flow behavior is obtained while rapid flow variations at the interface between the groove and land sections are inherently time averaged into the solution. Although lack of the above simplifying assumptions provides increased accuracy, CFD simulations can be expensive in terms of modeling time and computational power.

Early CFD solutions for seals began with taking advantage of the near axisymmetry of many seal geometries. A two-dimensional, axial-radial, gas seal solution was developed by Deitzen[36] using a non-specified finite difference technique to solve the 3-D N-S momentum equations, an energy equation, and the k-ϵ turbulence model, over a coarse two-dimensional grid. The circumferential dimension was removed by assuming a small circular whirl orbit and related perturbation of fluid flow variables. This method neglected some terms of the resulting equations, but demonstrated the

capability to model seal rotordynamic coefficients. The method was then extended to rectangularly grooved gas seals[37] where the solution was found to have improved accuracy over bulk methods, with significant increased computational cost at the time. This method seems to have since been abandoned due to the high computational costs in the early 1990's. Later seal work with CFD jumps straight to the full 3-D N-S solutions, presumably for reasons of convenience with commercial CFD software and the assumption that a more complex model will be more accurate.

Dietzen and Athavale[38–41] began the transition to 3-D FEA and finite volume CFD codes to model seal flows from the late 1980's through the 1990's. The current trend in seal CFD research[30–33,42–50] is to take advantage of commercial CFD software, often 3-D FEA codes, that are designed for a broad range of applications. The required expertise has transitioned towards creation of appropriate meshes and tweaking of options within these generalized codes rather than seal specific CFD code development. However, even neglecting the time and effort required to create a quality mesh of the fluid region and the availability of modern parallel computing clusters, a full seal model can take hours or days to solve a single case. Considering that it is necessary to run each seal geometry at multiple whirl speeds to determine the rotordynamic coefficients, performing large scale experimentation can be impractical for industrial applications though somewhat common in academia.

A hybrid CFD/bulk-flow method was first developed for annular labyrinth seals in 1996 by Athavale *et. al.*[41] This method was later independently developed for hole pattern and honeycomb seals by Migliorini *et. al.* in 2012.[20] Both methods can be applied to smooth look-through seals. These hybrid methods combine the positive features of both bulk-flow and CFD techniques. The method begins with a single concentric, with no whirl, small sector CFD simulation of a seal geometry. The flow variables are exported from this CFD simulation result to obtain a single control volume base state solution that can be applied to a bulk-flow method. This provides a more accurate and more detailed solution of the unperturbed flow within the seal than can be obtained by a normal single control volume method. The CFD solution can also be obtained quickly and at low computational cost due to the concentric and small sector nature of the model. This base state solution is then applied in place of the normal bulk-flow zeroth-order calculation and perturbed by standard bulk-flow methods to obtain stiffness and damping coefficients. The increased accuracy of the unperturbed flow increases the accuracy of the resulting coefficients obtained from the bulk-flow

without resorting to a full series of 3-D eccentric seal CFD models. As the friction factors necessary for the bulk-flow calculations can also be obtained from the simplified CFD model, this becomes a practical and efficient method for testing potential seal geometries for which no information is previously known.

Academically, published design optimization studies are exclusively the result of CFD simulations of varying complexity. Rhode, Ko, and Morrison[51] performed early optimization of leakage rate through step labyrinth annular seals. The leakage rate of the step seal was calculated using a numerical Navier-Stokes code based on the TEACH algorithm with a variation in the QUICK differencing scheme and the high Reynolds number k-ϵ turbulence model. Seven characteristic geometric parameters were varied over 16 simulation experiments. The simulation experiment with minimum leakage rate was selected to be investigated experimentally for verification of the numerical code. The predicted optimal seal geometry had a 60% less leakage than their baseline seal geometry, and suggested some significant factors relating step seal geometry to leakage rate. The results of this work show the benefits of optimizing seal geometry designs for improved leakage rate.

Schramm, *et. al.*[52] performed simulated annealing optimization of step labyrinth seal geometry. The step seal geometry shape was parameterized for only two design variables representing step position and step height. A three-dimensional CFD mesh was automatically generated and TASCflow3D was used to solve for the seal's flow properties. Nine hundred simulation experiments were performed with factor values selected by the optimization algorithm. Both factors converged to predicted optimum values after approximately 600 simulations, resulting in an improved leakage rate of greater than 10

Asok, *et. al.* 2007[53] employed an artificial neural network simulation model to optimize labyrinth seal groove geometries for minimal leakage rate. Initially five different aspect ratio square cavity labyrinth seal groove geometries were simulated in Fluent with the second-order upwind SIMPLEC algorithm. The CFD results for the square cavity labyrinth seal geometries were confirmed by physical experiment. Artificial neural network simulation and analytical modeling were then combined to predict the performance of new seal geometries based on the CFD results of the previous simulations. Additionally, based on the flow fields found in the square cavity grooves by CFD simulation, two new seal geometries were defined with curved cavity walls at the rear of

the grooves. This additional curve creates a counter rotating double vortex in the groove cavity resulting in a pressure differential increase of more than 75%. The results of this study suggest that investigation of novel groove geometries can yield significant performance increases.

Untaroiu, *et. al.*[54] also performed CFD simulation and verified with physical experiments. The four factor parameterized seal geometry was meshed and simulated using ANSYS CFX. The design factors include the seal tooth front and back angles, the tooth tip width, and the spacing between teeth. The CFD simulation results for five seal geometries were verified by physical experiment. Subsequently, design factor values selected based on the output of a genetic optimization algorithm. The genetic algorithm was used to generate design points for 38 simulated experiments and a sensitivity study was performed with this sample. This study demonstrates the effective use of a genetic optimization algorithm for prediction of local optimum design points.

Bellaouar, *et. al.*[55] performed a similar optimization of annular labyrinth seal tooth geometry using the multivariate Gauss-Seidel iteration method. The five parameterization factors under investigation include the seal tooth front and rear angles, and the rounding radii on each side of the base and tip of the seal tooth. Cosmos FloWorks 2009 for SolidWorks 2009 was the CFD code employed to model the performance of the test seal geometries. This study demonstrates the use of the Gauss-Seidel iteration method to optimize seal geometry for reduced leakage rates.

This author and colleagues at the University of Virginia's Rotating Machinery and Controls (ROMAC) Laboratory, have also performed multiple CFD studies to optimize annular seal geometry.[30–32,42,46–48,50] All of the seal geometry optimization studies mentioned suggest that future improvements in seal designs will require flexible or computationally efficient modeling tools for mass optimization studies. The success of such optimization studies with commercial CFD codes in academia suggests that similar performance improvements could be found for industrial applications if the computational efficiency of seal CFD analysis is improved.

1.2.3 Modeling Turbulence in Annular Pressure Seals

Annular pressure seal designs and applications exist for Reynodls numbers as low as 100^3 and up into the $100{,}000^4$ range even for liquid seals. Flow through these secondary passages can be laminar, turbulent, or somewhere in between. For a smooth seal geometry and a Reynolds

number using a characteristic length equal to twice the clearance, turbulent flow effects can be observed as early as Reynolds numbers of 1,800.[5] However, the turbulence in seal flow can delay becoming fully developed to Reynolds numbers as high as 12,000[5,56] depending on seal geometry. Comparatively, the acknowledged onset of turbulence in smooth pipe flow occurs at a Reynolds number of 2,300.[6,57] Design engineers will even add geometric features in the seal path or upstream of the seal to encourage additional turbulence in the flow, reducing leakage through increased shear from the wall boundary layers. As Reynolds number increases, laminar model for seal flow becomes increasingly inaccurate at predicting seal performance characteristics such as leakage, power-loss to torque shear, and rotordynamic response coefficients. Selection of an appropriate turbulence model for the seal design, or selection of a turbulence model that is flexible enough to cover a broad design space, is critical to a numerical seal flow analysis.

Primarily, laminar flow is only observed in annular seals where oil is the working fluid.[3] The greater viscosity of oils lowers the Reynolds number significantly, but oil seals are also frequently lower speed than water or gas seals. Chien[58] applied an early alternative turbulence model using a Taylor series expansion to the more typical kinetic energy and turbulent dissipation energy equations. Chochua[59] comapred Chien's model to the k-ϵ model and concluded that the latter model matched experimental results more closely for most cases tested. The two equation k-ϵ is frequently applied to both liquid[60] and gas seals whether straight through, honeycomb, or labyrinth geometries are used. In fact, gas seals are almost exclusively modeled using the k-ϵ turbulence model,[20,36,37,42,59,61–65] due to lower mesh density requirements from high flow velocities causing higher y+ values along the rotor and stator surfaces. The k-ϵ model has been applied at Reynolds numbers of 1,900,[63] 12,000,[66] and 3,000 to 100,000.[4] The largest weakness of the k-ϵ model with resect to seals is inaccuracy when simulating significant stream line curvature or secondary paths.[67] Patel and Chen *et. al.* investigated low Reynolds number turbulence models[68] and introduced a two-layer model combining the standard k-ϵ model with several one equation models[69,70] before settling on Wolfshtein's.[71] This two layer model was later compared, by Vilasmil *et. al.* ,[72] with the Re-Normalisation Group (RNG) modified k-ϵ model, the original k-ϵ model, and the Reynolds Stress equation for flows with Reynodls numbers from 2,000 to 60,000. Vilasmil observed that the experimental friction factor data was matched most closely by the Reynolds Stress equation results. Despite this result, the Reynolds Stress equation model is not typically applied to seals in

the literature.

The only model that is competative with the k-ϵ for seals in more recent years is the Shear Stress Transport (SST) model.[73–75] SST is actually a weighted blending of the k-ϵ and the k-ω model to increase the range of allowable y+ values,[76] but most authors apply it within the y+ range of the k-ω model $(y+ < 5)$. This has only become more common recently as computational resources have increased due to the high density mesh requirements of getting a y+ value that low.

1.2.4 CFD Methods Not Specific To Annular Seals

One of the drawbacks of modern commercial CFD software is the high requirements for user expertise to define the mesh grid, the boundary conditions, the solver domain and time step settings, and many more parameters. These complex paramteters allow for a software package, such as ANSYS, to accurately handle a wide variety of flow configurations, but significantly increase the time, engineer, and computational requirements. In contrast, specialized codes such as bulk-flow analysis methods are easy to learn, run quickly, and lack much of the flexibility and accuracy of commercial CFD codes. There exists a niche for seal analysis tools that bridge the gap between these methods. However, this code must employ modern techniques to maximize the comparative advantages since it will not be a full 3-D CFD code.

Annular pressure seal flow is nearly axisymmetric, as previously discussed, with only small variations due to rotor eccentricy around the concentric position. Barring the use of bi-polar cylindrical coordinates like used in drilling calcualtions[77,78] which doesn't reduced the size of the model, just the complexity; it will be most efficient to employ standard cylindrical coordinates like the bulk-flow codes. As discussed, large component of an engineer's time is used to create, troubleshoot, and test independence of the mesh grid when using commercial CFD software. The authors thus focused on numerical methods that reduce the dependence on mesh quality to stability and accuracy of solution. The first investigated numerical technique was the Boundary Element Method,[79–82] for its geometric flexibility and grid insensitive qualities. However this method relies on full matrices which quickly grow beyond current RAM and storage capacities when mesh density is increased to offset non-linear solution stiffness.

The opposite extreme of complexity was then considered in the form of the Finite Diference Method (FDM).[83,84] FDM is commonly applied to numerical solutions of differential equations and appreciated for its simplicity both in implementation and concept. FDM is also a popular method to hybridize with other techniques such as BEM or Finite Element Analsyis (FEA).[85–87] Unfortunately, FDM is not generally known for mesh insensitivity. To address this potential failing, the Mimetic Finite Difference Method (MFDM) was applied.[88–90] Oud[91,92] demonstrates that discretization schemes generated by the mimetic method can inherently conserve mass, momentum and kinetic energy; while also preserving the symmetry properties of the differential operators in the cylindrical coordinate system. The mimetic method is further elaborated in the related methods section of Chapter 2.

1.3 Dissertation Plan

Modern annular pressure seal design employs a combination of physical experiments and numerical simulations to accurately predict the effects of the seal on the total system. The common methods discussed in the literature for numerical simulation are extremes of simplicity, in the form of bulk-flow analysis, or complexity, in the form of full 3-D CFD analysis often using commercial CFD software. Bulk-flow analysis is a rapid and low computational cost method for testing design variations, but it requires knowledge of empirical coefficients to approximate wall shear stresses, entrance contraction pressure losses, and exit expansion effects. The bulk-flow method is also inherently constrained to simple rectangular geometry due to its 1-D nature. This greatly reduces the usefulness of the bulk-flow method in optimizing a seal design. Despite this, bulk-flow is still more popular in industrial settings than CFD because the CFD simulations required for these studies consume vastly more computational resources, engineer expertise, and time. There is a niche for numerical modeling methods that are more efficient than general CFD, but do not require extensive use of empirical coefficients. Previously a 2-D axial-radial analysis method was developed and tested for smooth and rectangularly grooved seals, but it never became mainstream due to the computational resources and numerical methods available at the time. This work demonstrates a similar 2-D axial-radial seal modeling method applied with modern numerical methods and coding

techniques to create a code to model annular pressure seals in a more computationally balanced way.

This work accomplishes improved computational efficiency by creating and investigating methods to reduce the mesh sizes, dimensionality, and stability of the computational analysis. The created methods offer the potential for greatly increased flow characterization within the seal when compared to bulk-flow, require no empirical coefficients within the fluid domain, and require less computational resources when compared to CFD. The objectives of this dissertation are:

1. **Create a mimetic discrete vector and tensor calculus (DVTC) for 3-D cylindrical differential vector operators:**

    - The model will apply a single assumption that the rotor surface moves in a small circular whirl orbit.
    - The discrete grid is 2-D in the axial and radial coordinate directions.

    An axial-radial grid is created by geometric perturbation of the radial coordinate using the rotor eccentricity as the perturbation variable. The small circular whirl assumption and the geometric perturbation are combined to remove the circumferential dependence of the original cylindrical coordinate differential vector operators. The mimetic DVTC operators preserve the identities and properties of the continous vector differential operators that make up the Navier-Stokes equation ensuring that the individual errors of the discrete approximations do not combine to violate the conservation of mass or momentum.

2. **Apply the mimetic DVTC to the Reynolds Averaged Navier-Stokes (RANS) equations to create an annular flow code:**

    - The computational and time cost of solution should be between bulk-flow and generalized CFD techniques, and closer to the cost of bulk-flow analysis.
    - The engineer expertise requirements should be closer to those of bulk-flow. CFD modeling requirements of mesh creation and boundary assignment should be automated.
    - The numerical techniques employed must be robust/stable.
    - The method must allow for future work expanding the code to generalized seal geometries.

- The annular flow code will accept Dirichlet or Neumann boundary conditions for each face to ease transition to a multi-domain method in the future.
- The DVTC operators are coded using only matrix operations through the shift matrix method to optimize the creation of solution matrices within Matlab.

The RANS conservation equations are solved for a zeroth-order non-linear concentric flow and a first-order linearized fluctuation of flow variables due to the whirling motion of the inner annular surface. The mimetic finite difference method provides a stable conservative discretization of the Navier-Stokes and turbulence modeling equations through pairs of primary and support discrete vector and tensor calculus (DVTC) operators. The annular flow modeling code is written in Matlab to take advantage of the well optimized matrix algebra operations and comprehensive debugging features. The combination of a mimetic spatial discretization and semi-implicit trapeziodal method allows for an extremely stable numerical model in space and time.

3. **Select and apply a turbulence model to approximate the Reynolds Stresses in the RANS equations:**

   - The turbulence model must model the transport of kinetic energy.
   - Like the RANS equations, the turbulence model is constructed with the mimetic DVTC operators through the shift matrix method.

   The Prandtl one-equation turbulence model is selected for simplicity of application and existing simulation data of direct numerical simulation (DNS) models for small clearance geometry. The additional advantage of the Prandtl one-equation model is that it is a complete turbulent kinetic energy (TKE) transport model and once it is constructed with the mimetic DVTC much of the discrete math requried for a more complex two-equation turbulence model is already accomplished.

4. **Validate the annular flow code against CFD simulation data and experimental results from the literature for annular pressure seals:**

- Validate the discrete RANS code without reynodls stress term by comparison to analytical solutions at low to medium Reynolds numbers.
- Compare the annular flow code with turbulence model to CFD simulation data for medium to high Reynolds numbers to verify the reasonableness of the TKE and eddy viscosity solutions.
- Demonstrate quantitative and qualitative agreement in code results when compared to physical experiment data for annular pressure seals in the literature.

Chapter 2

Background on Methods

2.1 Rotordynamics of Annular Pressure Seals

The rotordynamic forces generated by annular pressure seals, like journal bearings, are quantified using a mass-spring-damper analogy describing shaft vibration. In this analogy, the mass represents the local section of the shaft and any components attached to it. The shaft vibrates, bends on its supports, and rotates pushing and dragging against the working fluid in the seal. As with any mass-spring-damper system, turbomachines are subject to phenomena such as natural frequencies and corresponding bending modes of the shaft. The restorative force generated by the working fluid pushing radially against compression is expressed as a spring constant K. However, in annular seals, relatively large cross-coupled spring constants are generated as the working fluid is dragged into the smallest clearance region between the rotor and stator. The working fluid is pulled by the no-slip boundary on the rotor into a converging/diverging wedge, Figure 2.1, that creates a tangential pressure imbalance, resulting in a tangential push caused by a radial motion. The tangential force is represented rotordynamically as the off main diagonal terms in the stiffness matrix (**K**) and known as cross-coupled stiffness because a radial displacement causes a circumferential force. The seal component's damping depends largely on the properties of the working fluid, but can be positively influenced by larger volume and greater radial depth of the labyrinth groove features that give additional volume in which the viscous interaction of fluid particles can convert mechanical energy, and when the fluid is compressible, into which the clearance region's fluid may be displaced. The damping also increases the local restorative forces as it always acts against

motion proportionally to the speed of vibration. The effective mass term is more controversial in its application to seal rotordynamics with most authors neglecting its use. The mass term of a seal is not often calculated by bulk-flow methods but it is essential in calculation of rotordynamic coefficients from CFD simulations. Sufficiently fast and accurate analysis tools for annular seals would allow designers to customize seal geometries to improve total system stability.

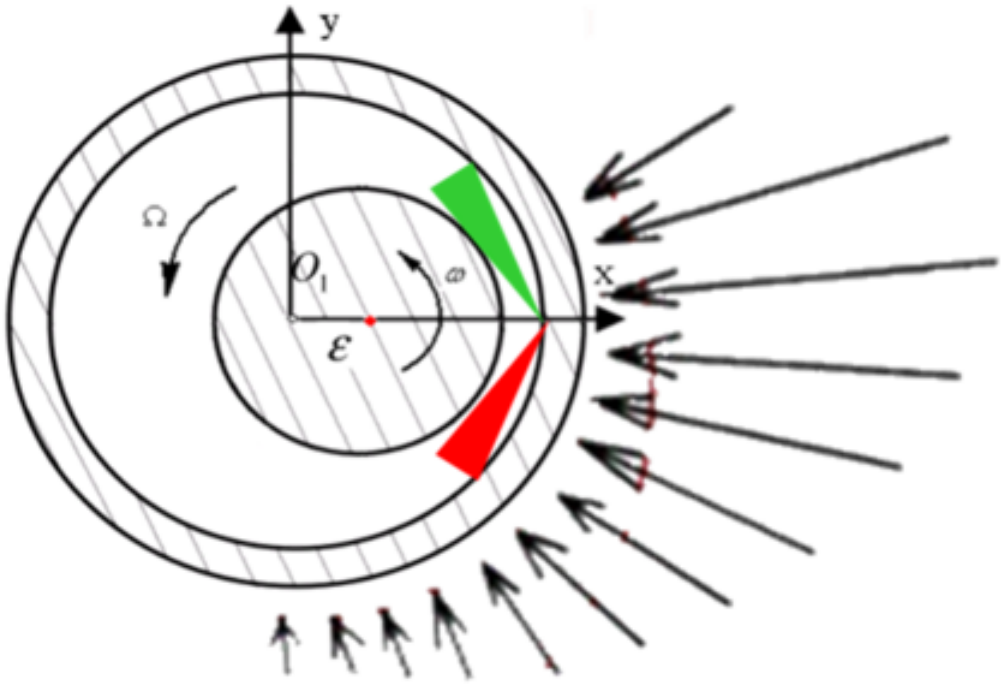

Figure 2.1: Rotordynamic seal response force profile, including converging (red) and diverging (green) pressure wedges.

All modern seal flow analysis methods numerically estimate the forces acting on the rotor by integrating the circumferential/axial pressure distribution over the rotor surface. These fluid forces acting on the rotor are calculated for a given seal geometry, fluid boundary conditions, rotor speed, and an assumed rotor whirling motion, Equation 2.1. The classical dynamics equations of motion for the vibrational system, Equation 2.2, are then manipulated to develop a function linking response forces to rotordynamic coefficients and whirl frequency, Equation 2.5 when the smallest clearance is at $\frac{\pi}{2}$ radians.

$$\vec{r} = \begin{bmatrix} x \\ y \end{bmatrix} = \begin{bmatrix} r\cos\theta \\ r\sin\theta \end{bmatrix} \Rightarrow \begin{bmatrix} \frac{x}{r} \\ \frac{y}{r} \end{bmatrix} = \begin{bmatrix} \cos(\Omega t + \theta) \\ \sin(\Omega t + \theta) \end{bmatrix} \tag{2.1}$$

$$\begin{bmatrix} -F_x \\ -F_y \end{bmatrix} = \begin{bmatrix} K_{xx} & K_{xy} \\ -K_{xy} & K_{xx} \end{bmatrix} \begin{bmatrix} x \\ y \end{bmatrix} + \begin{bmatrix} C_{xx} & C_{xy} \\ -C_{xy} & C_{xx} \end{bmatrix} \begin{bmatrix} \dot{x} \\ \dot{y} \end{bmatrix} + \begin{bmatrix} M_{xx} & M_{xy} \\ -M_{xy} & M_{xx} \end{bmatrix} \begin{bmatrix} \ddot{x} \\ \ddot{y} \end{bmatrix} \tag{2.2}$$

$$\begin{bmatrix} -\frac{F_x}{r} \\ -\frac{F_y}{r} \end{bmatrix} = \begin{bmatrix} K_{xx} & K_{xy} \\ -K_{xy} & K_{xx} \end{bmatrix} \begin{bmatrix} \frac{x}{r} \\ \frac{y}{r} \end{bmatrix} + \Omega \begin{bmatrix} C_{xx} & C_{xy} \\ -C_{xy} & C_{xx} \end{bmatrix} \begin{bmatrix} -\frac{y}{r} \\ \frac{x}{r} \end{bmatrix} - \Omega^2 \begin{bmatrix} M_{xx} & M_{xy} \\ -M_{xy} & M_{xx} \end{bmatrix} \begin{bmatrix} \frac{x}{r} \\ \frac{y}{r} \end{bmatrix} \tag{2.3}$$

$$\begin{bmatrix} -\frac{F_r}{r} \\ -\frac{F_\theta}{r} \end{bmatrix} = \begin{bmatrix} K_{xx} & K_{xy} \\ -K_{xy} & K_{xx} \end{bmatrix} \begin{bmatrix} 0 \\ 1 \end{bmatrix} + \Omega \begin{bmatrix} C_{xx} & C_{xy} \\ -C_{xy} & C_{xx} \end{bmatrix} \begin{bmatrix} -1 \\ 0 \end{bmatrix} - \Omega^2 \begin{bmatrix} M_{xx} & M_{xy} \\ -M_{xy} & M_{xx} \end{bmatrix} \begin{bmatrix} 0 \\ 1 \end{bmatrix} \tag{2.4}$$

$$\begin{aligned} -\frac{F_\theta}{r} &= K_{xy} - \Omega C_{xx} - \Omega^2 M_{xy} \qquad \text{smallest clearance at } (\Omega t + \theta) = \frac{\pi}{2} \\ -\frac{F_r}{r} &= K_{xx} + \Omega C_{xy} - \Omega^2 M_{xx} \end{aligned} \tag{2.5}$$

These rotordynamic coefficients are functions of eccentric whirl speed. As each equation is second order (quadratic) a minimum of four whirl speeds and force responses are required, three to allow calculation of each coefficient and at least one more to allow for calculation of confidence interval and other model fit statistics. Although the effective mass and cross-coupled damping terms may or may not be used for the rotordynamic stability calculations, it is necessary to include them in the regression modeling to accurately estimate the stiffness and damping coefficients.

2.2 Bulk-flow Analysis of Annular Pressure Seals

Bulk-Flow analysis grew as a natural extension of early 20th century work on using empirical Darcy-Weisbach friction factors to predict head loss in pipes and annular regions.[8–10] By assuming that the flow within an annular pressure seal is a ”thin film”, flow property radial variation is neglected allowing a single ”Bulk” to represent the entire radial clearance at each axial and circumferential location. The control volume of flow is drawn to include the entire radial clearance, Figure 2.2. Here the axial direction is represented by x and the radial clearance is c. The shear stresses are represented by R for rotor surface and S for stator surface respectively. The familiar momentum conservation equations are radially averaged in Equations 2.6 to 2.8. The control volume encompassing the fluid flow the labyrinth groove cavities is more complex. They are also constrained to specific groove

geometries (rectangles, semi-circles, ect.) with specific aspect ratios. This limit is due to typical bulk models failing to take into account the vortex size and positioning as well as the interactions between the groove volume and the below groove jet flow.

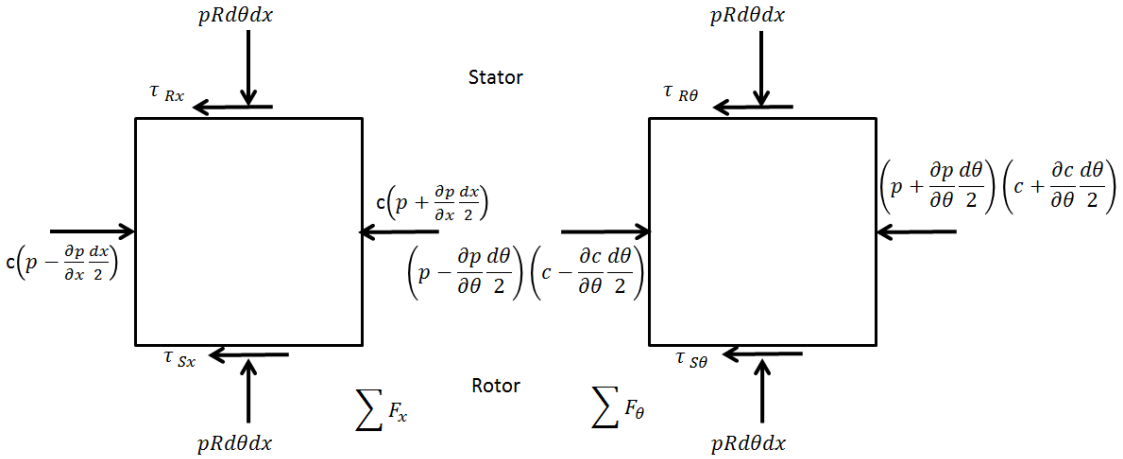

Figure 2.2: Free-body Diagram of Seal Control Volume, $\sum F_z$ on the left and $\sum F_\theta$ on the right

$$0 = \sum F_r = \int_{R-\frac{c}{2}}^{R+\frac{c}{2}} \left[\frac{d}{dt}\rho + \nabla\cdot(\rho w)\right] dr = \frac{d}{dt}(c) + \frac{\partial}{\partial x}(cw) + \frac{1}{R}\frac{\partial}{\partial \theta}(cv) \tag{2.6}$$

$$-\frac{c}{R}\frac{\partial p}{\partial \theta} - (\tau_{R\theta} + \tau_{S\theta}) = \sum F_\theta = \int_{R-\frac{c}{2}}^{R+\frac{c}{2}} \left[\frac{d}{dt}\rho v + \nabla\cdot(\rho v w)\right] dr = \frac{d}{dt}(c\rho w) + \frac{\partial}{\partial x}(\rho c v w) + \frac{1}{R}\frac{\partial}{\partial \theta}\left(\rho c v^2\right) \tag{2.7}$$

$$-c\frac{\partial p}{\partial x} - (\tau_{Rx} + \tau_{Sx}) = \sum F_x = \int_{R-\frac{c}{2}}^{R+\frac{c}{2}} \left[\frac{d}{dt}\rho w + \nabla\cdot(\rho w w)\right] dr = \frac{d}{dt}(c\rho w) + \frac{\partial}{\partial x}\left(\rho c w^2\right) + \frac{1}{R}\frac{\partial}{\partial \theta}(\rho c v w) \tag{2.8}$$

Wall shear stress acts in exact opposition to the direction of relative motion. With only a single radial value, it is impossible to calculate wall shear contributions to the momentum equations from the standard Cauchy stress tensor terms necessitating the substitution of approximations using the empirical friction factors, Equation 2.9. Note that here a Fanning friction factor is used instead of Darcy-Weisbach, the difference is a factor of 4. The relative velocities relating the bulk values to the rotor and stator walls are given by Equation 2.10. Using these magnitudes for relative velocity, the individual components of shear stress can be related to the resultant shear stress for each wall, Equation 2.11.

$$\tau = \frac{1}{2} f \rho |U|^2 \tag{2.9}$$

$$U_R = \left[w^2 + (v - R\omega)^2\right]^{\frac{1}{2}} \qquad U_S = \left[w^2 + v^2\right]^{\frac{1}{2}} \tag{2.10}$$

$$\begin{aligned} \tau_{Rx} &= \tau_R \frac{w}{U_R} & \tau_{Sx} &= \tau_S \frac{w}{U_S} \\ \tau_{Rx} &= \tau_R \frac{v - R\omega}{U_R} & \tau_{Rx} &= \tau_S \frac{v}{U_R} \end{aligned} \tag{2.11}$$

2.2.1 Friction Factors Models for Seals

There have been many models developed after Blasius' early equation to select pipe flow friction factors,[93] most of which are approximations to the Colebrook-White Equation.[94] However of the pipe flow type friction factor models, only the Blasius type friction factor[95] and friction factors based on a few select variations of the Colebrook equation have been applied to seals. The general Colebrook equation for friction factor estimation is Equation 2.12, however it is seldom used directly as it requires an iterative solution.

$$\frac{1}{\sqrt{f}} = -2\log\left(\frac{\epsilon}{3.7D} + \frac{2.51}{Re\sqrt{f}}\right) \tag{2.12}$$

A large body of early experimental work on turbulent flow between plates and through channels, pipes and annuli established that axial flow can be modeled by a power function of Reynolds number[96].[97] This lead to Prandtl's boundary layer equations[98] and Blasius' development of pipe flow friction factor empirical relationships[95] based on the assumption that near wall flow behavior is a power law function of Reynolds number implying that the shear stress can be similarly modeled. The analytical relationship for a turbulent Blasius friction factor is given by Equation 2.13.[18]

$$f = 0.079Re^{-\frac{1}{4}} \tag{2.13}$$

The earliest applications of a power law based friction factor to rotating annular flow was performed by Suzuki[11] in 1929. A single expression was developed for a friction coefficient, λ, based on a $\frac{1}{7}$th power law and employing an additional empirical factor β, seen in Equation 2.14. The radius used is the inner annulus radius and the U velocities are axial.

$$\lambda = \frac{0.3216}{Re_z^{\frac{1}{4}}} \times \frac{1}{2}\left\{\left[1 + 0.629\left(\frac{\omega R_i}{U_z}\right)^2\right]^{\frac{3}{8}} + \left[1 + 0.629\left(\beta\frac{\omega R_i}{U_z}\right)^2\right]^{\frac{3}{8}}\right\} \tag{2.14}$$

Another early application of friction factors to the analysis of annular flow was Yamada in 1962[12][13].[14] Yamada experimentally determined an axial flow resistance coefficient (λ) for smooth and grooved annular vertical regions with inner rotating cylinders and a working fluid of water. λ is defined in Equation 2.15, and the relationship for smooth turbulent annular regions is in Equations 2.16. These empirical relationships for λ are also based on a $\frac{1}{7}$ power law velocity distribution in the clearance. Equation 2.17 gives Yamada's torque coefficient definition and Equation 2.18 shows the relationship between torque and Reynolds number in the presence of axial flow and a rotating inner cylinder. In these equations r_1 is the inner radius, r_2 the outer radius, and u is the average circumferential velocity and the experiments were performed up to a rotational Reynolds number of 30,000.

$$\frac{\Delta p}{\rho} = \lambda \frac{L}{2\left(r_2 - r_1\right)} \frac{u_{avg}^2}{2g} \tag{2.15}$$

$$\lambda = 0.27 Re_{ax}^{-0.24} \left[1 + \left(\frac{7}{8}\right)^2 \left(\frac{Re_\omega}{2Re_{ax}}\right)^2\right]^{0.38} \tag{2.16}$$

$$C_f = \frac{\tau}{\rho \left(r_1 \omega\right)^2} \tag{2.17}$$

$$C_f = 0.00759 Re_\omega^{-0.24} \left[1 + \left(\frac{8}{7}\right)^2 \left(\frac{2Re_{ax}}{Re_\omega}\right)^2\right]^{0.38} \tag{2.18}$$

Childs and Dressman[99] performed experimental testing of turbulent seals with clearance to radius ratios ranging from 0.0106 to 0.0129, and axial and rotational Reynolds numbers up to 40,000. They found leakage and pressure differentials that were "reasonably well predicted" by Yamada's friction factor model. Yamada's friction factor model was later used in bulk-flow applications by Fenwick et. al.[100] Polkowski,[101] in 1984, models turbulent flow between coaxial rotating cylinders without a pressure gradient and develops a friction factor expression that was demonstrated is identical to Yamda's,[14] it was also demonstrated that a friction factor model developed by Gazley[102] is equivalent.

Black and Jenssen applied thin-film theory and perturbation to create the first bulk-flow model of annular seal flow[103] in 1969. They employed a single friction factor throughout the equations. Black and Jenssen's friction factor is defined like Yamada's with Equation 2.15 and also is based on a $\frac{1}{7}$ power law velocity distribution, however, the coefficients relating their turbulent friction factor to Reynolds number differ as seen in Equation 2.19. Black and Jenssen's experiments covered axial

Reynolds numbers ranging from 6,000-20,000 and rotational speeds ranging 2,000 to 8,000 RPM. They were not specific about what working fluid was used in the experiment.

$$\lambda = 0.079 Re_{ax}^{-1/4} \left[1 + \left(\frac{7}{8} \frac{Re_\omega}{Re_{ax}} \right)^2 \right]^{\frac{3}{8}} \tag{2.19}$$

In the early 1970's Hirs developed a general bulk-flow method for thin film lubricants[17].[104] Hirs employed only one empirical friction factor defined similarly to Equation 2.17 as a ratio of shear stress to kinetic energy. Hirs compared his theory to experimental results with Reynolds numbers ranging from 3,000 to 30,000. The following relationship was observed between Reynolds number and shear stresses, where τ_0 is the shear stress due to pressure driven flow, τ_1 is the shear stress due to a sliding wall, and τ_b is the combination shear stress observed at the sliding surface.

$$\frac{\tau_b}{\frac{1}{2}\rho U^2} = \frac{\tau_0 - \tau_1}{\frac{1}{2}\rho U^2} = -0.062 \left(\frac{\rho U h}{\mu} \right)^{-0.25} \tag{2.20}$$

Hirs also derived an equivalent expression for his friction factor model for easier comparison to Yamada's results, as shown in Equation 2.21. In this equation Re without a subscript is the axial Reynolds number, $n_0 = 0.066$ and $m_0 = -0.25$. These values were found to be very close to Yamada's coefficients.

$$\lambda = 4 n_0 Re^{m_0} \left[\frac{1}{4} \left(\frac{Re_\omega}{Re} \right)^2 + 1 \right]^{1+\frac{m_0}{2}} \tag{2.21}$$

Childs applied Hirs' lubrication bulk-flow equations to annular seal dynamics in 1983 to model interstage seals in a multi-stage centrifugal pump[105] . It is also noted that Hirs' and Black's[106] friction factors give very similar results. Hirs' friction factor equation modified for usage with bulk-flow models is given below.

$$f_s = n_s \left[\frac{2\rho H \left(U_z^2 + U_\theta^2 \right)^{\frac{1}{2}}}{\mu} \right]^m \tag{2.22}$$

$$f_r = n_r \left\{ \frac{2\rho H \left[U_z^2 + (U_\theta - r\omega)^2 \right]^{\frac{1}{2}}}{\mu} \right\}^m \tag{2.23}$$

The second friction factor model to be applied to annular pressure seals was an approximation of the Colebrook-White equation[94] proposed and plotted by Moody[107] for pipe flow applications,

seen in Equation 2.24 . The moody friction factor model is intended for use with Reynolds numbers between 4,000 and 3,000,000 and relative roughness from 0 to 0.05 for pipe flow and is ±15% accurate within this range. Nelson and Nguyen[108] observed in 1987 that Hirs' friction factor model, and by extension the other Blasius based models, tended to predict lower direct stiffness when used in Bulk-flow models than was experimentally measured. Specifically, the direct stiffness predictions were increasingly inaccurate as the ratio of relative roughness to seal clearance increased. In an attempt to correct this under prediction, Nelson and Nguyen chose to compare Hirs' friction factor equation to Moody's model. Their study found that for smooth seals the two friction factor models gave nearly identical results. As they varied the relative roughness ratio from 0 to 0.05, obtaining Moody friction factors between 0.0056 and 0.018, there were large differences in predicted stiffness and damping terms when compared to Hirs' friction factors. Particularly, the Moody friction factor model resulted in up to 44% more direct stiffness predicted and a larger predicted pressure gradient. The authors make no claim that the Moody friction factor model is best for annular seals, but they advocate increased complexity of friction factor model to allow bulk-flow models to account for non-smooth surface roughness.

$$f = 0.001375\left[1 + \left(20,000\frac{e}{D} + \frac{10^6}{Re}\right)^{\frac{1}{3}}\right] \tag{2.24}$$

The Moody friction factor type model has been applied to bulk-flow methods particularly in the case of modeling cryogenic liquids in work published in 1993 by Yang and San Andreas[109].[110] However going further, in 1999, Childs[111] comments that based on flat plate experiments done in the early 1990's the friction factor should increase if the relative roughness is decreased while Reynolds number is maintained at a constant value for certain geometries with tight clearance gaps between surfaces with macro scale roughness features. It is then concluded that, in general, friction factor models used for turbulent pipe flow are not adequate for bulk-flow applications to modeling hole-pattern annular seals.

In addition to the friction factor models originally developed for pipe flow, there are several other relationships developed with other theories in mind. Simon and Frene, in 1989[112] and in 1992,[4] applied a friction factor type model developed by Elrod[113] for turbulent fluid film bearing applications to model annular pressure seals with bulk-flow. This model chooses to approximate the local shear

stresses instead of specifically the wall shear stress and is developed by combining theories of Prandtl's mixing length with wall functions. The relationship for shear stresses is given below in Equations 2.25 to 2.28, where the ξ's represent frictional surface stresses. The equation is in Cartesian coordinates with z along the axial length of the seal, U and W are average velocities in the x and z directions respectively and I and J are given by Equations 2.29 and 2.30.

$$\xi_{xh} - \xi_{x0} = -k_v \frac{\mu}{h}\left(U_m - \frac{\sigma V}{2}\right) \tag{2.25}$$

$$\xi_{zh} - \xi_{z0} = -k_z \frac{\mu}{h} W_m \tag{2.26}$$

$$k_v = \left[J(1)\frac{\overline{I}}{I(1)} - \overline{J} + \frac{\overline{\mu} V \left[\frac{\sigma}{2} - \frac{\overline{I}}{I(1)}\right]}{h^2 \frac{\partial P}{\partial x}} \right]^{-1} \tag{2.27}$$

$$k_z = \left[J(1)\frac{\overline{I}}{I(1)} - \overline{J} \right]^{-1} \tag{2.28}$$

$$I(y^*) = \int_0^{y^*} \frac{dy^*}{1 + \frac{\epsilon}{\nu}} \tag{2.29}$$

$$J(y^*) = \int_0^{y^*} \frac{y^* dy^*}{1 + \frac{\epsilon}{\nu}} \tag{2.30}$$

The is a general consensus that friction factors are sufficient to reasonably model the shear stresses appearing in annular seals. However, there is no guidelines on which friciton factor model is more appropriate or reliable way to select a friction factor without some physical or simulation experiments. This works well for familiar geometries and operating conditions and for incremental improvements, but breaks down as potential designs diverge from the known cases.

2.2.2 Perturbation of Flow Variables

This reduces the 3-D Navier-Stokes momentum and mass conservation equations to 2-D by removing the radial dimension of the annulus. The circumferential dimension is then removed by assuming that the film thickness can be modeled as a sine-cosine function of time, fixing the whirling motion of the rotor's vibration to a circular or eliptical path. As the change in film thickness is equal to the rotor's eccentricity, this distance can usually be assumed to be small, much smaller than the clearance. Since this whirling motion is driving the fluid flow circumferentially, it is assumed that the flow variables will also exhibit some sine-cosine function dependence in

the circumferential direction. The method of multiple scales is then appllied, based on the small amplitude of the whirling motion relative to the clearance, to assume that the flow variables are functions of the concentric steady-state solution of the flow and a perturbation solution in the form of sine-cosine. The perturbation variables of clearance height, axial velocity, circumferential velocity and pressure are then introduced to the non-dimensional equations. This produces in two zeroth-order momentum equations allowing for solution of the velocity components and pressure using the inlet and outlet pressures of the seal as boundaries along with the no-slip walls on the rotor and stator. These results from the zeroth-order equations are then used as coefficients for the first-order perturbation equations. The eccentricity of a shaft that is vibrating while it rotates will result in a harmonic solution to the perturbation of the clearance height.[17,19,103] As expected from classical mechanics, the eccentricity of the spinning rotor will precess around its axis and account for the remaining time dependence in the non-dimensional equations. Similar harmonic solutions can be applied with separation-of-variables techniques to the other first order perturbation variables. These variables are also solved by numerical iteration with homogeneous boundary conditions. Rotordynamic forces are calculated by integrating the first order perturbation pressures along the axial length and circumferentially around the seal. This process is then repeated for at least two whirl speeds to provide estimates of the rotordynamic stiffness and damping coefficients associated with the annular seal.[114]

2.2.3 Two and Three Control Volumes

Two and three CV models are similar to the single CV model except for the need to include interaction between the clearance region and the groove cavities, as seen in Figure 2.3 for two and three CV models respectively. It can be seen that the only distinction between the two and three CV models is the addition of a simple CV with the same equations as a single CV model to account for the regions between grooves. Because of the similarities among the equations, the focus of this section will be on the methods of joining the clearance region of the seal to the grooves and what models are used for the groove cavities. Scharrer writes the continuity equations in terms of mass flow rate and uses a Pradtl mixing length hypothesis to determine the free shear stress and couple the two CV's.[19] The Pradtl mixing length hypothesis is a similar concept to

mean free path. It represents the length over which a fluid element is likely to maintain a separate momentum before it mixes with the fluid elements around it.[57] Thus, it is a measure of how far from the boundary between control volumes the recirculation begins to dominate the flow in a labyrinth groove. Scharrer also takes the most novel approach to modeling the recirculating flow inside the groove cavity, the second CV. The flow in the groove is modeled with a half-infinite turbulent jet, simulating flow entering the cavity with one direction and diffusing into multiple directions. Childs also models the connections between the first and second CV's of a two CV model with mass transfer rates and Prandtl's mixing length hyptothesis, however a more typical black box approach to the third control volume was used instead of assuming a special flow field.[1] Ha's three CV model but writes the continuity equation like above in the single CV model with the addition of the Prandtl mixing length hypothesis terms and a radial velocity at the boundary between second and third control volumes.[24] Each of the references that used Prandtl's mixing length used approximately the same values for it in an annular labyrinth seal as found by Rhode.[27] Nordmann's three CV model was the exception to the rule and does not appear to employ the mixing length.[28] Otherwise it is very similar to both the work of Childs and Ha. All four models employed an additional empirical coefficient to estimate pressure losses as the flow accelerates out of a groove cavity, in the case of a two CV model, or from region 2 to 1 in a three CV model.

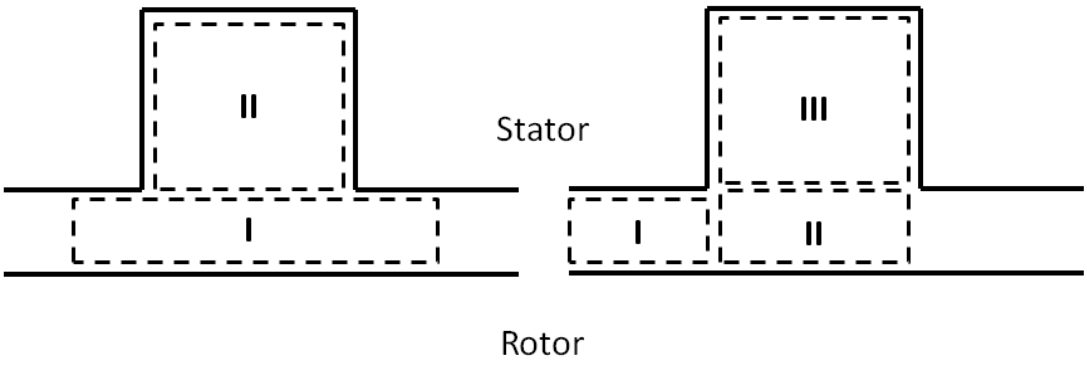

Figure 2.3: Left: two control-volume, Right: three control-volume

2.2.4 Hybrid CFD/bulk-flow method for first order results

The bulk-flow method employs empirical models for modelling the wall shear stresses. A hybrid method that replaces the zeroth order solution, and thus the dependence on shear stress approximation, with CFD solutions over a 3-D grid has been previously demonstrated in the literature.[20] This work demonstrates the application of the 2-D grid turbulent flow solution to the concentric seal geometry as a replacement for the zeroth order solution of traditional bulk-flow methods. The first order bulk-flow equations are employed with non-dimensional variables and characteristic quantities in, Equations 2.38 to 2.40 below, with radially averaged zeroth order solution data and numerically obtained local shear stress values from the near wall nodes. The local shear stress values are obtained numerically using laminar finite difference or turbulent wall functions from Section 4.2.1 that describes their use in the Prandtl one-equation turbulence model.

$$c = \frac{H^0}{L_c}\left(1 - \varepsilon e^{\imath(\tau+\theta)}\right) \tag{2.31}$$

$$v = v^0 + \varepsilon v^1 e^{\imath(\tau+\theta)} \tag{2.32}$$

$$w = w^0 + \varepsilon w^1 e^{\imath(\tau+\theta)} \tag{2.33}$$

$$P = P^0 + \varepsilon P^1 e^{\imath(\tau+\theta)} \tag{2.34}$$

$$0 = L_c \not{\ell} \frac{d}{d\tau}(c) + \frac{1}{L_c}\frac{\partial}{\partial z}(U_c L_c c w) + \frac{1}{L_c}\frac{1}{R}\frac{\partial}{\partial \theta}(U_c L_c c v) \tag{2.35}$$

$$-\frac{L_c P_c}{L_c}\frac{c}{R}\frac{\partial P}{\partial \theta} - P_c(\tau_{R\theta} + \tau_{S\theta}) = \not{\ell}\frac{d}{d\tau}(L_c U_c c \rho v) + \frac{1}{L_c}\frac{\partial}{\partial z}\left(L_c U_c^2 \rho c v w\right) + \frac{1}{L_c}\frac{1}{R}\frac{\partial}{\partial \theta}\left(L_c U_c^2 \rho c v^2\right) \tag{2.36}$$

$$-\frac{L_c P_c}{L_c} c \frac{\partial P}{\partial z} - P_c(\tau_{Rz} + \tau_{Sz}) = \not{\ell}\frac{d}{d\tau}(L_c U_c c \rho w) + \frac{1}{L_c}\frac{\partial}{\partial z}\left(L_c U_c^2 \rho c w^2\right) + \frac{1}{L_c}\frac{1}{R}\frac{\partial}{\partial \theta}\left(L_c U_c^2 \rho c v w\right) \tag{2.37}$$

The continuity equation has dimensions of velocity and was non-dimensionalized by dividing through by U_c. The momentum equations above have dimensions of pressure, so to non-dimensionalize the equations the characteristic pressure took the form $P_c = \rho U_c^2$ and the equations were divided by the newly defined P_c. Additionally, at this step the clearance was substituted from Equation 2.34 and the derivatives were expanded. As the hybrid method only requires the first order terms, the zeroth order terms were also discarded at this step.

$$0 = -\imath\frac{L_c\Omega}{U_c}\frac{\cancel{H^0}}{\cancel{L_c}} + \frac{\cancel{H^0}}{\cancel{L_c}}\frac{\partial}{\partial z}\left(w^1\right) + \frac{\cancel{H^0}}{\cancel{L_c}}\frac{\imath}{R}\left(v^1 - v^0\right) \tag{2.38}$$

$$-\frac{H^0}{L_c}\frac{\imath}{R}P^1 - \left(\tau^1_{R\theta} + \tau^1_{S\theta}\right) = \imath\frac{\cancel{L_c}\Omega}{U_c}\frac{H^0}{\cancel{L_c}}v^1 - \frac{H^0}{L_c}w^0\frac{\partial v^0}{\partial z} + \frac{H^0}{L_c}w^1\frac{\partial v^0}{\partial z} + \frac{H^0}{L_c}w^0\frac{\partial v^1}{\partial z} + \frac{H^0}{L_c}\frac{\imath}{R}v^0v^1 \tag{2.39}$$

$$-\frac{H^0}{L_c}\left(-\frac{\partial P^0}{\partial z} + \frac{\partial P^1}{\partial z}\right) - \left(\tau^1_{Rz} + \tau^1_{Sz}\right) = \imath\frac{\cancel{L_c}\Omega}{U_c}\frac{H^0}{\cancel{L_c}}w^1 + \frac{H^0}{L_c}w^0\frac{\partial w^1}{\partial z} + \frac{H^0}{L_c}\frac{\imath}{R}v^0w^1 \tag{2.40}$$

$$0 = -\imath\frac{L_c\Omega}{U_c} + \frac{\partial w^1}{\partial z} + \frac{\imath}{R}\left(v^1 - v^0\right) \tag{2.41}$$

$$-\frac{H^0}{L_c}\frac{\imath}{R}P^1 - \left(\tau^1_{R\theta} + \tau^1_{S\theta}\right) = \imath\frac{H^0\Omega}{U_c}v^1 - \frac{H^0}{L_c}w^0\frac{\partial v^0}{\partial z} + \frac{H^0}{L_c}w^1\frac{\partial v^0}{\partial z} + \frac{H^0}{L_c}w^0\frac{\partial v^1}{\partial z} + \frac{H^0}{L_c}\frac{\imath}{R}v^0v^1 \tag{2.42}$$

$$-\frac{H^0}{L_c}\left(-\frac{\partial P^0}{\partial z} + \frac{\partial P^1}{\partial z}\right) - \left(\tau^1_{Rz} + \tau^1_{Sz}\right) = \imath\frac{H^0\Omega}{U_c}w^1 + \frac{H^0}{L_c}w^0\frac{\partial w^1}{\partial z} + \frac{H^0}{L_c}\frac{\imath}{R}v^0w^1 \tag{2.43}$$

Note that the first order shear stress terms can be approximated from the zeroth order numerical results by the following relationship.

$$\begin{aligned} \tau^0_{-z} \propto w^0 const \Rightarrow & \tau^1_{-z} \propto w^1 const \\ & \frac{\tau^0_{-z}}{w^0} \approx \frac{\tau^1_{-z}}{w^1} \\ & \tau^1_{-z} \approx \frac{w^1}{w^0}\tau^0_{-z} \end{aligned} \tag{2.44}$$

Real Hybrid First Order Equations

$$0 = \frac{\partial w^R}{\partial z} - \frac{1}{R}v^I \tag{2.45}$$

$$\frac{H^0}{L_c}\frac{1}{R}P^I - \frac{v^R}{v^0}\left(\tau^0_{R\theta} + \tau^0_{S\theta}\right) = -\frac{H^0\Omega}{U_c}v^I - \frac{H^0}{L_c}w^0\frac{\partial v^0}{\partial z} + \frac{H^0}{L_c}w^R\frac{\partial v^0}{\partial z} + \frac{H^0}{L_c}w^0\frac{\partial v^R}{\partial z} - \frac{H^0}{L_c}\frac{1}{R}v^0v^I \tag{2.46}$$

$$\frac{H^0}{L_c}\left(\frac{\partial P^0}{\partial z} - \frac{\partial P^R}{\partial z}\right) - \frac{w^R}{w^0}\left(\tau^0_{Rz} + \tau^0_{Sz}\right) = -\frac{H^0\Omega}{U_c}w^I + \frac{H^0}{L_c}w^0\frac{\partial w^R}{\partial z} - \frac{H^0}{L_c}\frac{1}{R}v^0w^I \tag{2.47}$$

On a staggered axial grid, where circumferential velocity and pressure are stored in the cell centers and axial velocity is stored on the cell faces, this becomes:

$$0 = \frac{w^R_n - w^R_{n-1}}{\Delta z_k} - \frac{1}{R}v^I_k \tag{2.48}$$

$$
\begin{aligned}
0 =& -\frac{H^0}{L_c}\frac{1}{R}P_k^I + \frac{v_k^R}{v_k^0}\left(\tau_k^{0,R\theta} + \tau_k^{0,S\theta}\right) - \frac{H^0\Omega}{U_c}v_k^I \\
&+ \frac{H^0}{L_c}\left(-\frac{w_n^0 + w_{n-1}^0}{2} + \frac{w_n^R + w_{n-1}^R}{2}\right)\left(\frac{v_{k+1}^0 - v_k^0}{\Delta z_{k+1} + \Delta z_k} + \frac{v_k^0 - v_{k-1}^0}{\Delta z_k + \Delta z_{k-1}}\right) \\
&+ \frac{H^0}{L_c}\frac{w_n^0 + w_{n-1}^0}{2}\left(\frac{v_{k+1}^R - v_k^R}{\Delta z_{k+1} + \Delta z_k} + \frac{v_k^R - v_{k-1}^R}{\Delta z_k + \Delta z_{k-1}}\right) - \frac{H^0}{L_c}\frac{1}{R}v_k^0 v_k^I
\end{aligned} \tag{2.49}
$$

$$
\begin{aligned}
0 =& 2\frac{H^0}{L_c}\left(-\frac{P_{k+1}^0 - P_k^0}{\Delta z_{k+1} + \Delta z_k} + \frac{P_{k+1}^R - P_k^R}{\Delta z_{k+1} + \Delta z_k}\right) + \frac{w_n^R}{w_n^0}\left(\tau_n^{0,Rz} + \tau_n^{0,Sz}\right) - \frac{H^0\Omega}{U_c}w_n^I \\
&+ \frac{1}{2}\frac{H^0}{L_c}w_n^0\left(\frac{w_{n+1}^R - w_n^R}{\Delta z_k} + \frac{w_n^R - w_{n-1}^R}{\Delta z_{k-1}}\right) - \frac{H^0}{L_c}\frac{1}{R}\frac{\Delta z_{k+1}v_{k+1}^0 + \Delta z_k v_k^0}{\Delta z_{k+1} + \Delta z_k}w_n^I
\end{aligned} \tag{2.50}
$$

Imaginary Hybrid First Order Equations

$$
0 = -\frac{L_c\Omega}{U_c} + \frac{\partial w^I}{\partial z} + \frac{1}{R}\left(v^R - v^0\right) \tag{2.51}
$$

$$
-\frac{H^0}{L_c}\frac{1}{R}P^R - \frac{v^I}{v^0}\left(\tau_{R\theta}^0 + \tau_{S\theta}^0\right) = \frac{H^0\Omega}{U_c}v^R + \frac{H^0}{L_c}w^I\frac{\partial v^0}{\partial z} + \frac{H^0}{L_c}w^0\frac{\partial v^I}{\partial z} + \frac{H^0}{L_c}\frac{1}{R}v^0 v^R \tag{2.52}
$$

$$
-\frac{H^0}{L_c}\frac{\partial P^I}{\partial z} - \frac{w^I}{w^0}\left(\tau_{Rz}^0 + \tau_{Sz}^0\right) = \frac{H^0\Omega}{U_c}w^R + \frac{H^0}{L_c}w^0\frac{\partial w^I}{\partial z} + \frac{H^0}{L_c}\frac{1}{R}v^0 w^R \tag{2.53}
$$

On a staggered axial grid, where circumferential velocity and pressure are stored in the cell centers and axial velocity is stored on the cell faces, this becomes:

$$
0 = -\frac{L_c\Omega}{U_c} + \frac{w_n^I - w_{n-1}^I}{\Delta z_k} + \frac{1}{R}\left(v_k^R - v_k^0\right) \tag{2.54}
$$

$$
\begin{aligned}
0 =& \frac{H^0}{L_c}\frac{1}{R}P_k^R + \frac{v_k^I}{v_k^0}\left(\tau_k^{0,R\theta} + \tau_k^{0,S\theta}\right) + \frac{H^0\Omega}{U_c}v_k^R \\
&+ \frac{H^0}{L_c}\frac{w_n^I + w_{n-1}^I}{2}\left(\frac{v_{k+1}^0 - v_k^0}{\Delta z_{k+1} + \Delta z_k} + \frac{v_k^0 - v_{k-1}^0}{\Delta z_k + \Delta z_{k-1}}\right) \\
&+ \frac{H^0}{L_c}\frac{w_n^0 + w_{n-1}^0}{2}\left(\frac{v_{k+1}^I - v_k^I}{\Delta z_{k+1} + \Delta z_k} + \frac{v_k^I - v_{k-1}^I}{\Delta z_k + \Delta z_{k-1}}\right) + \frac{H^0}{L_c}\frac{1}{R}v_k^0 v_k^R
\end{aligned} \tag{2.55}
$$

$$
\begin{aligned}
0 =& 2\frac{H^0}{L_c}\frac{P_{k+1}^I - P_k^I}{\Delta z_{k+1} + \Delta z_k} + \frac{w_n^I}{w_n^0}\left(\tau_n^{0,Rz} + \tau_n^{0,Sz}\right) + \frac{H^0\Omega}{U_c}w_n^R \\
&+ \frac{1}{2}\frac{H^0}{L_c}w_n^0\left(\frac{w_{n+1}^I - w_n^I}{\Delta z_k} + \frac{w_n^I - w_{n-1}^I}{\Delta z_{k-1}}\right) + \frac{H^0}{L_c}\frac{1}{R}\frac{\Delta z_{k+1}v_{k+1}^0 + \Delta z_k v_k^0}{\Delta z_{k+1} + \Delta z_k}w_n^R
\end{aligned} \tag{2.56}
$$

2.3 The General Mimetic Finite Difference Method

The finite difference method (FDM)[83,84] is a general category of methods for solving partial differential equations (PDE's) in which continuous derivatives are replaced with discrete approximations, typically based on manipulations of Taylor series polynomials,[?] Equation 2.57. The accuracy of these approximations depends on the remainder terms in the manipulated Taylor series combinations once the desired derivative approximation is isolated. The scale of the error involved depends on the number of discrete nodes employed in the calculation, the degree of the derivative, and the position at which the desired derivative is located relative to the discrete nodes. For example, the right-sided finite difference scheme of Equation 2.58 is considered first order accurate since it's remainder term is proportional to Δx and the central difference scheme of Equation 2.59 is considered 2nd order accurate since it's remainder is proportional to $(\Delta x)^2$. However, the individual errors at each node do not necessarily predict the overall accuracy and stability of the method as a whole series of equations converted from the PDE.

$$f\left(x+\Delta x\right) = f\left(x\right) + \frac{\Delta x}{1!}\frac{\partial f\left(x\right)}{\partial x} + \frac{\left(\Delta x\right)^2}{2!}\frac{\partial^2 f\left(x\right)}{\partial x^2} + \cdots + \frac{\left(\Delta x\right)^n}{n!}\frac{\partial^n f\left(x\right)}{\partial x^n} + R_n\left(x\right) \tag{2.57}$$

$$\frac{\partial f\left(x\right)}{\partial x} = \frac{f\left(x+\Delta x\right) - f\left(x\right)}{\Delta x} - \frac{\Delta x}{2}\frac{\partial^2 f\left(x\right)}{\partial x^2} = \frac{f\left(x+\Delta x\right) - f\left(x\right)}{\Delta x} + \mathcal{O}\left(\Delta x\right) \tag{2.58}$$

$$\frac{\partial f\left(x\right)}{\partial x} = \frac{f\left(x+\Delta x\right) - f\left(x-\Delta x\right)}{2\Delta x} - \frac{\left(\Delta x\right)^2}{6}\frac{\partial^3 f\left(x\right)}{\partial x^3} = \frac{f\left(x+\Delta x\right) - f\left(x-\Delta x\right)}{2\Delta x} + \mathcal{O}\left(\Delta x\right)^2 \tag{2.59}$$

The mimetic finite difference method (MFDM) is designed to account for the interactions between the remainder error terms by creating finite difference schemes that mimic the properties of the continuous vector and tensor calculus (CVTC) operators that make up the original PDE with discrete vector and tensor calculus (DVTC) operator equivalents. These DVTC operators can also be designed according to the physical properties that the original continuum PDE's are intended to model.[88–90]

Like any numerical method for solving PDE's the initial step is to define the discretization of the domain with suitable degrees of freedom and discrete vector spaces to store each scalar, vector, and tenso valued variable. The degrees of freedom relates to the number of variables in the equation to be stored at each discrete location, the number of discrete nodes, faces, and edges at which these are located, and the geometry of the domain to be modeled. The grid sizing is

dependent on computational resource constraints and the expected scale of gradients in the PDE to be modeled. Higher gradient values typically need a more dense mesh to accurately model.

2.3.1 Natural Discretizations of Continuous Operators

The discrete schemes employed in the MFDM corresponds to the first-order differential operators, **grad**, **curl**, and **div**, that exist in the continuous PDE. A primary operator is selected to be derived from coordinate invariant CVTC definitions. These definitions for differential operators **grad**, **curl**, and **div** are given in Equations 2.60 to 2.62. The discretizations of these operators give intuitive transformations between vector spaces defined in a control volume.[88–90,115] For a central difference discrete scheme, the vector **div** operator naturally maps from vector values normal to the control volume's faces, **FC** space, to a scalar at the center, **CC** or cell centered space, of the control volume. Similarly, the vector **grad** operator maps from scalar **CN**, or corner node, space to the vector valued edge centered space, **EC**. The **curl** operator is different in that it needs two discrete forms, where the second one maps in reverse of the first. The primary discrete vector **curl** operator then would map from the center of the control volume's edges, **EC** space, to to the vector valued **FC** space. These constructions of the primary operators enforce basic CVTC properties such as **div curl** $\vec{\omega} \equiv 0$ and **curl grad** $\vec{u} \equiv 0$. The proof of these identities for the discrete operators is provided by Hyman's 1997 paper.[115]

$$\int_{\mathbf{x}_1}^{\mathbf{x}_2} \frac{\partial \vec{u}}{\partial \tau} dL = \int_{\mathbf{x}_1}^{\mathbf{x}_2} \mathbf{grad}\,(\vec{u}) \cdot \tau dL = \vec{u}\,(\mathbf{x}_2) - \vec{u}\,(\mathbf{x}_1) \tag{2.60}$$

$$\int_S (\mathbf{curl}\vec{u}) \cdot \hat{n} dS = \oint_{\partial S} \vec{u} \cdot \hat{\tau} dL \tag{2.61}$$

$$\int_V \mathbf{div}\vec{u} dV = \oint_S \vec{u} \cdot \hat{n} dS \tag{2.62}$$

2.3.2 The Adjoint Support Operators

Notice that the vector space mappings of these "naturally" obtained primary operators do not allow the construction of common CVTC combinations such as **div grad**, **grad div**, or **curl curl**. To perform these operations discretly it is necessary to create paired adjoint operators, $\overline{\mathbf{grad}}$, $\overline{\mathbf{curl}}$, and $\overline{\mathbf{div}}$, that complete the vector space transformation of the original operators in reverse. The support operator method (SOM)[116] is employed to ensure that these adjoint operators are

consistent with the primary pair and maintain the identites of the DVTC being constructed.[117] Each primary operator is paired with it's adjoint through a discrete equivalent to Green's integration by parts formulae in Equations 2.63 to 2.65.[88–90,117] The script $\mathscr{Div}$ and $\mathscr{Grad}$ are discrete tensor operators while the bold text represents vector operators. The discrete form of the volume integrals can be performed with volume weighted inner products, Equations 2.66 to 2.68, analagous to Hausdorff pre-Hilbert space inner products.[91,92,118,119] These equations are the inner products for the **CC**, **FC**, and **EC** vector spaces respectively located on a staggered grid that will be elaborated in Chapter 3.

$$\int_V p\mathbf{div}\vec{u}dV = -\int_V \mathbf{grad}p\cdot\vec{u}dV + \oint_S p\,(\vec{u}\cdot\hat{n})\,dS \tag{2.63}$$

$$\int_V \vec{u}\cdot\mathbf{curl}\vec{v}dV = \int_V \mathbf{curl}\vec{u}\cdot\vec{v}dV + \oint_S p\,(\vec{u}\times\vec{v})\,dS \tag{2.64}$$

$$\int_V p\mathscr{Div}\sigma_{\mathbf{qs}}dV = -\int_V \mathscr{Grad}\vec{u}\cdot\sigma_{qs}dV + \oint_S \vec{u}\cdot\left(\sigma_{qs}\cdot\hat{n}\right)dS \tag{2.65}$$

$$\langle a,b\rangle_{CC} \equiv \sum_{(i,j,k)} a_{i,j,k}b_{i,j,k}\left[\chi_i+\varepsilon h\left(R_S-\chi_i\right)\right]\Delta\chi_i\left(1-\varepsilon h\right)\Delta\theta\Delta z_k \tag{2.66}$$

$$\begin{aligned}\left\langle\vec{a},\vec{b}\right\rangle_{FC} \equiv \sum_{(i,j,k)} \frac{\Delta\chi_i\left(1-\varepsilon h\right)\Delta\theta\Delta z_k}{2}\Big\{&\left[\chi_{\ell-1}+\varepsilon h\left(R_S-\chi_{\ell-1}\right)\right]\vec{a}_{\chi_{\ell-1}}\vec{b}_{\chi_{\ell-1}}\\ &+\left[\chi_\ell+\varepsilon h\left(R_S-\chi_\ell\right)\right]\vec{a}_{\chi_\ell}\vec{b}_{\chi_\ell}+2\left[\chi_i+\varepsilon h\left(R_S-\chi_i\right)\right]\vec{a}_{\theta_j}\vec{b}_{\theta_j}\\ &+\left[\chi_i+\varepsilon h\left(R_S-\chi_i\right)\right]\left[\vec{a}_{z_{n-1}}\vec{b}_{z_{n-1}}+\vec{a}_{z_n}\vec{b}_{z_n}\right]\Big\}\end{aligned} \tag{2.67}$$

$$\begin{aligned}\left\langle\vec{a},\vec{b}\right\rangle_{EC} \equiv \sum_{(i,j,k)} \frac{\Delta\chi_i\left(1-\varepsilon h\right)\Delta\theta\Delta z_k}{2}\Big\{&\left[\chi_i+\varepsilon h\left(R_S-\chi_i\right)\right]\left[\vec{a}_{\theta_j,z_{n-1}}\vec{b}_{\theta_j,z_{n-1}}+\vec{a}_{\theta_j,z_n}\vec{b}_{\theta_j,z_n}\right]\\ &+\left[\chi_{\ell-1}+\varepsilon h\left(R_S-\chi_{\ell-1}\right)\right]\frac{\vec{a}_{\chi_{\ell-1},z_{n-1}}\vec{b}_{\chi_{\ell-1},z_{n-1}}+\vec{a}_{\chi_{\ell-1},z_n}\vec{b}_{\chi_{\ell-1},z_n}}{2}\\ &+\left[\chi_\ell+\varepsilon h\left(R_S-\chi_\ell\right)\right]\frac{\vec{a}_{\chi_\ell,z_{n-1}}\vec{b}_{\chi_\ell,z_{n-1}}+\vec{a}_{\chi_\ell,z_n}\vec{b}_{\chi_\ell,z_n}}{2}\\ &+\frac{\chi_i+\chi_{i-1}+\varepsilon h\left(2R_S-\chi_i-\chi_{i-1}\right)}{2}\vec{a}_{\chi_{\ell-1},\theta_j}\vec{b}_{\chi_{\ell-1},\theta_j}\\ &+\frac{\chi_i+\chi_{i+1}+\varepsilon h\left(2R_S-\chi_i-\chi_{i+1}\right)}{2}\vec{a}_{\chi_\ell,\theta_j}\vec{b}_{\chi_\ell,\theta_j}\Big\}\end{aligned} \tag{2.68}$$

The resulting adjoint DVTC operators have reversed mappings to the primary operator so $\overline{\mathbf{grad}}$ maps **CC** $\rightarrow$ **FC**, $\overline{\mathbf{curl}}$ maps **FC** $\rightarrow$ **EC**, and $\overline{\mathbf{div}}$ maps **EC** $\rightarrow$ **CN**. These adjoint operators maintain the same identites as the primary operators, $\overline{\mathbf{div}}\,\overline{\mathbf{curl}}\vec{\omega}\equiv 0$ and $\overline{\mathbf{curl}}\,\overline{\mathbf{grad}}\vec{u}\equiv 0$.[117] The primary and

SOM DVTC operators can then be combined to form discrete equivalents of any continuous PDE while preserving the original system behavior. The construction of the original primary operators and the inner product definitions result in conservative finite difference schems in general.[120,121] For example, the basic equaitons of gas dynamics, Equations 2.69 to 2.71, relate to the integral in Equation 2.72 with a zero pressure boundary condition. Converted to discrete mimetic operators and inner products, Equation 2.73, the equation is now equivalent to Equation 2.63.[88] Thus the mimetic operator construction ensures that the discretization scheme is energy conservative, which provides an unconditionally stable spatial discretization.[91]

$$\frac{1}{\rho}\frac{d\rho}{dt} = - \ \textbf{div}\ \vec{u} \tag{2.69}$$

$$\rho\frac{d\vec{u}}{dt} = - \ \textbf{grad}\ p \tag{2.70}$$

$$\rho\frac{de}{dt} = - \ p\ \textbf{div}\ \vec{u} \tag{2.71}$$

$$\frac{de}{dt} = \int_V \rho\left(\frac{d\vec{u}}{dt}\cdot\vec{u} + \frac{de}{dt}\right)dV = - \int_V (\vec{u}\cdot\ \textbf{grad}\ p + p\ \textbf{div}\ \vec{u})\,dV = 0 \tag{2.72}$$

$$\frac{de}{dt} = - \langle\vec{u},\ \textbf{grad}\ p\rangle_{\textbf{FC}} - \langle p,\ \textbf{div}\ \vec{u}\rangle_{\textbf{CC}} \tag{2.73}$$

2.4 Turbulence Modeling

Accurate turbulence modeling is of particular importance to annular pressure seal modeling due to the dissipation of kinetic energy that occurs. Annular pressure seals are used to prevent loss of pressure between regions of the rotor system that cannot be fully sealed. As such, any effects that reduce the leaking flow's motion are desirable. Adding turbulence modeling to a seal analysis method increases the accuracy of flow solutions and provides the opportunity to test the effect of various patterns of surface roughness more extensively.

Turbulent flow occurs at the high Reynolds numbers that often characterize turbomachinery flows. High Reynolds numbers indicate the ratio of inertial forces to viscous forces acting on a fluid element is immensely in favor of inertia. Any inconstancy in the flow can then cause effectively random abruptly fluctuating local 3-D unsteady variations in fluid velocity and pressure. Turbulent motion in fluids is often described as a collection of eddies, defined as local regions exhibiting high vorticity swirling, that are capable of continuous merging into large unsteady structures, splitting into

multiple smaller structures, and eventually dissipating due to viscous effects. Larger scale eddies transport significant energy not direclty associated with the aggregate fluid motion, increasing diffusion and fluid shear stresses.

2.4.1 Reynolds Averaging

While, turbulence is continuous and can calculated completely with the Navier-Stokes equations at a high enough numerical resolution, it is often more practical to describe turbulent motion as a statistical average effect over a chosen time scale, the method is termed Reynolds decomposition.[122] To achieve a model of this statistically averaged flow, the fluid properties of velocity, pressure, and density, are assumed to be composed of a mean component that represents the overall motion of the fluid, and a time fluctuating component accomidating the local transient eddy motion. By definition, the average of time fluctuating components over the chosen time scale is zero implying that the multiple of a mean value and time fluctating value also averages to zero. However, the multiple of two time fluctuating values does not necessarily average to zero. The Reynolds Averaged Navier-Stokes (RANS) equations result from substituting the mean and fluctating values for each flow variable into the original N-S conservation equations and integrating over a characteristic time scale related to the life expenctancy of a turbulent eddy in the flow. This Kolmogorov time scale is proportional to the changes of local kinetic energy contained in the turbulent eddies due to production and dissipaton of turbulence. The Kolmogorov scales for length, time, and velocity, are given in terms of turbulent energy dissipation, ϵ, and kinematic viscosity, ν in Equation 2.74.[123]

$$\ell_{\mathcal{K}} \equiv \left(\frac{\nu^3}{\epsilon}\right)^{\frac{1}{4}} \tag{2.74a}$$

$$\tau_{\mathcal{K}} \equiv \left(\frac{\nu}{\epsilon}\right)^{\frac{1}{2}} \tag{2.74b}$$

$$U_{\ell} \equiv (\nu\epsilon)^{\frac{1}{4}} \tag{2.74c}$$

2.4.2 Transport of Turbulent Kinetic Energy

Turbulent kinetic energy, k_t, is defined as a scalar quantity that is produced by fluid-fluid interactions forming eddies, exchanged and transported by eddy splitting, and transformed to heat by viscous dissipation. The eddy dissipation to heat occurs at the smallest turbulent scales, though still much larger than molecular scales, and thus transpires over short time scales. It is then assumed that this dissipation is independent of the larger, and therefore slower, eddy motion and the mean fluid transport. The motion within these small eddies is assumed to be a zero-sum game, averaging out to a net zero change over a Kolmorogorov time scale, but still contributing to the total energy of the flow. The kinetic energy in the small eddies within a control volume is thus balanced by convective transport, energy delivered from larger eddies, and the conversion to heat resulting in Kolmogorov's universal equilibrium theory[124].[125] The non-dimensionalized incompressible RANS momentum equation is given in Equation 2.75, where terms with bars over them are time averaged values and terms with ‘ are time fluctuating values. By definition, the time average of a time fluctuating value is zero, but not necessarily so for the multiple of two time fluctuating values, leading to the RANS equations being nearly identical to the typical N-S equations with an additional Reynolds Stress Tensor that appears as the multiple of the fluctuating time fluctuating velocities. This new Reynolds Stress Tensor, $\overline{u_s' u_q'}$, represents 6 new unknowns due to symmetry and sparks the "Closure Problem" of turbulence modeling.

$$2\frac{fH^0}{U_c\rho_c}\frac{\partial\left(\overline{\rho}\overline{\vec{u}}\right)}{\partial t}+\frac{1}{\rho_c}\nabla\cdot\left(\overline{\rho\vec{u}}\otimes\overline{\vec{u}}\right)= -\frac{\Delta P_c}{\rho_c U_c^2}\nabla P+\frac{1}{\rho_c L_c U_c}\nabla\cdot\left[\mu_c\left(\nabla\overline{\vec{u}}+\left\{\nabla\overline{\vec{u}}\right\}^T\right)-\rho\overline{\vec{u}'\vec{u}'}\right] \tag{2.75}$$

The Reynolds Stress Tensor resembles the definition of specific kinetic energy, $\frac{1}{2}\overline{u_q' u_q'}$, and was linked to the concept of turbulent kinetic energy in the eddies by Prandtl.[26] Full transport equations for the Reynolds Stress Tensor terms can be developed by taking the RANS equations prior to averaging, subtracting the mean flow terms, multiplying by the fluctuating velocity components, and performing the Reynolds averaging last. This 3-D Reynolds Stress transport equations results in 6 new equations and 22 new unkowns to replace the previous 6 unknowns, however the trace of this system of equations is equivalent to the scalar turbulent kinetic energy, as suggested by $u_q' u_q'$ in the

definition. The resulting transport equation for turbulent kinetic energy is given in Equation 2.76.

$$\frac{1}{2}\frac{\partial\left(\overline{u'_q u'_q}\right)}{\partial t} + \overbrace{u_s \frac{1}{2}\frac{\partial\left(\overline{u'_q u'_q}\right)}{\partial x_s}}^{\text{Advection}} = \overbrace{-\overline{u'_q u'_s}\frac{\partial \overline{u_q}}{\partial x_s}}^{\text{Production}} \overbrace{-\frac{\mu^0}{\rho_0}\overline{\frac{\partial u'_q}{\partial x_s}\frac{\partial u'_q}{\partial x_s}}}^{\text{Dissipation}} + \frac{\partial}{\partial x_s}\left[\overbrace{\frac{1}{2}\frac{\mu^0}{\rho_0}\frac{\partial\left(\overline{u'_q u'_q}\right)}{\partial x_s}}^{\text{Molecular Diffusion}} \overbrace{-\frac{1}{2}\overline{u'_q u'_q u'_s}}^{\text{Turbulent Transport}} \overbrace{-\frac{1}{\rho_0}\overline{p' u'_s}}^{\text{Pressure Diffusion}}\right] \tag{2.76}$$

This equation still has too many unknown variables, but begins to be more managable. The dissipation term is substituted for ϵ to be defined later by the particular turbulence model, but is within a small margin of $2\frac{\mu^0}{\rho_0}\overline{E'_{qs}E'_{qs}}$ for most flows without shocks.[126] The Reynolds Stress tensor has been represented by τ_{qs}. Further simplificaitons require more assumptions and are discussed in the following sections.

$$\frac{\partial k_t}{\partial t} + \overbrace{\vec{u}_s \cdot \nabla_s k_t}^{\text{Advection}} = \overbrace{\tau_{qs} \otimes \nabla_s \overline{u_q}}^{\text{Production}} \overbrace{-\epsilon}^{\text{Dissipation}} + \nabla_s \cdot \left[\overbrace{\frac{\mu^0}{\rho_0}\nabla_s k_t}^{\text{Molecular Diffusion}} \overbrace{-\frac{1}{2}\overline{u'_q u'_q u'_s}}^{\text{Turbulent Transport}} \overbrace{-\frac{1}{\rho_0}\overline{p' u'_s}}^{\text{Pressure Diffusion}}\right] \tag{2.77}$$

2.4.3 The Boussinesq Hypothesis: Linear Eddy Viscosity Model

Of the available methods to model these 6 unknowns in the Reynolds Stress tensor, one of the more commonly applied and earliest methods in approaching the closure problem is the application of the Boussinesq Hypothesis.[127] Boussinesq proposed that the Reynolds stress tensor, that describes turbulent shear and normal stresses, could be approximated by assuming the turbulent stress tensor can also be approximated with a Newtonian fluid model that has a separate empirical "eddy" viscosity from fluid's molecular viscosity. Instead of relating the trace terms in the turbulent constitutive equation to pressure, they are assumed to reflect the TKE. This approximation of Reynolds Stresses as a function of effective turbulent viscosity defined in Equation 2.78. The turbulent viscosity is, technically, defined through the Boussinesq Hypothesis, as no approximations were made to this point. However, the model is further simplified by assuming that turbulent viscosity

a scalar and estimated through additional calculation. The hypothesis lumps the motion within small eddies into the turbulent kinetic energy and effective turbulent viscosity terms, allowing the calculation of large eddy motion without need to significantly increase numerical resolution.

$$-\rho\overline{u_s' u_q'} \equiv 2\mu_t \left\{ \frac{1}{2}\left[\nabla\vec{u} + (\nabla\vec{u})^T\right] - \frac{1}{3}\nabla\cdot\vec{u}\delta_{qs} \right\} - \frac{2}{3}\rho k_t \delta_{qs} \tag{2.78}$$

Note that this approximation results in modificaitons to the primary non-dimensional and incompressible RANS momentum equations, see Equation 2.79.

$$\begin{aligned} 2\frac{fH^0}{U_c\rho_c}\frac{\partial\left(\overline{\rho}\overline{\vec{u}}\right)}{\partial t} + \frac{1}{\rho_c}\nabla\cdot\left(\overline{\rho\vec{u}}\otimes\overline{\vec{u}}\right) = \\ -\frac{\Delta P_c}{\rho_c U_c^2}\nabla P + \frac{1}{\rho_c L_c U_c}\nabla\cdot\left[\mu_c\left(\nabla\overline{\vec{u}} + \left\{\nabla\overline{\vec{u}}\right\}^T\right)\right. \\ \left. + \mu_t\left\{\nabla\vec{u} + (\nabla\vec{u})^T\right\} - \frac{2}{3}\rho k_t\delta_{qs}\right] \end{aligned} \tag{2.79}$$

Addtional assumptions are made to empirically replace the turbulent transport and pressure diffusion terms in Equation 2.77. The turbulent transport is approximated with gradient-diffusion and an empirically determined coefficient in Equation 2.80.[123] As with the turbulent eddy viscosity, the coefficient σ_k is assumed scalar making the vectors on either side of the equals sign parallel. The pressure diffusion effects are neglected based on DNS simulation results by Mansour, Kim and Moin.[128]

$$\frac{1}{2}\overline{u_q' u_q' u_s'} \approx -\frac{\mu_t}{\rho_0\sigma_k}\nabla_s k \tag{2.80}$$

2.4.4 Prandtl 1-Equation Model

Based on the Buckingham Pi Theorem and dimensional reasoning, Taylor[129] demonstrated that the dissipation of kinetic energy is proportional to $k_t^{\frac{3}{2}}/\ell_t$. Prandtl[26] ran with this ratio by adding a closure coefficient C_D to that proportionality and positing that the length scale is proportional to the Prandtl Mixing Length if the ratio of turbulent production to dissipation is steady. The turbulent kinetic energy transport equation for incompressible fluids is then re-written in the form of Prandtl's One-Equation Model for turbulence in Equation 2.81. The value of C_D is approximately 0.3 for thin boundary layers.

$$\frac{\partial k_t}{\partial t} + \vec{u}_s \cdot \nabla_s k_t = \left[\frac{\mu_t}{\rho_0} \left\{ \nabla_s \vec{u}_q + \left(\nabla_q \vec{u}_s \right)^T \right\} - \frac{2}{3} \rho k_t \delta_{ij} \right] \otimes \nabla_s \vec{u}_q - C_D \frac{k^{\frac{3}{2}}}{\ell_t} + \nabla_s \cdot \left[\frac{1}{\rho_0} \left(\mu_0 + \frac{\mu_t}{\sigma_k} \right) \nabla_s k_t \right] \tag{2.81}$$

$$\mu_t = \rho k_t^{\frac{1}{2}} \ell_t \tag{2.82}$$

2.5 The Shift-Matrix Coding Method

The Shifting-Matrix coding method as applied to fluid dynamics appears to have been pioneered by Sun and Salama.[130–133] This addition to CFD techniques does not improve the solution time, stability, or accuracy of the solution to the $\mathbf{A}\vec{x} = \vec{b}$ equation that is the eventual form of the majority of PDE numerical solution techniques. However, it still significantly improves the overall run time of a CFD code by taking advantage of certain aspects of programming languages. The concept in its most basic form is to construct $\mathbf{A}$ and $\vec{b}$ using only computational operations that are computationally efficient.

Programming languages such as Matlab, Mathematica, Python, and JavaScript are able to direclty perform tasks without previously compiling a program into machine-language instructions for a particular hardware combination. This makes such languages platform independent, flexible to variable type and scope, and convenient for a programmer to code, decipher, and debug a program, but also makes the end product less efficient as each code statement has to be passed through an interpreter that organizes it into machine language on the fly. A comparison can be made with compiled imperative programming languages like FORTRAN, C, C++, and C#. FOTRAN for example is rigid in variable type and scope, with such things assigned before the body of the program; is harder to read; and requires more steps to test and debug than an interpreted language. The trade-off is that it typically performs much more efficiently, which has made it a traditional staple in scientific computing.[134–136]

Particularly, loops such as DO FOR or DO WHILE are especially inefficient in interpreted languages.[83,137] To overcome the relative inefficiency of Matlab for the CFD task, it is necessary to first avoid loops except in the high-level iteration between variablue updating over time-steps, or psuedo-time in steady state. Conveniently, Matlab, being an abbreviation of ”matrix laboratory”, has long optimized and pre-compiled functions for efficient construction of matrices and performing

matrix algebra operations for both sparse and non-sparse matrices. This specialty of Matlab becomes an advantage when used to construct $\mathbf{A}$ and $\vec{b}$ as whole matrices and vectors instead of looping through component by component.

For the purposes of this study, basic finite difference and averaging operations must be performed through matrix algebra. Note specifically that every discrete mimetic operator in the MFDM method applied in this work involves a mapping between variables contained within multiple vector spaces with different ranges of indices on a staggered grid. Figure 2.4 shows a staggered grid with pressure located in each cell center and the velocity vector components located at the center of the cell's positive faces in their respective tangential directions. Each flow variable is stored in a vector array with elements unwrapped axial row by row. If there are N_z axial cells and N_r radial cells, the pressure and circumferential velocity arrays have $N_z \times N_r$ internal elements, $(N_z + 2) \times (N_r + 2)$ elements counting ghost cells. The pressure array is visualized in Equation 2.83. The radial velocity location is "shifted" radially by half a cell to the outward normal face and has $N_z \times (N_r - 1)$ elements, with out boundary/ghost cells, in the storage array. Similarly, the axial velocity has $(N_z - 1) \times N_r$ elements. Sun's shifting matrix technique[131] involves defining basic shifting matrices that "shift" a flow variable east, west, north, or south and increment the size of the flow variable's range in that direction by one. The $nm \times n\,(m + 1)$ east-shift matrix, $\mathbf{A}_E$, consistes of Equation 2.84 which is constructed with the Kronecker tensor product, aka outer product, of a n element identity matrix and an identity matrix with a row of zeros on top. The remaining shifting $\mathbf{A}$ matrices are given by Equations 2.85 to 2.87, with the north/south shifting matrices even simpler to construct.

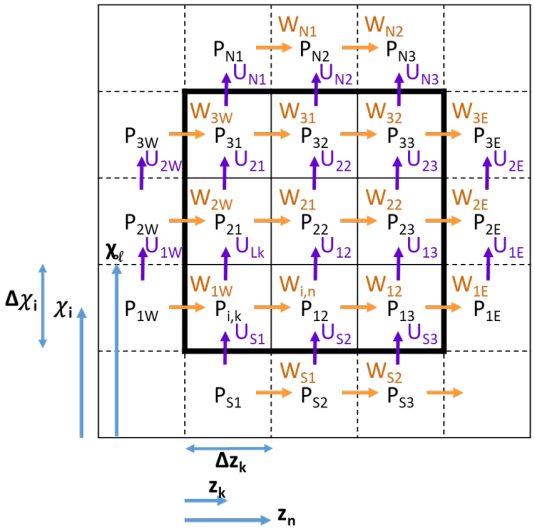

Figure 2.4: Discrete Staggered Grid

$$\vec{P}_{i,j,k} = \begin{bmatrix} P_{1,j,1} \\ P_{1,j,2} \\ P_{1,j,3} \\ \vdots \\ P_{1,j,N_z} \\ P_{2,j,2} \\ \vdots \\ P_{2,j,N_z} \\ \vdots \\ P_{N_r,j,N_z} \end{bmatrix} \tag{2.83}$$

$$[\mathbf{A}_E]_{nm\times n(m+1)} = \mathbf{I}_{n\times n} \otimes \begin{bmatrix} 0_{1\times m} \\ \mathbf{I}_{m\times m} \end{bmatrix} = \begin{bmatrix} \begin{bmatrix} 0_{1\times m} \\ \mathbf{I}_{m\times m} \end{bmatrix} & & & \\ & \begin{bmatrix} 0_{1\times m} \\ \mathbf{I}_{m\times m} \end{bmatrix} & & \\ & & \ddots & \\ & & & \begin{bmatrix} 0_{1\times m} \\ \mathbf{I}_{m\times m} \end{bmatrix} \end{bmatrix}_{nm\times n(m+1)} \tag{2.84}$$

$$[\mathbf{A}_W]_{nm\times n(m+1)} = \mathbf{I}_{n\times n} \otimes \begin{bmatrix} \mathbf{I}_{m\times m} \\ 0_{1\times m} \end{bmatrix} \tag{2.85}$$

$$[\mathbf{A}_N]_{(n+1)m\times nm} = \begin{bmatrix} 0_{m\times nm} \\ \mathbf{I}_{nm\times nm} \end{bmatrix} \tag{2.86}$$

$$[\mathbf{A}_S]_{(n+1)m\times nm} = \begin{bmatrix} \mathbf{I}_{nm\times nm} \\ 0_{m\times nm} \end{bmatrix} \tag{2.87}$$

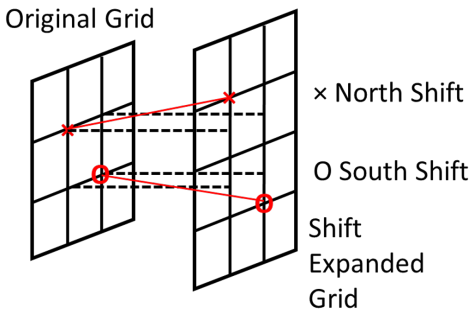

Figure 2.5: Discrete Staggered Grid

Sun[131] calls these $\mathbf{A}$ "Cell-to-Face" shifting matrices and the same matrices incremented from n to n+1 form "Face-to-Node" matrices. For example, Figure 2.5, the pressure array multipled by the north/south shifting matrices maps from the cell centered nodes to the radial face centered nodes by moving the value to the face centered node to the north or south respectively, while the same north/south shifting matrices with an appropriate chosie of n and m will map the velocity to the cell center that is north or south of it in the staggered grid. The $\mathbf{A}$ shifting matrices map locations within the variable's internal domain index range, while similar $\mathbf{B}$ shifting matrices, given by Equations 2.88 to 2.91, map the boundary and ghost cells. The pairs of north/south and east/west shift operations can combined to difference or average a flow variable, while a similar Kroneker tensor product can be applied to distribute the differencing/averaging scale for non-uniform grids. The discrete pressure gradient in the axial direction is given in terms of shift matrices by Equation 2.92 and radial weighted average of axial velocity is given by Equation 2.93. There are no boundary shift matrices in the axial pressure gradient because the mimetic discretization of pressure gradient does not include boundary/ghost cells. In contrast, the weighted radial average of axial velocity

uses the east/west boundary values.

$$[\mathbf{B}_E]_{n(m+1)\times n} = \mathbf{I}_{n\times n} \otimes \begin{bmatrix} 0_{m\times 1} \\ 1 \end{bmatrix} \tag{2.88}$$

$$[\mathbf{B}_W]_{n(m+1)\times n} = \mathbf{I}_{n\times n} \otimes \begin{bmatrix} 1 \\ 0_{m\times 1} \end{bmatrix} \tag{2.89}$$

$$[\mathbf{B}_N]_{(n+1)m\times m} = \begin{bmatrix} 0_{nm\times m} \\ \mathbf{I}_{m\times m} \end{bmatrix} \tag{2.90}$$

$$[\mathbf{B}_S]_{(n+1)m\times m} = \begin{bmatrix} \mathbf{I}_{m\times m} \\ 0_{nm\times m} \end{bmatrix} \tag{2.91}$$

$$\begin{aligned} \left[\mathbf{grad}_z P\right]_{(N_z-1)N_r} =& 2\frac{P_{i,j,k+1} - P_{i,j,k}}{\Delta z_k + \Delta z_{k+1}} \\ =& \left(\mathbf{I}_{N_r\times N_r} \otimes \left[\vec{\Delta} z_{(2:N_z)} + \vec{\Delta} z_{(1:N_z-1)}\right]\right) \\ & \left(\mathbf{A}_{E[N_r N_z\times N_r(N_z-1)]} - \mathbf{A}_{W[N_r N_z\times N_r(N_z-1)]}\right)\vec{P} \end{aligned} \tag{2.92}$$

$$\begin{aligned} \left[\overline{W}^r\right]_{(N_z+1)(N_r-1)} =& \frac{\Delta r_i w_{i,j,n} + \Delta r_{i+1} w_{i+1,j,n}}{\Delta r_i + \Delta r_{i+1}} \\ =& \left(\frac{1}{\left[\vec{\Delta} r_{(2:N_r+1)} + \vec{\Delta} r_{(1:N_r)}\right]} \otimes \mathbf{I}_{N_z+1\times N_z+1}\right) \\ & \left(\mathbf{A}_{N[(N_r-1)(N_z+1)\times N_r(N_z+1)]} + \mathbf{A}_{S[(N_r-1)(N_z+1)\times N_r(N_z+1)]}\right) \\ & \left(\vec{\Delta} r_{(1:N_r)} \otimes \mathbf{I}_{N_z+2\times N_z+2}\right) \\ & \Big[\mathbf{A}_{W N_r N_z\times N_r(N_z+1)} \mathbf{A}_{E N_r(N_z-1)\times N_r N_z} \vec{W} \\ & + \mathbf{A}_{E N_r N_z\times N_r(N_z+1)} \mathbf{B}_{E N_r N_z\times N_r} \vec{W}_{E,BC} \\ & + \mathbf{A}_{W N_r N_z\times N_r(N_z+1)} \mathbf{B}_{W N_r N_z\times N_r} \vec{W}_{W,BC}\Big] \end{aligned} \tag{2.93}$$

The study on Stokes' flow by Zhang in 2015[133] found that applying the shifting matrix method instead of loops in matlab decreased their code's runtime by orders of magnitude. They also found that the runtime of matlab code created with shifting matrices was a small fraction of the runtime for each of multiple tested FORTRAN implementations.

2.6 Commercial CFD Software - ANSYS CFX

ANSYS Workbench and CFX were commercial CFD softwares employed in this work for validation cases and the dynamic similarity models. ANSYS allows the creation of discretized finite element analysis (FEA) CFD models and solves the unsteady Reynolds Averaged Navier-Stokes (RANS) equations with a selected turbulence model.[138–140] The Navier-Stokes equations are sufficient to model any fluid flow when solved analyticaly or at high enough resolution. In practice it is not realistic to use numerical mesh grids fine enough to model the smaller turbulent features. For a simple geometry it may be possible to perform direct numerical simulation (DNS) to fully resolve the flow. However, for the majority of applictions the flows variables are time averaged with mean and fluctuating values by Reynolds Averaging (discussed in detail at Section 2.4.1). This results in the standard conservation of mass and three momentum equations, plus turbulence model to be solved in the discretized domain using FEA.

The Navier-Stokes equations do not have analytical solutions for flows as complex as those presented in this study. Instead, ANSYS CFX discretizes the fluid domain into small control volumes, or elements, using a user defined mesh. The fluid properties for the domain are stored at each node, or corner, of the control volumes. The RANS conservation equations and turbulence model are then constructed as integral FEA matrices. The flow properties are then found by application of a backwards, or implicit, Euler method to the governing equations. This numerical iteration method equates the differential form of the governing equations to change in flow properties between times t_0 and $t_0 + \Delta t$, through the integrated governing equations. In the case of a steady-state simulation, the time step both resolves turbulent time scales and functions as a limiter on the rate of convergence.

2.6.1 Finite Element Method

The finite element method is a subset of a wider range of numerical analysis techniques that are categorized as Galerkin methods[141] that convert continuous equations to discrete equations by assuming that the local solution has the form of a shape function between nodes and integrating the equations over these shape functions. Specifically FEA is a method of mean weighted residuals (MWR),[82,83,142] also known as the Rayleigh-Ritz method. If the a residual is defined as the difference

between the exact solution and the discretely obtained FEA solution at each node, Equation 2.94, the goal is to minimize the magnitude of these residuals like in least-squares linear regression. To perform this minimization, weighting functions for each node are applied as shape functions that approximate the true solution value between nodes, Equation 2.95. In solving the unsteady Navier-Stokes equations, the flow variables substituted into the discrete conservation equations results in the residual directly since the conservation equations should sum to zero. The integral in Equation 2.95 is typically performed by Gaussian quadrature[143] over the shape functions that weight the flow variables between nodes.

$$R(t, x_i) = S_{true} - S_{Discrete}(t, x_i) \tag{2.94}$$

$$0 = \int_{-1}^{1} \phi_{x_i} R(t, x_i) dx \tag{2.95}$$

Shape Functions

ANSYS CFX stores the flow variables and properties at each node of the domain. Algebraic shape functions are used as integrators and interpolators for the finite element method to smoothly connect these discrete nodal values throughout the domain. The sum of shape functions around a particular node describes the 'weight' of its influence on the local flow. The shape functions are given by S_i and the flow properties are represented by ϕ_j in Equation 2.96. The general solution to the discretized RANS equations is composed by the piecewise connection of all the shape functions throughout the domain.

$$\phi = \sum_{i}^{Nodes} (S_i \phi_i) \tag{2.96}$$

The specifics of the shape function employed vary with the number of nodes used to define each element and the geometric structure of the element, *i.e.* 4 or 8 nodes for a tetrahedral element, 6 or 12 nodes for a hexahedral element, and so on. The fluid domains in the present work are simple annular geometries that can be meshed as a single face and swept circumferentially. The radial-axial face is then a rectangular geometry and can be easily divided into rectangular elements and swept into hexahedral elements, though sometimes it is preferable to use triangles and thus sweep them into triangular prism elements. ANSYS CFX documentation provides the individual shape functions for each element type.[138–140]

Equation

Solution and Determination of Residuals

As with most finite element numerical solvers, the ANSYS CFX software collects the discretized and shape function weighted RANS equations into a matrix of linearized equations. Equation 2.97 is the generalized form of the resulting linear algebra expression. The variable ϕ_j represents the solution to the flow variables linearized by shape functions. Matrix $\mathbf{a_{ij}}$ consists of the differential operators in the RANS equations and b_i is a measure of solution residual errors. Each conservation equation is coupled, sacrifcing computer memory capcacity for improved efficiency and robustness of solution.

$$\mathbf{a_{ij}}\phi_j = b_i \tag{2.97}$$

The linear algebra solver employed by ANSYS CFX[138,140] is a combination of ILU factorization[144] and multigrid techniques.[145] ILU factorization refers to decomposing a matrix into the identity, upper, and lower component matrices and is a common linear algebra technique with many variations. Multigrid refers to the use of multiple grids of varying mesh density. The solver is first iterated with a fine mesh and then subseqently with a series of coursening grids to smooth the solution before interpolating the coarse solution back to the finer grids. The actual fine and course grids do not necessarily need to be individually created, instead an algebraic multigrid method can be applied to create matrix operators that perform restrictions and prolongations to simulate multiple grid levels from a single fine grid matrix. The smoothing that results from the prolongation and restriction mapping to and from the fine and coarse grids tend to remove high frequency noise from the solution. Additionally, the coarse grid structure will increase the rate of convergence due to the larger spatial steps between nodes creating a larger step in residuals.

2.6.2 ANSYS Turbulence Models

ANSYS CFX has many turbulence models available for selection,[138,140] however, the more commonly applied models in the literature for annular pressure seals are the $k-\epsilon$ and SST eddy viscosity models. Both models are two-equation models that consist of a transport equation for the turbulent kinetic energy and a representation of the eddy viscosity dissipation rate. Most turbulence models

are designed for accuracy over a particular range of operating parameters and grid types, the $k-\epsilon$ model and SST are not exceptions to this rule. The $k-\epsilon$ model has relatively strict requirements on y+ values for the first layer of elements inside the domain against a wall to be between 30 and 300. The SST turbulence model has much looser restrictions on y+ due to its nature as a smooth blending of the $k-\epsilon$ and $k-\omega$ models based on local y+ value. However, researchers typically treat the SST model as having the same y+ restrictions of the $k-\omega$ model, a local y+ value of less than 5, to ensure that the $k-\omega$ part of the model is being used. A y+ value of less than 5 is typically a high demand in terms of mesh size and results in computationally expensive models. The SST model attenuates this cost by allowing the turbulence model to transition to the $k-\epsilon$ requirements in parts of the fluid domain while maintaining the accuracy of the $k-\omega$ model where needed.

2-D Numerical Analysis of Incompressible Annular Seals by Mimetic FDM

Chapter 3

2-D Grid Laminar Annular Pressure Seal Code By Mimetic FDM

3.1 Mimmetic FDM in Perturbed Cylindrical Coordinates

The mimetic finite difference (MFD) method was selected as the numerical discretization procedure for this body of work due to its conservation and spatial stability properties. MFD methods were developed from work done by Shashkov and hyman in the mid to late 1990's and early 2000's,[115–117,120,146,147] and not available to the few authors who tested two-dimensional grids with finite difference methods and applied to annular pressure seals in the late 1980's.[36–38] Additionally, the MFD method lends itself well to vetorized coding which has been demonstrated to be considerably more computationally efficient, particularly when using Matlab.[133] Future application of the mimetic finite difference method is also more easily adaptable to less structured grid generation than other finite difference techniques.[88,89] The use of mimetic discretizations is novel in application to annular pressure seals, and rarely seen in turbomachinery applications in general. Additional novelty on the side of MFD techniques occurs from the effects of the complex variables, used in the perterbued radial coordinate definition, on the derived adjoint support operators.

3.1.1 Coordinate Perturbation, Definition, & Transformation

To apply the MFD method, the RANS momentum equations were transformed, from the standard incompressible form (A.2) to a form using a only a sequence of first order operators (3.1) and no second order differential operators. The sequence of operators was considered carefully to ensure that no operators require discrete information outside of the established vector spaces within the domain and its adjacent ghost cells along the boundaries.[115,117] While the original form could be preserved by applying tensor discrete operators to the viscous diffusion terms, the diffusion terms and the convection terms are more easily modeled using the vector discrete operators. It did still become necessary to formulate tensor operators for diffusion of eddy viscosity and production of turbulent kinetic energy in the following chapter, but that was not motivation to avoid simplification where possible. The transformation was accomplished by applicaiton of vector operation identities. Between these two steps the equation was non-dimensionalized by Reynolds Number scaling using a characteristic density, length, and velocity, Table A.1. For convenience sake, the characteristic pressure difference was taken ρU_c^2, so that the Euler number is 1 and the gradient of velocity could be conveniently combined into the total pressure without additional scaling parameters.

$$\begin{aligned} 0 &= St\frac{\partial\left(\vec{u}\right)}{\partial t} + \left(\nabla\times\vec{u}\right)\times\vec{u} + \frac{1}{2}\nabla\left(\vec{u}\cdot\vec{u}\right) + \nabla P + \frac{1}{Re}\nabla\times\nabla\times\vec{u} \\ &= St\frac{\partial\left(\vec{u}\right)}{\partial t} + N\left(\vec{u}\right) + \nabla P^T + \frac{1}{Re}C\left[\overline{C}\left(\vec{u}\right)\right] \end{aligned} \tag{3.1}$$

The coordinates were then transformed from standard cylindrical coordinates to a perturbed and eccentric whirling cylindrical coordinate system. The true radial position, r, of a given location was defined as a function of χ, θ, and t seen in Equation 3.4 as a stretching away from, and contraction towards, of the radial clearance depth around a fixed radial location selected at the stator surface, R_S. The position variable, θ, is the standard variable for angular position in cylindrical coordinates, and t indicates a function of time. The χ coordinate was defined as the concentric, non-whirling, radial position being perturbed by the whirling motion. Thus the χ radial coordinate is not a function of angle or time. The new coordinate system consisting of χ, θ, z, and t will accomidate a small circular whirling motion of the rotor about it's nominal geometric center.

$$\epsilon = \frac{h^1}{h^0} = \frac{Eccentricity}{Clearance} \tag{3.2}$$

$$\varepsilon = \epsilon e^{\imath(\Omega t+\theta)} \tag{3.3}$$

$$r = \chi + \varepsilon\left(R_S - \chi\right) \tag{3.4}$$

The core assumption of perturbation methods relies on the method of multiple scales[148] assumption that the perturbation effects of the eccentric whirl are small compared to the basline concentric behaviour about which the perturbation occurs. Thus the sum of effects incurred at each power of the perturbation variable ϵ were taken separately and conservation of dynamic properties such as mass, momentum, and energy, is maintained individually for each power of ϵ. This work truncated terms with powers ϵ^2 and higher. The truncation of terms necessitated defining some approximately equivalent expressions seen below in Equation 3.5 and each subsequent equation in this section.

$$\begin{aligned}\frac{1}{r} = \frac{1}{\chi + \varepsilon\left(R_S - \chi\right)} &\approx \overbrace{\frac{1}{\chi} - \varepsilon\frac{\left(R_S - \chi\right)}{\chi^2} + \varepsilon^2 h^2\frac{\left(R_S - \chi\right)^2}{\chi^3} - \varepsilon^3 h^3\frac{\left(R_S - \chi\right)^3}{\chi^4} + \ldots}^{\text{Taylor Expansion}} \\ &\approx \overbrace{\frac{1}{\chi} - \varepsilon\frac{\left(R_S - \chi\right)}{\chi^2}}^{\text{First 2 terms}}\end{aligned} \tag{3.5}$$

With the coordinate variable χ substituted into the RANS equations in place of r, the relevant derivatives to application of the chain rule are listed in Equations 3.6 to 3.11. Note that the chain rule terms relating to the dependence of coordinate r on θ and t must be applied even in RANS equation terms with no r variables.

$$\frac{\partial\chi}{\partial r} = \frac{1}{1-\varepsilon} \approx \overbrace{1 + \varepsilon + \varepsilon^2 h^2 + \varepsilon^3 h^3 + \ldots}^{\text{Taylor Expansion}} \approx \overbrace{1 + \varepsilon}^{\text{First 2 terms}} \tag{3.6}$$

$$\frac{\partial r\left(\chi,\theta,t\right)}{\partial\theta} = \frac{\partial\left[\chi + \epsilon e^{\imath(\Omega t+\theta)}\left(R_S - \chi\right)\right]}{\partial\theta} = \imath\varepsilon\left(R_S - r\right) \tag{3.7}$$

$$\frac{\partial r\left(\chi,\theta,t\right)}{\partial t} = \frac{\partial\left[\chi + \epsilon e^{\imath(\Omega t+\theta)}\left(R_S - \chi\right)\right]}{\partial t} = \imath\Omega\varepsilon\left(R_S - r\right) \tag{3.8}$$

The flow variables of the RANS equations were also perturbed using the small circular whirl expression of Equation 3.3:

$$\begin{bmatrix} u_{\ell,k} \\ v_{i,k} \\ w_{i,n} \\ P_{i,k} \\ P^T_{i,k} \\ k_{i,k} \end{bmatrix} = \begin{bmatrix} u^0_{\ell,k} + \varepsilon u^1_{\ell,k} \\ v^0_{i,k} + \varepsilon v^1_{i,k} \\ w^0_{i,n} + \varepsilon w^1_{i,n} \\ P^0_{i,k} + \varepsilon P^1_{i,k} \\ P^{T,0}_{i,k} + \varepsilon P^{T,1}_{i,k} \\ k^0_{i,k} \end{bmatrix} \tag{3.9}$$

For convenience, the real and imaginary components of the radial velocity are shown below with the variable multiplied by $\imath$ and distributed to the real and imaginary components. Note that the conjugate refered to in the mimetic support operator derivation does not correspond with a complex conjugate.

$$u^1_{\ell,j,k} = u^R_{\ell,j,k} + \imath u^I_{\ell,j,k} \Rightarrow \overline{u^1_{\ell,j,k}} = u^R_{\ell,j,k} - \imath u^I_{\ell,j,k} \tag{3.10a}$$

$$\imath u^1_{\ell,j,k} = -u^I_{\ell,j,k} + \imath u^R_{\ell,j,k} \Rightarrow \overline{\imath u^1_{\ell,j,k}} = u^I_{\ell,j,k} + \imath u^R_{\ell,j,k} \tag{3.10b}$$

The chain rule for each spatial derivative of a flow variable follows in Equation 3.11. Note that the extra terms in the total derivative with respect to angle and time reduce to partial derivatives of χ without the $(1+\varepsilon)$ factor as the second power of ε is truncated away.

$$\frac{d}{dr} = \frac{\partial}{\partial \chi}\frac{\partial \chi}{\partial r} \approx \frac{\partial}{\partial \chi}(1+\varepsilon) \tag{3.11a}$$

$$\frac{du}{d\theta} = \frac{\partial u}{\partial \phi} + \frac{\partial r}{\partial \phi}\frac{\partial u}{\partial r} \approx \frac{\partial u}{\partial \phi} + \imath\varepsilon(R_S - \chi)\frac{\partial u}{\partial \chi} \approx \imath\varepsilon u^1 + \imath\varepsilon(R_S - \chi)\frac{\partial u^0}{\partial \chi} \tag{3.11b}$$

$$\approx -\varepsilon u^I + \imath\varepsilon\left[u^R + (R_S - \chi)\frac{\partial u^0}{\partial \chi}\right] \tag{3.11c}$$

$$\frac{d}{dt} = \frac{\partial u}{\partial t} + \frac{\partial r}{\partial t}\frac{\partial u}{\partial r} \approx \imath\varepsilon\Omega u^1 + \imath\Omega\varepsilon(R_S - \chi)\frac{\partial u^0}{\partial \chi} \tag{3.11d}$$

$$\approx -\varepsilon\Omega u^I + \imath\varepsilon\Omega\left[u^R + (R_S - \chi)\frac{\partial u^0}{\partial \chi}\right] \tag{3.11e}$$

The time derivatives were then discretely approximated as follows using the taylor approximations and chain rule application shown in Equation 3.11. The discrete radial derivatives in the chain rule differed for radial velocity compared to circumferential and axial velocities due to the second

two variables being located in the radial center of each domain cell. These velocity derivatives were split into zeroth and first order terms to be added to the A matrix and B array respectively.

$$\frac{\partial u_{\ell,k}}{\partial t} \approx -\varepsilon\Omega u^I_{\ell,k} + i\varepsilon\Omega.\left[u^R_{\ell,k} + (R_S - \chi)\frac{\partial u^0_{\ell,k}}{\partial \chi}\right] \tag{3.12a}$$

$$\left(\frac{\partial u_{\ell,k}}{\partial t}\right)^R \approx -\Omega u^I_{\ell,k} \tag{3.12b}$$

$$\left(\frac{\partial u_{\ell,k}}{\partial t}\right)^I \approx \Omega u^R_{\ell,k} + \Omega h\,(R_S - \chi_\ell)\frac{u^0_{\ell+1,k} - u^0_{\ell-1,k}}{\Delta\chi_{i+1} + \Delta\chi_i} \tag{3.12c}$$

$$\frac{\partial v_{i,j+\frac{1}{2},k}}{\partial t} \approx -\varepsilon\Omega v^I_{i,k} + i\varepsilon\Omega.\left[v^R_{i,k} + (R_S - \chi)\frac{\partial v^0_{i,k}}{\partial \chi}\right] \tag{3.12d}$$

$$\left(\frac{\partial v_{i,k}}{\partial t}\right)^R \approx -\Omega v^I_{i,k} \tag{3.12e}$$

$$\left(\frac{\partial v_{i,k}}{\partial t}\right)^I \approx \Omega v^R_{i,k} + 2\Omega h\,(R_S - \chi_i)\frac{v^0_{i+1,k} - v^0_{i-1,k}}{\Delta\chi_{i+1} + 2\Delta\chi_i + \Delta\chi_{i-1}} \tag{3.12f}$$

$$\frac{\partial w_{i,n}}{\partial t} \approx -\varepsilon\Omega w^I_{i,n} + i\varepsilon\Omega.\left[w^R_{i,n} + (R_S - \chi)\frac{\partial w^0_{i,n}}{\partial \chi}\right] \tag{3.12g}$$

$$\left(\frac{\partial w_{i,n}}{\partial t}\right)^R \approx -\Omega w^I_{i,n} \tag{3.12h}$$

$$\left(\frac{\partial w_{i,n}}{\partial t}\right)^I \approx \Omega w^R_{i,n} + 2\Omega h\,(R_S - \chi_i)\frac{w^0_{i+1,n} - w^0_{i-1,n}}{\Delta\chi_{i+1} + 2\Delta\chi_i + \Delta\chi_{i-1}} \tag{3.12i}$$

3.2 Discrete Staggered 2-D Grid for the Navier-Stokes Equations

The fluid modeling of an annular pressure seal begins with the Navier-Stokes (NS) momentum equations. The general Reynolds scaling non-dimensional form of the incompressible NS equations are found in Equation 3.13. These equations were applied in the geometrically perturbed cylindrical coordinate system discussed in Section 3.1.1. Both the convection and diffusion components of the NS equation are second order tensors, to take advantage of simpler mimetic DVTC operators the components were reorganized into first order tensor operations through vector calculus identities in Equation 3.14. Note that the Euler number was removed in the second form by selecting a characteristic pressure differential equal to the denominator of the Euler Number's definition. The non-dimensionalization and tensor rank adjustments were developed in detail in Appendix A.

$$St\frac{\partial(\vec{u})}{\partial t} + \nabla\cdot(\vec{u}\otimes\vec{u}) = -Eu\nabla P + \frac{1}{Re}\left[\nabla^2\vec{u}\right] \tag{3.13}$$

$$\begin{aligned} 0 &= St\frac{\partial(\vec{u})}{\partial t} + (\nabla \times \vec{u}) \times \vec{u} + \frac{1}{2}\nabla(\vec{u} \cdot \vec{u}) + Eu\nabla P + \frac{1}{Re}\nabla \times \nabla \times \vec{u} \\ &= St\frac{\partial(\vec{u})}{\partial t} + N(\vec{u}) + \nabla P^T + \frac{1}{Re}C\left[\overline{C}(\vec{u})\right] \end{aligned} \tag{3.14}$$

As the mimetic approach customizes the operators to the discrete Hilbert spaces that makeup the selected staggered 2-D grid, in geometrically perturbed cylindrical coordiantes, it was first important to define the various grid locations. For the purposes of the grid definition it was assumed to have three basis vectors analagous to cylindrical coordinates. The coordinate directions consist of the concentric radial coordinate $\hat{\chi}$ basis, the circumferential coordinate angle $\hat{\theta}$ basis, and the axial coordinate $\hat{z}$ basis; with respective discrete distances of $\Delta\chi$, $\Delta\theta$, Δz. However, the grid was 2-D in the radial-axial directions; there were no grid variations with θ so there is no need to define an index or discrete distance in the $\hat{\theta}$ basis direction. The non-uniform distribution of the cell centered, (**CC**), grid locations depended on the discrete distances and indices i and k in each respective direction. Additional grid locations on the cell faces, (**FC**), were defined by adding half of the respective discrete distances so $i + \frac{1}{2} = \ell$ and $k + \frac{1}{2} = n$. The staggered grid was then constructed with N_z by N_χ cells in the axial and radial directions and a single cell in the circumferential direction. Flow variables were separated into distinct vector spaces that are cell centered (**CC**), face centered (**FC**), and edge centered (**CC**) seen in Equations 3.16a, 3.16b, and 3.16c respectively. Like the radial and axial velocities stored on the positive radial and axial faces respectively, the circumferential velocity was considered face centered on an infinitely thin circumferential face. The edge centered vector space existed in the positive corners of the infinitely thin rectangular prism and contained the vorticity flow variables. The cell centers contain the scalar flow variables such as pressure, total pressure, viscosity, density, and turbulent kinetic energy. This work consists of incompressible flow calculations, however, there is no conceptual difficulty in having the Reynolds number (and thus density) stored for each cell as an additional variable with the existing conservative discretization if discrete tensor operators are used for viscous diffusion and an additional equation of state is included allow for more unknowns.

$$\chi_i = R_{Rotor} + \sum_{q=1}^{i} \Delta\chi_q - \frac{\Delta\chi_i}{2}\, i \in \{1, 2, 3, \ldots N_\chi\} \tag{3.15a}$$

$$\chi_\ell = R_{Rotor} + \sum_{q=1}^{i} \Delta\chi_q\, i \in \{1, 2, 3, \ldots N_\chi\} \tag{3.15b}$$

$$z_k = \sum_{q=1}^{k} \Delta z_q - \frac{\Delta z_k}{2} \; k \in \{1, 2, 3, \ldots N_z\} \tag{3.15c}$$

$$z_n = \sum_{q=1}^{k} \Delta z_q \; k \in \{1, 2, 3, \ldots N_z\} \tag{3.15d}$$

$$P_{i,k} = P(\chi_i, \theta, z_k) = P^0_{i,k} + \varepsilon P^1_{i,k} = P^0_{i,k} + hcos(\Omega t + \theta) P^R_{i,k} + \imath hsin(\Omega t + \theta) P^I_{i,k} \tag{3.16a}$$

$$\begin{bmatrix} u_{\ell,k} \\ v_{i,k} \\ w_{i,n} \end{bmatrix} = \begin{bmatrix} u(\chi_\ell, \theta, z_k) \\ v(\chi_i, \theta, z_k) \\ w(\chi_i, \theta, z_n) \end{bmatrix} = \begin{bmatrix} u^0_{\ell,k} + \varepsilon u^1_{\ell,k} \\ v^0_{i,k} + \varepsilon v^1_{i,k} \\ w^0_{i,n} + \varepsilon w^1_{i,n} \end{bmatrix} = \begin{bmatrix} u^0_{\ell,k} + hcos(\Omega t + \theta) u^R_{\ell,k} + \imath hsin(\Omega t + \theta) u^I_{\ell,k} \\ v^0_{i,k} + hcos(\Omega t + \theta) v^R_{i,k} + \imath hsin(\Omega t + \theta) v^I_{i,k} \\ w^0_{i,n} + hcos(\Omega t + \theta) w^R_{i,n} + \imath hsin(\Omega t + \theta) w^I_{i,n} \end{bmatrix} \tag{3.16b}$$

$$\begin{bmatrix} \eta_{i,n} \\ \omega_{\ell,n} \\ \zeta_{\ell,k} \end{bmatrix} = \begin{bmatrix} \eta(\chi_i, \theta, z_n) \\ \omega(\chi_\ell, \theta, z_n) \\ \zeta(\chi_\ell, \theta, z_k) \end{bmatrix} = \begin{bmatrix} \eta^0_{i,n} + \varepsilon \eta^1_{i,n} \\ \omega^0_{\ell,n} + \varepsilon \omega^1_{\ell,n} \\ \zeta^0_{\ell,k} + \varepsilon \zeta^1_{\ell,k} \end{bmatrix} = \begin{bmatrix} \eta^0_{i,n} + hcos(\Omega t + \theta) \eta^R_{i,n} + \imath hsin(\Omega t + \theta) \eta^I_{i,n} \\ \omega^0_{\ell,n} + hcos(\Omega t + \theta) \omega^R_{\ell,n} + \imath hsin(\Omega t + \theta) \omega^I_{\ell,n} \\ \zeta^0_{\ell,k} + hcos(\Omega t + \theta) \zeta^R_{\ell,k} + \imath hsin(\Omega t + \theta) \zeta^I_{\ell,k} \end{bmatrix} \tag{3.16c}$$

As previously discussed, the mimetic method consists of constructing a unique DVTC for the vector spaces and grid defining the fluid domain. The DVTC consists of paired discrete operators that form Hilbert spaces with the flow variables. These discrete operators are derived as paired primary and derived operators. The primary operators were created from coordinate invariant definitions of the vector operators and the derived operators are arrived at through the support operator method that uses the defined Hilbert spaces. As Hilbert spaces are used, the inner products must be defined for each vector space in question. The **CC**, **FC**, and **EC** Hilbert spaces are defined with Equations 3.17, 3.18, and 3.19. The DVTC mimetic operators are combined in the following sections to create the the mass conservation equation and pressure gradient, diffusion and convection components of the NS momentum equations.

$$\langle a, b \rangle_{CC} \equiv \sum_{(i,k)} a_{i,k} b_{i,k} \left[\chi_i + \varepsilon \left(R_S - \chi_i\right)\right] \Delta\chi_i \left(1 - \varepsilon\right) \Delta\theta \Delta z_k \tag{3.17}$$

$$\begin{aligned} \left\langle \vec{a}, \vec{b} \right\rangle_{FC} \equiv \sum_{(i,k)} \frac{\Delta\chi_i \left(1 - \varepsilon\right) \Delta\theta \Delta z_k}{2} \Big\{ & \left[\chi_{\ell-1} + \varepsilon \left(R_S - \chi_{\ell-1}\right)\right] \vec{a}_{\chi_{\ell-1}} \vec{b}_{\chi_{\ell-1}} \\ & + \left[\chi_\ell + \varepsilon \left(R_S - \chi_\ell\right)\right] \vec{a}_{\chi_\ell} \vec{b}_{\chi_\ell} + 2 \left[\chi_i + \varepsilon \left(R_S - \chi_i\right)\right] \vec{a}_\theta \vec{b}_\theta \\ & + \left[\chi_i + \varepsilon \left(R_S - \chi_i\right)\right] \left[\vec{a}_{z_{n-1}} \vec{b}_{z_{n-1}} + \vec{a}_{z_n} \vec{b}_{z_n}\right] \Big\} \end{aligned} \tag{3.18}$$

$$\begin{aligned}\left\langle \vec{a},\vec{b}\right\rangle_{EC} \equiv \sum_{(i,k)} \frac{\Delta\chi_i\,(1-\varepsilon)\,\Delta\theta\Delta z_k}{2}\Bigg\{ & \\ & [\chi_i+\varepsilon\,(R_S-\chi_i)]\left[\vec{a}_{\theta,z_{n-1}}\vec{b}_{\theta,z_{n-1}}+\vec{a}_{\theta,z_n}\vec{b}_{\theta,z_n}\right] \\ & +[\chi_{\ell-1}+\varepsilon\,(R_S-\chi_{\ell-1})]\,\frac{\vec{a}_{\chi_{\ell-1},z_{n-1}}\vec{b}_{\chi_{\ell-1},z_{n-1}}+\vec{a}_{\chi_{\ell-1},z_n}\vec{b}_{\chi_{\ell-1},z_n}}{2} \\ & +[\chi_{\ell}+\varepsilon\,(R_S-\chi_{\ell})]\,\frac{\vec{a}_{\chi_{\ell},z_{n-1}}\vec{b}_{\chi_{\ell},z_{n-1}}+\vec{a}_{\chi_{\ell},z_n}\vec{b}_{\chi_{\ell},z_n}}{2} \\ & +\frac{\chi_i+\chi_{i-1}+\varepsilon\,(2R_S-\chi_i-\chi_{i-1})}{2}\vec{a}_{\chi_{\ell-1},\theta}\vec{b}_{\chi_{\ell-1},\theta} \\ & +\frac{\chi_i+\chi_{i+1}+\varepsilon\,(2R_S-\chi_i-\chi_{i+1})}{2}\vec{a}_{\chi_{\ell},\theta}\vec{b}_{\chi_{\ell},\theta}\Bigg\}\end{aligned} \tag{3.19}$$

3.3 Mass Conservation, $\nabla \cdot \vec{u}$

The mass conservation equation for an incompressible fluid is simply the divergence of velocity equal to zero. Divergence is a measure of flux in and out of a differential volume, thus for an incompressible fluid, density is constant, velocity flux is equal to mass flux. The primary discrete divergence operator is used from Appendix Section B.1.

3.3.1 Discrete Divergence Operator, Zeroth Order: $0 = (\nabla \cdot \vec{u})^0$

$$\mathbf{D_{FC}}^0\,(\vec{u}) = 0 = \frac{1}{\chi_i}\frac{\chi_\ell u^0_{\ell,k}-\chi_{\ell-1}u^0_{\ell-1,k}}{\Delta\chi_i}+\frac{w^0_{i,n}-w^0_{i,n-1}}{\Delta z_k} \tag{3.20}$$

3.3.2 Discrete Divergence Operator, Real First Order: $0 = (\nabla \cdot \vec{u})^R$

$$\begin{aligned}\mathbf{D_{FC}}^R\,(\vec{u}) = 0 = & \frac{1}{\chi_i}\frac{\chi_\ell u^0_{\ell,k}-\chi_{\ell-1}u^0_{\ell-1,k}}{\Delta\chi_i}+\frac{R_S}{\chi_i}\frac{u^0_{\ell,k}-u^0_{\ell-1,k}}{\Delta\chi_i} \\ & -\frac{R_S}{\chi_i^2}\frac{\chi_\ell u^0_{\ell,k}-\chi_{\ell-1}u^0_{\ell-1,k}}{\Delta\chi_i}+\frac{1}{\chi_i}\frac{\chi_\ell u^R_{\ell,k}-\chi_{\ell-1}u^R_{\ell-1,k}}{\Delta\chi_i} \\ & -\frac{1}{\chi_i}v^I_{i,k}+\frac{w^R_{i,n}-w^R_{i,n-1}}{\Delta z_k}\end{aligned} \tag{3.21}$$

3.3.3 Discrete Divergence Operator, Imaginary First Order: $0 = (\nabla \cdot \vec{u})^I$

$$\begin{aligned}\mathbf{D_{FC}}^I\,(\vec{u}) = 0 = & \frac{1}{\chi_i}\frac{\chi_\ell u^I_{\ell,k}-\chi_{\ell-1}u^I_{\ell-1,k}}{\Delta\chi_i} \\ & +\frac{1}{\chi_i}\left[v^R_{i,k}+2\,(R_S-\chi_i)\,\frac{v^0_{i+1,k}-v^0_{i-1,k}}{\Delta\chi_{i+1}+2\Delta\chi_i+\chi_{i-1}}\right]+\frac{w^I_{i,n}-w^I_{i,n-1}}{\Delta z_k}\end{aligned} \tag{3.22}$$

3.4 Discrete Pressure Gradient, ∇P^T

In 3.14, the convection term was split into vorticity crossed with velocity and a kinetic energy term $\frac{1}{2}\nabla\left(\vec{u}\cdot\vec{u}\right)$. Instead of separately defining an appropriate equivalent discrete operator for the gradient of the kinetic energy, this term is combined with the gradient of pressure to form the gradient of total pressure. Even though the kinetic energy term must be calculated later to determine the static pressure, it involves less error to calculate the potential instead of the gradient. To conveniently combine the kinetic energy and pressure gradients the characteristic pressure differential is selected to be ρU_c^2, resolving the Euler number to unity. The discrete scalar gradient operator is derived from the vector divergence operator in Appendix Section B.4.

3.4.1 Discrete Pressure Gradient Operator, Zeroth Order: $\left(\nabla P^T\right)^0$

$$\begin{bmatrix} \left(\overline{\mathbf{G_{CC}}}_{\chi} P\right)^0_{\ell,k} \\ \hdashline \left(\overline{\mathbf{G_{CC}}}_{\phi} P\right)^0_{i,k} \\ \hdashline \left(\overline{\mathbf{G_{CC}}}_{z} P\right)^0_{i,jn} \end{bmatrix} = \begin{bmatrix} 2\dfrac{P^0_{i+1,k} - P^0_{i,k}}{\Delta\chi_i + \Delta\chi_{i+1}} \\ \hdashline 0 \\ \hdashline 2\dfrac{P^0_{i,k+1} - P^0_{i,k}}{\Delta z_k + \Delta z_{k+1}} \end{bmatrix} \tag{3.23}$$

3.4.2 Discrete Pressure Gradient Operator, Real First Order: $\left(\nabla P^T\right)^R$

$$\begin{bmatrix} \left(\overline{\mathbf{G}_{\mathrm{CC}}}_{\chi} P\right)^R_{\ell,k} \\ \left(\overline{\mathbf{G}_{\mathrm{CC}}}_{\phi} P\right)^R_{i,k} \\ \left(\overline{\mathbf{G}_{\mathrm{CC}}}_{z} P\right)^R_{i,jn} \end{bmatrix} = \begin{bmatrix} 2\dfrac{P^0_{i+1,k} - P^0_{i,k}}{\Delta\chi_i + \Delta\chi_{i+1}} + 2\dfrac{P^R_{i+1,k} - P^R_{i,k}}{\Delta\chi_i + \Delta\chi_{i+1}} \\ -\dfrac{1}{\chi_i} P^I_{i,k} \\ 2\dfrac{P^R_{i,k+1} - P^R_{i,k}}{\Delta z_k + \Delta z_{k+1}} \end{bmatrix} \tag{3.24}$$

3.4.3 Discrete Pressure Gradient Operator, Imaginary First Order: $\left(\nabla P^T\right)^I$

$$\begin{bmatrix} \left(\overline{\mathbf{G}_{\mathrm{CC}}}_{\chi} P\right)^I_{\ell,k} \\ \left(\overline{\mathbf{G}_{\mathrm{CC}}}_{\phi} P\right)^I_{i,k} \\ \left(\overline{\mathbf{G}_{\mathrm{CC}}}_{z} P\right)^I_{i,jn} \end{bmatrix} = \begin{bmatrix} -2\dfrac{P^I_{i+1,k} - P^I_{i,k}}{\Delta\chi_i + \Delta\chi_{i+1}} \\ -\dfrac{1}{\chi_i} P^R_{i,k} + 2\dfrac{\Delta\chi_{i+1}}{\Delta\chi_i}\dfrac{R_S - \chi_{i+1}}{\chi_i}\dfrac{P^0_{i+1,k}}{\Delta\chi_{i+2} + 2\Delta\chi_{i+1} + \chi_i} \\ \qquad -2\dfrac{\Delta\chi_{i-1}}{\Delta\chi_i}\dfrac{R_S - \chi_{i-1}}{\chi_i}\dfrac{P^0_{i-1,k}}{\Delta\chi_i + 2\Delta\chi_{i-1} + \chi_{i-2}} \\ -2\dfrac{P^I_{i,k+1} - P^I_{i,k}}{\Delta z_k + \Delta z_{k+1}} \end{bmatrix} \tag{3.25}$$

3.5 Discrete Viscous Diffusion, $C\overline{C}\left(\vec{u}\right) = \nabla \times \nabla \times \vec{u}$

The diffusion term is transformed in 3.14 to a function of the sequentially applied curl operators on velocity. Appendix Sections C.1 and C.2 give the derivations of the curl operator and its conjugate, it is necessary to use the primary curl operator on its conjugate curl operator rather than sequentially applying the primary curl operator to maintain the correct mapping between vector spaces, beginning and ending in the **FC** space. Futhermore, boundary conditions must be applied consistently with the mimetic operators to preserve their replication of the continuous vector operators. The full diffusion equations are obtained by substituting the derived curl operator into the primary curl operator. The zeroth and first order equations are first substituted and then simplified in the following subsections.

3.5.1 Discrete Viscous Diffusion, Zeroth Order: $\left(\nabla \times \nabla \times \vec{u}\right)^0$

$$\vec{\mathbf{C}}^0 = \begin{bmatrix} C\left(\vec{\omega}\right)^0_{\ell,k} \\ \hdashline C\left(\vec{\omega}\right)^0_{i,k} \\ \hdashline C\left(\vec{\omega}\right)^0_{i,n} \end{bmatrix} = \begin{bmatrix} -2\dfrac{1}{\Delta z_k}\left\{\dfrac{u^0_{\ell,k+1}-u^0_{\ell,k}}{\Delta z_k+\Delta z_{k+1}} - \dfrac{w^0_{i+1,n}-w^0_{i,n}}{\Delta\chi_{i+1}+\Delta\chi_i} - \dfrac{u^0_{\ell,k}-u^0_{\ell,k-1}}{\Delta z_k+\Delta z_{k-1}} + \dfrac{w^0_{i+1,n-1}-w^0_{i,n-1}}{\Delta\chi_{i+1}+\Delta\chi_i}\right\} \\ \hdashline \dfrac{2}{\Delta z_k}\left\{-\dfrac{v^0_{i,k+1}-v^0_{i,k}}{\Delta z_k+\Delta z_{k+1}} + \dfrac{v^0_{i,k}-v^0_{i,k-1}}{\Delta z_k+\Delta z_{k-1}}\right\} - \dfrac{4}{\Delta\chi_i}\left\{\dfrac{1}{\chi_{i+1}+\chi_i}\dfrac{\chi_{i+1}v^0_{i+1,k}-\chi_i v^0_{i,k}}{\Delta\chi_i+\Delta\chi_{i+1}} - \dfrac{1}{\chi_{i-1}+\chi_i}\dfrac{\chi_i v^0_{i,k}-\chi_{i-1}v^0_{i-1,k}}{\Delta\chi_i+\Delta\chi_{i-1}}\right\} \\ \hdashline \dfrac{2}{\chi_i\Delta\chi_i}\left\{\chi_\ell\left(\dfrac{u^0_{\ell,k+1}-u^0_{\ell,k}}{\Delta z_k+\Delta z_{k+1}} - \dfrac{w^0_{i+1,n}-w^0_{i,n}}{\Delta\chi_i+\Delta\chi_{i+1}}\right) - \chi_{\ell-1}\left(\dfrac{u^0_{\ell-1,k+1}-u^0_{\ell-1,k}}{\Delta z_k+\Delta z_{k+1}} - \dfrac{w^0_{i,n}-w^0_{i-1,n}}{\Delta\chi_i+\Delta\chi_{i-1}}\right)\right\} \end{bmatrix} \tag{3.26}$$

3.5.2 Discrete Viscous Diffusion, Real First Order: $(\nabla \times \nabla \times \vec{u})^R$

$$C\left(\overline{\vec{\omega}}\right)^R_{\ell,k} = -\frac{1}{\chi_\ell}\overline{\zeta^I_{\ell,k}} - \frac{\overline{\omega^R_{\ell,n}} - \overline{\omega^R_{\ell,n-1}}}{\Delta z_k} \tag{3.27}$$

$$\begin{aligned}
C\left(\overline{\vec{\omega}}\right)^R_{\ell,k} =& +\frac{4}{\chi_\ell\left(\chi_{i+1}+\chi_i\right)}\frac{\chi_{i+1}v^I_{i+1,k} - \chi_i v^I_{i,k}}{\Delta\chi_i + \Delta\chi_{i+1}} \\
&+\frac{2}{\chi_\ell\left(\chi_{i+1}+\chi_i\right)}\left\{-u^R_{\ell,k} + \frac{\left(R_S-\chi_{\ell+1}\right)u^0_{\ell+1,k} - \left(R_S-\chi_{\ell-1}\right)u^0_{\ell-1,k}}{\Delta\chi_i+\Delta\chi_{i+1}}\right\} \\
&-\frac{2}{\Delta z_k}\left\{\left(\frac{u^R_{\ell,k+1}-u^R_{\ell,k}}{\Delta z_k+\Delta z_{k+1}} - \frac{w^0_{i+1,n}-w^0_{i,n}}{\Delta\chi_{i+1}+\Delta\chi_i} - \frac{w^R_{i+1,n}-w^R_{i,n}}{\Delta\chi_{i+1}+\Delta\chi_i}\right)\right. \\
&\left.-\left(\frac{u^R_{\ell,k}-u^R_{\ell,k-1}}{\Delta z_k+\Delta z_{k-1}} - \frac{w^0_{i+1,n-1}-w^0_{i,n-1}}{\Delta\chi_{i+1}+\Delta\chi_i} - \frac{w^R_{i+1,n-1}-w^R_{i,n-1}}{\Delta\chi_{i+1}+\Delta\chi_i}\right)\right\}
\end{aligned} \tag{3.28}$$

$$C\left(\overline{\vec{\omega}}\right)^R_{i,k} = \frac{\overline{\eta^R_{i,n}} - \overline{\eta^R_{i,n-1}}}{\Delta z_k} - \left(\frac{\zeta^0_{\ell,k}-\zeta^0_{\ell-1,k}}{\Delta\chi_i} + \frac{\overline{\zeta^R_{\ell,k}} - \overline{\zeta^R_{\ell-1,k}}}{\Delta\chi_i}\right) \tag{3.29}$$

$$\begin{aligned}
C\left(\overline{\vec{\omega}}\right)^R_{i,k} =& \frac{1}{\Delta z_k}\left\{-\frac{1}{\chi_i}w^I_{i,n} - 2\frac{v^R_{i,k+1}-v^R_{i,k}}{\Delta z_k+\Delta z_{k+1}} + \frac{1}{\chi_i}w^I_{i,n-1} + 2\frac{v^R_{i,k}-v^R_{i,k-1}}{\Delta z_k+\Delta z_{k-1}}\right\} \\
&-\frac{1}{\Delta\chi_i}\left\{4\frac{1}{\chi_{i+1}+\chi_i}\frac{\chi_{i+1}v^0_{i+1,k}-\chi_i v^0_{i,k}}{\Delta\chi_i+\Delta\chi_{i+1}} - 4\frac{1}{\chi_{i-1}+\chi_i}\frac{\chi_i v^0_{i,k}-\chi_{i-1}v^0_{i-1,k}}{\Delta\chi_i+\Delta\chi_{i-1}}\right\} \\
&-\frac{1}{\Delta\chi_i}\left\{\frac{4}{\chi_{i+1}+\chi_i}\frac{\chi_{i+1}v^0_{i+1,k}-\chi_i v^0_{i,k}}{\Delta\chi_i+\Delta\chi_{i+1}} + \frac{4}{\chi_{i+1}+\chi_i}\frac{\chi_{i+1}v^R_{i+1,k}-\chi_i v^R_{i,k}}{\Delta\chi_i+\Delta\chi_{i+1}}\right. \\
&\quad+\frac{4R_S}{\chi_{i+1}+\chi_i}\frac{v^0_{i+1,k}-v^0_{i,k}}{\Delta\chi_i+\Delta\chi_{i+1}} - \frac{8R_S}{\left(\chi_{i+1}+\chi_i\right)^2}\frac{\chi_{i+1}v^0_{i+1,k}-\chi_i v^0_{i,k}}{\Delta\chi_{i+1}+\Delta\chi_i} \\
&\quad+2\frac{1}{\chi_{i+1}+\chi_i}u^I_{\ell,k} \\
&\quad-\frac{4}{\chi_{i-1}+\chi_i}\frac{\chi_i v^0_{i,k}-\chi_{i-1}v^0_{i-1,k}}{\Delta\chi_i+\Delta\chi_{i-1}} - \frac{4}{\chi_{i-1}+\chi_i}\frac{\chi_i v^R_{i,k}-\chi_{i-1}v^R_{i-1,k}}{\Delta\chi_i+\Delta\chi_{i-1}} \\
&\quad-\frac{4R_S}{\chi_{i-1}+\chi_i}\frac{v^0_{i,k}-v^0_{i-1,k}}{\Delta\chi_i+\Delta\chi_{i-1}} + \frac{8R_S}{\left(\chi_{i-1}+\chi_i\right)^2}\frac{\chi_i v^0_{i,k}-\chi_{i-1}v^0_{i-1,k}}{\Delta\chi_{i-1}+\Delta\chi_i} \\
&\quad\left.-2\frac{1}{\chi_{i-1}+\chi_i}u^I_{\ell-1,k}\right\}
\end{aligned} \tag{3.30}$$

$$
\begin{aligned}
C\left(\vec{\overline{\omega}}\right)^{R}_{i,n} =& \frac{1}{\chi_i}\frac{\chi_\ell \omega^0_{\ell,n} - \chi_{\ell-1}\omega^0_{\ell-1,n}}{\Delta\chi_i} - \frac{R_S}{\chi_i^2}\frac{\chi_\ell \omega^0_{\ell,n} - \chi_{\ell-1}\omega^0_{\ell-1,n}}{\Delta\chi_i} \\
&+ \frac{R_S}{\chi_i}\frac{\omega^0_{\ell,n} - \omega^0_{\ell-1,n}}{\Delta\chi_i} + \frac{1}{\chi_i}\frac{\chi_\ell \overline{\omega^R_{\ell,n}} - \chi_{\ell-1}\overline{\omega^R_{\ell-1,n}}}{\Delta\chi_i} + \frac{1}{\chi_i}\overline{\eta^I_{i,n}}
\end{aligned}
\tag{3.31}
$$

$$
\begin{aligned}
C\left(\vec{\overline{\omega}}\right)^{R}_{i,n} =& \frac{2}{\chi_i\Delta\chi_i}\left(1-\frac{R_S}{\chi_i}\right)\left[\chi_\ell\left(\frac{u^0_{\ell,k+1}-u^0_{\ell,k}}{\Delta z_k+\Delta z_{k+1}} - \frac{w^0_{i+1,n}-w^0_{i,n}}{\Delta\chi_i+\Delta\chi_{i+1}}\right)\right. \\
&\left. - \chi_{\ell-1}\left(\frac{u^0_{\ell-1,k+1}-u^0_{\ell-1,k}}{\Delta z_k+\Delta z_{k+1}} - \frac{w^0_{i,n}-w^0_{i-1,n}}{\Delta\chi_i+\Delta\chi_{i-1}}\right)\right] \\
&+ 2\frac{R_S}{\chi_i\Delta\chi_i}\left[\left(\frac{u^0_{\ell,k+1}-u^0_{\ell,k}}{\Delta z_k+\Delta z_{k+1}} - \frac{w^0_{i+1,n}-w^0_{i,n}}{\Delta\chi_i+\Delta\chi_{i+1}}\right)\right. \\
&\left. - \left(\frac{u^0_{\ell-1,k+1}-u^0_{\ell-1,k}}{\Delta z_k+\Delta z_{k+1}} - \frac{w^0_{i,n}-w^0_{i-1,n}}{\Delta\chi_i+\Delta\chi_{i-1}}\right)\right] \\
&+ \frac{2}{\chi_i\Delta\chi_i}\left[\chi_\ell\left(\frac{u^R_{\ell,k+1}-u^R_{\ell,k}}{\Delta z_k+\Delta z_{k+1}} - \frac{w^0_{i+1,n}-w^0_{i,n}}{\Delta\chi_{i+1}+\Delta\chi_i} - \frac{w^R_{i+1,n}-w^R_{i,n}}{\Delta\chi_{i+1}+\Delta\chi_i}\right)\right. \\
&\left. - \chi_{\ell-1}\left(\frac{u^R_{\ell-1,k+1}-u^R_{\ell-1,k}}{\Delta z_k+\Delta z_{k+1}} - \frac{w^0_{i,n}-w^0_{i-1,n}}{\Delta\chi_{i-1}+\Delta\chi_i} - \frac{w^R_{i,n}-w^R_{i-1,n}}{\Delta\chi_{i-1}+\Delta\chi_i}\right)\right] \\
&+ \frac{1}{\chi_i}\left\{-\frac{1}{\chi_i}w^R_{i,n} + 2\frac{v^I_{i,k+1}-v^I_{i,k}}{\Delta z_k+\Delta z_{k+1}}\right. \\
&\left. + \frac{2}{\chi_i\Delta\chi_i}\left[\frac{\Delta\chi_{i+1}\left(R_S-\chi_{i+1}\right)w^0_{i+1,n}}{\Delta\chi_i+2\Delta\chi_{i+1}+\Delta\chi_{i+2}} - \frac{\Delta\chi_{i-1}\left(R_S-\chi_{i-1}\right)w^0_{i-1,n}}{\Delta\chi_{i-2}+2\Delta\chi_{i-1}+\Delta\chi_i}\right]\right\}
\end{aligned}
\tag{3.32}
$$

3.5.3 Discrete Viscous Diffusion, Imaginary First Order: $(\nabla \times \nabla \times \vec{u})^I$

$$C\left(\overline{\vec{\omega}}\right)^I_{\ell,k} = \frac{1}{\chi_\ell}\left[\overline{\zeta^R_{\ell,k}} + (R_S - \chi_\ell)\,\frac{\zeta^0_{\ell+1,k} - \zeta^0_{\ell-1,k}}{\Delta\chi_i + \Delta\chi_{i+1}}\right] - \frac{\overline{\omega^I_{\ell,n}} - \overline{\omega^I_{\ell,n-1}}}{\Delta z_k} \tag{3.33}$$

$$\begin{aligned}
C\left(\overline{\vec{\omega}}\right)^I_{\ell,k} = \frac{1}{\chi_\ell}\Bigg[& \frac{4}{\chi_{i+1}+\chi_i}\frac{\chi_{i+1}v^0_{i+1,k} - \chi_i v^0_{i,k}}{\Delta\chi_i + \Delta\chi_{i+1}} + \frac{4}{\chi_{i+1}+\chi_i}\frac{\chi_{i+1}v^R_{i+1,k} - \chi_i v^R_{i,k}}{\Delta\chi_i + \Delta\chi_{i+1}} \\
& + \frac{4R_S}{\chi_{i+1}+\chi_i}\frac{v^0_{i+1,k} - v^0_{i,k}}{\Delta\chi_i + \Delta\chi_{i+1}} - \frac{8R_S}{(\chi_{i+1}+\chi_i)^2}\frac{\chi_{i+1}v^0_{i+1,k} - \chi_i v^0_{i,k}}{\Delta\chi_{i+1} + \Delta\chi_i} \\
& + 2\frac{1}{\chi_{i+1}+\chi_i}\,u^I_{\ell,k} \\
& + 4\frac{R_S - \chi_\ell}{\Delta\chi_i + \Delta\chi_{i+1}} \\
& \left\{\frac{1}{\chi_{i+1}+\chi_{i+2}}\frac{\chi_{i+2}v^0_{i+2,k} - \chi_{i+1}v^0_{i+1,k}}{\Delta\chi_{i+2} + \Delta\chi_{i+1}} - \frac{1}{\chi_{i-1}+\chi_i}\frac{\chi_i v^0_{i,k} - \chi_{i-1}v^0_{i-1,k}}{\Delta\chi_i + \Delta\chi_{i-1}}\right\}\Bigg] \\
& + \frac{2}{\Delta z_k}\left\{\left(\frac{u^I_{\ell,k+1} - u^I_{\ell,k}}{\Delta z_k + \Delta z_{k+1}} - \frac{w^I_{i+1,n} - w^I_{i,n}}{\Delta\chi_{i+1} + \Delta\chi_i}\right)\right. \\
& \left. - \left(\frac{u^I_{\ell,k} - u^I_{\ell,k-1}}{\Delta z_k + \Delta z_{k-1}} - \frac{w^I_{i+1,n-1} - w^I_{i,n-1}}{\Delta\chi_{i+1} + \Delta\chi_i}\right)\right\}
\end{aligned} \tag{3.34}$$

$$C\left(\vec{\omega}\right)_{i,k}^{I}=\frac{\overline{\eta_{i,n}^{I}}-\overline{\eta_{i,n-1}^{I}}}{\Delta z_k}-\frac{\overline{\zeta_{\ell,k}^{I}}-\overline{\zeta_{\ell-1,k}^{I}}}{\Delta\chi_i} \tag{3.35}$$

$$\begin{aligned}
C\left(\vec{\omega}\right)_{i,k}^{I}=&\frac{1}{\Delta z_k}\left\{-\frac{1}{\chi_i}\,w_{i,n}^{R}+2\,\frac{v_{i,k+1}^{I}-v_{i,k}^{I}}{\Delta z_k+\Delta z_{k+1}}\right.\\
&+\frac{2}{\chi_i\Delta\chi_i}\left[\frac{\Delta\chi_{i+1}\left(R_S-\chi_{i+1}\right)w_{i+1,n}^{0}}{\Delta\chi_i+2\Delta\chi_{i+1}+\Delta\chi_{i+2}}-\frac{\Delta\chi_{i-1}\left(R_S-\chi_{i-1}\right)w_{i-1,n}^{0}}{\Delta\chi_{i-2}+2\Delta\chi_{i-1}+\Delta\chi_i}\right]\\
&+\frac{1}{\chi_i}\,w_{i,n-1}^{R}-2\,\frac{v_{i,k}^{I}-v_{i,k-1}^{I}}{\Delta z_k+\Delta z_{k-1}}\\
&\left.-\frac{2}{\chi_i\Delta\chi_i}\left[\frac{\Delta\chi_{i+1}\left(R_S-\chi_{i+1}\right)w_{i+1,n-1}^{0}}{\Delta\chi_i+2\Delta\chi_{i+1}+\Delta\chi_{i+2}}-\frac{\Delta\chi_{i-1}\left(R_S-\chi_{i-1}\right)w_{i-1,n-1}^{0}}{\Delta\chi_{i-2}+2\Delta\chi_{i-1}+\Delta\chi_i}\right]\right\}\\
&+\frac{1}{\Delta\chi_i}\left\{\frac{4}{\chi_{i+1}+\chi_i}\,\frac{\chi_{i+1}v_{i+1,k}^{I}-\chi_i v_{i,k}^{I}}{\Delta\chi_i+\Delta\chi_{i+1}}\right.\\
&+2\frac{1}{\chi_{i+1}+\chi_i}\left[-u_{\ell,k}^{R}+\frac{\left(R_S-\chi_{\ell+1}\right)u_{\ell+1,k}^{0}-\left(R_S-\chi_{\ell-1}\right)u_{\ell-1,k}^{0}}{\Delta\chi_i+\Delta\chi_{i+1}}\right]\\
&-\frac{4}{\chi_{i-1}+\chi_i}\,\frac{\chi_i v_{i,k}^{I}-\chi_{i-1}v_{i-1,k}^{I}}{\Delta\chi_i+\Delta\chi_{i-1}}\\
&\left.-2\frac{1}{\chi_{i-1}+\chi_i}\left[-u_{\ell-1,k}^{R}+\frac{\left(R_S-\chi_{\ell}\right)u_{\ell,k}^{0}-\left(R_S-\chi_{\ell-2}\right)u_{\ell-2,k}^{0}}{\Delta\chi_i+\Delta\chi_{i-1}}\right]\right\}
\end{aligned} \tag{3.36}$$

$$\begin{aligned}
C\left(\vec{\omega}\right)_{i,n}^{I}=&\frac{1}{\chi_i}\,\frac{\chi_\ell\overline{\omega_{\ell,n}^{I}}-\chi_{\ell-1}\overline{\omega_{\ell-1,n}^{I}}}{\Delta\chi_i}\\
&-\frac{1}{\chi_i}\left[\overline{\eta_{i,n}^{R}}+2\left(R_S-\chi_i\right)\frac{\eta_{i+1,n}^{0}-\eta_{i-1,n}^{0}}{\Delta\chi_{i-1}+2\Delta\chi_i+\Delta\chi_{i+1}}\right]
\end{aligned} \tag{3.37}$$

$$\begin{aligned}
C\left(\vec{\omega}\right)_{i,n}^{I}=&-\frac{2}{\chi_i\Delta\chi_i}\left[\chi_\ell\left(\frac{u_{\ell,k+1}^{I}-u_{\ell,k}^{I}}{\Delta z_k+\Delta z_{k+1}}-\frac{w_{i+1,n}^{I}-w_{i,n}^{I}}{\Delta\chi_{i+1}+\Delta\chi_i}\right)\right.\\
&\left.-\chi_{\ell-1}\left(\frac{u_{\ell-1,k+1}^{I}-u_{\ell-1,k}^{I}}{\Delta z_k+\Delta z_{k+1}}-\frac{w_{i,n}^{I}-w_{i-1,n}^{I}}{\Delta\chi_{i-1}+\Delta\chi_i}\right)\right]\\
&-\frac{1}{\chi_i}\left[-\frac{1}{\chi_i}\,w_{i,n}^{I}-2\,\frac{v_{i,k+1}^{R}-v_{i,k}^{R}}{\Delta z_k+\Delta z_{k+1}}\right.\\
&\left.+2\frac{R_S-\chi_i}{\Delta\chi_{i-1}+2\Delta\chi_i+\Delta\chi_{i+1}}\left\{-2\frac{v_{i+1,k+1}^{0}-v_{i+1,k}^{0}}{\Delta z_k+\Delta z_{k+1}}+2\frac{v_{i-1,k+1}^{0}-v_{i-1,k}^{0}}{\Delta z_k+\Delta z_{k+1}}\right\}\right]
\end{aligned} \tag{3.38}$$

3.6 Discrete Convection, $N(\vec{u},\vec{\omega}) = (\nabla \times \vec{u}) \times \vec{u}$

Oud[91] converts the convection terms into a function of the velocity and vorticity terms, A.17, to maintian consistency and take advantage of the discrete operators selected for the mimetic method. The discrete form of the convection terms is given in Equation 3.40 from Oud's work. Oud constructed the averaging of vorticities and velocities to allow conservation of both momentum and energy. The conservation of energy is checked through assuring that $\langle N(\vec{\omega}), \rangle_{FC} = 0$.

A similar convection averaging was performed below for the perturbed coordinate system on the two-dimensional grid. To create this convection averaging operator, Equation 3.41 which describes the face centered inner product space, is set to zero and a discretization for the circumferential momentum average is selected. This allows the calculation of consistent averaging for ζ and η in the radial and axial convection components. Circumferential convection is assumed to be averaged using the combination of Equations 3.43 and 3.44. Recall that while Oud's work used $j + \frac{1}{2}$ for the circumferential velocity location, this work employs a 2-D grid and thus all relevent vorticities and circumferential velocity exist on the j location only.

To apply these convection components to the numerical code, they were next substituted with the perturbed flow variables of velocity and vorticity to prepare for distinguishing the zeroth order and first order components. Simultaneously, the equations were simplified by collection of the velocity terms into their radially and axially averaged values.

$$N(\vec{u}) = \begin{bmatrix} (\omega w - \zeta v)_{\ell,k} \\ (\zeta u - \eta w)_{i,k} \\ (\eta v - \omega u)_{i,n} \end{bmatrix} \tag{3.39}$$

$$N(\vec{u}) = \begin{bmatrix} \frac{1}{2}\left[\omega_{\ell,n-1}\frac{\Delta r_i w_{i,n-1}+\Delta r_{i+1}w_{i+1,n-1}}{\Delta r_i+\Delta r_{i+1}} + \omega_{\ell,n}\frac{\Delta r_i w_{i,n}+\Delta r_{i+1}w_{i+1,n}}{\Delta r_i+\Delta r_{i+1}}\right] \\ \quad -\frac{r_i+r_{i+1}}{8}\left[\zeta_{\ell,j-\frac{1}{2},k}\left(\frac{v_{i,j-\frac{1}{2},k}}{r_i}+\frac{v_{i+1,m-1,k}}{r_{i+1}}\right)+\zeta_{\ell,j+\frac{1}{2},k}\left(\frac{v_{i,j+\frac{1}{2},k}}{r_i}+\frac{v_{i+1,j+\frac{1}{2},k}}{r_{i+1}}\right)\right] \\ \hdashline \frac{1}{2r_i^2\Delta r_i}\left[r_{\ell-1}\frac{r_{i-1}+r_i}{2}\frac{\Delta r_{i-1}+\Delta r_i}{2}\zeta_{\ell-1,j+\frac{1}{2},k}\frac{u_{\ell-1,k}+u_{\ell-1,j+1,k}}{2}\right. \\ \quad \left. +r_{\ell+1}\frac{r_{i+1}+r_i}{2}\frac{\Delta r_{i+1}+\Delta r_i}{2}\zeta_{\ell,j+\frac{1}{2},k}\frac{u_{\ell,k}+u_{\ell,j+1,k}}{2}\right] \\ \quad -\frac{1}{2}\left[\eta_{i,j+\frac{1}{2},n-1}\frac{w_{i,n-1}+w_{i,j+1,n-1}}{2}+\eta_{i,j+\frac{1}{2},n}\frac{w_{i,n}+w_{i,j+1,n}}{2}\right] \\ \hdashline \frac{1}{2}\left[\eta_{i,j-\frac{1}{2},n}\frac{\Delta z_k v_{i,j-\frac{1}{2},k}+\Delta z_{k+1}v_{i,j-\frac{1}{2},k+1}}{\Delta z_k+\Delta z_{k+1}}+\eta_{i,j+\frac{1}{2},n}\frac{\Delta z_k v_{i,j+\frac{1}{2},k}+\Delta z_{k+1}v_{i,j+\frac{1}{2},k+1}}{\Delta z_k+\Delta z_{k+1}}\right] \\ \quad -\frac{1}{2r_i}\left[r_{\ell-1}\omega_{\ell-1,n}\frac{\Delta z_k u_{\ell-1,k}+\Delta z_{k+1}u_{\ell-1,k+1}}{\Delta z_k+\Delta z_{k+1}}+r_\ell\omega_{\ell,n}\frac{\Delta z_k u_{\ell,k}+\Delta z_{k+1}u_{\ell,k+1}}{\Delta z_k+\Delta z_{k+1}}\right] \end{bmatrix} \tag{3.40}$$

$$\begin{aligned}\left\langle\vec{\mathbf{N}},\vec{u}\right\rangle_{FC} \equiv \sum_{(i,k)}\frac{\Delta\chi_i(1-\varepsilon)\Delta\theta\Delta z_k}{2}\Big\{&[\chi_{\ell-1}+\varepsilon(R_S-\chi_{\ell-1})]\,\vec{\mathbf{N}}_{\chi_{\ell-1}}u_{\ell-1,k} \\ &+[\chi_\ell+\varepsilon(R_S-\chi_\ell)]\,\vec{\mathbf{N}}_{\chi_\ell}u_{\ell,k}+2[\chi_i+\varepsilon(R_S-\chi_i)]\,\vec{\mathbf{N}}_{\theta_j}v_{i,k} \\ &+[\chi_i+\varepsilon(R_S-\chi_i)]\left[\vec{\mathbf{N}}_{z_{n-1}}w_{i,n-1}+\vec{\mathbf{N}}_{z_n}w_{i,n}\right]\Big\}\end{aligned} \tag{3.41}$$

$$\vec{\mathbf{N}}_{\chi_{\ell-1}} = \not\ell\,(\omega_{??},\zeta_{??}) \tag{3.42a}$$

$$\vec{\mathbf{N}}_{\chi_\ell} = \not\ell\,(\omega_{??},\zeta_{??}) \tag{3.42b}$$

$$\vec{\mathbf{N}}_{\theta_j} = \not\ell\left(\eta_{i,m,n-1},\eta_{i,m,n},\zeta_{\ell-1,m,k},\zeta_{\ell,m,k}\right) \tag{3.42c}$$

$$\vec{\mathbf{N}}_{z_{n-1}} = \not\ell\,(\eta_{??},\omega_{??}) \tag{3.42d}$$

$$\vec{\mathbf{N}}_{z_n} = \not\ell\,(\eta_{??},\omega_{??}) \tag{3.42e}$$

$$\vec{\mathbf{N}}^{\,\eta}_{\mathbf{i},\mathbf{k}_\theta}(\eta_{i,n},\eta_{i,n-1}) = -\frac{1}{2}\left[\eta_{i,n-1}w_{i,n-1}+\eta_{i,n}w_{i,n}\right] \tag{3.43}$$

$$\begin{aligned}&\vec{\mathbf{N}}^{\,\zeta}_{\mathbf{i},\mathbf{k}_\theta}(\zeta_{\ell-1,k},\zeta_{\ell,k}) = \\ &\frac{1}{2\Delta\chi_i}\left(\frac{1}{\chi_i}-\varepsilon\frac{(R_S-\chi_i)}{\chi_i^2}\right)^2 \\ &\Big\{[\chi_{\ell-1}+\varepsilon(R_S-\chi_{\ell-1})]\,\frac{\chi_i+\chi_{i-1}+\varepsilon(2R_S-\chi_i-\chi_{i+1})}{2}\,\frac{\Delta\chi_{i-1}+\Delta\chi_i}{2}\zeta_{\ell-1,k}u_{\ell-1,k} \\ &+[\chi_\ell+\varepsilon(R_S-\chi_\ell)]\,\frac{\chi_i+\chi_{i+1}+\varepsilon(2R_S-\chi_i-\chi_{i+1})}{2}\,\frac{\Delta\chi_{i+1}+\Delta\chi_i}{2}\zeta_{\ell,k}u_{\ell,k}\Big\}\end{aligned} \tag{3.44}$$

3.6.1 Gathering $\eta_{i,n}$ terms for circumferential/axial convection

Gather $\eta_{i,n}$ terms from cells (i,k) and (i,k+1). Equation 3.46 provides two relationships to define the circumferential and axial convection components related to η. Equation 3.46 has a factor of two on the $\vec{\mathbf{N}}_\theta$ term to account for the fact that it is one number being applied at the + and - circumferential faces of the cell.

$$\begin{aligned}\left\langle \vec{\mathbf{N}}, \vec{u} \right\rangle_{FC} |_{\eta_{i,n}} = 0 = \\ \left.\begin{aligned} &+ \frac{\Delta\chi_i (1-\varepsilon)\Delta\theta\Delta z_k}{2} \left\{ 2\left[\chi_i + \varepsilon(R_S - \chi_i)\right] v_{i,k} \vec{\mathbf{N}}_{\theta_j} \left(\eta_{i,m,n-1}, \eta_{i,m,n}\right) \right. \\ &\left. + \left[\chi_i + \varepsilon(R_S - \chi_i)\right] \left[\vec{\mathbf{N}}_{z_{n-1}} w_{i,n-1} + \vec{\mathbf{N}}_{z_n} w_{i,n} \right] \right\} \end{aligned} \right\} (i,k) \\ \left.\begin{aligned} &+ \frac{\Delta\chi_i (1-\varepsilon)\Delta\theta\Delta z_{k+1}}{2} \left\{ 2\left[\chi_i + \varepsilon(R_S - \chi_i)\right] v_{i,k} \vec{\mathbf{N}}_{\theta_j} \left(\eta_{i,m,n}, \eta_{i,m,n+1}\right) \right. \\ &\left. + \left[\chi_i + \varepsilon(R_S - \chi_i)\right] \left[\vec{\mathbf{N}}_{z_n} w_{i,n} + \vec{\mathbf{N}}_{z_{n+1}} w_{i,n+1} \right] \right\} \end{aligned} \right\} (i,k+1)\end{aligned} \tag{3.45}$$

$$\begin{aligned}\Delta z_{k+1}\left[\vec{\mathbf{N}}_{z_n} w_{i,n} + \vec{\mathbf{N}}_{z_{n+1}} w_{i,n+1}\right] + \Delta z_k \left[\vec{\mathbf{N}}_{z_{n-1}} w_{i,n-1} + \vec{\mathbf{N}}_{z_n} w_{i,n}\right] = &- 2\Delta z_k v_{i,k} \vec{\mathbf{N}}_{\theta_j}\left(\eta_{i,m,n-1}, \eta_{i,m,n}\right) \\ &- 2\Delta z_{k+1} v_{i,k} \vec{\mathbf{N}}_{\theta_j}\left(\eta_{i,m,n}, \eta_{i,m,n+1}\right)\end{aligned} \tag{3.46}$$

At this point, the assumed circumferential convection averaging components are substituted in and it becomes clear that the axial convection component averaging can be modeled on Oud's work, where $j+\frac{1}{2}$ and $j-\frac{1}{2}$ are the same location, and thus have the same values for each flow variable at those two locations. Note that if instead, a pseudo three dimensional grid was used where velocity was face centered at $+\frac{\Delta\theta}{2}$ from the cell center, the averaging depends on some assumed $\Delta\theta$ value which can be arbitrarily chosen as long as it obeys the $\Delta << 1$ rule of finite difference methods. An infinitely thin element corresponds to selecting the limit of that circumferential distance going to zero.

$$\vec{\mathbf{N}}_{z_n} = \eta_{i,n} \frac{\Delta z_k v_{i,j-\frac{1}{2},k} + \Delta z_{k+1} v_{i,j-\frac{1}{2},k+1}}{\Delta z_k + \Delta z_{k+1}} \tag{3.47}$$

$$(\Delta z_{k+1} + \Delta z_k)\,\eta_{i,n} \frac{\Delta z_k v_{i,j-\frac{1}{2},k} + \Delta z_{k+1} v_{i,j-\frac{1}{2},k+1}}{\Delta z_k + \Delta z_{k+1}} w_{i,n} = \left(\Delta z_k v_{i,k} + \Delta z_{k+1} v_{i,k}\right) \eta_{i,n} w_{i,n} \tag{3.48}$$

$$\left(\vec{\mathbf{N}}_z\right)^\eta = \left(\eta^0_{i,n} + \varepsilon\eta^1_{i,n}\right)\left(\frac{\Delta z_k v^0_{i,k} + \Delta z_{k+1} v^0_{i,k+1}}{\Delta z_k + \Delta z_{k+1}} + \varepsilon \frac{\Delta z_k v^1_{i,k} + \Delta z_{k+1} v^1_{i,k+1}}{\Delta z_k + \Delta z_{k+1}}\right) \tag{3.49}$$

3.6.2 Gathering $\zeta_{\ell,k}$ terms for radial/circumferential convection

Gather $\zeta_{\ell,k}$ terms from cells (i,k) and (i+1,k). A step was skipped to assume a version of Oud's averaging and the inner product of the convection components with velocity was confirmed to be zero.

$$\begin{aligned}\left\langle \vec{\mathbf{C}}, \vec{\overline{u}} \right\rangle_{FC} |_{\zeta_{\ell,k}} = \\ + \Delta\chi_i \Big\{ \left[\chi_{\ell-1} + \varepsilon\left(R_S - \chi_{\ell-1}\right)\right] \vec{\mathbf{N}}_{\chi_{\ell-1}} u_{\ell-1,k} \\ + \left[\chi_\ell + \varepsilon\left(R_S - \chi_\ell\right)\right] \vec{\mathbf{N}}_{\chi_\ell} u_{\ell,k} + 2\left[\chi_i + \varepsilon\left(R_S - \chi_i\right)\right] v_{i,k} \vec{\mathbf{N}}_{\theta_j}\left(\zeta_{\ell-1,m,k}, \zeta_{\ell,m,k}\right) \Big\} (i,k) \\ + \Delta\chi_{i+1} \Big\{ \left[\chi_\ell + \varepsilon\left(R_S - \chi_\ell\right)\right] \vec{\mathbf{N}}_{\chi_\ell} u_{\ell,k} \\ + \left[\chi_{\ell+1} + \varepsilon\left(R_S - \chi_{\ell+1}\right)\right] \vec{\mathbf{N}}_{\chi_{\ell+1}} u_{\ell+1,k} + 2\left[\chi_{i+1} + \varepsilon\left(R_S - \chi_{i+1}\right)\right] v_{i+1,k} \vec{\mathbf{N}}_{\theta_j}\left(\zeta_{\ell,m,k}, \zeta_{\ell+1,m,k}\right) \Big\} (i+1,k)\end{aligned} \tag{3.50}$$

$$\begin{aligned}\vec{\mathbf{N}}_{\chi_\ell} = -\frac{\chi_i + \chi_{i+1} + \varepsilon\left(2R_S - \chi_i - \chi_{i+1}\right)}{4} \zeta_{\ell,k} \Bigg[\\ \left(\frac{1}{\chi_i} - \varepsilon\frac{\left(R_S - \chi_i\right)}{\chi_i^2}\right) v_{i,k} + \left(\frac{1}{\chi_{i+1}} - \varepsilon\frac{\left(R_S - \chi_{i+1}\right)}{\chi_{i+1}^2}\right) v_{i+1,k} \Bigg]\end{aligned} \tag{3.51}$$

$$\begin{aligned}\frac{\chi_i + \chi_{i+1} + \varepsilon\left(2R_S - \chi_i - \chi_{i+1}\right)}{4} \left[\left(\frac{1}{\chi_i} - \varepsilon\frac{\left(R_S - \chi_i\right)}{\chi_i^2}\right) v_{i,k} + \left(\frac{1}{\chi_{i+1}} - \varepsilon\frac{\left(R_S - \chi_{i+1}\right)}{\chi_{i+1}^2}\right) v_{i+1,k}\right] = \\ v_{i,k}\left(\frac{1}{\chi_i} - \varepsilon\frac{\left(R_S - \chi_i\right)}{\chi_i^2}\right) \frac{\chi_i + \chi_{i+1} + \varepsilon\left(2R_S - \chi_i - \chi_{i+1}\right)}{2} \frac{1}{2} \\ + v_{i+1,k}\left(\frac{1}{\chi_{i+1}} - \varepsilon\frac{\left(R_S - \chi_{i+1}\right)}{\chi_{i+1}^2}\right) \frac{\chi_i + \chi_{i+1} + \varepsilon\left(2R_S - \chi_i - \chi_{i+1}\right)}{2} \frac{1}{2}\end{aligned} \tag{3.52}$$

$$\begin{aligned}\vec{\mathbf{N}}_{\mathbf{i}_\chi}^{\zeta} = -\frac{\chi_i + \chi_{i+1} + \varepsilon\left(2R_S - \chi_i - \chi_{i+1}\right)}{4} \left[\zeta_{\ell,k}^0 + \varepsilon\zeta_{\ell,k}^1\right] \\ \left[\left(\frac{1}{\chi_i} - \varepsilon\frac{\left(R_S - \chi_i\right)}{\chi_i^2}\right)\left[v_{i,k}^0 + \varepsilon v_{i,k}^1\right] \right. \\ \left. + \left(\frac{1}{\chi_{i+1}} - \varepsilon\frac{\left(R_S - \chi_{i+1}\right)}{\chi_{i+1}^2}\right)\left[v_{i+1,k}^0 + \varepsilon v_{i+1,k}^1\right]\right]\end{aligned} \tag{3.53}$$

3.6.3 The Convection Averaging Operator

$$N(\vec{u}) = \begin{bmatrix} \frac{1}{2}\left[\omega_{\ell,n-1}\frac{\Delta\chi_i w_{i,n-1} + \Delta\chi_{i+1} w_{i+1,n-1}}{\Delta\chi_i + \Delta\chi_{i+1}} + \omega_{\ell,n}\frac{\Delta\chi_i w_{i,n} + \Delta\chi_{i+1} w_{i+1,n}}{\Delta\chi_i + \Delta\chi_{i+1}}\right] \\ \quad + \left(\vec{\mathbf{N}}_\chi\right)^{\zeta}_{i,k} \\ \hdashline \vec{\mathbf{N}}^{\ \zeta}_{\mathbf{i,k}\theta}\left(\zeta_{\ell-1,k}, \zeta_{\ell,k}\right) + \vec{\mathbf{N}}^{\ \eta}_{\mathbf{i,k}\theta}\left(\eta_{i,n}, \eta_{i,n-1}\right) \\ \hdashline \left(\vec{\mathbf{N}}_z\right)^{\eta}_{i,k} \\ -\frac{1}{2}\left(\frac{1}{\chi_i} - \varepsilon\frac{(R_S - \chi_i)}{\chi_i^2}\right)\left[\left[\chi_{\ell-1} + \varepsilon\left(R_S - \chi_{\ell-1}\right)\right]\omega_{\ell-1,n}\frac{\Delta z_k u_{\ell-1,k} + \Delta z_{k+1} u_{\ell-1,k+1}}{\Delta z_k + \Delta z_{k+1}}\right. \\ \quad \left. + \left[\chi_\ell + \varepsilon\left(R_S - \chi_\ell\right)\right]\omega_{\ell,n}\frac{\Delta z_k u_{\ell,k} + \Delta z_{k+1} u_{\ell,k+1}}{\Delta z_k + \Delta z_{k+1}}\right] \end{bmatrix} \tag{3.54}$$

$$\begin{aligned} N_\chi(\vec{u}) =& \frac{1}{2}\left[\omega^0_{\ell,n-1}\frac{\Delta\chi_i w^0_{i,n-1} + \Delta\chi_{i+1} w^0_{i+1,n-1}}{\Delta\chi_i + \Delta\chi_{i+1}} + \omega^0_{\ell,n}\frac{\Delta\chi_i w^0_{i,n} + \Delta\chi_{i+1} w^0_{i+1,n}}{\Delta\chi_i + \Delta\chi_{i+1}}\right] \\ & \frac{1}{2}\varepsilon\left[\omega^0_{\ell,n-1}\frac{\Delta\chi_i w^1_{i,n-1} + \Delta\chi_{i+1} w^1_{i+1,n-1}}{\Delta\chi_i + \Delta\chi_{i+1}} + \omega^1_{\ell,n-1}\frac{\Delta\chi_i w^0_{i,n-1} + \Delta\chi_{i+1} w^0_{i+1,n-1}}{\Delta\chi_i + \Delta\chi_{i+1}}\right. \\ & \qquad \left. + \omega^0_{\ell,n}\frac{\Delta\chi_i w^1_{i,n} + \Delta\chi_{i+1} w^1_{i+1,n}}{\Delta\chi_i + \Delta\chi_{i+1}} + \omega^1_{\ell,n-1}\frac{\Delta\chi_i w^0_{i,n} + \Delta\chi_{i+1} w^0_{i+1,n}}{\Delta\chi_i + \Delta\chi_{i+1}}\right] \\ & -\frac{\chi_i + \chi_{i+1}}{4}\zeta^0_{\ell,k}\left[\frac{v^0_{i,k}}{\chi_i} + \frac{v^0_{i+1,k}}{\chi_{i+1}}\right] \\ & -\varepsilon\frac{\chi_i + \chi_{i+1}}{4}\left[\zeta^0_{\ell,k}\left(\frac{v^1_{i,k}}{\chi_i} + \frac{v^1_{i+1,k}}{\chi_{i+1}}\right) + \zeta^1_{\ell,k}\left(\frac{v^0_{i,k}}{\chi_i} + \frac{v^0_{i+1,k}}{\chi_{i+1}}\right)\right] \\ & -\frac{\varepsilon\left(2R_S - \chi_i - \chi_{i+1}\right)}{4}\zeta^0_{\ell,k}\left[\frac{v^0_{i,k}}{\chi_i} + \frac{v^0_{i+1,k}}{\chi_{i+1}}\right] \\ & +\frac{\chi_i + \chi_{i+1}}{4}\zeta^0_{\ell,k}\left[\varepsilon\frac{(R_S - \chi_i)}{\chi_i^2}v^0_{i,k} + \varepsilon\frac{(R_S - \chi_{i+1})}{\chi^2_{i+1}}v^0_{i+1,k}\right] \end{aligned} \tag{3.55}$$

$$
\begin{aligned}
N_\theta(\vec{u}) =& \frac{1}{2\Delta\chi_i}\frac{1}{\chi_i^2}\left(\chi_{\ell-1}\frac{\chi_i+\chi_{i-1}}{2}\frac{\Delta\chi_{i-1}+\Delta\chi_i}{2}\left\{\zeta^0_{\ell-1,k}u^0_{\ell-1,k}+\varepsilon\left[\zeta^0_{\ell-1,k}u^1_{\ell-1,k}+\zeta^1_{\ell-1,k}u^0_{\ell-1,k}\right]\right\}\right.\\
&\left.+\chi_\ell\frac{\chi_i+\chi_{i+1}}{2}\frac{\Delta\chi_{i+1}+\Delta\chi_i}{2}\left\{\zeta^0_{\ell,k}u^0_{\ell,k}+\varepsilon\left[\zeta^0_{\ell,k}u^1_{\ell,k}+\zeta^1_{\ell,k}u^0_{\ell,k}\right]\right\}\right)\\
&-\frac{1}{2\Delta\chi_i}2\varepsilon\frac{(R_S-\chi_i)}{\chi_i^3}\left(\chi_{\ell-1}\frac{\chi_i+\chi_{i-1}}{2}\frac{\Delta\chi_{i-1}+\Delta\chi_i}{2}\zeta^0_{\ell-1,k}u^0_{\ell-1,k}\right.\\
&\left.+\chi_\ell\frac{\chi_i+\chi_{i+1}}{2}\frac{\Delta\chi_{i+1}+\Delta\chi_i}{2}\zeta^0_{\ell,k}u^0_{\ell,k}\right)\\
&+\frac{1}{2\Delta\chi_i}\frac{1}{\chi_i^2}\left(\varepsilon(R_S-\chi_{\ell-1})\frac{\chi_i+\chi_{i-1}}{2}\frac{\Delta\chi_{i-1}+\Delta\chi_i}{2}\zeta^0_{\ell-1,k}u^0_{\ell-1,k}\right.\\
&\left.+\varepsilon(R_S-\chi_\ell)\frac{\chi_i+\chi_{i+1}}{2}\frac{\Delta\chi_{i+1}+\Delta\chi_i}{2}\zeta^0_{\ell,k}u^0_{\ell,k}\right)\\
&+\frac{1}{2\Delta\chi_i}\frac{1}{\chi_i^2}\left(\chi_{\ell-1}\frac{\varepsilon(2R_S-\chi_i-\chi_{i+1})}{2}\frac{\Delta\chi_{i-1}+\Delta\chi_i}{2}\zeta^0_{\ell-1,k}u^0_{\ell-1,k}\right.\\
&\left.+\chi_\ell\frac{\varepsilon(2R_S-\chi_i-\chi_{i+1})}{2}\frac{\Delta\chi_{i+1}+\Delta\chi_i}{2}\zeta^0_{\ell,k}u^0_{\ell,k}\right)\\
&-\frac{1}{2}\left\{\eta^0_{i,n-1}w^0_{i,n-1}+\varepsilon\left[\eta^0_{i,n-1}w^1_{i,n-1}+\eta^1_{i,n-1}w^0_{i,n-1}\right]\right.\\
&\left.+\eta^0_{i,n}w^0_{i,n}+\varepsilon\left[\eta^0_{i,n}w^1_{i,n}+\eta^1_{i,n}w^0_{i,n}\right]\right\}
\end{aligned}
\tag{3.56}
$$

$$
\begin{aligned}
N_z(\vec{u}) =& \eta^0_{i,n}\frac{\Delta z_k v^0_{i,k}+\Delta z_{k+1}v^0_{i,k+1}}{\Delta z_k+\Delta z_{k+1}}\\
&+\varepsilon\left(\eta^0_{i,n}\frac{\Delta z_k v^1_{i,k}+\Delta z_{k+1}v^1_{i,k+1}}{\Delta z_k+\Delta z_{k+1}}+\eta^1_{i,n}\frac{\Delta z_k v^0_{i,k}+\Delta z_{k+1}v^0_{i,k+1}}{\Delta z_k+\Delta z_{k+1}}\right)\\
&-\frac{1}{2}\frac{1}{\chi_i}\left[\chi_{\ell-1}\omega^0_{\ell-1,n}\frac{\Delta z_k u^0_{\ell-1,k}+\Delta z_{k+1}u^0_{\ell-1,k+1}}{\Delta z_k+\Delta z_{k+1}}+\chi_\ell\omega^0_{\ell,n}\frac{\Delta z_k u^0_{\ell,k}+\Delta z_{k+1}u^0_{\ell,k+1}}{\Delta z_k+\Delta z_{k+1}}\right]\\
&-\frac{1}{2}\frac{\varepsilon}{\chi_i}\left[\chi_{\ell-1}\omega^0_{\ell-1,n}\frac{\Delta z_k u^1_{\ell-1,k}+\Delta z_{k+1}u^1_{\ell-1,k+1}}{\Delta z_k+\Delta z_{k+1}}+\chi_\ell\omega^0_{\ell,n}\frac{\Delta z_k u^1_{\ell,k}+\Delta z_{k+1}u^1_{\ell,k+1}}{\Delta z_k+\Delta z_{k+1}}\right]\\
&-\frac{1}{2}\frac{\varepsilon}{\chi_i}\left[\chi_{\ell-1}\omega^1_{\ell-1,n}\frac{\Delta z_k u^0_{\ell-1,k}+\Delta z_{k+1}u^0_{\ell-1,k+1}}{\Delta z_k+\Delta z_{k+1}}+\chi_\ell\omega^1_{\ell,n}\frac{\Delta z_k u^0_{\ell,k}+\Delta z_{k+1}u^0_{\ell,k+1}}{\Delta z_k+\Delta z_{k+1}}\right]\\
&+\frac{1}{2}\varepsilon\frac{(R_S-\chi_i)}{\chi_i^2}\left[\chi_{\ell-1}\omega^0_{\ell-1,n}\frac{\Delta z_k u^0_{\ell-1,k}+\Delta z_{k+1}u^0_{\ell-1,k+1}}{\Delta z_k+\Delta z_{k+1}}+\chi_\ell\omega^0_{\ell,n}\frac{\Delta z_k u^0_{\ell,k}+\Delta z_{k+1}u^0_{\ell,k+1}}{\Delta z_k+\Delta z_{k+1}}\right]\\
&-\frac{1}{2}\frac{\varepsilon}{\chi_i}\left[(R_S-\chi_{\ell-1})\omega^0_{\ell-1,n}\frac{\Delta z_k u^0_{\ell-1,k}+\Delta z_{k+1}u^0_{\ell-1,k+1}}{\Delta z_k+\Delta z_{k+1}}+(R_S-\chi_\ell)\omega^0_{\ell,n}\frac{\Delta z_k u^0_{\ell,k}+\Delta z_{k+1}u^0_{\ell,k+1}}{\Delta z_k+\Delta z_{k+1}}\right]
\end{aligned}
\tag{3.57}
$$

3.6.4 Discrete Convection, Zeroth Order: $N^0(\vec{u},\vec{\omega}) = (\nabla\times\vec{u})\times\vec{u}^0$

$$
\begin{aligned}
N^0_\chi(\vec{u}) =& \frac{1}{2}\left[\omega^0_{\ell,n-1}\frac{\Delta\chi_i w^0_{i,n-1}+\Delta\chi_{i+1}w^0_{i+1,n-1}}{\Delta\chi_i+\Delta\chi_{i+1}}+\omega^0_{\ell,n}\frac{\Delta\chi_i w^0_{i,n}+\Delta\chi_{i+1}w^0_{i+1,n}}{\Delta\chi_i+\Delta\chi_{i+1}}\right]\\
&-\frac{\chi_i+\chi_{i+1}}{4}\zeta^0_{\ell,k}\left[\frac{v^0_{i,k}}{\chi_i}+\frac{v^0_{i+1,k}}{\chi_{i+1}}\right]
\end{aligned}
\tag{3.58}
$$

$$
\begin{aligned}
N_\theta^0(\vec{u}) =& \frac{1}{2\Delta\chi_i}\frac{1}{\chi_i^2}\left[\chi_{\ell-1}\frac{\chi_i+\chi_{i-1}}{2}\frac{\Delta\chi_{i-1}+\Delta\chi_i}{2}\zeta^0_{\ell-1,k}u^0_{\ell-1,k} + \chi_\ell\frac{\chi_i+\chi_{i+1}}{2}\frac{\Delta\chi_{i+1}+\Delta\chi_i}{2}\zeta^0_{\ell,k}u^0_{\ell,k}\right] \\
&- \frac{1}{2}\left[\eta^0_{i,n-1}w^0_{i,n-1} + \eta^0_{i,n}w^0_{i,n}\right]
\end{aligned}
\tag{3.59}
$$

$$
\begin{aligned}
N_z^0(\vec{u}) =& \eta^0_{i,n}\frac{\Delta z_k v^0_{i,k} + \Delta z_{k+1}v^0_{i,k+1}}{\Delta z_k + \Delta z_{k+1}} \\
&- \frac{1}{2}\frac{1}{\chi_i}\left[\chi_{\ell-1}\omega^0_{\ell-1,n}\frac{\Delta z_k u^0_{\ell-1,k} + \Delta z_{k+1}u^0_{\ell-1,k+1}}{\Delta z_k + \Delta z_{k+1}} + \chi_\ell\omega^0_{\ell,n}\frac{\Delta z_k u^0_{\ell,k} + \Delta z_{k+1}u^0_{\ell,k+1}}{\Delta z_k + \Delta z_{k+1}}\right]
\end{aligned}
\tag{3.60}
$$

$$
N^0(\vec{u}) = \left[\begin{array}{c}
\left(\dfrac{u^0_{\ell,k}-u^0_{\ell,k-1}}{\Delta z_k+\Delta z_{k-1}} - \dfrac{w^0_{i+1,n-1}-w^0_{i,n-1}}{\Delta\chi_{i+1}+\Delta\chi_i}\right)\overline{w^0_{i,n-1}}^{\chi} \\
+\left(\dfrac{u^0_{\ell,k+1}-u^0_{\ell,k}}{\Delta z_k+\Delta z_{k+1}} - \dfrac{w^0_{i+1,n}-w^0_{i,n}}{\Delta\chi_{i+1}+\Delta\chi_i}\right)\overline{w^0_{i,n}}^{\chi} \\
-\dfrac{\chi_{i+1}v^0_{i+1,k}-\chi_i v^0_{i,k}}{\Delta\chi_i+\Delta\chi_{i+1}}\overline{v^0_{i,k}}^{\chi} \\
\hdashline
\dfrac{1}{2\Delta\chi_i}\dfrac{1}{\chi_i^2}\left[\chi_{\ell-1}\left(\chi_i v^0_{i1,k}-\chi_{i-1}v^0_{i-1,k}\right)u^0_{\ell-1,k}\right. \\
\left.+\chi_\ell\left(\chi_{i+1}v^0_{i+1,k}-\chi_i v^0_{i,k}\right)u^0_{\ell,k}\right] \\
+\dfrac{v^0_{i,k}-v^0_{i,k-1}}{\Delta z_k+\Delta z_{k-1}}w^0_{i,n-1} + \dfrac{v^0_{i,k+1}-v^0_{i,k}}{\Delta z_k+\Delta z_{k+1}}w^0_{i,n} \\
\hdashline
-2\dfrac{v^0_{i,k+1}-v^0_{i,k}}{\Delta z_k+\Delta z_{k+1}}\overline{v^0_{i,k}}^{z} \\
-\dfrac{1}{\chi_i}\left\{\chi_{\ell-1}\left(\dfrac{u^0_{\ell-1,k+1}-u^0_{\ell-1,k}}{\Delta z_k+\Delta z_{k+1}} - \dfrac{w^0_{i,n}-w^0_{i-1,n}}{\Delta\chi_{i-1}+\Delta\chi_i}\right)\overline{u^0_{\ell-1,k}}^{z}\right. \\
\left.+\chi_\ell\left(\dfrac{u^0_{\ell,k+1}-u^0_{\ell,k}}{\Delta z_k+\Delta z_{k+1}} - \dfrac{w^0_{i+1,n}-w^0_{i,n}}{\Delta\chi_{i+1}+\Delta\chi_i}\right)\overline{u^0_{\ell,k}}^{z}\right\}
\end{array}\right]
\tag{3.61}
$$

3.6.5 Discrete Convection, First Order: $N^1(\vec{u},\vec{\omega}) = (\nabla \times \vec{u}) \times \vec{u}$

$$
\begin{aligned}
N^1_\chi(\vec{u}) =& \frac{1}{2}\left[\omega^0_{\ell,n-1}\frac{\Delta\chi_i w^1_{i,n-1}+\Delta\chi_{i+1}w^1_{i+1,n-1}}{\Delta\chi_i+\Delta\chi_{i+1}}+\omega^1_{\ell,n-1}\frac{\Delta\chi_i w^0_{i,n-1}+\Delta\chi_{i+1}w^0_{i+1,n-1}}{\Delta\chi_i+\Delta\chi_{i+1}}\right.\\
&\left.+\omega^0_{\ell,n}\frac{\Delta\chi_i w^1_{i,n}+\Delta\chi_{i+1}w^1_{i+1,n}}{\Delta\chi_i+\Delta\chi_{i+1}}+\omega^1_{\ell,n-1}\frac{\Delta\chi_i w^0_{i,n}+\Delta\chi_{i+1}w^0_{i+1,n}}{\Delta\chi_i+\Delta\chi_{i+1}}\right]\\
&-\frac{\chi_i+\chi_{i+1}}{4}\left[\zeta^0_{\ell,k}\left(\frac{v^1_{i,k}}{\chi_i}+\frac{v^1_{i+1,k}}{\chi_{i+1}}\right)+\zeta^1_{\ell,k}\left(\frac{v^0_{i,k}}{\chi_i}+\frac{v^0_{i+1,k}}{\chi_{i+1}}\right)\right]\\
&-\frac{(2R_S-\chi_i-\chi_{i+1})}{4}\zeta^0_{\ell,k}\left[\frac{v^0_{i,k}}{\chi_i}+\frac{v^0_{i+1,k}}{\chi_{i+1}}\right]\\
&+\frac{\chi_i+\chi_{i+1}}{4}\zeta^0_{\ell,k}\left[\frac{(R_S-\chi_i)}{\chi_i^2}v^0_{i,k}+\frac{(R_S-\chi_{i+1})}{\chi^2_{i+1}}v^0_{i+1,k}\right]
\end{aligned}
\tag{3.62}
$$

$$
\begin{aligned}
N^1_\chi(\vec{u}) =& \frac{1}{2}\left[\omega^0_{\ell,n-1}\frac{\Delta\chi_i w^1_{i,n-1}+\Delta\chi_{i+1}w^1_{i+1,n-1}}{\Delta\chi_i+\Delta\chi_{i+1}}+\omega^1_{\ell,n-1}\frac{\Delta\chi_i w^0_{i,n-1}+\Delta\chi_{i+1}w^0_{i+1,n-1}}{\Delta\chi_i+\Delta\chi_{i+1}}\right.\\
&\left.+\omega^0_{\ell,n}\frac{\Delta\chi_i w^1_{i,n}+\Delta\chi_{i+1}w^1_{i+1,n}}{\Delta\chi_i+\Delta\chi_{i+1}}+\omega^1_{\ell,n-1}\frac{\Delta\chi_i w^0_{i,n}+\Delta\chi_{i+1}w^0_{i+1,n}}{\Delta\chi_i+\Delta\chi_{i+1}}\right]\\
&-\frac{\chi_i+\chi_{i+1}}{4}\left[\zeta^0_{\ell,k}\left(\frac{v^1_{i,k}}{\chi_i}+\frac{v^1_{i+1,k}}{\chi_{i+1}}\right)+\zeta^1_{\ell,k}\left(\frac{v^0_{i,k}}{\chi_i}+\frac{v^0_{i+1,k}}{\chi_{i+1}}\right)\right]\\
&-\frac{R_S}{2}\zeta^0_{\ell,k}\left[\frac{v^0_{i,k}}{\chi_i}+\frac{v^0_{i+1,k}}{\chi_{i+1}}\right]+\frac{\chi_i+\chi_{i+1}}{4}\zeta^0_{\ell,k}\left[\cancel{\frac{v^0_{i,k}}{\chi_i}}+\cancel{\frac{v^0_{i+1,k}}{\chi_{i+1}}}\right]\\
&+\frac{\chi_i+\chi_{i+1}}{4}\zeta^0_{\ell,k}\left[\left(\frac{R_S}{\chi_i^2}-\cancel{\frac{1}{\chi_i}}\right)v^0_{i,k}+\left(\frac{R_S}{\chi^2_{i+1}}-\cancel{\frac{1}{\chi_{i+1}}}\right)v^0_{i+1,k}\right]
\end{aligned}
\tag{3.63}
$$

$$
\begin{aligned}
N^1_\chi(\vec{u}) =& \frac{1}{2}\left[\omega^0_{\ell,n-1}\frac{\Delta\chi_i w^1_{i,n-1}+\Delta\chi_{i+1}w^1_{i+1,n-1}}{\Delta\chi_i+\Delta\chi_{i+1}}+\omega^1_{\ell,n-1}\frac{\Delta\chi_i w^0_{i,n-1}+\Delta\chi_{i+1}w^0_{i+1,n-1}}{\Delta\chi_i+\Delta\chi_{i+1}}\right.\\
&\left.+\omega^0_{\ell,n}\frac{\Delta\chi_i w^1_{i,n}+\Delta\chi_{i+1}w^1_{i+1,n}}{\Delta\chi_i+\Delta\chi_{i+1}}+\omega^1_{\ell,n-1}\frac{\Delta\chi_i w^0_{i,n}+\Delta\chi_{i+1}w^0_{i+1,n}}{\Delta\chi_i+\Delta\chi_{i+1}}\right]\\
&-\frac{\chi_i+\chi_{i+1}}{4}\left[\zeta^0_{\ell,k}\left(\frac{v^1_{i,k}}{\chi_i}+\frac{v^1_{i+1,k}}{\chi_{i+1}}\right)+\zeta^1_{\ell,k}\left(\frac{v^0_{i,k}}{\chi_i}+\frac{v^0_{i+1,k}}{\chi_{i+1}}\right)\right]\\
&-\frac{R_S}{2}\zeta^0_{\ell,k}\left[\frac{v^0_{i,k}}{\chi_i}+\frac{v^0_{i+1,k}}{\chi_{i+1}}\right]+R_S\frac{\chi_i+\chi_{i+1}}{4}\zeta^0_{\ell,k}\left[\frac{1}{\chi_i^2}v^0_{i,k}+\frac{1}{\chi^2_{i+1}}v^0_{i+1,k}\right]
\end{aligned}
\tag{3.64}
$$

$$
\begin{aligned}
N^1_\theta(\vec{u}) =& \frac{1}{2\Delta\chi_i}\frac{1}{\chi_i^2}\left(\chi_{\ell-1}\frac{\chi_i+\chi_{i-1}}{2}\frac{\Delta\chi_{i-1}+\Delta\chi_i}{2}\left\{\zeta^0_{\ell-1,k}u^1_{\ell-1,k}+\zeta^1_{\ell-1,k}u^0_{\ell-1,k}\right\}\right.\\
&\left.+\chi_\ell\frac{\chi_i+\chi_{i+1}}{2}\frac{\Delta\chi_{i+1}+\Delta\chi_i}{2}\left\{\zeta^0_{\ell,k}u^1_{\ell,k}+\zeta^1_{\ell,k}u^0_{\ell,k}\right\}\right)\\
&-\frac{1}{\Delta\chi_i}\frac{(R_S-\cancel{\chi_i})}{\chi_i^3}\left(\chi_{\ell-1}\frac{\chi_i+\chi_{i-1}}{2}\frac{\Delta\chi_{i-1}+\Delta\chi_i}{2}\zeta^0_{\ell-1,k}u^0_{\ell-1,k}\right.\\
&\left.+\chi_\ell\frac{\chi_i+\chi_{i+1}}{2}\frac{\Delta\chi_{i+1}+\Delta\chi_i}{2}\zeta^0_{\ell,k}u^0_{\ell,k}\right)\\
&+\frac{1}{2\Delta\chi_i}\frac{1}{\chi_i^2}\left((R_S\cancel{\chi}+\chi_{\ell-1})\frac{\chi_i+\chi_{i-1}}{2}\frac{\Delta\chi_{i-1}+\Delta\chi_i}{2}\zeta^0_{\ell-1,k}u^0_{\ell-1,k}\right.\\
&\left.+(R_S\cancel{\chi}+\chi_\ell)\frac{\chi_i+\chi_{i+1}}{2}\frac{\Delta\chi_{i+1}+\Delta\chi_i}{2}\zeta^0_{\ell,k}u^0_{\ell,k}\right)\\
&+\frac{1}{2\Delta\chi_i}\frac{1}{\chi_i^2}\left(\chi_{\ell-1}\frac{(2R_S-\chi_i-\chi_{i-1})}{2}\frac{\Delta\chi_{i-1}+\Delta\chi_i}{2}\zeta^0_{\ell-1,k}u^0_{\ell-1,k}\right.\\
&\left.+\chi_\ell\frac{(2R_S-\chi_i-\chi_{i+1})}{2}\frac{\Delta\chi_{i+1}+\Delta\chi_i}{2}\zeta^0_{\ell,k}u^0_{\ell,k}\right)\\
&-\frac{1}{2}\left\{\eta^0_{i,n-1}w^1_{i,n-1}+\eta^1_{i,n-1}w^0_{i,n-1}+\eta^0_{i,n}w^1_{i,n}+\eta^1_{i,n}w^0_{i,n}\right\}
\end{aligned}
\tag{3.65}
$$

$$
\begin{aligned}
N^1_\theta(\vec{u}) =& \frac{1}{2\Delta\chi_i}\frac{1}{\chi_i^2}\left(\chi_{\ell-1}\frac{\chi_i+\chi_{i-1}}{2}\frac{\Delta\chi_{i-1}+\Delta\chi_i}{2}\left[\zeta^0_{\ell-1,k}u^1_{\ell-1,k}+\zeta^1_{\ell-1,k}u^0_{\ell-1,k}\right]\right.\\
&\left.+\chi_\ell\frac{\chi_i+\chi_{i+1}}{2}\frac{\Delta\chi_{i+1}+\Delta\chi_i}{2}\left[\zeta^0_{\ell,k}u^1_{\ell,k}+\zeta^1_{\ell,k}u^0_{\ell,k}\right]\right)\\
&-\frac{1}{\Delta\chi_i}\frac{R_S}{\chi_i^3}\left(\chi_{\ell-1}\frac{\chi_i+\chi_{i-1}}{2}\frac{\Delta\chi_{i-1}+\Delta\chi_i}{2}\zeta^0_{\ell-1,k}u^0_{\ell-1,k}\right.\\
&\left.+\chi_\ell\frac{\chi_i+\chi_{i+1}}{2}\frac{\Delta\chi_{i+1}+\Delta\chi_i}{2}\zeta^0_{\ell,k}u^0_{\ell,k}\right)\\
&+\frac{1}{2\Delta\chi_i}\frac{1}{\chi_i^2}\left((R_S+\chi_{\ell-1})\frac{\chi_i+\chi_{i-1}}{2}\frac{\Delta\chi_{i-1}+\Delta\chi_i}{2}\zeta^0_{\ell-1,k}u^0_{\ell-1,k}\right.\\
&\left.+(R_S+\chi_\ell)\frac{\chi_i+\chi_{i+1}}{2}\frac{\Delta\chi_{i+1}+\Delta\chi_i}{2}\zeta^0_{\ell,k}u^0_{\ell,k}\right)\\
&+\frac{1}{2\Delta\chi_i}\frac{1}{\chi_i^2}\left(\chi_{\ell-1}\frac{(2R_S-\chi_i-\chi_{i-1})}{2}\frac{\Delta\chi_{i-1}+\Delta\chi_i}{2}\zeta^0_{\ell-1,k}u^0_{\ell-1,k}\right.\\
&\left.+\chi_\ell\frac{(2R_S-\chi_i-\chi_{i+1})}{2}\frac{\Delta\chi_{i+1}+\Delta\chi_i}{2}\zeta^0_{\ell,k}u^0_{\ell,k}\right)\\
&-\frac{1}{2}\left\{\eta^0_{i,n-1}w^1_{i,n-1}+\eta^1_{i,n-1}w^0_{i,n-1}+\eta^0_{i,n}w^1_{i,n}+\eta^1_{i,n}w^0_{i,n}\right\}
\end{aligned}
\tag{3.66}
$$

$$
\begin{aligned}
N_z^1(\vec{u}) =& \eta_{i,n}^0 \frac{\Delta z_k v_{i,k}^1 + \Delta z_{k+1} v_{i,k+1}^1}{\Delta z_k + \Delta z_{k+1}} + \eta_{i,n}^1 \frac{\Delta z_k v_{i,k}^0 + \Delta z_{k+1} v_{i,k+1}^0}{\Delta z_k + \Delta z_{k+1}} \\
& - \frac{1}{2}\frac{1}{\chi_i}\left[\chi_{\ell-1}\omega_{\ell-1,n}^0 \frac{\Delta z_k u_{\ell-1,k}^1 + \Delta z_{k+1} u_{\ell-1,k+1}^1}{\Delta z_k + \Delta z_{k+1}} + \chi_\ell \omega_{\ell,n}^0 \frac{\Delta z_k u_{\ell,k}^1 + \Delta z_{k+1} u_{\ell,k+1}^1}{\Delta z_k + \Delta z_{k+1}}\right] \\
& - \frac{1}{2}\frac{1}{\chi_i}\left[\chi_{\ell-1}\omega_{\ell-1,n}^1 \frac{\Delta z_k u_{\ell-1,k}^0 + \Delta z_{k+1} u_{\ell-1,k+1}^0}{\Delta z_k + \Delta z_{k+1}} + \chi_\ell \omega_{\ell,n}^1 \frac{\Delta z_k u_{\ell,k}^0 + \Delta z_{k+1} u_{\ell,k+1}^0}{\Delta z_k + \Delta z_{k+1}}\right] \\
& + \frac{1}{2}\frac{(R_S - \cancel{\chi_i})}{\chi_i^2}\left[\chi_{\ell-1}\omega_{\ell-1,n}^0 \frac{\Delta z_k u_{\ell-1,k}^0 + \Delta z_{k+1} u_{\ell-1,k+1}^0}{\Delta z_k + \Delta z_{k+1}} + \chi_\ell \omega_{\ell,n}^0 \frac{\Delta z_k u_{\ell,k}^0 + \Delta z_{k+1} u_{\ell,k+1}^0}{\Delta z_k + \Delta z_{k+1}}\right] \\
& - \frac{1}{2}\frac{1}{\chi_i}\left[(R_S - \cancel{\chi_{\ell-1}})\,\omega_{\ell-1,n}^0 \frac{\Delta z_k u_{\ell-1,k}^0 + \Delta z_{k+1} u_{\ell-1,k+1}^0}{\Delta z_k + \Delta z_{k+1}} + (R_S - \cancel{\chi_\ell})\,\omega_{\ell,n}^0 \frac{\Delta z_k u_{\ell,k}^0 + \Delta z_{k+1} u_{\ell,k+1}^0}{\Delta z_k + \Delta z_{k+1}}\right]
\end{aligned}
\tag{3.67}
$$

$$
\begin{aligned}
N_z^1(\vec{u}) =& \eta_{i,n}^0 \frac{\Delta z_k v_{i,k}^1 + \Delta z_{k+1} v_{i,k+1}^1}{\Delta z_k + \Delta z_{k+1}} + \eta_{i,n}^1 \frac{\Delta z_k v_{i,k}^0 + \Delta z_{k+1} v_{i,k+1}^0}{\Delta z_k + \Delta z_{k+1}} \\
& - \frac{1}{2}\frac{1}{\chi_i}\left[\chi_{\ell-1}\omega_{\ell-1,n}^0 \frac{\Delta z_k u_{\ell-1,k}^1 + \Delta z_{k+1} u_{\ell-1,k+1}^1}{\Delta z_k + \Delta z_{k+1}} + \chi_\ell \omega_{\ell,n}^0 \frac{\Delta z_k u_{\ell,k}^1 + \Delta z_{k+1} u_{\ell,k+1}^1}{\Delta z_k + \Delta z_{k+1}}\right] \\
& - \frac{1}{2}\frac{1}{\chi_i}\left[\chi_{\ell-1}\omega_{\ell-1,n}^1 \frac{\Delta z_k u_{\ell-1,k}^0 + \Delta z_{k+1} u_{\ell-1,k+1}^0}{\Delta z_k + \Delta z_{k+1}} + \chi_\ell \omega_{\ell,n}^1 \frac{\Delta z_k u_{\ell,k}^0 + \Delta z_{k+1} u_{\ell,k+1}^0}{\Delta z_k + \Delta z_{k+1}}\right] \\
& + \frac{1}{2}\frac{R_S}{\chi_i^2}\left[\chi_{\ell-1}\omega_{\ell-1,n}^0 \frac{\Delta z_k u_{\ell-1,k}^0 + \Delta z_{k+1} u_{\ell-1,k+1}^0}{\Delta z_k + \Delta z_{k+1}} + \chi_\ell \omega_{\ell,n}^0 \frac{\Delta z_k u_{\ell,k}^0 + \Delta z_{k+1} u_{\ell,k+1}^0}{\Delta z_k + \Delta z_{k+1}}\right] \\
& - \frac{1}{2}\frac{R_S}{\chi_i}\left[\omega_{\ell-1,n}^0 \frac{\Delta z_k u_{\ell-1,k}^0 + \Delta z_{k+1} u_{\ell-1,k+1}^0}{\Delta z_k + \Delta z_{k+1}} + \omega_{\ell,n}^0 \frac{\Delta z_k u_{\ell,k}^0 + \Delta z_{k+1} u_{\ell,k+1}^0}{\Delta z_k + \Delta z_{k+1}}\right]
\end{aligned}
\tag{3.68}
$$

3.6.6 Discrete Convection, Real First Order: $N^R(\vec{u},\vec{\omega}) = (\nabla\times\vec{u})\times\vec{u}$

$$
\begin{aligned}
N^R_\chi(\vec{u}) =& \frac{1}{2}\Bigg[\omega^0_{\ell,n-1}\,\frac{\Delta\chi_i w^R_{i,n-1}+\Delta\chi_{i+1}w^R_{i+1,n-1}}{\Delta\chi_i+\Delta\chi_{i+1}} + \omega^R_{\ell,n-1}\,\frac{\Delta\chi_i w^0_{i,n-1}+\Delta\chi_{i+1}w^0_{i+1,n-1}}{\Delta\chi_i+\Delta\chi_{i+1}} \\
&+ \omega^0_{\ell,n}\,\frac{\Delta\chi_i w^R_{i,n}+\Delta\chi_{i+1}w^R_{i+1,n}}{\Delta\chi_i+\Delta\chi_{i+1}} + \omega^R_{\ell,n-1}\,\frac{\Delta\chi_i w^0_{i,n}+\Delta\chi_{i+1}w^0_{i+1,n}}{\Delta\chi_i+\Delta\chi_{i+1}}\Bigg] \\
&- \frac{\chi_i+\chi_{i+1}}{4}\left[\zeta^0_{\ell,k}\left(\frac{v^R_{i,k}}{\chi_i}+\frac{v^R_{i+1,k}}{\chi_{i+1}}\right) + \zeta^R_{\ell,k}\left(\frac{v^0_{i,k}}{\chi_i}+\frac{v^0_{i+1,k}}{\chi_{i+1}}\right)\right] \\
&- \frac{R_S}{2}\zeta^0_{\ell,k}\left[\frac{v^0_{i,k}}{\chi_i}+\frac{v^0_{i+1,k}}{\chi_{i+1}}\right] + \frac{\chi_i+\chi_{i+1}}{4}\zeta^0_{\ell,k}\left[\frac{R_S}{\chi_i^2}v^0_{i,k}+\frac{R_S}{\chi^2_{i+1}}v^0_{i+1,k}\right]
\end{aligned}
\tag{3.69}
$$

$$
\begin{aligned}
N^R_\chi(\vec{u}) =& \left(\frac{u^0_{\ell,k}-u^0_{\ell,k-1}}{\Delta z_k+\Delta z_{k-1}} - \frac{w^0_{i+1,n-1}-w^0_{i,n-1}}{\Delta\chi_{i+1}+\Delta\chi_i}\right)\frac{\Delta\chi_i w^R_{i,n-1}+\Delta\chi_{i+1}w^R_{i+1,n-1}}{\Delta\chi_i+\Delta\chi_{i+1}} \\
&+ \left(\frac{u^R_{\ell,k}-u^R_{\ell,k-1}}{\Delta z_k+\Delta z_{k-1}} - \frac{w^0_{i+1,n-1}-w^0_{i,n-1}}{\Delta\chi_{i+1}+\Delta\chi_i} - \frac{w^R_{i+1,n-1}-w^R_{i,n-1}}{\Delta\chi_{i+1}+\Delta\chi_i}\right)\frac{\Delta\chi_i w^0_{i,n-1}+\Delta\chi_{i+1}w^0_{i+1,n-1}}{\Delta\chi_i+\Delta\chi_{i+1}} \\
&+ \left(\frac{u^0_{\ell,k+1}-u^0_{\ell,k}}{\Delta z_k+\Delta z_{k+1}} - \frac{w^0_{i+1,n}-w^0_{i,n}}{\Delta\chi_{i+1}+\Delta\chi_i}\right)\frac{\Delta\chi_i w^R_{i,n}+\Delta\chi_{i+1}w^R_{i+1,n}}{\Delta\chi_i+\Delta\chi_{i+1}} \\
&+ \left(\frac{u^R_{\ell,k+1}-u^R_{\ell,k}}{\Delta z_k+\Delta z_{k+1}} - \frac{w^0_{i+1,n}-w^0_{i,n}}{\Delta\chi_{i+1}+\Delta\chi_i} - \frac{w^R_{i+1,n}-w^R_{i,n}}{\Delta\chi_{i+1}+\Delta\chi_i}\right)\frac{\Delta\chi_i w^0_{i,n}+\Delta\chi_{i+1}w^0_{i+1,n}}{\Delta\chi_i+\Delta\chi_{i+1}} \\
&- \frac{\chi_i+\chi_{i+1}}{4}\Bigg[\frac{4}{\chi_{i+1}+\chi_i}\frac{\chi_{i+1}v^0_{i+1,k}-\chi_i v^0_{i,k}}{\Delta\chi_i+\Delta\chi_{i+1}}\left(\frac{v^R_{i,k}}{\chi_i}+\frac{v^R_{i+1,k}}{\chi_{i+1}}\right) \\
&\quad+\Bigg\{\frac{4}{\chi_{i+1}+\chi_i}\frac{\chi_{i+1}v^0_{i+1,k}-\chi_i v^0_{i,k}}{\Delta\chi_i+\Delta\chi_{i+1}} + \frac{4}{\chi_{i+1}+\chi_i}\frac{\chi_{i+1}v^R_{i+1,k}-\chi_i v^R_{i,k}}{\Delta\chi_i+\Delta\chi_{i+1}} \\
&\qquad+\frac{4R_S}{\chi_{i+1}+\chi_i}\frac{v^0_{i+1,k}-v^0_{i,k}}{\Delta\chi_i+\Delta\chi_{i+1}} - \frac{8R_S}{(\chi_{i+1}+\chi_i)^2}\frac{\chi_{i+1}v^0_{i+1,k}-\chi_i v^0_{i,k}}{\Delta\chi_{i+1}+\Delta\chi_i} \\
&\qquad+2\frac{1}{\chi_{i+1}+\chi_i}u^I_{\ell,k}\Bigg\}\left(\frac{v^0_{i,k}}{\chi_i}+\frac{v^0_{i+1,k}}{\chi_{i+1}}\right)\Bigg] \\
&- \frac{R_S}{2}\frac{4}{\chi_{i+1}+\chi_i}\frac{\chi_{i+1}v^0_{i+1,k}-\chi_i v^0_{i,k}}{\Delta\chi_i+\Delta\chi_{i+1}}\left[\frac{v^0_{i,k}}{\chi_i}+\frac{v^0_{i+1,k}}{\chi_{i+1}}\right] \\
&+ \frac{\chi_i+\chi_{i+1}}{4}\frac{4}{\chi_{i+1}+\chi_i}\frac{\chi_{i+1}v^0_{i+1,k}-\chi_i v^0_{i,k}}{\Delta\chi_i+\Delta\chi_{i+1}}\left[\frac{R_S}{\chi_i^2}v^0_{i,k}+\frac{R_S}{\chi^2_{i+1}}v^0_{i+1,k}\right]
\end{aligned}
\tag{3.70}
$$

$$
\begin{aligned}
N_{\chi}^{R}(\vec{u}) = &\left(\frac{u_{\ell,k}^{0}-u_{\ell,k-1}^{0}}{\Delta z_k+\Delta z_{k-1}}-\frac{w_{i+1,n-1}^{0}-w_{i,n-1}^{0}}{\Delta\chi_{i+1}+\Delta\chi_i}\right)\frac{\Delta\chi_i w_{i,n-1}^{R}+\Delta\chi_{i+1}w_{i+1,n-1}^{R}}{\Delta\chi_i+\Delta\chi_{i+1}}\\
&+\left(\frac{u_{\ell,k}^{R}-u_{\ell,k-1}^{R}}{\Delta z_k+\Delta z_{k-1}}-\frac{w_{i+1,n-1}^{0}-w_{i,n-1}^{0}}{\Delta\chi_{i+1}+\Delta\chi_i}-\frac{w_{i+1,n-1}^{R}-w_{i,n-1}^{R}}{\Delta\chi_{i+1}+\Delta\chi_i}\right)\frac{\Delta\chi_i w_{i,n-1}^{0}+\Delta\chi_{i+1}w_{i+1,n-1}^{0}}{\Delta\chi_i+\Delta\chi_{i+1}}\\
&+\left(\frac{u_{\ell,k+1}^{0}-u_{\ell,k}^{0}}{\Delta z_k+\Delta z_{k+1}}-\frac{w_{i+1,n}^{0}-w_{i,n}^{0}}{\Delta\chi_{i+1}+\Delta\chi_i}\right)\frac{\Delta\chi_i w_{i,n}^{R}+\Delta\chi_{i+1}w_{i+1,n}^{R}}{\Delta\chi_i+\Delta\chi_{i+1}}\\
&+\left(\frac{u_{\ell,k+1}^{R}-u_{\ell,k}^{R}}{\Delta z_k+\Delta z_{k+1}}-\frac{w_{i+1,n}^{0}-w_{i,n}^{0}}{\Delta\chi_{i+1}+\Delta\chi_i}-\frac{w_{i+1,n}^{R}-w_{i,n}^{R}}{\Delta\chi_{i+1}+\Delta\chi_i}\right)\frac{\Delta\chi_i w_{i,n}^{0}+\Delta\chi_{i+1}w_{i+1,n}^{0}}{\Delta\chi_i+\Delta\chi_{i+1}}\\
&-\left[\frac{\chi_{i+1}v_{i+1,k}^{0}-\chi_i v_{i,k}^{0}}{\Delta\chi_i+\Delta\chi_{i+1}}\left(\frac{v_{i,k}^{R}}{\chi_i}+\frac{v_{i+1,k}^{R}}{\chi_{i+1}}\right)\right.\\
&\quad+\left(\frac{v_{i,k}^{0}}{\chi_i}+\frac{v_{i+1,k}^{0}}{\chi_{i+1}}\right)\left\{\frac{\chi_{i+1}v_{i+1,k}^{0}-\chi_i v_{i,k}^{0}}{\Delta\chi_i+\Delta\chi_{i+1}}+\frac{\chi_{i+1}v_{i+1,k}^{R}-\chi_i v_{i,k}^{R}}{\Delta\chi_i+\Delta\chi_{i+1}}\right.\\
&\qquad\left.\left.+R_S\frac{v_{i+1,k}^{0}-v_{i,k}^{0}}{\Delta\chi_i+\Delta\chi_{i+1}}-\cancel{\frac{2R_S}{\chi_{i+1}+\chi_i}\frac{\chi_{i+1}v_{i+1,k}^{0}-\chi_i v_{i,k}^{0}}{\Delta\chi_{i+1}+\Delta\chi_i}}+\frac{1}{2}u_{\ell,k}^{I}\right\}\right]\\
&-\cancel{\frac{2R_S}{\chi_{i+1}+\chi_i}\frac{\chi_{i+1}v_{i+1,k}^{0}-\chi_i v_{i,k}^{0}}{\Delta\chi_i+\Delta\chi_{i+1}}\left[\frac{v_{i,k}^{0}}{\chi_i}+\frac{v_{i+1,k}^{0}}{\chi_{i+1}}\right]}\\
&+\frac{\chi_{i+1}v_{i+1,k}^{0}-\chi_i v_{i,k}^{0}}{\Delta\chi_i+\Delta\chi_{i+1}}\left[\frac{R_S}{\chi_i^2}v_{i,k}^{0}+\frac{R_S}{\chi_{i+1}^2}v_{i+1,k}^{0}\right]
\end{aligned}
\tag{3.71}
$$

$$
\begin{aligned}
N_{\chi}^{R}(\vec{u}) = &\left(\frac{u_{\ell,k}^{0}-u_{\ell,k-1}^{0}}{\Delta z_k+\Delta z_{k-1}}-\frac{w_{i+1,n-1}^{0}-w_{i,n-1}^{0}}{\Delta\chi_{i+1}+\Delta\chi_i}\right)\frac{\Delta\chi_i w_{i,n-1}^{R}+\Delta\chi_{i+1}w_{i+1,n-1}^{R}}{\Delta\chi_i+\Delta\chi_{i+1}}\\
&+\left(\frac{u_{\ell,k}^{R}-u_{\ell,k-1}^{R}}{\Delta z_k+\Delta z_{k-1}}-\frac{w_{i+1,n-1}^{0}-w_{i,n-1}^{0}}{\Delta\chi_{i+1}+\Delta\chi_i}-\frac{w_{i+1,n-1}^{R}-w_{i,n-1}^{R}}{\Delta\chi_{i+1}+\Delta\chi_i}\right)\frac{\Delta\chi_i w_{i,n-1}^{0}+\Delta\chi_{i+1}w_{i+1,n-1}^{0}}{\Delta\chi_i+\Delta\chi_{i+1}}\\
&+\left(\frac{u_{\ell,k+1}^{0}-u_{\ell,k}^{0}}{\Delta z_k+\Delta z_{k+1}}-\frac{w_{i+1,n}^{0}-w_{i,n}^{0}}{\Delta\chi_{i+1}+\Delta\chi_i}\right)\frac{\Delta\chi_i w_{i,n}^{R}+\Delta\chi_{i+1}w_{i+1,n}^{R}}{\Delta\chi_i+\Delta\chi_{i+1}}\\
&+\left(\frac{u_{\ell,k+1}^{R}-u_{\ell,k}^{R}}{\Delta z_k+\Delta z_{k+1}}-\frac{w_{i+1,n}^{0}-w_{i,n}^{0}}{\Delta\chi_{i+1}+\Delta\chi_i}-\frac{w_{i+1,n}^{R}-w_{i,n}^{R}}{\Delta\chi_{i+1}+\Delta\chi_i}\right)\frac{\Delta\chi_i w_{i,n}^{0}+\Delta\chi_{i+1}w_{i+1,n}^{0}}{\Delta\chi_i+\Delta\chi_{i+1}}\\
&-\frac{\chi_{i+1}v_{i+1,k}^{0}-\chi_i v_{i,k}^{0}}{\Delta\chi_i+\Delta\chi_{i+1}}\left(\frac{v_{i,k}^{R}}{\chi_i}+\frac{v_{i+1,k}^{R}}{\chi_{i+1}}\right)\\
&-\left(\frac{v_{i,k}^{0}}{\chi_i}+\frac{v_{i+1,k}^{0}}{\chi_{i+1}}\right)\\
&\quad\left\{\frac{\chi_{i+1}v_{i+1,k}^{0}-\chi_i v_{i,k}^{0}}{\Delta\chi_i+\Delta\chi_{i+1}}+\frac{\chi_{i+1}v_{i+1,k}^{R}-\chi_i v_{i,k}^{R}}{\Delta\chi_i+\Delta\chi_{i+1}}+R_S\frac{v_{i+1,k}^{0}-v_{i,k}^{0}}{\Delta\chi_i+\Delta\chi_{i+1}}+\frac{1}{2}u_{\ell,k}^{I}\right\}\\
&+\frac{\chi_{i+1}v_{i+1,k}^{0}-\chi_i v_{i,k}^{0}}{\Delta\chi_i+\Delta\chi_{i+1}}\left[\frac{R_S}{\chi_i^2}v_{i,k}^{0}+\frac{R_S}{\chi_{i+1}^2}v_{i+1,k}^{0}\right]
\end{aligned}
\tag{3.72}
$$

$$
\begin{aligned}
N_\theta^R(\vec{u}) =& \frac{1}{2\Delta\chi_i}\frac{1}{\chi_i^2}\left(\chi_{\ell-1}\frac{\chi_i+\chi_{i-1}}{2}\frac{\Delta\chi_{i-1}+\Delta\chi_i}{2}\left\{\zeta^0_{\ell-1,k}\,u^{\boldsymbol{R}}_{\ell-1,k} + \zeta^{\boldsymbol{R}}_{\ell-1,k}\,u^0_{\ell-1,k}\right\}\right.\\
&\left. + \chi_\ell\frac{\chi_i+\chi_{i+1}}{2}\frac{\Delta\chi_{i+1}+\Delta\chi_i}{2}\left\{\zeta^0_{\ell,k}\,u^{\boldsymbol{R}}_{\ell,k} + \zeta^{\boldsymbol{R}}_{\ell,k}\,u^0_{\ell,k}\right\}\right)\\
&- \frac{1}{\Delta\chi_i}\frac{R_S}{\chi_i^3}\left(\chi_{\ell-1}\frac{\chi_i+\chi_{i-1}}{2}\frac{\Delta\chi_{i-1}+\Delta\chi_i}{2}\zeta^0_{\ell-1,k}u^0_{\ell-1,k} + \chi_\ell\frac{\chi_i+\chi_{i+1}}{2}\frac{\Delta\chi_{i+1}+\Delta\chi_i}{2}\zeta^0_{\ell,k}u^0_{\ell,k}\right)\\
&+ \frac{1}{2\Delta\chi_i}\frac{1}{\chi_i^2}\left((R_S+\chi_{\ell-1})\frac{\chi_i+\chi_{i-1}}{2}\frac{\Delta\chi_{i-1}+\Delta\chi_i}{2}\zeta^0_{\ell-1,k}u^0_{\ell-1,k} + (R_S+\chi_\ell)\frac{\chi_i+\chi_{i+1}}{2}\frac{\Delta\chi_{i+1}+\Delta\chi_i}{2}\zeta^0_{\ell,k}u^0_{\ell,k}\right)\\
&+ \frac{1}{2\Delta\chi_i}\frac{1}{\chi_i^2}\left(\chi_{\ell-1}\frac{(2R_S-\chi_i-\chi_{i-1})}{2}\frac{\Delta\chi_{i-1}+\Delta\chi_i}{2}\zeta^0_{\ell-1,k}u^0_{\ell-1,k} + \chi_\ell\frac{(2R_S-\chi_i-\chi_{i+1})}{2}\frac{\Delta\chi_{i+1}+\Delta\chi_i}{2}\zeta^0_{\ell,k}u^0_{\ell,k}\right)\\
&- \frac{1}{2}\left\{\eta^0_{i,n-1}\,w^{\boldsymbol{R}}_{i,n-1} + \eta^{\boldsymbol{R}}_{i,n-1}\,w^0_{i,n-1} + \eta^0_{i,n}\,w^{\boldsymbol{R}}_{i,n} + \eta^{\boldsymbol{R}}_{i,n}\,w^0_{i,n}\right\}
\end{aligned}
\tag{3.73}
$$

$$
\begin{aligned}
N_\theta^R(\vec{u}) =& \frac{1}{2\Delta\chi_i}\frac{1}{\chi_i^2}\left(\chi_{\ell-1}\frac{\chi_i+\chi_{i-1}}{2}\frac{\Delta\chi_{i-1}+\Delta\chi_i}{2}\left\{\frac{4}{\chi_{i-1}+\chi_i}\frac{\chi_i v^0_{i,k}-\chi_{i-1}v^0_{i-1,k}}{\Delta\chi_i+\Delta\chi_{i-1}}\,u^{\boldsymbol{R}}_{\ell-1,k}\right.\right.\\
&\left.\left. + u^0_{\ell-1,k}\left[\frac{4}{\chi_{i-1}+\chi_i}\frac{\chi_i v^0_{i,k}-\chi_{i-1}v^0_{i-1,k}}{\Delta\chi_i+\Delta\chi_{i-1}} + \frac{4}{\chi_{i-1}+\chi_i}\frac{\chi_i v^{\boldsymbol{R}}_{i,k}-\chi_{i-1}v^{\boldsymbol{R}}_{i-1,k}}{\Delta\chi_i+\Delta\chi_{i-1}}\right.\right.\right.\\
&\left.\left.\left. + \frac{4R_S}{\chi_{i-1}+\chi_i}\frac{v^0_{i,k}-v^0_{i-1,k}}{\Delta\chi_i+\Delta\chi_{i-1}} - \frac{8R_S}{(\chi_{i-1}+\chi_i)^2}\frac{\chi_i v^0_{i,k}-\chi_{i-1}v^0_{i-1,k}}{\Delta\chi_{i-1}+\Delta\chi_i} + 2\frac{1}{\chi_{i-1}+\chi_i}\,u^{\boldsymbol{I}}_{\ell-1,k}\right]\right\}\\
&+ \chi_\ell\frac{\chi_i+\chi_{i+1}}{2}\frac{\Delta\chi_{i+1}+\Delta\chi_i}{2}\left\{\frac{4}{\chi_{i+1}+\chi_i}\frac{\chi_{i+1}v^0_{i+1,k}-\chi_i v^0_{i,k}}{\Delta\chi_i+\Delta\chi_{i+1}}\,u^{\boldsymbol{R}}_{\ell,k}\right.\\
&\left. + u^0_{\ell,k}\left[\frac{4}{\chi_{i+1}+\chi_i}\frac{\chi_{i+1}v^0_{i+1,k}-\chi_i v^0_{i,k}}{\Delta\chi_i+\Delta\chi_{i+1}} + \frac{4}{\chi_{i+1}+\chi_i}\frac{\chi_{i+1}v^{\boldsymbol{R}}_{i+1,k}-\chi_i v^{\boldsymbol{R}}_{i,k}}{\Delta\chi_i+\Delta\chi_{i+1}}\right.\right.\\
&\left.\left. + \frac{4R_S}{\chi_{i+1}+\chi_i}\frac{v^0_{i+1,k}-v^0_{i,k}}{\Delta\chi_i+\Delta\chi_{i+1}} - \frac{8R_S}{(\chi_{i+1}+\chi_i)^2}\frac{\chi_{i+1}v^0_{i+1,k}-\chi_i v^0_{i,k}}{\Delta\chi_{i+1}+\Delta\chi_i} + 2\frac{1}{\chi_{i+1}+\chi_i}\,u^{\boldsymbol{I}}_{\ell,k}\right]\right\}\right)\\
&- \frac{1}{\Delta\chi_i}\frac{R_S}{\chi_i^3}\left(\chi_{\ell-1}\frac{\chi_i+\chi_{i-1}}{2}\frac{\Delta\chi_{i-1}+\Delta\chi_i}{2}\frac{4}{\chi_{i-1}+\chi_i}\frac{\chi_i v^0_{i,k}-\chi_{i-1}v^0_{i-1,k}}{\Delta\chi_i+\Delta\chi_{i-1}}u^0_{\ell-1,k}\right.\\
&\left. + \chi_\ell\frac{\chi_i+\chi_{i+1}}{2}\frac{\Delta\chi_{i+1}+\Delta\chi_i}{2}\frac{4}{\chi_{i+1}+\chi_i}\frac{\chi_{i+1}v^0_{i+1,k}-\chi_i v^0_{i,k}}{\Delta\chi_i+\Delta\chi_{i+1}}u^0_{\ell,k}\right)\\
&+ \frac{1}{2\Delta\chi_i}\frac{1}{\chi_i^2}\left((R_S+\chi_{\ell-1})\frac{\chi_i+\chi_{i-1}}{2}\frac{\Delta\chi_{i-1}+\Delta\chi_i}{2}\frac{4}{\chi_{i-1}+\chi_i}\frac{\chi_i v^0_{i,k}-\chi_{i-1}v^0_{i-1,k}}{\Delta\chi_i+\Delta\chi_{i-1}}u^0_{\ell-1,k}\right.\\
&\left. + (R_S+\chi_\ell)\frac{\chi_i+\chi_{i+1}}{2}\frac{\Delta\chi_{i+1}+\Delta\chi_i}{2}\frac{4}{\chi_{i+1}+\chi_i}\frac{\chi_{i+1}v^0_{i+1,k}-\chi_i v^0_{i,k}}{\Delta\chi_i+\Delta\chi_{i+1}}u^0_{\ell,k}\right)\\
&+ \frac{1}{2\Delta\chi_i}\frac{1}{\chi_i^2}\left(\chi_{\ell-1}\frac{(2R_S-\chi_i-\chi_{i-1})}{2}\frac{\Delta\chi_{i-1}+\Delta\chi_i}{2}\frac{4}{\chi_{i-1}+\chi_i}\frac{\chi_i v^0_{i,k}-\chi_{i-1}v^0_{i-1,k}}{\Delta\chi_i+\Delta\chi_{i-1}}u^0_{\ell-1,k}\right.\\
&\left. + \chi_\ell\frac{(2R_S-\chi_i-\chi_{i+1})}{2}\frac{\Delta\chi_{i+1}+\Delta\chi_i}{2}\frac{4}{\chi_{i+1}+\chi_i}\frac{\chi_{i+1}v^0_{i+1,k}-\chi_i v^0_{i,k}}{\Delta\chi_i+\Delta\chi_{i+1}}u^0_{\ell,k}\right)\\
&+\frac{1}{2}\left\{+2\frac{v^0_{i,k}-v^0_{i,k-1}}{\Delta z_k+\Delta z_{k-1}}\,w^{\boldsymbol{R}}_{i,n-1} + \left(\frac{1}{\chi_i}\,w^{\boldsymbol{I}}_{i,n-1} + 2\frac{v^{\boldsymbol{R}}_{i,k}-v^{\boldsymbol{R}}_{i,k-1}}{\Delta z_k+\Delta z_{k-1}}\right)w^0_{i,n-1}\right.\\
&\left. +2\frac{v^0_{i,k+1}-v^0_{i,k}}{\Delta z_k+\Delta z_{k+1}}\,w^{\boldsymbol{R}}_{i,n} + \left(\frac{1}{\chi_i}\,w^{\boldsymbol{I}}_{i,n} + 2\frac{v^{\boldsymbol{R}}_{i,k+1}-v^{\boldsymbol{R}}_{i,k}}{\Delta z_k+\Delta z_{k+1}}\right)w^0_{i,n}\right\}
\end{aligned}
\tag{3.74}
$$

$$
\begin{aligned}
N_\theta^R(\vec{u}) = & \frac{1}{2\Delta\chi_i}\frac{1}{\chi_i^2}\chi_{\ell-1}\left\{\left(\chi_i v_{i,k}^0 - \chi_{i-1}v_{i-1,k}^0\right) u_{\ell-1,k}^R \right. \\
& + u_{\ell-1,k}^0\left[\cancel{\left(\chi_i v_{i,k}^0 - \chi_{i-1}v_{i-1,k}^0\right)} + \left(\chi_i v_{i,k}^R - \chi_{i-1}v_{i-1,k}^R\right)\right. \\
& + R_S\left(v_{i,k}^0 - v_{i-1,k}^0\right) - \cancel{\frac{2R_S}{\chi_{i-1}+\chi_i}\left(\chi_i v_{i,k}^0 - \chi_{i-1}v_{i-1,k}^0\right)} \\
& \left.\left. + \frac{\Delta\chi_{i-1}+\Delta\chi_i}{2} u_{\ell-1,k}^I\right]\right\} \\
& + \frac{1}{2\Delta\chi_i}\frac{1}{\chi_i^2}\chi_\ell\left\{\left(\chi_{i+1}v_{i+1,k}^0 - \chi_i v_{i,k}^0\right) u_{\ell,k}^R \right. \\
& + u_{\ell,k}^0\left[\cancel{\left(\chi_{i+1}v_{i+1,k}^0 - \chi_i v_{i,k}^0\right)} + \left(\chi_{i+1}v_{i+1,k}^R - \chi_i v_{i,k}^R\right)\right. \\
& + R_S\left(v_{i+1,k}^0 - v_{i,k}^0\right) - \cancel{\frac{2R_S}{\chi_{i+1}+\chi_i}\left(\chi_{i+1}v_{i+1,k}^0 - \chi_i v_{i,k}^0\right)} \\
& \left.\left. + \frac{\Delta\chi_{i+1}+\Delta\chi_i}{2} u_{\ell,k}^I\right]\right\} \\
& - \frac{1}{\Delta\chi_i}\frac{R_S}{\chi_i^3}\left[\chi_{\ell-1}\left(\chi_i v_{i,k}^0 - \chi_{i-1}v_{i-1,k}^0\right)u_{\ell-1,k}^0 + \chi_\ell\left(\chi_{i+1}v_{i+1,k}^0 - \chi_i v_{i,k}^0\right)u_{\ell,k}^0\right] \\
& + \frac{1}{2\Delta\chi_i}\frac{1}{\chi_i^2}\left[(R_S+\chi_{\ell-1})\left(\chi_i v_{i,k}^0 - \chi_{i-1}v_{i-1,k}^0\right)u_{\ell-1,k}^0 + (R_S+\chi_\ell)\left(\chi_{i+1}v_{i+1,k}^0 - \chi_i v_{i,k}^0\right)u_{\ell,k}^0\right] \\
& + \frac{1}{2\Delta\chi_i}\frac{1}{\chi_i^2}\left[\left(\cancel{\frac{2R_S}{\chi_{i-1}+\chi_i}} - 1\right)\chi_{\ell-1}\left(\chi_i v_{i,k}^0 - \chi_{i-1}v_{i-1,k}^0\right)u_{\ell-1,k}^0\right. \\
& \left. + \left(\cancel{\frac{2R_S}{\chi_{i+1}+\chi_i}} - 1\right)\chi_\ell\left(\chi_{i+1}v_{i+1,k}^0 - \chi_i v_{i,k}^0\right)u_{\ell,k}^0\right] \\
& + \frac{v_{i,k}^0 - v_{i,k-1}^0}{\Delta z_k + \Delta z_{k-1}} w_{i,n-1}^R + \left(\frac{1}{2\chi_i} w_{i,n-1}^I + \frac{v_{i,k}^R - v_{i,k-1}^R}{\Delta z_k + \Delta z_{k-1}}\right) w_{i,n-1}^0 \\
& + \frac{v_{i,k+1}^0 - v_{i,k}^0}{\Delta z_k + \Delta z_{k+1}} w_{i,n}^R + \left(\frac{1}{2\chi_i} w_{i,n}^I + \frac{v_{i,k+1}^R - v_{i,k}^R}{\Delta z_k + \Delta z_{k+1}}\right) w_{i,n}^0
\end{aligned}
\tag{3.75}
$$

$$
\begin{aligned}
N_\theta^R(\vec{u}) =& \frac{1}{2\Delta\chi_i}\frac{1}{\chi_i^2}\chi_{\ell-1}\left\{\left(\chi_i v_{i,k}^0 - \chi_{i-1}v_{i-1,k}^0\right) u_{\ell-1,k}^R \right.\\
&\left. + u_{\ell-1,k}^0\left[\left(\chi_i v_{i,k}^R - \chi_{i-1}v_{i-1,k}^R\right) + R_S\left(v_{i,k}^0 - v_{i-1,k}^0\right) + \frac{\Delta\chi_{i-1}+\Delta\chi_i}{2} u_{\ell-1,k}^I\right]\right\}\\
&+ \frac{1}{2\Delta\chi_i}\frac{1}{\chi_i^2}\chi_\ell\left\{\left(\chi_{i+1}v_{i+1,k}^0 - \chi_i v_{i,k}^0\right) u_{\ell,k}^R \right.\\
&\left. + u_{\ell,k}^0\left[\left(\chi_{i+1}v_{i+1,k}^R - \chi_i v_{i,k}^R\right) + R_S\left(v_{i+1,k}^0 - v_{i,k}^0\right) + \frac{\Delta\chi_{i+1}+\Delta\chi_i}{2} u_{\ell,k}^I\right]\right\}\\
&- \frac{1}{\Delta\chi_i}\frac{R_S}{\chi_i^3}\left[\chi_{\ell-1}\left(\chi_i v_{i,k}^0 - \chi_{i-1}v_{i-1,k}^0\right)u_{\ell-1,k}^0 + \chi_\ell\left(\chi_{i+1}v_{i+1,k}^0 - \chi_i v_{i,k}^0\right)u_{\ell,k}^0\right]\\
&+ \frac{1}{2\Delta\chi_i}\frac{1}{\chi_i^2}\left[(R_S+\chi_{\ell-1})\left(\chi_i v_{i,k}^0 - \chi_{i-1}v_{i-1,k}^0\right)u_{\ell-1,k}^0 + (R_S+\chi_\ell)\left(\chi_{i+1}v_{i+1,k}^0 - \chi_i v_{i,k}^0\right)u_{\ell,k}^0\right]\\
&+ \frac{v_{i,k}^0 - v_{i,k-1}^0}{\Delta z_k + \Delta z_{k-1}} w_{i,n-1}^R + \left(\frac{1}{2\chi_i} w_{i,n-1}^I + \frac{v_{i,k}^R - v_{i,k-1}^R}{\Delta z_k + \Delta z_{k-1}}\right) w_{i,n-1}^0\\
&+ \frac{v_{i,k+1}^0 - v_{i,k}^0}{\Delta z_k + \Delta z_{k+1}} w_{i,n}^R + \left(\frac{1}{2\chi_i} w_{i,n}^I + \frac{v_{i,k+1}^R - v_{i,k}^R}{\Delta z_k + \Delta z_{k+1}}\right) w_{i,n}^0
\end{aligned}
\tag{3.76}
$$

$$
\begin{aligned}
N_z^R(\vec{u}) = &\left(\eta_{i,n}^0 \frac{\Delta z_k v_{i,k}^R + \Delta z_{k+1} v_{i,k+1}^R}{\Delta z_k + \Delta z_{k+1}} + \eta_{i,n}^R \frac{\Delta z_k v_{i,k}^0 + \Delta z_{k+1} v_{i,k+1}^0}{\Delta z_k + \Delta z_{k+1}}\right) \\
&- \frac{1}{2}\frac{1}{\chi_i}\left[\chi_{\ell-1}\omega_{\ell-1,n}^0 \frac{\Delta z_k u_{\ell-1,k}^R + \Delta z_{k+1} u_{\ell-1,k+1}^R}{\Delta z_k + \Delta z_{k+1}} + \chi_\ell \omega_{\ell,n}^0 \frac{\Delta z_k u_{\ell,k}^R + \Delta z_{k+1} u_{\ell,k+1}^R}{\Delta z_k + \Delta z_{k+1}}\right] \\
&- \frac{1}{2}\frac{1}{\chi_i}\left[\chi_{\ell-1}\omega_{\ell-1,n}^R \frac{\Delta z_k u_{\ell-1,k}^0 + \Delta z_{k+1} u_{\ell-1,k+1}^0}{\Delta z_k + \Delta z_{k+1}} + \chi_\ell \omega_{\ell,n}^R \frac{\Delta z_k u_{\ell,k}^0 + \Delta z_{k+1} u_{\ell,k+1}^0}{\Delta z_k + \Delta z_{k+1}}\right] \\
&+ \frac{1}{2}\frac{R_S}{\chi_i^2}\left[\chi_{\ell-1}\omega_{\ell-1,n}^0 \frac{\Delta z_k u_{\ell-1,k}^0 + \Delta z_{k+1} u_{\ell-1,k+1}^0}{\Delta z_k + \Delta z_{k+1}} + \chi_\ell \omega_{\ell,n}^0 \frac{\Delta z_k u_{\ell,k}^0 + \Delta z_{k+1} u_{\ell,k+1}^0}{\Delta z_k + \Delta z_{k+1}}\right] \\
&- \frac{1}{2}\frac{R_S}{\chi_i}\left[\omega_{\ell-1,n}^0 \frac{\Delta z_k u_{\ell-1,k}^0 + \Delta z_{k+1} u_{\ell-1,k+1}^0}{\Delta z_k + \Delta z_{k+1}} + \omega_{\ell,n}^0 \frac{\Delta z_k u_{\ell,k}^0 + \Delta z_{k+1} u_{\ell,k+1}^0}{\Delta z_k + \Delta z_{k+1}}\right]
\end{aligned}
\tag{3.77}
$$

$$
\begin{aligned}
N_z^R(\vec{u}) = &-2\frac{v_{i,k+1}^0 - v_{i,k}^0}{\Delta z_k + \Delta z_{k+1}} \frac{\Delta z_k v_{i,k}^R + \Delta z_{k+1} v_{i,k+1}^R}{\Delta z_k + \Delta z_{k+1}} \\
&- \left[\frac{1}{\chi_i} w_{i,n}^I + 2\frac{v_{i,k+1}^R - v_{i,k}^R}{\Delta z_k + \Delta z_{k+1}}\right] \frac{\Delta z_k v_{i,k}^0 + \Delta z_{k+1} v_{i,k+1}^0}{\Delta z_k + \Delta z_{k+1}} \\
&- \frac{1}{\chi_i}\left[\chi_{\ell-1}\left\{\frac{u_{\ell-1,k+1}^0 - u_{\ell-1,k}^0}{\Delta z_k + \Delta z_{k+1}} - \frac{w_{i,n}^0 - w_{i-1,n}^0}{\Delta\chi_{i-1} + \Delta\chi_i}\right\} \frac{\Delta z_k u_{\ell-1,k}^R + \Delta z_{k+1} u_{\ell-1,k+1}^R}{\Delta z_k + \Delta z_{k+1}}\right. \\
&\qquad \left. + \chi_\ell\left\{\frac{u_{\ell,k+1}^0 - u_{\ell,k}^0}{\Delta z_k + \Delta z_{k+1}} - \frac{w_{i+1,n}^0 - w_{i,n}^0}{\Delta\chi_{i+1} + \Delta\chi_i}\right\} \frac{\Delta z_k u_{\ell,k}^R + \Delta z_{k+1} u_{\ell,k+1}^R}{\Delta z_k + \Delta z_{k+1}}\right] \\
&- \frac{1}{\chi_i}\left[\chi_{\ell-1}\frac{\Delta z_k u_{\ell-1,k}^0 + \Delta z_{k+1} u_{\ell-1,k+1}^0}{\Delta z_k + \Delta z_{k+1}}\right. \\
&\qquad \left\{\frac{u_{\ell-1,k+1}^R - u_{\ell-1,k}^R}{\Delta z_k + \Delta z_{k+1}} - \frac{w_{i,n}^0 - w_{i-1,n}^0}{\Delta\chi_{i-1} + \Delta\chi_i} - \frac{w_{i,n}^R - w_{i-1,n}^R}{\Delta\chi_{i-1} + \Delta\chi_i}\right\} \\
&\qquad + \chi_\ell \frac{\Delta z_k u_{\ell,k}^0 + \Delta z_{k+1} u_{\ell,k+1}^0}{\Delta z_k + \Delta z_{k+1}} \\
&\qquad \left.\left\{\frac{u_{\ell,k+1}^R - u_{\ell,k}^R}{\Delta z_k + \Delta z_{k+1}} - \frac{w_{i+1,n}^0 - w_{i,n}^0}{\Delta\chi_{i+1} + \Delta\chi_i} - \frac{w_{i+1,n}^R - w_{i,n}^R}{\Delta\chi_{i+1} + \Delta\chi_i}\right\}\right] \\
&+ \frac{R_S}{\chi_i^2}\left[\chi_{\ell-1}\left\{\frac{u_{\ell-1,k+1}^0 - u_{\ell-1,k}^0}{\Delta z_k + \Delta z_{k+1}} - \frac{w_{i,n}^0 - w_{i-1,n}^0}{\Delta\chi_{i-1} + \Delta\chi_i}\right\} \frac{\Delta z_k u_{\ell-1,k}^0 + \Delta z_{k+1} u_{\ell-1,k+1}^0}{\Delta z_k + \Delta z_{k+1}}\right. \\
&\qquad \left. + \chi_\ell\left\{\frac{u_{\ell,k+1}^0 - u_{\ell,k}^0}{\Delta z_k + \Delta z_{k+1}} - \frac{w_{i+1,n}^0 - w_{i,n}^0}{\Delta\chi_{i+1} + \Delta\chi_i}\right\} \frac{\Delta z_k u_{\ell,k}^0 + \Delta z_{k+1} u_{\ell,k+1}^0}{\Delta z_k + \Delta z_{k+1}}\right] \\
&- \frac{R_S}{\chi_i}\left[\left\{\frac{u_{\ell-1,k+1}^0 - u_{\ell-1,k}^0}{\Delta z_k + \Delta z_{k+1}} - \frac{w_{i,n}^0 - w_{i-1,n}^0}{\Delta\chi_{i-1} + \Delta\chi_i}\right\} \frac{\Delta z_k u_{\ell-1,k}^0 + \Delta z_{k+1} u_{\ell-1,k+1}^0}{\Delta z_k + \Delta z_{k+1}}\right. \\
&\qquad \left. + \left\{\frac{u_{\ell,k+1}^0 - u_{\ell,k}^0}{\Delta z_k + \Delta z_{k+1}} - \frac{w_{i+1,n}^0 - w_{i,n}^0}{\Delta\chi_{i+1} + \Delta\chi_i}\right\} \frac{\Delta z_k u_{\ell,k}^0 + \Delta z_{k+1} u_{\ell,k+1}^0}{\Delta z_k + \Delta z_{k+1}}\right]
\end{aligned}
\tag{3.78}
$$

$$
\begin{aligned}
N_z^R(\vec{u}) = & -2\frac{v^0_{i,k+1}-v^0_{i,k}}{\Delta z_k+\Delta z_{k+1}}\,\frac{\Delta z_k v^R_{i,k}+\Delta z_{k+1}v^R_{i,k+1}}{\Delta z_k+\Delta z_{k+1}} \\
& -\left[\frac{1}{\chi_i}\,w^I_{i,n}+2\,\frac{v^R_{i,k+1}-v^R_{i,k}}{\Delta z_k+\Delta z_{k+1}}\right]\frac{\Delta z_k v^0_{i,k}+\Delta z_{k+1}v^0_{i,k+1}}{\Delta z_k+\Delta z_{k+1}} \\
& -\frac{1}{\chi_i}\left[\chi_{\ell-1}\left\{\frac{u^0_{\ell-1,k+1}-u^0_{\ell-1,k}}{\Delta z_k+\Delta z_{k+1}}-\frac{w^0_{i,n}-w^0_{i-1,n}}{\Delta\chi_{i-1}+\Delta\chi_i}\right\}\frac{\Delta z_k u^R_{\ell-1,k}+\Delta z_{k+1}u^R_{\ell-1,k+1}}{\Delta z_k+\Delta z_{k+1}}\right. \\
& \qquad \left.+\chi_\ell\left\{\frac{u^0_{\ell,k+1}-u^0_{\ell,k}}{\Delta z_k+\Delta z_{k+1}}-\frac{w^0_{i+1,n}-w^0_{i,n}}{\Delta\chi_{i+1}+\Delta\chi_i}\right\}\frac{\Delta z_k u^R_{\ell,k}+\Delta z_{k+1}u^R_{\ell,k+1}}{\Delta z_k+\Delta z_{k+1}}\right] \\
& -\frac{1}{\chi_i}\left[\chi_{\ell-1}\frac{\Delta z_k u^0_{\ell-1,k}+\Delta z_{k+1}u^0_{\ell-1,k+1}}{\Delta z_k+\Delta z_{k+1}}\right. \\
& \qquad \left.\left\{\frac{u^R_{\ell-1,k+1}-u^R_{\ell-1,k}}{\Delta z_k+\Delta z_{k+1}}-\frac{w^0_{i,n}-w^0_{i-1,n}}{\Delta\chi_{i-1}+\Delta\chi_i}-\frac{w^R_{i,n}-w^R_{i-1,n}}{\Delta\chi_{i-1}+\Delta\chi_i}\right\}\right. \\
& \qquad +\chi_\ell\frac{\Delta z_k u^0_{\ell,k}+\Delta z_{k+1}u^0_{\ell,k+1}}{\Delta z_k+\Delta z_{k+1}} \\
& \qquad \left.\left.\left\{\frac{u^R_{\ell,k+1}-u^R_{\ell,k}}{\Delta z_k+\Delta z_{k+1}}-\frac{w^0_{i+1,n}-w^0_{i,n}}{\Delta\chi_{i+1}+\Delta\chi_i}-\frac{w^R_{i+1,n}-w^R_{i,n}}{\Delta\chi_{i+1}+\Delta\chi_i}\right\}\right]\right. \\
& +\frac{R_S}{\chi_i^2}\left[\chi_{\ell-1}\left\{\frac{u^0_{\ell-1,k+1}-u^0_{\ell-1,k}}{\Delta z_k+\Delta z_{k+1}}-\frac{w^0_{i,n}-w^0_{i-1,n}}{\Delta\chi_{i-1}+\Delta\chi_i}\right\}\frac{\Delta z_k u^0_{\ell-1,k}+\Delta z_{k+1}u^0_{\ell-1,k+1}}{\Delta z_k+\Delta z_{k+1}}\right. \\
& \qquad \left.+\chi_\ell\left\{\frac{u^0_{\ell,k+1}-u^0_{\ell,k}}{\Delta z_k+\Delta z_{k+1}}-\frac{w^0_{i+1,n}-w^0_{i,n}}{\Delta\chi_{i+1}+\Delta\chi_i}\right\}\frac{\Delta z_k u^0_{\ell,k}+\Delta z_{k+1}u^0_{\ell,k+1}}{\Delta z_k+\Delta z_{k+1}}\right] \\
& -\frac{R_S}{\chi_i}\left[\left\{\frac{u^0_{\ell-1,k+1}-u^0_{\ell-1,k}}{\Delta z_k+\Delta z_{k+1}}-\frac{w^0_{i,n}-w^0_{i-1,n}}{\Delta\chi_{i-1}+\Delta\chi_i}\right\}\frac{\Delta z_k u^0_{\ell-1,k}+\Delta z_{k+1}u^0_{\ell-1,k+1}}{\Delta z_k+\Delta z_{k+1}}\right. \\
& \qquad \left.+\left\{\frac{u^0_{\ell,k+1}-u^0_{\ell,k}}{\Delta z_k+\Delta z_{k+1}}-\frac{w^0_{i+1,n}-w^0_{i,n}}{\Delta\chi_{i+1}+\Delta\chi_i}\right\}\frac{\Delta z_k u^0_{\ell,k}+\Delta z_{k+1}u^0_{\ell,k+1}}{\Delta z_k+\Delta z_{k+1}}\right]
\end{aligned}
\tag{3.79}
$$

3.6.7 Discrete Convection, Imaginary First Order: $N^I(\vec{u},\vec{\omega}) = (\nabla \times \vec{u}) \times \vec{u}$

$$
\begin{aligned}
N^I_\chi(\vec{u}) = &\frac{1}{2}\left[\omega^0_{\ell,n-1}\,\frac{\Delta\chi_i w^I_{i,n-1} + \Delta\chi_{i+1} w^I_{i+1,n-1}}{\Delta\chi_i + \Delta\chi_{i+1}} + \omega^I_{\ell,n-1}\,\frac{\Delta\chi_i w^0_{i,n-1} + \Delta\chi_{i+1} w^0_{i+1,n-1}}{\Delta\chi_i + \Delta\chi_{i+1}}\right.\\
&\left. + \omega^0_{\ell,n}\,\frac{\Delta\chi_i w^I_{i,n} + \Delta\chi_{i+1} w^I_{i+1,n}}{\Delta\chi_i + \Delta\chi_{i+1}} + \omega^I_{\ell,n}\,\frac{\Delta\chi_i w^0_{i,n} + \Delta\chi_{i+1} w^0_{i+1,n}}{\Delta\chi_i + \Delta\chi_{i+1}}\right]\\
&- \frac{\chi_i + \chi_{i+1}}{4}\left[\zeta^0_{\ell,k}\left(\frac{v^I_{i,k}}{\chi_i} + \frac{v^I_{i+1,k}}{\chi_{i+1}}\right) + \zeta^I_{\ell,k}\left(\frac{v^0_{i,k}}{\chi_i} + \frac{v^0_{i+1,k}}{\chi_{i+1}}\right)\right]
\end{aligned}
\tag{3.80}
$$

$$
\begin{aligned}
N^I_\chi(\vec{u}) = &\left(\frac{u^0_{\ell,k} - u^0_{\ell,k-1}}{\Delta z_k + \Delta z_{k-1}} - \frac{w^0_{i+1,n-1} - w^0_{i,n-1}}{\Delta\chi_{i+1} + \Delta\chi_i}\right)\frac{\Delta\chi_i w^I_{i,n-1} + \Delta\chi_{i+1} w^I_{i+1,n-1}}{\Delta\chi_i + \Delta\chi_{i+1}}\\
&-\left(\frac{u^I_{\ell,k} - u^I_{\ell,k-1}}{\Delta z_k + \Delta z_{k-1}} - \frac{w^I_{i+1,n-1} - w^I_{i,n-1}}{\Delta\chi_{i+1} + \Delta\chi_i}\right)\frac{\Delta\chi_i w^0_{i,n-1} + \Delta\chi_{i+1} w^0_{i+1,n-1}}{\Delta\chi_i + \Delta\chi_{i+1}}\\
&+\left(\frac{u^0_{\ell,k+1} - u^0_{\ell,k}}{\Delta z_k + \Delta z_{k+1}} - \frac{w^0_{i+1,n} - w^0_{i,n}}{\Delta\chi_{i+1} + \Delta\chi_i}\right)\frac{\Delta\chi_i w^I_{i,n} + \Delta\chi_{i+1} w^I_{i+1,n}}{\Delta\chi_i + \Delta\chi_{i+1}}\\
&-\left(\frac{u^I_{\ell,k+1} - u^I_{\ell,k}}{\Delta z_k + \Delta z_{k+1}} - \frac{w^I_{i+1,n} - w^I_{i,n}}{\Delta\chi_{i+1} + \Delta\chi_i}\right)\frac{\Delta\chi_i w^0_{i,n} + \Delta\chi_{i+1} w^0_{i+1,n}}{\Delta\chi_i + \Delta\chi_{i+1}}\\
&- \frac{\chi_i + \chi_{i+1}}{4}\left[\frac{4}{\chi_{i+1} + \chi_i}\frac{\chi_{i+1} v^0_{i+1,k} - \chi_i v^0_{i,k}}{\Delta\chi_i + \Delta\chi_{i+1}}\left(\frac{v^I_{i,k}}{\chi_i} + \frac{v^I_{i+1,k}}{\chi_{i+1}}\right)\right.\\
&+\left(\frac{v^0_{i,k}}{\chi_i} + \frac{v^0_{i+1,k}}{\chi_{i+1}}\right)\left\{-\frac{4}{\chi_{i+1} + \chi_i}\frac{\chi_{i+1} v^I_{i+1,k} - \chi_i v^I_{i,k}}{\Delta\chi_i + \Delta\chi_{i+1}}\right.\\
&\left.\left.\left.-2\frac{1}{\chi_{i+1} + \chi_i}\left(-u^R_{\ell,k} + \frac{(R_S - \chi_{\ell+1})\,u^0_{\ell+1,k} - (R_S - \chi_{\ell-1})\,u^0_{\ell-1,k}}{\Delta\chi_i + \Delta\chi_{i+1}}\right)\right\}\right]
\end{aligned}
\tag{3.81}
$$

$$
\begin{aligned}
N^I_\chi(\vec{u}) = &\left(\frac{u^0_{\ell,k} - u^0_{\ell,k-1}}{\Delta z_k + \Delta z_{k-1}} - \frac{w^0_{i+1,n-1} - w^0_{i,n-1}}{\Delta\chi_{i+1} + \Delta\chi_i}\right)\frac{\Delta\chi_i w^I_{i,n-1} + \Delta\chi_{i+1} w^I_{i+1,n-1}}{\Delta\chi_i + \Delta\chi_{i+1}}\\
&-\left(\frac{u^I_{\ell,k} - u^I_{\ell,k-1}}{\Delta z_k + \Delta z_{k-1}} - \frac{w^I_{i+1,n-1} - w^I_{i,n-1}}{\Delta\chi_{i+1} + \Delta\chi_i}\right)\frac{\Delta\chi_i w^0_{i,n-1} + \Delta\chi_{i+1} w^0_{i+1,n-1}}{\Delta\chi_i + \Delta\chi_{i+1}}\\
&+\left(\frac{u^0_{\ell,k+1} - u^0_{\ell,k}}{\Delta z_k + \Delta z_{k+1}} - \frac{w^0_{i+1,n} - w^0_{i,n}}{\Delta\chi_{i+1} + \Delta\chi_i}\right)\frac{\Delta\chi_i w^I_{i,n} + \Delta\chi_{i+1} w^I_{i+1,n}}{\Delta\chi_i + \Delta\chi_{i+1}}\\
&-\left(\frac{u^I_{\ell,k+1} - u^I_{\ell,k}}{\Delta z_k + \Delta z_{k+1}} - \frac{w^I_{i+1,n} - w^I_{i,n}}{\Delta\chi_{i+1} + \Delta\chi_i}\right)\frac{\Delta\chi_i w^0_{i,n} + \Delta\chi_{i+1} w^0_{i+1,n}}{\Delta\chi_i + \Delta\chi_{i+1}}\\
&-\left[\frac{\chi_{i+1} v^0_{i+1,k} - \chi_i v^0_{i,k}}{\Delta\chi_i + \Delta\chi_{i+1}}\left(\frac{v^I_{i,k}}{\chi_i} + \frac{v^I_{i+1,k}}{\chi_{i+1}}\right) - \left(\frac{v^0_{i,k}}{\chi_i} + \frac{v^0_{i+1,k}}{\chi_{i+1}}\right)\frac{\chi_{i+1} v^I_{i+1,k} - \chi_i v^I_{i,k}}{\Delta\chi_i + \Delta\chi_{i+1}}\right.\\
&\left.+\frac{1}{2}\left(\frac{v^0_{i,k}}{\chi_i} + \frac{v^0_{i+1,k}}{\chi_{i+1}}\right)\left(+u^R_{\ell,k} - \frac{(R_S - \chi_{\ell+1})\,u^0_{\ell+1,k} - (R_S - \chi_{\ell-1})\,u^0_{\ell-1,k}}{\Delta\chi_i + \Delta\chi_{i+1}}\right)\right]
\end{aligned}
\tag{3.82}
$$

$$
\begin{aligned}
N_\theta^I(\vec{u}) = & \frac{1}{2\Delta\chi_i}\frac{1}{\chi_i^2}\left(\chi_{\ell-1}\frac{\chi_i+\chi_{i-1}}{2}\frac{\Delta\chi_{i-1}+\Delta\chi_i}{2}\left\{\zeta^0_{\ell-1,k}\,u^I_{\ell-1,k}+\zeta^I_{\ell-1,k}\,u^0_{\ell-1,k}\right\}\right.\\
& \left.+\chi_\ell\frac{\chi_i+\chi_{i+1}}{2}\frac{\Delta\chi_{i+1}+\Delta\chi_i}{2}\left\{\zeta^0_{\ell,k}\,u^I_{\ell,k}+\zeta^I_{\ell,k}\,u^0_{\ell,k}\right\}\right)\\
& -\frac{1}{2}\left\{\eta^0_{i,n-1}\,w^I_{i,n-1}+\eta^I_{i,n-1}\,w^0_{i,n-1}+\eta^0_{i,n}\,w^I_{i,n}+\eta^I_{i,n}\,w^0_{i,n}\right\}
\end{aligned}
\tag{3.83}
$$

$$
\begin{aligned}
N_\theta^I(\vec{u}) = & \frac{1}{2\Delta\chi_i}\frac{1}{\chi_i^2}\left(\chi_{\ell-1}\frac{\chi_i+\chi_{i-1}}{2}\frac{\Delta\chi_{i-1}+\Delta\chi_i}{2}\right.\\
& \left\{\frac{4}{\chi_{i-1}+\chi_i}\frac{\chi_i v^0_{i,k}-\chi_{i-1}v^0_{i-1,k}}{\Delta\chi_i+\Delta\chi_{i-1}}\,u^I_{\ell-1,k}\right.\\
& +u^0_{\ell-1,k}\left[-\frac{4}{\chi_{i-1}+\chi_i}\frac{\chi_i v^I_{i,k}-\chi_{i-1}v^I_{i-1,k}}{\Delta\chi_i+\Delta\chi_{i-1}}\right.\\
& \left.\left.\left.-2\frac{1}{\chi_{i-1}+\chi_i}\left(-u^R_{\ell-1,k}+\frac{(R_S-\chi_\ell)\,u^0_{\ell,k}-(R_S-\chi_{\ell-2})\,u^0_{\ell-2,k}}{\Delta\chi_i+\Delta\chi_{i-1}}\right)\right]\right\}\right.\\
& +\chi_\ell\frac{\chi_i+\chi_{i+1}}{2}\frac{\Delta\chi_{i+1}+\Delta\chi_i}{2}\\
& \left\{\frac{4}{\chi_{i+1}+\chi_i}\frac{\chi_{i+1}v^0_{i+1,k}-\chi_i v^0_{i,k}}{\Delta\chi_i+\Delta\chi_{i+1}}\,u^I_{\ell,k}\right.\\
& +u^0_{\ell,k}\left[-\frac{4}{\chi_{i+1}+\chi_i}\frac{\chi_{i+1}v^I_{i+1,k}-\chi_i v^I_{i,k}}{\Delta\chi_i+\Delta\chi_{i+1}}\right.\\
& \left.\left.\left.\left.-2\frac{1}{\chi_{i+1}+\chi_i}\left(-u^R_{\ell,k}+\frac{(R_S-\chi_{\ell+1})\,u^0_{\ell+1,k}-(R_S-\chi_{\ell-1})\,u^0_{\ell-1,k}}{\Delta\chi_i+\Delta\chi_{i+1}}\right)\right]\right\}\right)\\
& -\frac{1}{2}\left\{-2\frac{v^0_{i,k}-v^0_{i,k-1}}{\Delta z_k+\Delta z_{k-1}}\,w^I_{i,n-1}\right.\\
& +\left[-\frac{1}{\chi_i}w^R_{i,n-1}+2\frac{v^I_{i,k}-v^I_{i,k-1}}{\Delta z_k+\Delta z_{k-1}}\right.\\
& \left.\left.+\frac{2}{\chi_i\Delta\chi_i}\left(\frac{\Delta\chi_{i+1}\,(R_S-\chi_{i+1})\,w^0_{i+1,n-1}}{\Delta\chi_i+2\Delta\chi_{i+1}+\Delta\chi_{i+2}}-\frac{\Delta\chi_{i-1}\,(R_S-\chi_{i-1})\,w^0_{i-1,n-1}}{\Delta\chi_{i-2}+2\Delta\chi_{i-1}+\Delta\chi_i}\right)\right]w^0_{i,n-1}\right.\\
& -2\frac{v^0_{i,k+1}-v^0_{i,k}}{\Delta z_k+\Delta z_{k+1}}\,w^I_{i,n}\\
& +\left[-\frac{1}{\chi_i}w^R_{i,n}+2\frac{v^I_{i,k+1}-v^I_{i,k}}{\Delta z_k+\Delta z_{k+1}}\right.\\
& \left.\left.\left.+\frac{2}{\chi_i\Delta\chi_i}\left(\frac{\Delta\chi_{i+1}\,(R_S-\chi_{i+1})\,w^0_{i+1,n}}{\Delta\chi_i+2\Delta\chi_{i+1}+\Delta\chi_{i+2}}-\frac{\Delta\chi_{i-1}\,(R_S-\chi_{i-1})\,w^0_{i-1,n}}{\Delta\chi_{i-2}+2\Delta\chi_{i-1}+\Delta\chi_i}\right)\right]w^0_{i,n}\right\}
\end{aligned}
\tag{3.84}
$$

$$
\begin{aligned}
N_\theta^I(\vec{u}) =& \frac{1}{2\Delta\chi_i}\frac{1}{\chi_i^2}\chi_{\ell-1}\left\{\left(\chi_i v_{i,k}^0 - \chi_{i-1}v_{i-1,k}^0\right) u_{\ell-1,k}^I \right.\\
&+ u_{\ell-1,k}^0\left[-\left(\chi_i v_{i,k}^I - \chi_{i-1}v_{i-1,k}^I\right)\right.\\
&\left.\left.-\frac{1}{2}\left(-\left[\Delta\chi_i + \Delta\chi_{i-1}\right] u_{\ell-1,k}^R + \left(R_S - \chi_\ell\right)u_{\ell,k}^0 - \left(R_S - \chi_{\ell-2}\right)u_{\ell-2,k}^0\right)\right]\right\}\\
&+ \frac{1}{2\Delta\chi_i}\frac{1}{\chi_i^2}\chi_\ell\left\{\left(\chi_{i+1}v_{i+1,k}^0 - \chi_i v_{i,k}^0\right) u_{\ell,k}^I\right.\\
&+ u_{\ell,k}^0\left[-\left(\chi_{i+1}v_{i+1,k}^I - \chi_i v_{i,k}^I\right)\right.\\
&\left.\left.-\frac{1}{2}\left(-\left[\Delta\chi_i + \Delta\chi_{i+1}\right] u_{\ell,k}^R + \left(R_S - \chi_{\ell+1}\right)u_{\ell+1,k}^0 - \left(R_S - \chi_{\ell-1}\right)u_{\ell-1,k}^0\right)\right]\right\}\\
&+ \frac{v_{i,k}^0 - v_{i,k-1}^0}{\Delta z_k + \Delta z_{k-1}} w_{i,n-1}^I + \frac{v_{i,k+1}^0 - v_{i,k}^0}{\Delta z_k + \Delta z_{k+1}} w_{i,n}^I\\
&- \left[-\frac{1}{2\chi_i} w_{i,n-1}^R + \frac{v_{i,k}^I - v_{i,k-1}^I}{\Delta z_k + \Delta z_{k-1}}\right.\\
&\left.+\frac{1}{\chi_i\Delta\chi_i}\left(\frac{\Delta\chi_{i+1}\left(R_S - \chi_{i+1}\right)w_{i+1,n-1}^0}{\Delta\chi_i + 2\Delta\chi_{i+1} + \Delta\chi_{i+2}} - \frac{\Delta\chi_{i-1}\left(R_S - \chi_{i-1}\right)w_{i-1,n-1}^0}{\Delta\chi_{i-2} + 2\Delta\chi_{i-1} + \Delta\chi_i}\right)\right] w_{i,n-1}^0\\
&- \left[-\frac{1}{2\chi_i} w_{i,n}^R + \frac{v_{i,k+1}^I - v_{i,k}^I}{\Delta z_k + \Delta z_{k+1}}\right.\\
&\left.+\frac{1}{\chi_i\Delta\chi_i}\left(\frac{\Delta\chi_{i+1}\left(R_S - \chi_{i+1}\right)w_{i+1,n}^0}{\Delta\chi_i + 2\Delta\chi_{i+1} + \Delta\chi_{i+2}} - \frac{\Delta\chi_{i-1}\left(R_S - \chi_{i-1}\right)w_{i-1,n}^0}{\Delta\chi_{i-2} + 2\Delta\chi_{i-1} + \Delta\chi_i}\right)\right] w_{i,n}^0
\end{aligned}
\tag{3.85}
$$

$$
\begin{aligned}
N_z^I(\vec{u}) = & \left(\eta_{i,n}^0 \frac{\Delta z_k v_{i,k}^I + \Delta z_{k+1} v_{i,k+1}^I}{\Delta z_k + \Delta z_{k+1}} + \eta_{i,n}^I \frac{\Delta z_k v_{i,k}^0 + \Delta z_{k+1} v_{i,k+1}^0}{\Delta z_k + \Delta z_{k+1}} \right) \\
& - \frac{1}{2}\frac{1}{\chi_i}\left[\chi_{\ell-1}\omega_{\ell-1,n}^0 \frac{\Delta z_k u_{\ell-1,k}^I + \Delta z_{k+1} u_{\ell-1,k+1}^I}{\Delta z_k + \Delta z_{k+1}} + \chi_\ell \omega_{\ell,n}^0 \frac{\Delta z_k u_{\ell,k}^I + \Delta z_{k+1} u_{\ell,k+1}^I}{\Delta z_k + \Delta z_{k+1}} \right] \\
& - \frac{1}{2}\frac{1}{\chi_i}\left[\chi_{\ell-1}\omega_{\ell-1,n}^I \frac{\Delta z_k u_{\ell-1,k}^0 + \Delta z_{k+1} u_{\ell-1,k+1}^0}{\Delta z_k + \Delta z_{k+1}} + \chi_\ell \omega_{\ell,n}^I \frac{\Delta z_k u_{\ell,k}^0 + \Delta z_{k+1} u_{\ell,k+1}^0}{\Delta z_k + \Delta z_{k+1}} \right]
\end{aligned}
\tag{3.86}
$$

$$
\begin{aligned}
N_z^I(\vec{u}) = & -2\frac{v_{i,k+1}^0 - v_{i,k}^0}{\Delta z_k + \Delta z_{k+1}} \frac{\Delta z_k v_{i,k}^I + \Delta z_{k+1} v_{i,k+1}^I}{\Delta z_k + \Delta z_{k+1}} \\
& + \frac{\Delta z_k v_{i,k}^0 + \Delta z_{k+1} v_{i,k+1}^0}{\Delta z_k + \Delta z_{k+1}} \left\{ -\frac{1}{\chi_i} w_{i,n}^R + 2 \frac{v_{i,k+1}^I - v_{i,k}^I}{\Delta z_k + \Delta z_{k+1}} \right. \\
& \qquad \left. + \frac{2}{\chi_i \Delta\chi_i}\left[\frac{\Delta\chi_{i+1}(R_S - \chi_{i+1}) w_{i+1,n}^0}{\Delta\chi_i + 2\Delta\chi_{i+1} + \Delta\chi_{i+2}} - \frac{\Delta\chi_{i-1}(R_S - \chi_{i-1}) w_{i-1,n}^0}{\Delta\chi_{i-2} + 2\Delta\chi_{i-1} + \Delta\chi_i} \right] \right\} \\
& - \frac{1}{\chi_i}\left[\chi_{\ell-1} \frac{\Delta z_k u_{\ell-1,k}^I + \Delta z_{k+1} u_{\ell-1,k+1}^I}{\Delta z_k + \Delta z_{k+1}} \left(\frac{u_{\ell-1,k+1}^0 - u_{\ell-1,k}^0}{\Delta z_k + \Delta z_{k+1}} - \frac{w_{i,n}^0 - w_{i-1,n}^0}{\Delta\chi_{i-1} + \Delta\chi_i} \right) \right. \\
& \qquad \left. + \chi_\ell \frac{\Delta z_k u_{\ell,k}^I + \Delta z_{k+1} u_{\ell,k+1}^I}{\Delta z_k + \Delta z_{k+1}} \left(\frac{u_{\ell,k+1}^0 - u_{\ell,k}^0}{\Delta z_k + \Delta z_{k+1}} - \frac{w_{i+1,n}^0 - w_{i,n}^0}{\Delta\chi_{i+1} + \Delta\chi_i} \right) \right] \\
& + \frac{1}{\chi_i}\left[\chi_{\ell-1} \frac{\Delta z_k u_{\ell-1,k}^0 + \Delta z_{k+1} u_{\ell-1,k+1}^0}{\Delta z_k + \Delta z_{k+1}} \left(\frac{u_{\ell-1,k+1}^I - u_{\ell-1,k}^I}{\Delta z_k + \Delta z_{k+1}} - \frac{w_{i,n}^I - w_{i-1,n}^I}{\Delta\chi_{i-1} + \Delta\chi_i} \right) \right. \\
& \qquad \left. + \chi_\ell \frac{\Delta z_k u_{\ell,k}^0 + \Delta z_{k+1} u_{\ell,k+1}^0}{\Delta z_k + \Delta z_{k+1}} \left(\frac{u_{\ell,k+1}^I - u_{\ell,k}^I}{\Delta z_k + \Delta z_{k+1}} - \frac{w_{i+1,n}^I - w_{i,n}^I}{\Delta\chi_{i+1} + \Delta\chi_i} \right) \right]
\end{aligned}
\tag{3.87}
$$

3.7 Boundary Conditions of Smooth Annular Pressure Seals

The Navier-Stokes momentum equations are second order PDE's requiring two boundary conditions for each coordinate dimension. No boundary needs to be specified in the circumferential direction as that coordinate dimension is removed through application of the small whirl orbit perturbation solution around an axisymmetric solution for a concentric rotor. Also absent is the need for axial ghost cell boundary conditions for pressure, as pressure is obtained implicitly from the momentum and mass conservation equations. A radial boundary condition for pressure is necessary due to the circumferential pressure gradient's radial dependence in the perturbed coordinate system. This radial, zeroth order, pressure boundary condition is assigned for a standard no slip wall as Neumann zero gradient conditions on the Rotor and Stator surfaces. Additionally, the pressure solution results in a gauge pressure that must be set relative to the absolute pressure of the surroundings by selecting a single mass conservation equation for a cell on the seal outlet boundary and replacing it with a direct asssignment of that cell's pressure to the reference value, typically zero for convenience.

The basic seal geometry parameters and boundary conditions for each flow variable are given in Table 3.1. The velocity boundary conditions are specified for the zeroth order, concentric solution, and the real and imaginary components of the first order perturbation solutions. Considering the second order PDE's being solved, 6 velocity boundaries must be defined for each velocity component. Beginning with the zeroth order solution, an annular seal's operating conditions are usually defined with a pressure differential, ΔP; a pre-swirl circumferential velocity ratio on the inlet PR; and a rotor rotational speed specified by revolutions per minute, RPM, or as the rotor surface speed. The radial velocity on the inlet is assumed to be zero without any knowledge of upstream conditions. Without the axial pressure boundary conditions allowed by solving the pressure Poisson Equation (PPE), the inflow to the seal must be defined by an inlet axial velocity w_W and a specified circumferential velocity on the inlet, v_W. To match a given pressure differential, an initial axial inlet velocity is guessed and a pressure profile is solved. The inlet axial velocity is then iterated by Brent's Method[149,150] to match the desired pressure differential. The Brent's method is an optimization algorithm to obtain zeros of a continuous objective function by combining three other methods: the bisection method,[151] the secand method,[152] and inverse quadratic interpolation.[153,154] The

algorithm switches between the individual methods to either increase speed or robustness of convergence. The exit velocity conditions are defined as Neumann boundaries with zero value to allow for flow profiles that are not fully developed. The Rotor and Stator boundaries are defined with Dirichlet conditions of zero value due to a no-slip wall.

Table 3.1: Seal Defining Variables and Boundary Conditions

Variable	**Symbol**	$0^{\mathbf{th}}$ **Order**	**Real** $1^{\mathbf{st}}$ **Ord.**	**Imag.** $1^{\mathbf{st}}$ **Ord.**
Length	L_S	L_S	-	-
Clearance	H^0	H^0	-	-
Eccentricity	H^1	-	H^1	H^1
Radius	R_S	R_S	-	-
Viscosity	μ	μ	-	-
Density	ρ	ρ	-	-
Pre-Swirl	Pr	$\frac{v_W}{R\omega}$	-	-
Rotor Speed	ω	ω	-	-
Whirl Speed	Ω	-	Ω	Ω
Radial Vel.	u_W	$u_W^0 = 0$	$u_W^R = 0$	$u_W^I = 0$
	u_E	$\frac{\partial u_E^0}{\partial z} = 0$	$u_E^R = 0$	$u_E^I = 0$
	u_S	$u_S^0 = 0$	$u_S^R = 0$	$u_S^I = (\Omega - \omega) H^0$
	u_N	$u_N^0 = 0$	$u_N^R = 0$	$u_N^I = 0$
Angular Vel.	v_W	$\frac{\partial v_W^0}{\partial z} = 0$ **OR** v_W^0	$\frac{\partial v_W^R}{\partial z} = 0$	$\frac{\partial v_W^I}{\partial z} = 0$
	v_E	$\frac{\partial v_E^0}{\partial z} = 0$	$\frac{\partial v_E^R}{\partial z} = 0$	$\frac{\partial v_E^I}{\partial z} = 0$
	v_S	$v_S^0 = \omega R_S$	$v_S^R = 0$	$v_S^I = \Omega H^0$
	v_N	$v_N^0 = 0$	$v_N^R = 0$	$v_N^I = 0$
Axial Vel.	w_W	$w_W^0 = f(\Delta P, \xi_{In})$	$w_W^R = f(P_W^R, \xi_{In})$	$w_W^I = f(P_W^I, \xi_{In})$
	w_E	$\frac{\partial w_E^0}{\partial z} = 0$	$w_E^R = f(P_E^R, \xi_{Out})$	$w_E^I = f(P_E^I, \xi_{Out})$
	w_S	$w_S^0 = 0$	$w_S^R = 0$	$w_S^I = 0$
	w_N	$w_N^0 = 0$	$w_N^R = 0$	$w_N^I = 0$
Press. Diff.	ΔP	ΔP^0	-	-
		$f\left(w_W^0, \zeta_{In}, \zeta_{Out}\right)$	-	-
Ref. Press.	P_{REF}	P_{REF}	-	-
TKE	k_W	$\frac{\partial k_W}{\partial z} = 0$	-	-
	k_E	$\frac{\partial k_E}{\partial z} = 0$	-	-
	k_S	$\frac{\partial k_S}{\partial \chi} = 0$	-	-
	k_N	$\frac{\partial k_N}{\partial \chi} = 0$	-	-

The boundary conditions are derived from the physical system and the definition of the coordinate system. Remember that the coordinate system has been perturbed from R to χ by a small circular orbit at Ω whirl frequency.

$$h = \frac{H^1}{H^0} = \frac{Eccentricity}{Clearance} \tag{3.88}$$

$$\varepsilon = \epsilon e^{i(\Omega t+\theta)} \tag{3.89}$$

$$r = \chi + \varepsilon h\left(R_S - \chi\right) \tag{3.90}$$

$$r = \chi + h\left(\cos\theta + i\sin\theta\right)\left(R_S - \chi\right) \tag{3.91}$$

At $\theta = 0$ the sine term disappears and the cosine term becomes 1. If we further assume that we are at the χ_{Rotor} modified radial coordinate that is equal to the shaft radius, then the equivalent radial coordinate in classical cylindrical coordinates becomes the following:

$$r_{Rotor} = \chi_{Rotor} + h\left(R_S - \chi_{Rotor}\right) = \chi_{Rotor} + hH^0 = \chi_{Rotor} + H^1 \tag{3.92}$$

This indicates that the real world radial position at $\theta = 0$ is shaft radius + eccentricity. As the coordinate transformation is based on a stator surface that is fixed in both modified and original cylindrical coordinates, this means that the clearance gap is smallest at $\theta = 0$.

The surface of the rotor can be defined with the following polar complex forms. The rotor surface speed is related to the variable ω which is given in hz or RPM. Similarly, the whirl speed is defined using the variable Ω in the same units. Using complex polar coordinates, the vector that defines a point on the rotor surface can be defined as follows:

$$\vec{r}_{RotorSurface} = R_{Rotor}e^{i(\omega t+\theta_0)} + H^0\frac{H^1}{H^0}e^{i(\Omega t+\theta_0)} \tag{3.93}$$

In order to combine the terms for these two rotations, whirling motion must be modified by adding and subtracting the shaft rotation for a net zero change.

$$\vec{r}_{RotorSurface} = R_{Rotor}e^{i(\omega t+\theta_0)} + H^0\frac{H^1}{H^0}e^{i\{\Omega t-\omega t+\omega t+\theta_0\}} \tag{3.94}$$

$$\vec{r}_{RotorSurface} = R_{Rotor}e^{i(\omega t+\theta_0)} + H^0\frac{H^1}{H^0}e^{i\{(\Omega-\omega)t\}}e^{i(\omega t+\theta_0)} \tag{3.95}$$

The following equation describes the actual position of the rotor surface relative to its own center in the bracketed term and the surface rotation in the rightmost term.

$$\vec{r}_{RotorSurface} = \left[R_{Rotor} + H^0 \frac{H^1}{H^0} e^{i\{(\Omega-\omega)t\}} \right] e^{i(\omega t+\theta_0)} \tag{3.96}$$

The radial velocity of the rotor surface can then be calculated as the time derivative of the bracketed term in the previous equation.

$$\frac{\partial}{\partial t} RadialMagnitude = \frac{\partial}{\partial t} \left[R_{Rotor} + H^0 \frac{H^1}{H^0} e^{i\{(\Omega-\omega)t\}} \right] \tag{3.97}$$

$$u_{Rotor} = i\,(\Omega-\omega)\,H^0 \frac{H^1}{H^0} e^{i\{(\Omega-\omega)t\}} \tag{3.98}$$

The linear angular velocity is the derivative of each exponential term with respect to time and re-multiplied by their respective radii.

$$\frac{\partial}{\partial t}\vec{r}_{RotorSurface} = \frac{\partial}{\partial t} \left[R_{Rotor} e^{i(\omega t+\theta_0)} + H^0 \frac{H^1}{H^0} e^{i(\Omega t+\theta_0)} \right] \tag{3.99}$$

$$v_{Rotor} = \omega R_{Rotor} e^{i(\omega t+\theta_0)} + \Omega H^0 \frac{H^1}{H^0} i e^{i(\Omega t+\theta_0)} \tag{3.100}$$

The pressure difference increases or decreases based on flow curvature leading into the seal clearance or exiting from the clearance region. This is often approximated based on some empirical factors that modify the pressure differential by a ratio of the equivalent Bernoulli stagnation pressure corresponding to either the velocity through the seal clearance or a function of seal clearance velocity and upstream or downstream velocities.

$$\Delta P^0_{Combined} = \Delta P^0_{Loss,Inlet} + \Delta P^0_{Seal} - \Delta P^0_{Recovery,Outlet} \tag{3.101a}$$

$$\Delta P^0_{Loss,Inlet} = \frac{1+\zeta_{Inlet}}{2} \rho \left(W^0_{Average} \right)^2 \tag{3.101b}$$

$$\Delta P^0_{Recovery,Outlet} = \frac{1-\zeta_{Exit}}{2} \rho \left(W^0_{Average} \right)^2 \tag{3.101c}$$

When the pressure differential is known and the velocity through the seal is unknown, the program iterates over seal inlet axial velocities and calculates inlet losses and exit recovery to match the total pressure differential. The first order boundary conditions for axial velocity are similarly calculated based on the first order pressure profile. This relationship is also based on the inlet loss and exit recovery factors and models the ”Lomakin” effect’s impact on the velocity boundary terms.

$$\Delta P^{R}_{Inlet} = (1 + \zeta_{Inlet})\, \rho W^{0}_{Average} W^{R}_{Inlet,Average} \tag{3.102a}$$

$$\Delta P^{I}_{Inlet} = (1 + \zeta_{Inlet})\, \rho W^{0}_{Average} W^{I}_{Inlet,Average} \tag{3.102b}$$

$$\Delta P^{R}_{Outlet} = (1 - \zeta_{Exit})\, \rho W^{0}_{Average} W^{R}_{Exit,Average} \tag{3.103a}$$

$$\Delta P^{I}_{Outlet} = (1 - \zeta_{Exit})\, \rho W^{0}_{Average} W^{I}_{Exit,Average} \tag{3.103b}$$

$$W^{R}_{Inlet,Average} = \frac{\Delta P^{R}_{Inlet}}{(1 + \zeta_{Inlet})\, \rho W^{0}_{Average}} \tag{3.104a}$$

$$W^{I}_{Inlet,Average} = \frac{\Delta P^{I}_{Inlet}}{(1 + \zeta_{Inlet})\, \rho W^{0}_{Average}} \tag{3.104b}$$

$$W^{R}_{Exit,Average} = \frac{\Delta P^{R}_{Outlet}}{(1 - \zeta_{Exit})\, \rho W^{0}_{Average}} \tag{3.105a}$$

$$W^{I}_{Exit,Average} = \frac{\Delta P^{I}_{Outlet}}{(1 - \zeta_{Exit})\, \rho W^{0}_{Average}} \tag{3.105b}$$

3.8 Numerical Iteration to RANS Solutions

While the MFD method provides spatial stability of the discretization, it does not have any claims to stability of iteration over time. Because the N-S equations are inherently non-linear, the equations are linearized for solution by applying a velocity multiple from a previous iteration step. Most codes take a pseudo-time approach even when solving steady state problems, and of course a time-stepping approach to transient solutions, to control the rate of change of the velocity solution as it is iterated towards a converged equilibrium. Oud[91] selects an implicit midpoint method in time (Implicit Euler) to iterate with an unspecified Krylov method. However, their implicit midpoint method seems to be a half implicit trapezoidal method instead. A similar trapezoidal method is given below in Equations 3.110 to 3.120. To obtain an implicit form of the solution, the $\mathbf{A}$ matrix is split into q and $q + 1$ time-steps by Equations 3.109 and 3.119. While the work by Oud split the mass conservation equation with the trapezoidal method, Gresho *et al.* suggests that this split can cause an oscillation in the solution on the order of $2\Delta t$ when the inputs are not well posed.[155] Gresho also says that switching to a fully implicit mass conservation solution can hide this oscillation. Ideally this work would include perfectly posed inputs, but determining the perfect boundary conditions for velocity is

not necessary for a decently converged and accurate solution. Future improvements or switching to the Pressure Poisson Equation form of the continuity equation would allow changing back to a trapezoidal continuity solution iteration. Note that the Reynolds Stress terms based on turbulent eddy viscosity are already included in this splitting of equation terms into $\underline{\underline{\mathbf{A}}}$ and $\underline{\mathbf{b}}$ components prior to their introduction and discussion in the next chapter.

$$\mathrm{St}\frac{d\vec{u}}{d\tau} + \overline{\mathbf{G}}P^T = -\mathbf{N}\left(\vec{u},\vec{u}\right) - \frac{1}{\mathrm{Re}}\mathbf{C}\overline{\mathbf{C}}\left(\vec{u}\right) + \overline{\mathscr{D}}\left[\frac{2}{\mathrm{Re}^t}\underline{\underline{\mathbf{E}}}\left(\vec{u}\right) - \frac{2}{3}k^t \cdot \underline{\underline{\mathbf{I}}}\right] \tag{3.106}$$

$$0 = \mathbf{D}\vec{u} \tag{3.107}$$

$$\begin{aligned}\frac{d\vec{u}}{d\tau} &= \frac{d}{d\tau}\left(\vec{u^0} + \varepsilon h\vec{u^1}\right)\\ &= \frac{d\vec{u^0}}{d\tau} + \frac{d}{d\tau}\left(\epsilon e^{\imath(\Omega t+\phi)}h\vec{u^1}\right)\\ &= \frac{\vec{u}^{0,g+1} - \vec{u}^{0,g}}{\Delta\tau} + \imath\Omega\varepsilon h\vec{u}^{1,g+\frac{1}{2}} - \imath\Omega\varepsilon h\left(R_S - \chi\right)\frac{\partial\vec{u}^{0,g+\frac{1}{2}}}{\partial\chi}\end{aligned} \tag{3.108}$$

$$\vec{u}^{0,g+\frac{1}{2}} + \varepsilon h\vec{u}^{1,g+\frac{1}{2}} = \frac{1}{2}\left(\vec{u}^{0,g} + \varepsilon h\vec{u}^{1,g} + \vec{u}^{0,g+1} + \varepsilon h\vec{u}^{1,g+1}\right) \tag{3.109}$$

$$\begin{aligned}\mathrm{St}\frac{\vec{u}^{0,g+1} - \vec{u}^{0,g}}{\Delta\tau} + \mathrm{St}\imath\Omega\varepsilon h\vec{u}^{1,g+\frac{1}{2}} - \mathrm{St}\imath\Omega\varepsilon h\left(R_S - \chi\right)\frac{\partial\vec{u}^{0,g+\frac{1}{2}}}{\partial\chi} + \overline{\mathbf{G}}P^{T\,0,g+1} + \varepsilon h\overline{\mathbf{G}}P^{T\,1,g+1} =\\ -\mathbf{N}^0\left(\vec{u}^{0,g+\frac{1}{2}},\vec{u}^{0,g}\right) - \frac{1}{\mathrm{Re}}\mathbf{C}^0\overline{\mathbf{C}}^0\left(\vec{u}^{0,g+\frac{1}{2}}\right) + \overline{\mathscr{D}}^0\left[\frac{2}{\mathrm{Re}^t}\underline{\underline{\mathbf{E}}}^0\left(\vec{u}^{0,g+\frac{1}{2}}\right) - \frac{2}{3}k^{0,t,g}\cdot\underline{\underline{\mathbf{I}}}\right]\\ -\varepsilon h\mathbf{N}^1\left(\vec{u}^{1,g+\frac{1}{2}},\vec{u}^{1,g}\right) - \varepsilon h\frac{1}{\mathrm{Re}}\mathbf{C}^1\overline{\mathbf{C}}^1\left(\vec{u}^{1,g+\frac{1}{2}}\right) + \varepsilon h\overline{\mathscr{D}}^1\left[\frac{2}{\mathrm{Re}^t}\underline{\underline{\mathbf{E}}}^1\left(\vec{u}^{1,g+\frac{1}{2}}\right)\right]\end{aligned} \tag{3.110}$$

$$-\mathbf{D}\left(\vec{u}^{0,g+1} + \varepsilon h\vec{u}^{0,g+1}\right) = -\left\{\mathbf{D}^0\left(\vec{u}^{0,g+1}\right)_{\underline{\underline{\mathbf{A}}}} + \varepsilon h\mathbf{D}^1\left(\vec{u}^{0,g+1}\right)_{\underline{\underline{\mathbf{A}}}} + \mathbf{D}^0\left(\vec{u}^{0,g+1}\right)_{\underline{\mathbf{b}}} + \varepsilon h\mathbf{D}^1\left(\vec{u}^{0,g+1}\right)_{\underline{\mathbf{b}}}\right\} \tag{3.111}$$

3.8.1 Zeroth Order Iteratation

Note that, as discussed above, for the concentric zeroth order solution, the physics is technically steady-state. The discrete time derivative is maintained to allow time-stepping iteration from the initial values to the final steady solution. However, the Strouhal number used for the zeroth order calculations is folded into the time step variable, with adaptive time step selection, for iterative stability instead of the whirl speed that defines the first order equation's Strouhal number or the constant that is typicaly used for steady state turbulent solutions.

$$\begin{aligned}
&\vec{u}^{0,g+1} + \frac{\Delta\tau}{\mathrm{St}}\overline{\mathbf{G}}P^{T,g+1} + \frac{1}{2}\frac{\Delta\tau}{\mathrm{St}}\left\{\mathbf{N}\left(\vec{u}^{0,g+1},\vec{u}^{0,g}\right) + \frac{1}{\mathrm{Re}}\mathbf{C}\overline{\mathbf{C}}\left(\vec{u}^{g+1}\right) - \overline{\mathscr{D}}\left[\frac{2}{\mathrm{Re}^t}\underline{\underline{\mathbf{E}}}\left(\vec{u}^{g+1}\right)\right]\right\}_{\mathbf{A}\underline{\underline{\mathbf{0}}}+} \\
&\quad = \vec{u}^{0,g} - \frac{1}{2}\frac{\Delta\tau}{\mathrm{St}}\left\{\mathbf{N}\left(\vec{u}^{0,g},\vec{u}^{0,g}\right) + \frac{1}{\mathrm{Re}}\mathbf{C}\overline{\mathbf{C}}^0\left(\vec{u}^{g}\right) - \overline{\mathscr{D}}\left[\frac{2}{\mathrm{Re}^t}\underline{\underline{\mathbf{E}}}\left(\vec{u}^{g}\right)\right]\right\}_{\mathbf{A}\underline{\underline{\mathbf{0}}}-} \\
&\quad\quad - \frac{\Delta\tau}{\mathrm{St}}\left\{\mathbf{N}\left(\vec{u}^{0,g},\vec{u}^{0,g}\right) + \frac{1}{\mathrm{Re}}\mathbf{C}\overline{\mathbf{C}}\left(\vec{u}^{g}\right) - \overline{\mathscr{D}}\left[\frac{2}{\mathrm{Re}^t}\underline{\underline{\mathbf{E}}}\left(\vec{u}^{g}\right) - \frac{2}{3}k^{t,g}\cdot\underline{\underline{\mathbf{I}}}\right]\right\}_{\underline{\mathbf{b}}}
\end{aligned} \tag{3.112}$$

$$\begin{bmatrix} \underline{\underline{\mathbf{I}}} + \frac{1}{2}\frac{\Delta\tau}{\mathrm{St}}\left(\mathbf{A}\underline{\underline{\mathbf{0}}}+\right) & \frac{\Delta\tau}{\mathrm{St}}\underline{\mathbf{G}} \\ -\underline{\mathbf{D}} & 0 \end{bmatrix}\begin{pmatrix}\vec{u}^{0,g+1}\\ P^{T,g+1}\end{pmatrix} = \begin{bmatrix} \underline{\underline{\mathbf{I}}} - \frac{1}{2}\frac{\Delta\tau}{\mathrm{St}}\left(\mathbf{A}\underline{\underline{\mathbf{0}}}-\right) & 0 \\ 0 & 0 \end{bmatrix}\begin{pmatrix}\vec{u}^{0,g}\\ P^{T,g}\end{pmatrix} - \frac{\Delta\tau}{\mathrm{St}}\underline{\mathbf{b}} \tag{3.113}$$

$$\begin{pmatrix}\vec{u}^{0,g+1}\\ P^{T,g+1}\end{pmatrix} = \begin{bmatrix} \underline{\underline{\mathbf{I}}} + \frac{1}{2}\frac{\Delta\tau}{\mathrm{St}}\left(\mathbf{A}\underline{\underline{\mathbf{0}}}+\right) & \frac{\Delta\tau}{\mathrm{St}}\underline{\mathbf{G}} \\ -\underline{\mathbf{D}} & 0 \end{bmatrix}^{-1}\left\{\begin{bmatrix} \underline{\underline{\mathbf{I}}} - \frac{1}{2}\frac{\Delta\tau}{\mathrm{St}}\left(\mathbf{A}\underline{\underline{\mathbf{0}}}-\right) & 0 \\ 0 & 0 \end{bmatrix}\begin{pmatrix}\vec{u}^{0,g}\\ P^{T,g}\end{pmatrix} - \frac{\Delta\tau}{\mathrm{St}}\underline{\mathbf{b}}\right\} \tag{3.114}$$

3.8.2 First Order Iteratation

The first order iteration procedure is different from that of the zeroth order solution due to the time derivative being a known quantity derived from the small circular perturbation. This means that there is no time-step applied to the first order solution as the discrete first order time derivative has no $\Delta\tau$. Also note that the first order equations are a linear expansion and thus more numerically stable than the zeroth order equations. This increased stability means that there is no need to split the matrix into current and future steps. Instead a fully implicit solution can be sought as seen below.

$$\begin{aligned}
&\mathrm{St}\imath\Omega\varepsilon h\vec{u}^{1,g+\frac{1}{2}} - \mathrm{St}\imath\Omega\varepsilon h\left(R_S-\chi\right)\frac{\partial\vec{u}^{0,g+\frac{1}{2}}}{\partial\chi} + \varepsilon h\overline{\mathbf{G}}P^{T\,1,g+1} = \\
&\quad - \varepsilon h\mathbf{N}^1\left(\vec{u}^{1,g+\frac{1}{2}},\vec{u}^{1,g}\right) - \varepsilon h\frac{1}{\mathrm{Re}}\mathbf{C}^1\overline{\mathbf{C}}^1\left(\vec{u}^{1,g+\frac{1}{2}}\right) + \varepsilon h\overline{\mathscr{D}}^1\left[\frac{2}{\mathrm{Re}^t}\underline{\underline{\mathbf{E}}}^1\left(\vec{u}^{1,g+\frac{1}{2}}\right)\right]
\end{aligned} \tag{3.115}$$

$$\begin{aligned}
&\mathrm{St}\imath\Omega\vec{u}^{1,g+1} + \overline{\mathbf{G}}P^{T\,1,g+1} \\
&\quad + \mathbf{N}^1\left(\vec{u}^{1,g+1},\vec{u}^{1,g}\right)_{\mathbf{A}\underline{\underline{\mathbf{1}}}+} + \frac{1}{\mathrm{Re}}\mathbf{C}^1\overline{\mathbf{C}}^1\left(\vec{u}^{1,g+1}\right)_{\mathbf{A}\underline{\underline{\mathbf{1}}}+} - \overline{\mathscr{D}}^1\left[\frac{2}{\mathrm{Re}^t}\underline{\underline{\mathbf{E}}}^1\left(\vec{u}^{1,g+1}\right)\right]_{\mathbf{A}\underline{\underline{\mathbf{1}}}+} = \\
&\quad - \left\{-\mathrm{St}\imath\Omega\left(R_S-\chi\right)\frac{\partial\vec{u}^{0,g}}{\partial\chi}\right\}_{\mathbf{b}\underline{\underline{\mathbf{1}}}\mathbf{t}} - \mathbf{N}^1\left(\vec{u}^{1,g},\vec{u}^{1,g}\right)_{\mathbf{b}\underline{\underline{\mathbf{1}}}} \\
&\quad - \frac{1}{\mathrm{Re}}\mathbf{C}^1\overline{\mathbf{C}}^1\left(\vec{u}^{1,g}\right)_{\mathbf{b}\underline{\underline{\mathbf{1}}}} + \overline{\mathscr{D}}^1\left[\frac{2}{\mathrm{Re}^t}\underline{\underline{\mathbf{E}}}^1\left(\vec{u}^{1,g}\right)\right]_{\mathbf{b}\underline{\underline{\mathbf{1}}}}
\end{aligned} \tag{3.116}$$

The real form of the first order RANS equations follows:

$$
\begin{aligned}
&-\mathbf{I}\left(\mathrm{St}\Omega\vec{u}^{1,g+1}\right)+\mathbf{R}\left(\overline{\mathbf{G}}P^{T\,1,g+1}\right)\\
&\quad\mathbf{R}\left(+\mathbf{N}^{1}\left(\vec{u}^{1,g+1},\vec{u}^{1,g}\right)_{\mathbf{A\underline{1}+}}+\frac{1}{\mathrm{Re}}\mathbf{C}^{1}\overline{\mathbf{C}}^{1}\left(\vec{u}^{1,g+1}\right)_{\mathbf{A\underline{1}+}}-\overline{\mathscr{D}}^{1}\left[\frac{2}{\mathrm{Re}^{t}}\underline{\underline{\mathbf{E}}}^{1}\left(\vec{u}^{1,g+1}\right)\right]_{\mathbf{A\underline{1}+}}\right)=\\
&\quad+\mathbf{I}\left(\mathrm{St}\Omega\vec{u}^{1,g}\right)-\mathbf{R}\left(\mathbf{N}^{1}\left(\vec{u}^{1,g},\vec{u}^{1,g}\right)_{\mathbf{\underline{b}1}}+\frac{1}{\mathrm{Re}}\mathbf{C}^{1}\overline{\mathbf{C}}^{1}\left(\vec{u}^{1,g}\right)_{\mathbf{\underline{b}1}}-\overline{\mathscr{D}}^{1}\left[\frac{2}{\mathrm{Re}^{t}}\underline{\underline{\mathbf{E}}}^{1}\left(\vec{u}^{1,g}\right)\right]_{\mathbf{\underline{b}1}}\right)
\end{aligned}
\tag{3.117}
$$

The imaginary form of the first order RANS equations is similarly:

$$
\begin{aligned}
&\mathbf{R}\left(\mathrm{St}\Omega\vec{u}^{1,g+1}\right)+\mathbf{I}\left(\overline{\mathbf{G}}P^{T\,1,g+1}\right)\\
&\quad+\mathbf{I}\left(\mathbf{N}^{1}\left(\vec{u}^{1,g+1},\vec{u}^{1,g}\right)_{\mathbf{A\underline{1}+}}+\frac{1}{\mathrm{Re}}\mathbf{C}^{1}\overline{\mathbf{C}}^{1}\left(\vec{u}^{1,g+1}\right)_{\mathbf{A\underline{1}+}}-\overline{\mathscr{D}}^{1}\left[\frac{2}{\mathrm{Re}^{t}}\underline{\underline{\mathbf{E}}}^{1}\left(\vec{u}^{1,g+1}\right)\right]_{\mathbf{A\underline{1}+}}\right)=\\
&\quad-\mathbf{R}\left(\mathrm{St}\Omega\vec{u}^{1,g+1}\right)-\left\{-\mathrm{St}\Omega\left(R_S-\chi\right)\frac{\partial\vec{u}^{0,g}}{\partial\chi}\right\}_{\mathbf{\underline{b}1t}}\\
&\quad-\mathbf{I}\left(\mathbf{N}^{1}\left(\vec{u}^{1,g},\vec{u}^{1,g}\right)_{\mathbf{\underline{b}1}}+\frac{1}{\mathrm{Re}}\mathbf{C}^{1}\overline{\mathbf{C}}^{1}\left(\vec{u}^{1,g}\right)_{\mathbf{\underline{b}1}}-\overline{\mathscr{D}}^{1}\left[\frac{2}{\mathrm{Re}^{t}}\underline{\underline{\mathbf{E}}}^{1}\left(\vec{u}^{1,g}\right)\right]_{\mathbf{\underline{b}1}}\right)
\end{aligned}
\tag{3.118}
$$

The combination of real and imaginary forms results in the final matrix form below:

$$
\begin{bmatrix}
\mathbf{R}\left\{\mathbf{A\underline{1}+}\left(Ur,Wr\right)\right\} & -\mathrm{St}\Omega\underline{\underline{\mathbf{I}}}+\mathbf{R}\left\{\mathbf{A\underline{1}+}\left(Vi\right)\right\} & \mathbf{R}\left\{\underline{\underline{\mathbf{G}}}\left(Pr\right)\right\} & 0\\
\mathrm{St}\Omega\underline{\underline{\mathbf{I}}}+\mathbf{I}\left\{\mathbf{A\underline{1}+}\left(Vr\right)\right\} & \mathbf{I}\left\{\mathbf{A\underline{1}+}\left(Ui,Wi\right)\right\} & 0 & \mathbf{I}\left\{\underline{\underline{\mathbf{G}}}\left(Pi\right)\right\}\\
\mathbf{R}\left\{-\underline{\underline{\mathbf{D}}}\left(Ur,Wr\right)\right\} & \mathbf{R}\left\{-\underline{\underline{\mathbf{D}}}\left(Vi\right)\right\} & 0 & 0\\
\mathbf{I}\left\{-\underline{\underline{\mathbf{D}}}\left(Vr\right)\right\} & \mathbf{R}\left\{-\underline{\underline{\mathbf{D}}}\left(Ur,Wr\right)\right\} & 0 & 0
\end{bmatrix}
\begin{pmatrix}
\vec{u}^{R,g+1}\\
\vec{u}^{I,g+1}\\
P^{T,R,g+1}\\
P^{T,I,g+1}
\end{pmatrix}
=-\mathbf{\underline{b}1t}-\mathbf{\underline{b}1}
\tag{3.119}
$$

$$
\begin{pmatrix}
\vec{u}^{R,g+1}\\
\vec{u}^{I,g+1}\\
P^{T,R,g+1}\\
P^{T,I,g+1}
\end{pmatrix}
=
\begin{bmatrix}
\mathbf{R}\left\{\mathbf{A\underline{1}+}\left(Ur,Wr\right)\right\} & -\mathrm{St}\Omega\underline{\underline{\mathbf{I}}}+\mathbf{R}\left\{\mathbf{A\underline{1}+}\left(Vi\right)\right\} & \mathbf{R}\left\{\underline{\underline{\mathbf{G}}}\left(Pr\right)\right\} & 0\\
\mathrm{St}\Omega\underline{\underline{\mathbf{I}}}+\mathbf{I}\left\{\mathbf{A\underline{1}+}\left(Vr\right)\right\} & \mathbf{I}\left\{\mathbf{A\underline{1}+}\left(Ui,Wi\right)\right\} & 0 & \mathbf{I}\left\{\underline{\underline{\mathbf{G}}}\left(Pi\right)\right\}\\
\mathbf{R}\left\{-\underline{\underline{\mathbf{D}}}\left(Ur,Wr\right)\right\} & \mathbf{R}\left\{-\underline{\underline{\mathbf{D}}}\left(Vi\right)\right\} & 0 & 0\\
\mathbf{I}\left\{-\underline{\underline{\mathbf{D}}}\left(Vr\right)\right\} & \mathbf{R}\left\{-\underline{\underline{\mathbf{D}}}\left(Ur,Wr\right)\right\} & 0 & 0
\end{bmatrix}^{-1}
\tag{3.120}
$$

$$
\left\{-\mathbf{\underline{b}1t}-\mathbf{\underline{b}1}\right\}
$$

Note that each first order pressure gradient above is a gradient of total pressure, Equation 3.121, and not static pressure. To obtain first order static pressure from the first order total pressure and the zeroth and first order velocities it is necessary to perturb the definition of total pressure

in Equation 3.124. The real component of the static pressure is given by Equation 3.126 and the imaginary component by Equation 3.127.

$$P_T = P_T^0 + h\left(P_T^R cos\theta + \imath P_T^I sin\theta\right) \tag{3.121}$$

$$P_T = P_S + \frac{\rho}{2}\left(u^2 + v^2 + w^2\right) \tag{3.122}$$

$$\begin{aligned} P_T^0 + h\left(P_T^R cos\theta + \imath P_T^I sin\theta\right) =& P_S^0 + h\left(P_S^R cos\theta + \imath P_S^I sin\theta\right) \\ &+ \frac{\rho}{2}\left[\left(u^0 + h\left[u^R cos\theta + \imath u^I sin\theta\right]\right)^2\right. \\ &\quad + \left(v^0 + h\left[v^R cos\theta + \imath v^I sin\theta\right]\right)^2 \\ &\quad \left. + \left(w^0 + h\left[w^R cos\theta + \imath w^I sin\theta\right]\right)^2\right] \end{aligned} \tag{3.123}$$

$$\begin{aligned} P_T^0 + h\left(P_T^R cos\theta + \imath P_T^I sin\theta\right) =& P_S^0 + h\left(P_S^R cos\theta + \imath P_S^I sin\theta\right) \\ &+ \frac{\rho}{2}\left(\left[u^0\right]^2 + 2hu^0\left[u^R cos\theta + \imath u^I sin\theta\right] + h^2\left[u^R cos\theta\right]^2 - h^2\left[u^I sin\theta\right]^2\right. \\ &\quad + \left[v^0\right]^2 + 2hv^0\left[v^R cos\theta + \imath v^I sin\theta\right] + h^2\left[v^R cos\theta\right]^2 - h^2\left[v^I sin\theta\right]^2 \\ &\quad \left. + \left[w^0\right]^2 + 2hw^0\left[w^R cos\theta + \imath w^I sin\theta\right] + h^2\left[w^R cos\theta\right]^2 - h^2\left[w^I sin\theta\right]^2\right) \end{aligned} \tag{3.124}$$

$$\begin{aligned} h\left(P_T^R cos\theta + \imath P_T^I sin\theta\right) =& h\left(P_S^R cos\theta + \imath P_S^I sin\theta\right) \\ &+ \frac{\rho}{2}\left(2hu^0\left[u^R cos\theta + \imath u^I sin\theta\right]\right. \\ &\quad + 2hv^0\left[v^R cos\theta + \imath v^I sin\theta\right] \\ &\quad \left. + 2hw^0\left[w^R cos\theta + \imath w^I sin\theta\right]\right) \end{aligned} \tag{3.125}$$

$$P_T^R = P_S^R + \rho h\left(u^0 u^R + v^0 v^R + w^0 w^R\right) \tag{3.126}$$

$$P_T^I = P_S^I + \rho h\left(u^0 u^I + v^0 v^I + w^0 w^I\right) \tag{3.127}$$

3.8.3 Adaptive time-stepping

The selected time-step size in the above numerical schemes affects the stability and speed of convergence to a steady solution. The initial time-step size was determined by a standard two-dimensional Courant-Friedrichs-Lewy (CFL) condition,[156,157] Equation 3.128. This commonly applied method bases the time-step size on the spatial discretization and the characteristic velocities in the flow domain. However, the CFL condition is a guideline and not a hard limit on the time-step size for stability.

$$\Delta t_{CFL} \leq St \frac{1}{\frac{\max(w_W)}{\max(\Delta_Y)} \frac{\max(v_S)}{\max(\Delta z)}} \tag{3.128}$$

It was decided to allow the time-step size to vary adaptively based on instantaneous estimates for the numerical discretization truncation errors of the spatial and temporal schemes. Pan *et. al.* 2021[158] demonstrated an adaptive time-stepping method compatible with compressible flow solvers. Their adaptation function for time-step size is designed to maintain parity between the temporal truncation error and the product of the time-step and the spatial truncation error. The goal was then to maximize the time-step size without reducing accuracy by increasing the temporal truncation error above the spatial truncation error. The local spatial truncation error was estimated for each node using Equation 3.129 as a function of the change in the momentum and conservation equations from one iteration step to the next. Note that for brevity the equations below are presented in terms of a standard $Ax = B$ matrix equation rather than the detailed matrices given in the previous sections. The component spatial truncation error for each set of equations was combined within the individual cells using the **FC** vector space inner product, Equation 3.18 providing Equation 3.130. The temporal truncation error necessitated a different method to estimate. The most direct method to obtain an estimate of truncation error was to apply another temporal discretization scheme, Equation 3.131, and then compare prediction for the subsequent time-step from each temporal scheme. A third order explicit-implicit backwards finite difference scheme (BFD3) was selected for the extra temporal discretization. The temporal truncation error, Equation 3.132, is likewise summed locally for each cell using the **FC** vector space inner product. Equation 3.133 was then applied to obtain new values for each cell's local time-step. These potential new time-steps are then averaged with a weighted sum of the local temporal truncation errors, in Equation 3.134, and the

maximum value is selected based on Equation 3.135. As the extra temporal discretization required multiple historical values for the flow variables, and to avoid an extra matrix division step at every iteration, the time-step size adaptation is applied every 10 iteration steps.

$$\epsilon_{\mathbf{S},\mathbf{x}}{}^{g} = \text{abs}\left(\underline{\underline{\mathbf{A}}}^{g} x^{g} + b^{g} - \underline{\underline{\mathbf{A}}}^{g-1} x^{g-1} - b^{g-1}\right) \tag{3.129}$$

$$\begin{aligned}\epsilon_{S,CC}^{g} = \Bigg\{ & \left[\frac{\left(\Delta\chi_{i+1} + \Delta\chi_i\right)\epsilon_{\mathbf{S},\mathbf{u}_{\ell,k}}^{g} + \left(\Delta\chi_i + \Delta\chi_{i-1}\right)\epsilon_{\mathbf{S},\mathbf{u}_{\ell-1,k}}^{g}}{2\Delta\chi_i}\right]^2 \\ & + \left[\epsilon_{\mathbf{S},\mathbf{v}_{i,k}}^{g}\right]^2 + \left[\frac{\left(\Delta z_{k+1} + \Delta z_k\right)\epsilon_{\mathbf{S},\mathbf{u}_{i,n}}^{g} + \left(\Delta z_k + \Delta z_{k-1}\right)\epsilon_{\mathbf{S},\mathbf{u}_{i,n-1}}^{g}}{2\Delta z_k}\right]^2 \\ & + \left[\epsilon_{\mathbf{S},\nabla\cdot\mathbf{u}_{i,k}}^{g}\right]^2 + \left[\epsilon_{\mathbf{S},\mathbf{k}_{i,k}}^{g}\right]^2\Bigg\}^{\frac{1}{2}}\end{aligned} \tag{3.130}$$

$$x_{BFD3}^{g+1} = \left[\Delta t^{g}\underline{\underline{\mathbf{A}}}^{g} - \frac{11}{6}\underline{\underline{\mathbf{I}}}\right]^{-1}\left[-\Delta t^{g} b^{g} - 3x^{g-1} + \frac{3}{2}x^{g-2} - \frac{1}{3}x^{g-3}\right] \tag{3.131}$$

$$\epsilon_{t,x}^{g} = \text{abs}\left(x_{Mid}^{g+1} - x_{BFD3}^{g+1}\right) \tag{3.132}$$

$$\Delta t_{i,k}^{g+1} = \Delta t^{g}\left[\frac{\frac{1}{2}\Delta t^{g}\epsilon_{S,CC}^{g} + 1.5^2\left(x^{g+1} - x^{g}\right)}{\epsilon_{t,x}^{g} + \left(x^{g+1} - x^{g}\right)}\right]^{\frac{1}{2}} \tag{3.133}$$

$$\Delta t^{g+1} = \frac{\sum_{i,k}\epsilon_{t,x}^{g}\cdot\Delta t_{i,k}^{g+1}}{\sum_{i,k}\epsilon_{t,x}^{g}} \tag{3.134}$$

$$\Delta t^{g+1} = \min\left(\max\left[\Delta t^{g+1}, 10^{-8}, 0.1\times MaxError\right], 100\Delta t_{CFL}\right) \tag{3.135}$$

3.9 Validation of RANS Code Solutions Without Reynolds Stresses

The RANS equations without the Reynolds Stress tensor are equivalent to the un-averaged Navier-Stokes momentum equations, making the code a laminar or DNS numerical solution. As a laminar code, analytical solutions exist for simple flow cases such as classical Poiseuille (pressure driven flow between two surfaces) and Couette (fluid between a moving and stationary surface, driven by the moving surface) flows. The established analytical solutions for annular laminar Poiseuille, Equation 3.136, and Couette, Equation 3.137, flows were provided in terms of no-slip wall boundaries and Dirichlet velocity boundary conditions.[6] The expected profiles for the analytically calculable flows were compared to the numerically obtained results in the following sections.

$$w = -\frac{\partial p}{\partial z}\frac{1}{4\mu}\left(R_R^2 - r^2\right)\left(R_S^2 - R_R^2\right)\frac{\ln\left(\frac{r}{R_R}\right)}{\ln\left(\frac{R_S}{R_R}\right)} \tag{3.136}$$

$$v = \omega R_R \frac{\left(\frac{R_S}{r} - \frac{r}{R_R}\right)}{\left(\frac{R_S}{R_R} - \frac{R_R}{R_S}\right)} \tag{3.137}$$

Annular pressure seals consist of a pressure driven flow between a rotating shaft and a fixed stator. While turbulent effects dominate the flow at high Reynolds numbers, at low Reynolds numbers the seal flow can be modeled as a superposition of the Poiseuille and Couette flow analytical solutions. The fundamentals of the 2-D seal code were thus validated against multiple Poiseuille, Couette, and combined flow cases to ensure the baseline functionality and stability of the solutions. Only the zeroth order laminar validation results are shown in this section. The first order laminar validation results are given with respect to the rotordynamic coefficients of San Andres' oil seal[159] in Section 5.1. For purely laminar test cases compared directly to analytical solutions numerical grids with radial element counts were tested with regularly spaced and growth-rate spaced cells numbering from 10 to 60 radial elements and 100 to 1,000 axial elements; at mean inlet velocities of 0.1 to 0.6 $\left[\frac{\mathrm{m}}{\mathrm{s}}\right]$ (Axial Reynolds Numbers of 173 and 1,039); and rotor speeeds of 0 to 50 [RPM] (Circumferential Reynolds Numbers of 0 and 1088).

3.9.1 Poiseuille Flow Validation

The first comparison between analyitcal and numerical solutions was for pressure driven flow between a stationary concentric rotor and stator. The velocity boundary conditions on the rotor and stator assigned as homogeneous Dirichlet no-slip conditions, and all velocity boundary conditions at the inlet and outlet, other than the inlet axial velocity boundary condition, were applied as homogeneous Neumann conditions. The only boundary condition defined for pressure was a single node at the outlet specified at 0 Pa gauge pressure. With an inlet mean velocity of 0.1 $\left[\frac{\mathrm{m}}{\mathrm{s}}\right]$ (Axial Reynolds Number of 173), the profile of the axial velocity was given by Equation 3.136 and can be seen in Figure 3.1 as the dashed line which can be compared to the numerically obtained profile of points. The devaition between the analytical velocity profile and the numerically obtained outlet profile was less than 0.002 % at any given grid node for a grid size of 30 radial by 300

axial elements. The coarsest mesh pressure drop across the seal deviated from the analytically obtained solution by an rms percent difference of 1.98 % and the finest by 0.059 %. The pressure drop for all tested Poiseuille flow cases at any mesh size deviated by an rms percent difference of 1.69 %. These pressure drop rms percent difference numbers were also tested for combined Couette-Poiseuille flow cases with all cases showing 1.29 % difference for any combined flow.

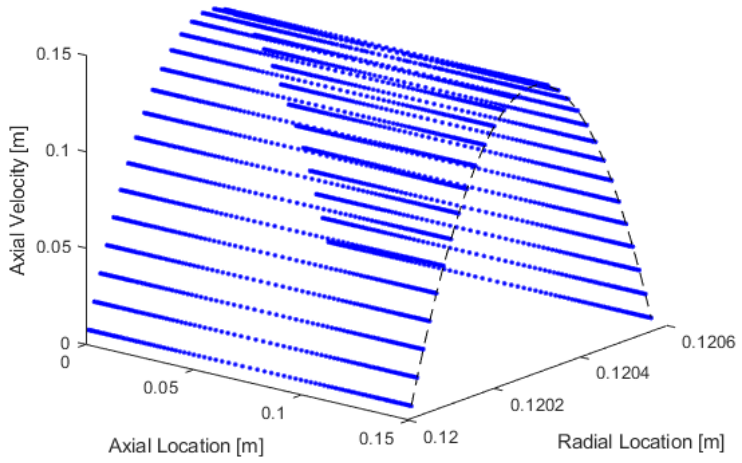

Figure 3.1: Axial velocity profile for Poiseuille flow at 0.1 $\left[\frac{\mathrm{m}}{\mathrm{s}}\right]$ mean inlet velocity

3.9.2 Couette Flow Validation

The second comparison between analyitcal and numerically obtained solutions was performed with annular Couette flow between a stationary stator and a concentric rotating rotor shaft. Equation 3.137 describes the circumferential velocity of the fluid in steady state. Figure 3.2 shows the circumferential velocity profile obtained numerically as a profile of points and the analytical solution as a dashed line at the domain exit for a seal with a 50 [RPM] rotor speed. The rotor and stator surfaces were again defined with Dirichlet boundaries and the inlet and outlet velocities were assigned with homogeneous Neumann conditions. However, the rotor circumferential velocity boundary is a non-homogeneous Dirichlet condition at the rotor surface speed. The resulting velocity profile rms percent difference between analytical and numerical solutions is less than 0.29 % for any given grid node at a grid size of 30 radial by 300 axial elements. The coarsest mesh

deviated from the analytically obtained solution by an rms percent difference of 0.27 % and the finest by 1.83 %.

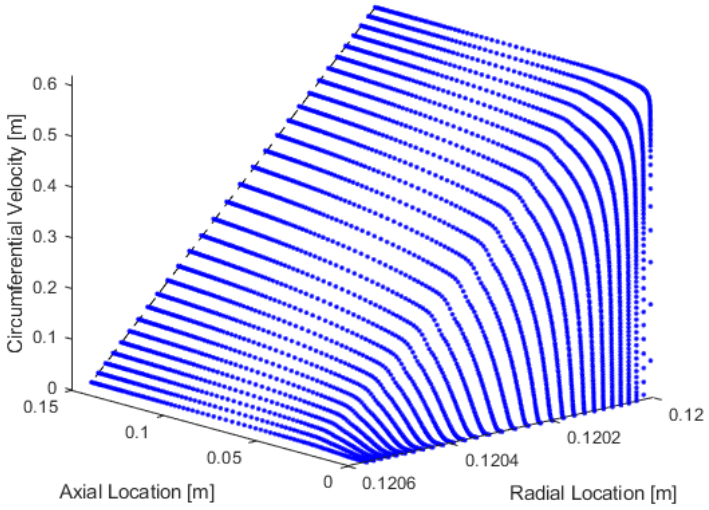

Figure 3.2: Circumferential velocity profile for Couette flow at 50 $[\mathrm{RPM}]$ rotor speed

Chapter 4

Eddy Viscosity Turbulence Model by Mimetic FDM

4.1 Discrete Turbulence Modeling

The discretization of terms for turbulence modeling comes in two parts. First, the momentum equations were augmented with the tensor gradient and tensor divergence operators, and averaging of scalar **CC** kinetic energy values to model the linear turbulent eddy viscosity effects. The additional momentum equation terms were completed for the zeroth and first order forms of the equations to include turbulence effects in the full solution. Then the selected Prandtl 1-Equation turbulence model was discreteized for the zeroth order solution only. The first order solution of turbulent eddy viscosity was deemed negligible as the scale of turbulence velocity fluctations in the kinetic energy transport equation is already assumed to be small.

As discussed in Section 2.4.3, Equation 3.14 is augmented with the Reynolds Stress tensor terms that are approximated with a linear eddy viscosity assumption. The resulting momentum equations with turbulence effects is seen in Equation 2.79. The non-dimensionalization coefficient of the kinetic energy term works out to be $\frac{\rho_0 U_c^2}{\rho_0 U_c^2} = 1$. Note that the two Reynolds number coefficients are not combined through summing because Re_t is not a constant in space and thus cannot be pulled out of the divergence operation.

$$0 = St\frac{\partial \vec{u}}{\partial t} + N\left(\vec{u}\right) + \nabla P^T + \frac{1}{Re} C\left[\overline{C}\left(\vec{u}\right)\right] - \overline{\mathscr{D}}\left[\frac{1}{Re_t}\mathbf{E}\left(\vec{u}\right) - \frac{2}{3}k_t\delta_{qs}\right] \tag{4.1}$$

4.1.1 Discrete Eddy Viscosity Diffusion

The 0^{th} and 1^{th} order components of momentum for the terms with tensor divergence and gradients including the turbulent Reynolds number and turbulent kinetic energy scalars are discretized using the discrete tensor operators in Appendix D. The terms are substituted from equations in Section D.2 into the tensor divergence operators in Section D.3 to create the discrete form of Equation 4.1's right most terms. The turbulent reynolds number and turbulent kinetic energy terms are stored in the $\mathbf{CC}$ vector space, and the Reynolds number requires averaging or linear interpolation to the $\mathbf{EC}$ vector space to properly combine with the established discrete tensor operators. Note that the turbulent Reynolds number scalar has only a 0^{th} order value.

$$\overline{\mathscr{D}}\left[\frac{2}{Re_t}\mathbf{E}\left(\vec{u}\right)-\frac{2}{3}k_t\delta_{qs}\right]=\overline{\mathscr{D}}\left[\tau_{qs}\right] \tag{4.2}$$

The $\mathbf{EC}$ vector space terms in Equation 4.2 represent the Reynolds Stresses and are given below to be later substituted into the discrete tensor divergence operators. The linear interopolation of the turbulent Reynolds number is performed analagously to the averages radial averages of circumferential velocity in the tensor gradient operator for the radial locations and

$$\frac{\overline{\mu}_{i,k}}{\rho_c L_c U_c}=\frac{1}{\overline{\overline{Re^t_{i,k}}^{\chi}}}=k^{\frac{1}{2}}_{i,k}\ell^t_{i,k} \tag{4.3}$$

$$\frac{\overline{\mu}^t_{\ell,k}}{\rho_c L_c U_c}=\frac{1}{\overline{\overline{Re^t_{\ell,k}}^{\chi}}}=\frac{\Delta\chi_{i+1}k^{\frac{1}{2}}_{i+1,k}\ell^t_{i+1,k}+\Delta\chi_i k^{\frac{1}{2}}_{i,k}\ell^t_{i,k}}{\Delta\chi_{i+1}+\Delta\chi_i} \tag{4.4}$$

$$\frac{1}{\overline{\overline{Re^t_{i,n}}^{z}}}=\frac{\Delta z_{k+1}k^{\frac{1}{2}}_{i,k+1}\ell^t_{i,k+1}+\Delta z_k k^{\frac{1}{2}}_{i,k}\ell^t_{i,k}}{\Delta z_{k+1}+\Delta z_k} \tag{4.5}$$

$$\begin{aligned}\frac{1}{\overline{\overline{Re^t_{\ell,n}}^{\chi z}}}=\frac{1}{\Delta z_{k+1}+\Delta z_k}\Bigg[&\Delta z_{k+1}\frac{\Delta\chi_{i+1}k^{\frac{1}{2}}_{i+1,k+1}\ell^t_{i+1,k+1}+\Delta\chi_i k^{\frac{1}{2}}_{i,k+1}\ell^t_{i,k+1}}{\Delta\chi_{i+1}+\Delta\chi_i}\\&+\Delta z_k\frac{\Delta\chi_{i+1}k^{\frac{1}{2}}_{i+1,k}\ell^t_{i+1,k}+\Delta\chi_i k^{\frac{1}{2}}_{i,k}\ell^t_{i,k}}{\Delta\chi_{i+1}+\Delta\chi_i}\Bigg]\end{aligned} \tag{4.6}$$

Zeroth Order Discrete Reynolds Stress Terms

$$\left(\tau^{\chi\chi}_{\mathbf{i,k}}\right)^0 = \frac{2}{Re^t_{i,k}}\left(\frac{1}{\chi_i}\frac{\chi_\ell u^0_{\ell,k} - \chi_{\ell-1}u^0_{\ell-1,k}}{\Delta\chi_i} - \frac{1}{\chi_i}\frac{u^0_{\ell,k} + u^0_{\ell-1,k}}{2}\right) - \frac{2}{3}k^t_{i,k} \tag{4.7a}$$

$$\left(\tau^{\theta\theta}_{\mathbf{i,k}}\right)^0 = \frac{2}{Re^t_{i,k}}\left(\frac{1}{\chi_i}\frac{u^0_{\ell,k} + u^0_{\ell-1,k}}{2}\right) - \frac{2}{3}k^t_{i,k} \tag{4.7b}$$

$$\left(\tau^{\mathbf{zz}}_{\mathbf{i,k}}\right)^0 = \frac{2}{Re^t_{i,k}}\left(\frac{w^0_{i,k,n} - w^0_{i,k,n-1}}{\Delta z_k}\right) - \frac{2}{3}k^t_{i,k} \tag{4.7c}$$

$$\left(\tau^{\chi\theta}_{\ell,\mathbf{k}}\right)^0 = \frac{1}{\overline{\overline{Re^t_{\ell,k}}}^{\chi}}\left(\frac{4}{\chi_{i+1}+\chi_i}\frac{\chi_{i+1}v^0_{i+1,k} - \chi_i v^0_{i,k}}{\Delta\chi_i + \Delta\chi_{i+1}} - 2\frac{v^0_{i+1,k} + v^0_{i,k}}{\chi_i + \chi_{i+1}}\right) \tag{4.7d}$$

$$\left(\tau^{\theta\mathbf{z}}_{\mathbf{i,n}}\right)^0 = \frac{2}{\overline{\overline{Re^t_{i,n}}}^{z}}\left(\frac{v^0_{i,k+1} - v^0_{i,k}}{\Delta z_k + \Delta z_{k+1}}\right) \tag{4.7e}$$

$$\left(\tau^{\mathbf{z}\chi}_{\ell,\mathbf{n}}\right)^0 = \frac{2}{\overline{\overline{Re^t_{\ell,n}}}^{\chi z}}\left(\frac{u^0_{\ell,k+1} - u^0_{\ell,k}}{\Delta z_k + \Delta z_{k+1}} + \frac{w^0_{i+1,n} - w^0_{i,n}}{\Delta\chi_{i+1} + \Delta\chi_i}\right) \tag{4.7f}$$

First Order Discrete Reynolds Stress Terms

$$\left(\tau^{\chi\chi}_{\mathbf{i,k}}\right)^1 = \frac{2}{Re^t_{i,k}}\left[\frac{1}{\chi_i}\frac{\chi_\ell u^0_{\ell,k} - \chi_{\ell-1}u^0_{\ell-1,k}}{\Delta\chi_i} - \frac{(R_S-\chi_i)}{\chi_i^2}\frac{\chi_\ell u^0_{\ell,k} - \chi_{\ell-1}u^0_{\ell-1,k}}{\Delta\chi_i} + \frac{1}{\chi_i}\frac{\left(\chi_\ell u^1_{\ell,k} + (R_S-\chi_\ell)\,u^0_{\ell,k}\right) - \left(\chi_{\ell-1}u^1_{\ell-1,k} + (R_S-\chi_{\ell-1})\,u^0_{\ell-1,k}\right)}{\Delta\chi_i} + \frac{(R_S-\chi_i)}{\chi_i^2}\frac{u^0_{\ell,k}+u^0_{\ell-1,k}}{2} - \frac{u^1_{\ell,k}+u^1_{\ell-1,k}}{2\chi_i}\right] \tag{4.8a}$$

$$\left(\tau^{\theta\theta}_{\mathbf{i,k}}\right)^1 = \frac{2}{Re^t_{i,k}}\left[\frac{1}{\chi_i}\left\{\left(-v^I_{i,k}+\imath v^R_{i,k}\right)+2\imath\,(R_S-\chi_i)\,\frac{v^0_{i+1,k}-v^0_{i-1,k}}{\Delta\chi_{i+1}+2\Delta\chi_i+\chi_{i-1}}\right\} - \frac{(R_S-\chi_i)}{\chi_i^2}\frac{u^0_{\ell,k}+u^0_{\ell-1,k}}{2} + \frac{u^1_{\ell,k}+u^1_{\ell-1,k}}{2\chi_i}\right] \tag{4.8b}$$

$$\left(\tau^{zz}_{\mathbf{i,k}}\right)^1 = \frac{2}{Re^t_{i,k}}\left(\frac{w^1_{i,k,n}-w^1_{i,k,n-1}}{\Delta z_k}\right) \tag{4.8c}$$

$$\left(\tau^{\chi\theta}_{\ell,\mathbf{k}}\right)^1 = \frac{2}{\overline{Re^t_{\ell,k}}^{\chi}}\left[\frac{1}{\chi_{i+1}+\chi_i}\left\{\left(-u^I_{\ell,k}+\imath u^R_{\ell,k}\right)+\imath\frac{(R_S-\chi_{\ell+1})\,u^0_{\ell+1,k}-(R_S-\chi_{\ell-1})\,u^0_{\ell-1,k}}{\Delta\chi_i+\Delta\chi_{i+1}}\right\} + \frac{2}{\chi_{i+1}+\chi_i}\frac{\chi_{i+1}v^0_{i+1,k}-\chi_i v^0_{i,k}}{\Delta\chi_i+\Delta\chi_{i+1}} + \frac{2}{\chi_{i+1}+\chi_i}\frac{\chi_{i+1}v^1_{i+1,k}-\chi_i v^1_{i,k}}{\Delta\chi_i+\Delta\chi_{i+1}} + 2\frac{R_S}{\chi_{i+1}+\chi_i}\frac{v^0_{i+1,k}-v^0_{i,k}}{\Delta\chi_i+\Delta\chi_{i+1}} - 4\frac{R_S}{(\chi_{i+1}+\chi_i)^2}\frac{\chi_{i+1}v^0_{i+1,k}-\chi_i v^0_{i,k}}{\Delta\chi_i+\Delta\chi_{i+1}} + \frac{(2R_S-\chi_i-\chi_{i+1})}{(\chi_i+\chi_{i+1})^2}\left(v^0_{i+1,k}+v^0_{i,k}\right) - \frac{v^1_{i+1,k}+v^1_{i,k}}{\chi_i+\chi_{i+1}}\right] \tag{4.8d}$$

$$\left(\tau^{\theta z}_{\mathbf{i,n}}\right)^1 = \frac{2}{\overline{Re^t_{i,n}}^{z}}\left[\frac{v^1_{i,k+1}-v^1_{i,k}}{\Delta z_k+\Delta z_{k+1}} + \frac{1}{2\chi_i}\left(-w^I_{i,n}+\imath w^R_{i,n}\right) + \imath\frac{\Delta\chi_{i+1}}{\chi_i\Delta\chi_i}\left(\frac{(R_S-\chi_{i+1})\,w^0_{i+1,n}}{\Delta\chi_i+2\Delta\chi_{i+1}+\Delta\chi_{i+2}}\right) - \imath\frac{\Delta\chi_{i-1}}{\chi_i\Delta\chi_i}\left(\frac{(R_S-\chi_{i-1})\,w^0_{i-1,n}}{\Delta\chi_{i-2}+2\Delta\chi_{i-1}+\Delta\chi_i}\right)\right] \tag{4.8e}$$

$$\left(\tau^{z\chi}_{\ell,\mathbf{n}}\right)^1 = \frac{2}{\overline{Re^t_{\ell,n}}^{\chi z}}\left(\frac{u^1_{\ell,k+1}-u^1_{\ell,k}}{\Delta z_k+\Delta z_{k+1}} + \frac{w^0_{i+1,n}-w^0_{i,n}}{\Delta\chi_{i+1}+\Delta\chi_i} + \frac{w^1_{i+1,n}-w^1_{i,n}}{\Delta\chi_{i+1}+\Delta\chi_i}\right) \tag{4.8f}$$

Real First Order Discrete Reynolds Stress Terms

$$\left(\tau^{\chi\chi}_{\mathbf{i,k}}\right)^R = \frac{2}{Re^t_{i,k}}\left[\frac{1}{\chi_i}\frac{\chi_\ell u^0_{\ell,k} - \chi_{\ell-1}u^0_{\ell-1,k}}{\Delta\chi_i} - \frac{(R_S-\chi_i)}{\chi_i^2}\frac{\chi_\ell u^0_{\ell,k} - \chi_{\ell-1}u^0_{\ell-1,k}}{\Delta\chi_i} + \frac{1}{\chi_i}\frac{\left(\chi_\ell u^R_{\ell,k} + (R_S-\chi_\ell)\,u^0_{\ell,k}\right) - \left(\chi_{\ell-1}u^R_{\ell-1,k} + (R_S-\chi_{\ell-1})\,u^0_{\ell-1,k}\right)}{\Delta\chi_i} + \frac{(R_S-\chi_i)}{\chi_i^2}\frac{u^0_{\ell,k}+u^0_{\ell-1,k}}{2} - \frac{u^R_{\ell,k}+u^R_{\ell-1,k}}{2\chi_i}\right] \tag{4.9a}$$

$$\left(\tau^{\theta\theta}_{\mathbf{i,k}}\right)^R = \frac{2}{Re^t_{i,k}}\left[-\frac{1}{\chi_i}v^I_{i,k} - \frac{(R_S-\chi_i)}{\chi_i^2}\frac{u^0_{\ell,k}+u^0_{\ell-1,k}}{2} + \frac{u^R_{\ell,k}+u^R_{\ell-1,k}}{2\chi_i}\right] \tag{4.9b}$$

$$\left(\tau^{\mathbf{zz}}_{\mathbf{i,k}}\right)^R = \frac{2}{Re^t_{i,k}}\left(\frac{w^R_{i,k,n} - w^R_{i,k,n-1}}{\Delta z_k}\right) \tag{4.9c}$$

$$\left(\tau^{\chi\theta}_{\ell,\mathbf{k}}\right)^R = \frac{2}{\overline{\overline{Re^t_{\ell,k}}}^{\chi}}\left[-\frac{1}{\chi_{i+1}+\chi_i}u^I_{\ell,k} + \frac{2}{\chi_{i+1}+\chi_i}\frac{\chi_{i+1}v^0_{i+1,k} - \chi_i v^0_{i,k}}{\Delta\chi_i + \Delta\chi_{i+1}} + \frac{2}{\chi_{i+1}+\chi_i}\frac{\chi_{i+1}v^R_{i+1,k} - \chi_i v^R_{i,k}}{\Delta\chi_i + \Delta\chi_{i+1}} + 2\frac{R_S}{\chi_{i+1}+\chi_i}\frac{v^0_{i+1,k} - v^0_{i,k}}{\Delta\chi_i + \Delta\chi_{i+1}} - 4\frac{R_S}{(\chi_{i+1}+\chi_i)^2}\frac{\chi_{i+1}v^0_{i+1,k} - \chi_i v^0_{i,k}}{\Delta\chi_i + \Delta\chi_{i+1}} + \frac{(2R_S - \chi_i - \chi_{i+1})}{(\chi_i+\chi_{i+1})^2}\left(v^0_{i+1,k} + v^0_{i,k}\right) - \frac{v^R_{i+1,k} + v^R_{i,k}}{\chi_i + \chi_{i+1}}\right] \tag{4.9d}$$

$$\left(\tau^{\theta\mathbf{z}}_{\mathbf{i,n}}\right)^R = \frac{2}{\overline{\overline{Re^t_{i,n}}}^{z}}\left[\frac{v^R_{i,k+1} - v^R_{i,k}}{\Delta z_k + \Delta z_{k+1}} - \frac{1}{2\chi_i}w^I_{i,n}\right] \tag{4.9e}$$

$$\left(\tau^{\mathbf{z}\chi}_{\ell,\mathbf{n}}\right)^R = \frac{2}{\overline{\overline{Re^t_{\ell,n}}}^{\chi z}}\left(\frac{u^R_{\ell,k+1} - u^R_{\ell,k}}{\Delta z_k + \Delta z_{k+1}} + \frac{w^0_{i+1,n} - w^0_{i,n}}{\Delta\chi_{i+1} + \Delta\chi_i} + \frac{w^R_{i+1,n} - w^R_{i,n}}{\Delta\chi_{i+1} + \Delta\chi_i}\right) \tag{4.9f}$$

Imaginary First Order Discrete Reynolds Stress Terms

$$\left(\tau^{\chi\chi}_{\mathbf{i,k}}\right)^I = \frac{2}{Re^t_{i,k}}\left[\frac{1}{\chi_i}\frac{\chi_\ell u^I_{\ell,k} - \chi_{\ell-1}u^I_{\ell-1,k}}{\Delta\chi_i} - \frac{u^I_{\ell,k} + u^I_{\ell-1,k}}{2\chi_i}\right] \tag{4.10a}$$

$$\left(\tau^{\theta\theta}_{\mathbf{i,k}}\right)^I = \frac{2}{Re^t_{i,k}}\left[\frac{u^I_{\ell,k} + u^I_{\ell-1,k}}{2\chi_i} + \frac{1}{\chi_i}\left\{v^R_{i,k} + 2\left(R_S - \chi_i\right)\frac{v^0_{i+1,k} - v^0_{i-1,k}}{\Delta\chi_{i+1} + 2\Delta\chi_i + \chi_{i-1}}\right\}\right] \tag{4.10b}$$

$$\left(\tau^{\mathbf{zz}}_{\mathbf{i,k}}\right)^I = \frac{2}{Re^t_{i,k}}\left(\frac{w^I_{i,k,n} - w^I_{i,k,n-1}}{\Delta z_k}\right) \tag{4.10c}$$

$$\begin{aligned}\left(\tau^{\chi\theta}_{\ell,\mathbf{k}}\right)^I = \frac{2}{\overline{\overline{Re^t_{\ell,k}}}^{\chi}}\Bigg[&\frac{1}{\chi_{i+1}+\chi_i}\left\{u^R_{\ell,k} + \frac{\left(R_S - \chi_{\ell+1}\right)u^0_{\ell+1,k} - \left(R_S - \chi_{\ell-1}\right)u^0_{\ell-1,k}}{\Delta\chi_i + \Delta\chi_{i+1}}\right\}\\ &+\frac{2}{\chi_{i+1}+\chi_i}\frac{\chi_{i+1}v^I_{i+1,k} - \chi_i v^I_{i,k}}{\Delta\chi_i + \Delta\chi_{i+1}} - \frac{v^I_{i+1,k} + v^I_{i,k}}{\chi_i + \chi_{i+1}}\Bigg]\end{aligned} \tag{4.10d}$$

$$\begin{aligned}\left(\tau^{\theta\mathbf{z}}_{\mathbf{i,n}}\right)^I = \frac{2}{\overline{\overline{Re^t_{i,n}}}^{z}}\Bigg[&\frac{v^I_{i,k+1} - v^I_{i,k}}{\Delta z_k + \Delta z_{k+1}} + \frac{1}{2\chi_i}w^R_{i,n}\\ &+\frac{\Delta\chi_{i+1}}{\chi_i\Delta\chi_i}\left(\frac{\left(R_S - \chi_{i+1}\right)w^0_{i+1,n}}{\Delta\chi_i + 2\Delta\chi_{i+1} + \Delta\chi_{i+2}}\right) - \frac{\Delta\chi_{i-1}}{\chi_i\Delta\chi_i}\left(\frac{\left(R_S - \chi_{i-1}\right)w^0_{i-1,n}}{\Delta\chi_{i-2} + 2\Delta\chi_{i-1} + \Delta\chi_i}\right)\Bigg]\end{aligned} \tag{4.10e}$$

$$\left(\tau^{\mathbf{z}\chi}_{\ell,\mathbf{n}}\right)^I = \frac{2}{\overline{\overline{Re^t_{\ell,n}}}^{\chi z}}\left(\frac{u^I_{\ell,k+1} - u^I_{\ell,k}}{\Delta z_k + \Delta z_{k+1}} + \frac{w^I_{i+1,n} - w^I_{i,n}}{\Delta\chi_{i+1} + \Delta\chi_i}\right) \tag{4.10f}$$

Equation 4.2 has three directional components to be discretized, one for each of the momentum equations.

Zeroth Order Discrete Eddy Viscosity Operator: $\overline{\mathscr{D}^0}\left(\tau\right)$

$$\begin{bmatrix} \overline{\mathscr{D}}^{0,\chi}\left[\tau_{qs}\right]_{\ell,k} \\ \overline{\mathscr{D}}^{0,\theta}\left[\tau_{qs}\right]_{i,k} \\ \overline{\mathscr{D}}^{0,z}\left[\tau_{qs}\right]_{i,n} \end{bmatrix} = \begin{bmatrix} 2\dfrac{\tau^{\chi\chi}_{\mathbf{i+1,k}}{}^{0} - \tau^{\chi\chi 0}_{\mathbf{i,k}}}{\Delta\chi_i + \Delta\chi_{i+1}} + \dfrac{\tau^{\chi\mathbf{z}}_{\ell,\mathbf{n}}{}^{0} - \tau^{\chi\mathbf{z}}_{\ell,\mathbf{n-1}}{}^{0}}{\Delta z_k} \\ + \dfrac{1}{\chi_\ell}\left(\dfrac{\Delta\chi_i\tau^{\chi\chi 0}_{\mathbf{i,k}} + \Delta\chi_{i+1}\tau^{\chi\chi}_{\mathbf{i+1,k}}{}^{0}}{\Delta\chi_i + \Delta\chi_{i+1}} - \dfrac{\Delta\chi_i\tau^{\theta\theta 0}_{\mathbf{i,k}} + \Delta\chi_{i+1}\tau^{\theta\theta}_{\mathbf{i+1,k}}{}^{0}}{\Delta\chi_i + \Delta\chi_{i+1}}\right) \\ \dfrac{\tau^{\theta\chi 0}_{\ell,\mathbf{k}} - \tau^{\theta\chi}_{\ell-\mathbf{1,k}}{}^{0}}{\Delta\chi_i} + \dfrac{\tau^{\theta\mathbf{z}0}_{\mathbf{i,n}} - \tau^{\theta\mathbf{z}}_{\mathbf{i,n-1}}{}^{0}}{\Delta z_k} \\ + \dfrac{1}{\chi_i}\dfrac{\left(\Delta\chi_{i-1} + \Delta\chi_i\right)\tau^{\theta\chi}_{\ell-\mathbf{1,k}}{}^{0} + \left(\Delta\chi_i + \Delta\chi_{i+1}\right)\tau^{\theta\chi 0}_{\ell,\mathbf{k}}}{2\Delta\chi_i} \\ \dfrac{1}{\chi_i\Delta\chi_i}\left(\chi_\ell\tau^{\mathbf{z}\chi}_{\ell,\mathbf{n}}{}^{0} - \chi_{\ell-1}\tau^{\mathbf{z}\chi}_{\ell-\mathbf{1,n}}{}^{0}\right) + \dfrac{\tau^{\mathbf{zz}}_{\mathbf{i,k+1}}{}^{0} - \tau^{\mathbf{zz}0}_{\mathbf{i,k}}}{\Delta z_k} \end{bmatrix} \tag{4.11}$$

Real First Order Discrete Eddy Viscosity Operator: $\overline{\mathscr{D}^R}\left(\tau\right)$

$$\begin{bmatrix} \overline{\mathscr{D}}^{R,\chi}\left[\tau_{qs}\right]_{\ell,k} \\ \overline{\mathscr{D}}^{R,\theta}\left[\tau_{qs}\right]_{i,k} \\ \overline{\mathscr{D}}^{R,z}\left[\tau_{qs}\right]_{i,n} \end{bmatrix} = \begin{bmatrix} 2\dfrac{\tau^{\chi\chi\ 0}_{\mathbf{i+1,k}}-\tau^{\chi\chi 0}_{\mathbf{i,k}}}{\Delta\chi_i+\Delta\chi_{i+1}}+2\dfrac{\tau^{\chi\chi\ R}_{\mathbf{i+1,k}}-\tau^{\chi\chi R}_{\mathbf{i,k}}}{\Delta\chi_i+\Delta\chi_{i+1}}+\dfrac{\tau^{\chi\mathbf{z}\ R}_{\ell,\mathbf{n}}-\tau^{\chi\mathbf{z}\ \ R}_{\ell,\mathbf{n-1}}}{\Delta z_k}-\dfrac{1}{\chi_\ell}\tau^{\chi\theta I}_{\ell,\mathbf{k}} \\ -\dfrac{(R_S-\chi_\ell)}{\chi_\ell^2}\left(\dfrac{\Delta\chi_i\tau^{\chi\chi 0}_{\mathbf{i,k}}+\Delta\chi_{i+1}\tau^{\chi\chi\ 0}_{\mathbf{i+1,k}}}{\Delta\chi_i+\Delta\chi_{i+1}}-\dfrac{\Delta\chi_i\tau^{\theta\theta 0}_{\mathbf{i,k}}+\Delta\chi_{i+1}\tau^{\theta\theta\ 0}_{\mathbf{i+1,k}}}{\Delta\chi_i+\Delta\chi_{i+1}}\right) \\ +\dfrac{1}{\chi_\ell}\left(\dfrac{\Delta\chi_i\tau^{\chi\chi R}_{\mathbf{i,k}}+\Delta\chi_{i+1}\tau^{\chi\chi\ R}_{\mathbf{i+1,k}}}{\Delta\chi_i+\Delta\chi_{i+1}}-\dfrac{\Delta\chi_i\tau^{\theta\theta R}_{\mathbf{i,k}}+\Delta\chi_{i+1}\tau^{\theta\theta\ R}_{\mathbf{i+1,k}}}{\Delta\chi_i+\Delta\chi_{i+1}}\right) \\ \dfrac{\tau^{\theta\chi 0}_{\ell,\mathbf{k}}-\tau^{\theta\chi\ \ 0}_{\ell-1,\mathbf{k}}}{\Delta\chi_i}+\dfrac{\tau^{\theta\chi R}_{\ell,\mathbf{k}}-\tau^{\theta\chi\ \ R}_{\ell-1,\mathbf{k}}}{\Delta\chi_i}+\dfrac{\tau^{\theta\mathbf{z}R}_{\mathbf{i,n}}-\tau^{\theta\mathbf{z}\ \ R}_{\mathbf{i,n-1}}}{\Delta z_k}-\dfrac{\tau^{\theta\theta I}_{\mathbf{i,k}}}{\chi_i} \\ -\dfrac{(R_S-\chi_i)}{\chi_i^2}\dfrac{(\Delta\chi_{i-1}+\Delta\chi_i)\,\tau^{\theta\chi\ \ 0}_{\ell-1,\mathbf{k}}+(\Delta\chi_i+\Delta\chi_{i+1})\,\tau^{\theta\chi 0}_{\ell,\mathbf{k}}}{4\Delta\chi_i} \\ +\dfrac{1}{\chi_i}\dfrac{(\Delta\chi_{i-1}+\Delta\chi_i)\,\tau^{\theta\chi\ \ R}_{\ell-1,\mathbf{k}}+(\Delta\chi_i+\Delta\chi_{i+1})\,\tau^{\theta\chi R}_{\ell,\mathbf{k}}}{4\Delta\chi_i} \\ -\dfrac{(R_S-\chi_i)}{\chi_i^2}\dfrac{(\Delta\chi_{i-1}+\Delta\chi_i)\,\tau^{\chi\theta\ \ 0}_{\ell-1,\mathbf{k}}+(\Delta\chi_i+\Delta\chi_{i+1})\,\tau^{\chi\theta 0}_{\ell,\mathbf{k}}}{4\Delta\chi_i} \\ +\dfrac{1}{\chi_i}\dfrac{(\Delta\chi_{i-1}+\Delta\chi_i)\,\tau^{\chi\theta\ \ R}_{\ell-1,\mathbf{k}}+(\Delta\chi_i+\Delta\chi_{i+1})\,\tau^{\chi\theta R}_{\ell,\mathbf{k}}}{4\Delta\chi_i} \\ \dfrac{1}{\chi_i\Delta\chi_i}\left((R_S-\chi_\ell)\,\tau^{\mathbf{z}\chi\ 0}_{\ell,\mathbf{n}}-(R_S-\chi_{\ell-1})\,\tau^{\mathbf{z}\chi\ \ 0}_{\ell-1,\mathbf{n}}\right) \\ -\dfrac{1}{\Delta\chi_i}\dfrac{(R_S-\chi_i)}{\chi_i^2}\left(\chi_\ell\tau^{\mathbf{z}\chi\ 0}_{\ell,\mathbf{n}}-\chi_{\ell-1}\tau^{\mathbf{z}\chi\ \ 0}_{\ell-1,\mathbf{n}}\right) \\ +\dfrac{1}{\chi_i\Delta\chi_i}\left(\chi_\ell\tau^{\mathbf{z}\chi\ 0}_{\ell,\mathbf{n}}-\chi_{\ell-1}\tau^{\mathbf{z}\chi\ \ 0}_{\ell-1,\mathbf{n}}\right)+\dfrac{1}{\chi_i\Delta\chi_i}\left(\chi_\ell\tau^{\mathbf{z}\chi\ R}_{\ell,\mathbf{n}}-\chi_{\ell-1}\tau^{\mathbf{z}\chi\ \ R}_{\ell-1,\mathbf{n}}\right) \\ -\dfrac{1}{\chi_i}\tau^{\mathbf{z}\theta I}_{\mathbf{i,n}}+\dfrac{\tau^{\mathbf{zz}\ \ R}_{\mathbf{i,k+1}}-\tau^{\mathbf{zz}\ R}_{\mathbf{i,k}}}{\Delta z_k} \end{bmatrix} \tag{4.12}$$

Imaginary First Order Discrete Tensor Divergence Operator: $\overline{\mathscr{D}^I}\left(\tau\right)$

$$\begin{bmatrix} \overline{\mathscr{D}}^{I,\chi}\left[\tau_{qs}\right]_{\ell,k} \\ \overline{\mathscr{D}}^{I,\theta}\left[\tau_{qs}\right]_{i,k} \\ \overline{\mathscr{D}}^{I,z}\left[\tau_{qs}\right]_{i,n} \end{bmatrix} = \begin{bmatrix} -2\dfrac{\tau^{\chi\chi\ I}_{\mathbf{i+1,k}} - \tau^{\chi\chi I}_{\mathbf{i,k}}}{\Delta\chi_i + \Delta\chi_{i+1}} - \dfrac{\tau^{\chi\mathbf{z}\ I}_{\ell,\mathbf{n}} - \tau^{\chi\mathbf{z}\ \ I}_{\ell,\mathbf{n-1}}}{\Delta z_k} \\ -\dfrac{1}{\chi_\ell}\tau^{\chi\theta R}_{\ell,\mathbf{k}} + \dfrac{(R_S-\chi_\ell)}{\chi_\ell}\dfrac{\tau^{\chi\theta\ \ 0}_{\ell+1,\mathbf{k}} - \tau^{\chi\theta\ \ 0}_{\ell-1,\mathbf{k}}}{\Delta\chi_i + \Delta\chi_{i+1}} \\ -\dfrac{1}{\chi_\ell}\left(\dfrac{\Delta\chi_i\tau^{\chi\chi\ I}_{\mathbf{i,k}} + \Delta\chi_{i+1}\tau^{\chi\chi\ \ I}_{\mathbf{i+1,k}}}{\Delta\chi_i + \Delta\chi_{i+1}} - \dfrac{\Delta\chi_i\tau^{\theta\theta I}_{\mathbf{i,k}} + \Delta\chi_{i+1}\tau^{\theta\theta\ \ I}_{\mathbf{i+1,k}}}{\Delta\chi_i + \Delta\chi_{i+1}}\right) \\ \hdashline -\dfrac{\tau^{\theta\chi I}_{\ell,\mathbf{k}} - \tau^{\theta\chi\ \ I}_{\ell-1,\mathbf{k}}}{\Delta\chi_i} - \dfrac{\tau^{\theta\mathbf{z}I}_{\mathbf{i,n}} - \tau^{\theta\mathbf{z}\ \ I}_{\mathbf{i,n-1}}}{\Delta z_k} - \dfrac{\tau^{\theta\theta R}_{\mathbf{i,k}}}{\chi_i} \\ +2\dfrac{1}{\chi_i}\dfrac{\Delta\chi_{i+1}}{\Delta\chi_i}\dfrac{(R_S-\chi_{i+1})\,\tau^{\theta\theta\ \ 0}_{\mathbf{i+1,k}}}{\Delta\chi_{i+2}+2\Delta\chi_{i+1}+\Delta\chi_i} - 2\dfrac{1}{\chi_i}\dfrac{\Delta\chi_{i-1}}{\Delta\chi_i}\dfrac{(R_S-\chi_{i-1})\,\tau^{\theta\theta\ \ 0}_{\mathbf{i-1,k}}}{\Delta\chi_i+2\Delta\chi_{i-1}+\Delta\chi_{i-2}} \\ -\dfrac{1}{\chi_i}\dfrac{(\Delta\chi_{i-1}+\Delta\chi_i)\,\tau^{\theta\chi\ \ I}_{\ell-1,\mathbf{k}} + (\Delta\chi_i+\Delta\chi_{i+1})\,\tau^{\theta\chi\ I}_{\ell,\mathbf{k}}}{4\Delta\chi_i} \\ -\dfrac{1}{\chi_i}\dfrac{(\Delta\chi_{i-1}+\Delta\chi_i)\,\tau^{\chi\theta\ \ I}_{\ell-1,\mathbf{k}} + (\Delta\chi_i+\Delta\chi_{i+1})\,\tau^{\chi\theta I}_{\ell,\mathbf{k}}}{4\Delta\chi_i} \\ \hdashline -\dfrac{1}{\chi_i\Delta\chi_i}\left(\chi_\ell\tau^{\mathbf{z}\chi\ I}_{\ell,\mathbf{n}} - \chi_{\ell-1}\tau^{\mathbf{z}\chi\ \ I}_{\ell-1,\mathbf{n}}\right) \\ -\dfrac{1}{\chi_i}\tau^{\mathbf{z}\theta R}_{\mathbf{i,n}} + 2\dfrac{(R_S-\chi_i)}{\chi_i}\dfrac{\tau^{\mathbf{z}\theta\ \ 0}_{\mathbf{i+1,n}} - \tau^{\mathbf{z}\theta\ \ 0}_{\mathbf{i-1,n}}}{\Delta\chi_{i-1}+2\Delta\chi_i+\Delta\chi_{i+1}} \\ -\dfrac{\tau^{\mathbf{zz}\ \ I}_{\mathbf{i,k+1}} - \tau^{\mathbf{zz}\,I}_{\mathbf{i,k}}}{\Delta z_k} \end{bmatrix} \tag{4.13}$$

4.2 Discrete Turbulent Kinetic Energy Transport: Prandtl 1-Equation

The turbulent kinetic energy (TKE) variable is stored in the $\mathbf{CC}$ vector space, enabling convenient use of the vector gradient and divergence operators from the mass conservation and momentum pressure terms to perform analogous operations in the TKE transport equation. The complexity of the discrete form of the TKE equation comes from the production component's tensor product that must be converted from the $\mathbf{EC}$ vector space to the $\mathbf{CC}$. Conveniently, this discrete operation is analagous to the $\mathbf{EC}$ inner product given by Equation 3.19 that describes the discrete contraction of two $\mathbf{EC}$ vector space variables to single cell value. Just like in the previous section, the turbulent Reynolds number is averaged to the $\mathbf{EC}$ vector space along with the TKE variable inside the production term. Similarly, the dot product of velocity with the gradient of TKE is evaluated in the $\mathbf{CC}$ vector space using Equation 3.18. Because the TKE transport equation refers to the energy

contained in small eddies, it is assumed that the 1^{th} order components are negligible, thus only the 0^{th} order form is used herein.

$$\mathrm{St}\frac{\partial k_t}{\partial t} + \vec{u}_s \cdot \mathbf{G}_s\left(k_t\right) = \left[\frac{2}{Re_t}\mathbf{E}\left(\vec{u}\right) - \frac{2}{3}k_t\delta_{qs}\right] \otimes \mathcal{G}_s\vec{u}_q - C_D\frac{k^{\frac{3}{2}}}{\ell_t} + \mathbf{D}_s\left[\frac{1}{Re_T}\mathbf{G}_s\left(k_t\right)\right] \tag{4.14}$$

$$\mathrm{St}\frac{\partial k_t}{\partial t} + \vec{u}_s^0 \cdot \mathbf{G}_s^0\left(k_t\right) = {\tau_{\mathbf{qs}}}^0 \otimes \mathcal{G}_s\vec{u}_q^0 - C_D\frac{k^{\frac{3}{2}}}{\ell_t} + \mathbf{D}_s^0\left[\frac{1}{Re_T}\mathbf{G}_s^0\left(k_t\right)\right] \tag{4.15}$$

$$Re_t = \frac{\rho_c L_c U_c}{\mu_t} = \frac{\rho_c L_c U_c}{U_c k_t^{\frac{1}{2}} L_c \ell_t} \Rightarrow \frac{1}{Re_t} = \frac{\mu_t}{\rho_c L_c U_c} = k_t^{\frac{1}{2}}\ell_t \tag{4.16}$$

$$\frac{1}{Re_T} = \frac{1}{\rho_c L_c U_c}\left(\mu_c + \frac{\mu_t}{\sigma_k}\right) = \frac{1}{Re_c} + \frac{1}{\sigma_k Re_t} = \frac{1}{Re_c} + \frac{k_t^{\frac{1}{2}}\ell_t}{\sigma_k} \tag{4.17}$$

$$C_D \approx 0.30 \tag{4.18}$$

$$\sigma_k = 1 \tag{4.19}$$

$$\begin{aligned}\left\{\vec{u}^0 \cdot \mathbf{G}^0\left(k_t\right)\right\}_{i,k} =& \frac{\chi_{\ell-1}}{\chi_i}u^0_{\ell-1,k}\frac{k^{t,0}_{i,k} - k^{t,0}_{i-1,k}}{\Delta\chi_i + \Delta\chi_{i-1}} + \frac{\chi_\ell}{\chi_i}u^0_{\ell,k}\frac{k^{t,0}_{i+1,k} - k^{t,0}_{i,k}}{\Delta\chi_i + \Delta\chi_{i+1}} \\ &+ w^0_{i,n-1}\frac{k^{t,0}_{i,k} - k^{t,0}_{i,k-1}}{\Delta z_k + \Delta z_{k-1}} + w^0_{i,n}\frac{k^{t,0}_{i,k+1} - k^{t,0}_{i,k}}{\Delta z_k + \Delta z_{k+1}}\end{aligned} \tag{4.20}$$

$$\begin{aligned}\left\{\tau^0 \otimes \mathcal{G}\vec{u}^0\right\}_{i,k} =& \left(\tau^{\chi\chi^0}\mathcal{G}^\chi\vec{u}^0_\chi\right)_{i,k} + \left(\tau^{\theta\theta^0}\mathcal{G}^\theta\vec{u}^0_\theta\right)_{i,k} + \left(\tau^{\mathbf{zz}0}\mathcal{G}^z\vec{u}^0_z\right)_{i,k} \\ &+ \frac{\chi_i + \chi_{i-1}}{4\chi_i}\left(\tau^{\chi\theta^0}\mathcal{G}^\theta\vec{u}^0_\chi\right)_{\ell-1,k} + \frac{\chi_i + \chi_{i+1}}{4\chi_i}\left(\tau^{\chi\theta^0}\mathcal{G}^\theta\vec{u}^0_\chi\right)_{\ell,k} \\ &+ \frac{\chi_{\ell-1}}{4\chi_i}\left[\left(\tau^{\chi\mathbf{z}0}\mathcal{G}^z\vec{u}^0_\chi\right)_{\ell-1,n-1} + \left(\tau^{\chi\mathbf{z}0}\mathcal{G}^z\vec{u}^0_\chi\right)_{\ell-1,n}\right] \\ &+ \frac{\chi_\ell}{4\chi_i}\left[\left(\tau^{\chi\mathbf{z}0}\mathcal{G}^z\vec{u}^0_\chi\right)_{\ell,n-1} + \left(\tau^{\chi\mathbf{z}0}\mathcal{G}^z\vec{u}^0_\chi\right)_{\ell,n}\right] \\ &+ \frac{\chi_i + \chi_{i-1}}{4\chi_i}\left(\tau^{\theta\chi^0}\mathcal{G}^\chi\vec{u}^0_\theta\right)_{\ell-1,k} + \frac{\chi_i + \chi_{i+1}}{4\chi_i}\left(\tau^{\theta\chi^0}\mathcal{G}^\chi\vec{u}^0_\theta\right)_{\ell,k} \\ &+ \frac{1}{2}\left[\left(\tau^{\theta\mathbf{z}^0}\mathcal{G}^z\vec{u}^0_\theta\right)_{i,n-1} + \left(\tau^{\theta\mathbf{z}0}\mathcal{G}^z\vec{u}^0_\theta\right)_{i,n}\right] \\ &+ \frac{\chi_{\ell-1}}{4\chi_i}\left[\left(\tau^{\mathbf{z}\chi^0}\mathcal{G}^\chi\vec{u}^0_z\right)_{\ell-1,n-1} + \left(\tau^{\mathbf{z}\chi^0}\mathcal{G}^\chi\vec{u}^0_z\right)_{\ell-1,n}\right] \\ &+ \frac{\chi_\ell}{4\chi_i}\left[\left(\tau^{\mathbf{z}\chi^0}\mathcal{G}^\chi\vec{u}^0_z\right)_{\ell,n-1} + \left(\tau^{\mathbf{z}\chi^0}\mathcal{G}^\chi\vec{u}^0_z\right)_{\ell,n}\right] \\ &+ \frac{1}{2}\left[\left(\tau^{\mathbf{z}\theta^0}\cancel{\mathcal{G}^\theta\vec{u}^0_z}\right)_{i,n-1} + \left(\tau^{\mathbf{z}\theta^0}\cancel{\mathcal{G}^\theta\vec{u}^0_z}\right)_{i,n}\right]\end{aligned} \tag{4.21}$$

$$
\begin{aligned}
\left\{\tau^0 \otimes \mathcal{G}\vec{u}^0\right\}_{i,k} = &\left(\tau^{\chi\chi^0}\mathcal{G}^\chi \vec{u}_\chi^0\right)_{i,k} + \left(\tau^{\theta\theta^0}\mathcal{G}^\theta \vec{u}_\theta^0\right)_{i,k} + \left(\tau^{\mathbf{zz}0}\mathcal{G}^z \vec{u}_z^0\right)_{i,k} \\
&+ \frac{\chi_i + \chi_{i-1}}{4\chi_i}\left[\tau^{\chi\theta^0}\left(\mathcal{G}^\theta \vec{u}_\chi^0 + \mathcal{G}^\chi \vec{u}_\theta^0\right)\right]_{\ell-1,k} \\
&+ \frac{\chi_i + \chi_{i+1}}{4\chi_i}\left[\tau^{\chi\theta^0}\left(\mathcal{G}^\theta \vec{u}_\chi^0 + \mathcal{G}^\chi \vec{u}_\theta^0\right)\right]_{\ell,k} \\
&+ \frac{\chi_{\ell-1}}{4\chi_i}\left[\left\{\tau^{\chi\mathbf{z}0}\left(\mathcal{G}^z \vec{u}_\chi^0 + \mathcal{G}^\chi \vec{u}_z^0\right)\right\}_{\ell-1,n-1} + \left\{\tau^{\chi\mathbf{z}0}\left(\mathcal{G}^z \vec{u}_\chi^0 + \mathcal{G}^\chi \vec{u}_z^0\right)\right\}_{\ell-1,n}\right] \\
&\quad + \frac{\chi_\ell}{4\chi_i}\left[\left\{\tau^{\chi\mathbf{z}0}\left(\mathcal{G}^z \vec{u}_\chi^0 + \mathcal{G}^\chi \vec{u}_z^0\right)\right\}_{\ell,n-1} + \left\{\tau^{\chi\mathbf{z}0}\left(\mathcal{G}^z \vec{u}_\chi^0 + \mathcal{G}^\chi \vec{u}_z^0\right)\right\}_{\ell,n}\right] \\
&+ \frac{1}{2}\left[\left(\tau^{\theta\mathbf{z}0}\mathcal{G}^z \vec{u}_\theta^0\right)_{i,n-1} + \left(\tau^{\theta\mathbf{z}0}\mathcal{G}^z \vec{u}_\theta^0\right)_{i,n}\right]
\end{aligned}
\tag{4.22}
$$

$$
\begin{aligned}
\left\{\tau^0 \otimes \mathcal{G}\vec{u}^0\right\}_{i,k} = &\left[\frac{2}{Re^t}\left(\underline{\underline{E}}^{\chi\chi^0}\right)^2\right]_{i,k} + \left[\frac{2}{Re^t}\left(\underline{\underline{E}}^{\theta\theta^0}\right)^2\right]_{i,k} + \left[\frac{2}{Re^t}\left(\underline{\underline{E}}^{zz^0}\right)^2\right]_{i,k} - \frac{2}{3}k_t\cancel{(\nabla\cdot\vec{u})} \\
&+ \frac{\chi_i + \chi_{i-1}}{4\chi_i}\left[\frac{2}{\overline{\overline{Re^t}}^\chi}\underline{\underline{E}}^{\chi\theta^0}\left(\mathcal{G}^\theta \vec{u}_\chi^0 + \mathcal{G}^\chi \vec{u}_\theta^0\right)\right]_{\ell-1,k} \\
&+ \frac{\chi_i + \chi_{i+1}}{4\chi_i}\left[\frac{2}{\overline{\overline{Re^t}}^\chi}\underline{\underline{E}}^{\chi\theta^0}\left(\mathcal{G}^\theta \vec{u}_\chi^0 + \mathcal{G}^\chi \vec{u}_\theta^0\right)\right]_{\ell,k} \\
&+ \frac{\chi_{\ell-1}}{4\chi_i}\left[\left\{\frac{2}{\overline{\overline{Re^t_{\ell,n}}}^{\chi z}}\underline{\underline{E}}^{\chi z0}\left(\mathcal{G}^z \vec{u}_\chi^0 + \mathcal{G}^\chi \vec{u}_z^0\right)\right\}_{\ell-1,n-1} + \left\{\frac{2}{\overline{\overline{Re^t_{\ell,n}}}^{\chi z}}\underline{\underline{E}}^{\chi z0}\left(\mathcal{G}^z \vec{u}_\chi^0 + \mathcal{G}^\chi \vec{u}_z^0\right)\right\}_{\ell-1,n}\right] \\
&\quad + \frac{\chi_\ell}{4\chi_i}\left[\left\{\frac{2}{\overline{\overline{Re^t_{\ell,n}}}^{\chi z}}\underline{\underline{E}}^{\chi z0}\left(\mathcal{G}^z \vec{u}_\chi^0 + \mathcal{G}^\chi \vec{u}_z^0\right)\right\}_{\ell,n-1} + \left\{\frac{2}{\overline{\overline{Re^t_{\ell,n}}}^{\chi z}}\underline{\underline{E}}^{\chi z0}\left(\mathcal{G}^z \vec{u}_\chi^0 + \mathcal{G}^\chi \vec{u}_z^0\right)\right\}_{\ell,n}\right] \\
&+ \frac{1}{2}\left[\left(\frac{2}{\overline{\overline{Re^t}}^z}\underline{\underline{E}}^{\theta z^0}\mathcal{G}^z \vec{u}_\theta^0\right)_{i,n-1} + \left(\frac{2}{\overline{\overline{Re^t}}^z}\underline{\underline{E}}^{\theta z^0}\mathcal{G}^z \vec{u}_\theta^0\right)_{i,n}\right]
\end{aligned}
\tag{4.23}
$$

$$\begin{aligned}\left\{\tau^0 \otimes \mathcal{G}\vec{u}^0\right\}_{i,k} = &\left[\frac{2}{Re^t}\left(\underline{\underline{E}}^{\chi\chi 0}\right)^2\right]_{i,k} + \left[\frac{2}{Re^t}\left(\underline{\underline{E}}^{\theta\theta 0}\right)^2\right]_{i,k} + \left[\frac{2}{Re^t}\left(\underline{\underline{E}}^{zz 0}\right)^2\right]_{i,k} - \frac{2}{3}k_t\cancel{(\nabla\cdot\vec{u})} \\ &+ \frac{\chi_i + \chi_{i-1}}{\chi_i}\left[\frac{1}{\overline{\overline{Re^t}}^{\chi}}\left(\underline{\underline{E}}^{\chi\theta 0}\right)^2\right]_{\ell-1,k} + \frac{\chi_i + \chi_{i+1}}{\chi_i}\left[\frac{1}{\overline{\overline{Re^t}}^{\chi}}\left(\underline{\underline{E}}^{\chi\theta 0}\right)^2\right]_{\ell,k} \\ &+ \frac{\chi_{\ell-1}}{\chi_i}\left[\left\{\frac{1}{\overline{\overline{Re^t_{\ell,n}}}^{\chi z}}\left(\underline{\underline{E}}^{\chi z 0}\right)^2\right\}_{\ell-1,n-1} + \left\{\frac{1}{\overline{\overline{Re^t_{\ell,n}}}^{\chi z}}\left(\underline{\underline{E}}^{\chi z 0}\right)^2\right\}_{\ell-1,n}\right] \\ &+ \frac{\chi_\ell}{\chi_i}\left[\left\{\frac{1}{\overline{\overline{Re^t_{\ell,n}}}^{\chi z}}\left(\underline{\underline{E}}^{\chi z 0}\right)^2\right\}_{\ell,n-1} + \left\{\frac{1}{\overline{\overline{Re^t_{\ell,n}}}^{\chi z}}\left(\underline{\underline{E}}^{\chi z 0}\right)^2\right\}_{\ell,n}\right] \\ &+ \left[\frac{2}{\overline{\overline{Re^t}}^{z}}\left(\underline{\underline{E}}^{\theta z 0}\right)^2\right]_{i,n-1} + \left[\frac{2}{\overline{\overline{Re^t}}^{z}}\left(\underline{\underline{E}}^{\theta z 0}\right)^2\right]_{i,n}\end{aligned} \tag{4.24}$$

$$\left(\mathcal{G}^{\chi}\vec{u}^0_{\chi}\right)^0_{i,k} = \frac{1}{\chi_i}\frac{\chi_\ell u^0_{\ell,k} - \chi_{\ell-1}u^0_{\ell-1,k}}{\Delta\chi_i} - \frac{1}{\chi_i}\frac{u^0_{\ell,k} + u^0_{\ell-1,k}}{2} \tag{4.25}$$

$$\left(\mathcal{G}^{\theta}\vec{u}^0_{\chi}\right)^0_{\ell,k} = -\frac{v^0_{i+1,k} + v^0_{i,k}}{\chi_i + \chi_{i+1}} \tag{4.26}$$

$$\left(\mathcal{G}^{z}\vec{u}^0_{\chi}\right)^0_{\ell,n} = 2\frac{u^0_{\ell,k+1} - u^0_{\ell,k}}{\Delta z_k + \Delta z_{k+1}} \tag{4.27}$$

$$\left(\mathcal{G}^{\chi}\vec{u}^0_{\theta}\right)^0_{\ell,k} = \frac{4}{\chi_{i+1} + \chi_i}\frac{\chi_{i+1}v^0_{i+1,k} - \chi_i v^0_{i,k}}{\Delta\chi_i + \Delta\chi_{i+1}} - \frac{v^0_{i+1,k} + v^0_{i,k}}{\chi_i + \chi_{i+1}} \tag{4.28}$$

$$\left(\mathcal{G}^{\theta}\vec{u}^0_{\theta}\right)^0_{i,k} = \frac{1}{\chi_i}\frac{u^0_{\ell,k} + u^0_{\ell-1,k}}{2} \tag{4.29}$$

$$\left(\mathcal{G}^{z}\vec{u}^0_{\theta}\right)^0_{i,n} = 2\frac{v^0_{i,k+1} - v^0_{i,k}}{\Delta z_k + \Delta z_{k+1}} \tag{4.30}$$

$$\left(\mathcal{G}^{\chi}\vec{u}^0_{z}\right)^0_{\ell,n} = 2\frac{w^0_{i+1,n} - w^0_{i,n}}{\Delta\chi_{i+1} + \Delta\chi_i} \tag{4.31}$$

$$\left(\mathcal{G}^{\theta}\vec{u}^0_{z}\right)^0_{i,n} = 0 \tag{4.32}$$

$$\left(\mathcal{G}^{z}\vec{u}^0_{z}\right)^0_{i,k} = \frac{w^0_{i,k,n} - w^0_{i,k,n-1}}{\Delta z_k} \tag{4.33}$$

$$
\begin{aligned}
\left\{\tau^0 \otimes \mathscr{G}\vec{u}^0\right\}_{i,k} =& \tau^{\chi\chi 0}_{i,k}\left(\frac{1}{\chi_i}\frac{\chi_\ell u^0_{\ell,k} - \chi_{\ell-1}u^0_{\ell-1,k}}{\Delta\chi_i} - \frac{1}{\chi_i}\frac{u^0_{\ell,k}+u^0_{\ell-1,k}}{2}\right)\\
&- \tau^{\chi\theta 0}_{\ell-1,k}\frac{v^0_{i,k}+v^0_{i-1,k}}{4\chi_i} - \tau^{\chi\theta 0}_{\ell,k}\frac{v^0_{i+1,k}+v^0_{i,k}}{4\chi_i}\\
&+ \frac{\chi_{\ell-1}}{2\chi_i}\left[\tau^{\chi\mathbf{z}0}_{\ell-1,n-1}\frac{u^0_{\ell-1,k}-u^0_{\ell-1,k-1}}{\Delta z_{k-1}+\Delta z_k} + \tau^{\chi\mathbf{z}0}_{\ell-1,n}\frac{u^0_{\ell-1,k+1}-u^0_{\ell-1,k}}{\Delta z_k+\Delta z_{k+1}}\right]\\
&+ \frac{\chi_\ell}{2\chi_i}\left[\tau^{\chi\mathbf{z}0}_{\ell,n-1}\frac{u^0_{\ell,k}-u^0_{\ell,k-1}}{\Delta z_{k-1}+\Delta z_k} + \tau^{\chi\mathbf{z}0}_{\ell,n}\frac{u^0_{\ell,k+1}-u^0_{\ell,k}}{\Delta z_k+\Delta z_{k+1}}\right]\\
&+ \tau^{\theta\chi 0}_{\ell-1,k}\left(\frac{1}{\chi_i}\frac{\chi_i v^0_{i,k} - \chi_{i-1}v^0_{i-1,k}}{\Delta\chi_i+\Delta\chi_{i-1}} - \frac{v^0_{i,k}+v^0_{i-1,k}}{4\chi_i}\right)\\
&+ \tau^{\theta\chi 0}_{\ell,k}\left(\frac{1}{\chi_i}\frac{\chi_{i+1} v^0_{i+1,k} - \chi_i v^0_{i,k}}{\Delta\chi_i+\Delta\chi_{i+1}} - \frac{v^0_{i+1,k}+v^0_{i,k}}{4\chi_i}\right)\\
&+ \tau^{\theta\theta 0}_{i,k}\frac{1}{\chi_i}\frac{u^0_{\ell,k}+u^0_{\ell-1,k}}{2} + \tau^{\mathbf{z}\mathbf{z}0}_{i,k}\frac{w^0_{i,k,n}-w^0_{i,k,n-1}}{\Delta z_k}\\
&+ \tau^{\theta\mathbf{z}0}_{i,n-1}\frac{v^0_{i,k}-v^0_{i,k-1}}{\Delta z_k+\Delta z_{k-1}} + \tau^{\theta\mathbf{z}0}_{i,n}\frac{v^0_{i,k+1}-v^0_{i,k}}{\Delta z_k+\Delta z_{k+1}}\\
&+ \frac{\chi_{\ell-1}}{2\chi_i}\left[\tau^{\mathbf{z}\chi 0}_{\ell-1,n-1}\frac{w^0_{i,n-1}-w^0_{i-1,n-1}}{\Delta\chi_{i-1}+\Delta\chi_i} + \tau^{\mathbf{z}\chi 0}_{\ell-1,n}\frac{w^0_{i,n}-w^0_{i-1,n}}{\Delta\chi_{i-1}+\Delta\chi_i}\right]\\
&+ \frac{\chi_\ell}{2\chi_i}\left[\tau^{\mathbf{z}\chi 0}_{\ell,n-1}\frac{w^0_{i+1,n-1}-w^0_{i,n-1}}{\Delta\chi_{i+1}+\Delta\chi_i} + \tau^{\mathbf{z}\chi 0}_{\ell,n}\frac{w^0_{i+1,n}-w^0_{i,n}}{\Delta\chi_{i+1}+\Delta\chi_i}\right]
\end{aligned}
\tag{4.34}
$$

$$
\begin{aligned}
\left\{\tau^0 \otimes \mathcal{G}\vec{u}^0\right\}_{i,k} =& \tau^{\chi\chi 0}_{i,k}\left(\frac{1}{\chi_i}\frac{\chi_\ell u^0_{\ell,k} - \chi_{\ell-1}u^0_{\ell-1,k}}{\Delta\chi_i} - \frac{1}{\chi_i}\frac{u^0_{\ell,k}+u^0_{\ell-1,k}}{2}\right)\\
&+ \tau^{\theta\theta 0}_{i,k}\frac{1}{\chi_i}\frac{u^0_{\ell,k}+u^0_{\ell-1,k}}{2} + \tau^{\mathbf{zz}0}_{i,k}\frac{w^0_{i,k,n}-w^0_{i,k,n-1}}{\Delta z_k}\\
&+ \tau^{\chi\theta 0}_{\ell-1,k}\left(\frac{1}{\chi_i}\frac{\chi_i v^0_{i,k} - \chi_{i-1}v^0_{i-1,k}}{\Delta\chi_i+\Delta\chi_{i-1}} - \frac{v^0_{i,k}+v^0_{i-1,k}}{2\chi_i}\right)\\
&+ \tau^{\chi\theta 0}_{\ell,k}\left(\frac{1}{\chi_i}\frac{\chi_{i+1} v^0_{i+1,k} - \chi_i v^0_{i,k}}{\Delta\chi_i+\Delta\chi_{i+1}} - \frac{v^0_{i+1,k}+v^0_{i,k}}{2\chi_i}\right)\\
&+ \tau^{\theta\mathbf{z}0}_{i,n-1}\frac{v^0_{i,k}-v^0_{i,k-1}}{\Delta z_k+\Delta z_{k-1}} + \tau^{\theta\mathbf{z}0}_{i,n}\frac{v^0_{i,k+1}-v^0_{i,k}}{\Delta z_k+\Delta z_{k+1}}\\
&+ \frac{\chi_{\ell-1}}{2\chi_i}\tau^{\mathbf{z}\chi 0}_{\ell-1,n-1}\left[\frac{u^0_{\ell-1,k}-u^0_{\ell-1,k-1}}{\Delta z_{k-1}+\Delta z_k} + \frac{w^0_{i,n-1}-w^0_{i-1,n-1}}{\Delta\chi_{i-1}+\Delta\chi_i}\right]\\
&+ \frac{\chi_{\ell-1}}{2\chi_i}\tau^{\mathbf{z}\chi 0}_{\ell-1,n}\left[\frac{u^0_{\ell-1,k+1}-u^0_{\ell-1,k}}{\Delta z_k+\Delta z_{k+1}} + \frac{w^0_{i,n}-w^0_{i-1,n}}{\Delta\chi_{i-1}+\Delta\chi_i}\right]\\
&+ \frac{\chi_\ell}{2\chi_i}\tau^{\mathbf{z}\chi 0}_{\ell,n-1}\left[\frac{u^0_{\ell,k}-u^0_{\ell,k-1}}{\Delta z_{k-1}+\Delta z_k} + \frac{w^0_{i+1,n-1}-w^0_{i,n-1}}{\Delta\chi_{i+1}+\Delta\chi_i}\right]\\
&+ \frac{\chi_\ell}{2\chi_i}\tau^{\mathbf{z}\chi 0}_{\ell,n}\left[\frac{u^0_{\ell,k+1}-u^0_{\ell,k}}{\Delta z_k+\Delta z_{k+1}} + \frac{w^0_{i+1,n}-w^0_{i,n}}{\Delta\chi_{i+1}+\Delta\chi_i}\right]
\end{aligned}
\tag{4.35}
$$

$$
\begin{aligned}
\left\{\mathbf{D}^0\left[\frac{1}{Re}\mathbf{G}^0\left(k_t\right)\right]\right\}_{i,k} =& \left[\frac{1}{Re}+\frac{1}{\overline{\overline{Re^t_{\ell,k}}^{\chi}}}\right]\frac{2\chi_\ell}{\chi_i\Delta\chi_i}\frac{k^{t,0}_{i+1,k}-k^{t,0}_{i,k}}{\Delta\chi_i+\Delta\chi_{i+1}}\\
&- \left[\frac{1}{Re}+\frac{1}{\overline{\overline{Re^t_{\ell-1,k}}^{\chi}}}\right]\frac{2\chi_{\ell-1}}{\chi_i\Delta\chi_i}\frac{k^{t,0}_{i,k}-k^{t,0}_{i-1,k}}{\Delta\chi_i+\Delta\chi_{i-1}}\\
&+ \left[\frac{1}{Re}+\frac{1}{\overline{\overline{Re^t_{i,n}}^{z}}}\right]2\frac{k^{t,0}_{i,k+1}-k^{t,0}_{i,k}}{\Delta z_k\left(\Delta z_k+\Delta z_{k+1}\right)}\\
&- \left[\frac{1}{Re}+\frac{1}{\overline{\overline{Re^t_{i,n-1}}^{z}}}\right]2\frac{k^{t,0}_{i,k}-k^{t,0}_{i,k-1}}{\Delta z_k\left(\Delta z_k+\Delta z_{k-1}\right)}
\end{aligned}
\tag{4.36}
$$

Note that the tensor Reynolds stresses in the TKE production terms are symmetric since they are based on the strain rate tensor. This allows the simplification of Equation 4.34 to Equation 4.35. The boundary conditions for TKE must be assigned at each face on the inlet, outlet, rotor and stator. The TKE on the walls along the rotor and stator boundary faces is zero because of the no-slip condition. The inlet and outlet boundary values for TKE are more complicated. Like ANSYS CFX Solver,[138] a constant value for the TKE could be estimated along the mass flow inlet boundary

or a Neumann condition could be applied to the TKE with zero gradient. On the outlet, ANSYS CFX applies a constant gradient to the TKE, which is equivalent to declaring the second derivative of TKE to be zero on the boundary in the direction of flow.

The boundaries on TKE are selected to be zero gradient at the inlet to the seal and constant gradient at the seal exit (not necessarily zero). These boundary conditions are seleced to avoid having to estimate turbulent values at the inlet and exit prior to the solution. The discrete forms of implementation for the inlet and outlet boundary conditions are in Equation 4.37. The zero gradient condition on the inlet is implemented implicitly, while the exit constant gradient boundary condition is a combination of implicit and explicit implementation, both with ghost cells as needed. The constant gradient boundary is applied based on the finite difference estimation of the second order derivative of TKE at the wall location of $n \pm \frac{1}{2}$.[84] On the rotor and stator surfaces, the TKE is of course equal to zero as a Dirichlet boundary condition due to the no-slip walls not allowing velocity fluctiation.

$$\begin{aligned} \frac{k}{\partial z}_{Inlet} = 0 = & \frac{k_{i,1} - k_{i,W}}{\Delta z_0 + \Delta z_1} + \frac{\Delta z_0 + \Delta z_1}{2} \frac{\partial^2 k}{\partial z^2}_{Inlet} \\ \Rightarrow & k_{i,W} = k_{i,1} \end{aligned} \tag{4.37}$$

4.2.1 Turbulent Length Scale, and Turbulence Model Empirical Coefficients

With a discrete TKE transport equation established, the two remaining empirical coefficients are σ_k and ℓ_t. The turbulent transport and pressure diffusion closure coefficient, σ_k, associated with the assumed gradient-diffusion of turbulence is typically assumed to be equal to 1.[123] The turbulent length scale, ℓ_t, is more complicated to estimate. Prandtl originated a characteristic ”mixing” length to the eddy viscosity model and described the concept of ”Boundary Layers” creating the foundation for the ”law of the wall”, Equations 4.39 to 4.41.[160] The law of the wall describes the logorithmic growth of non-dimensional velocity parallel to a no-slip wall as the reference point is moved perpendicularly to the wall and relates it to shear stress acting on the wall. Prandtl related the magnitude of the partial derivative of the parallel velocity with respect to the normal distance from the wall multiplied by the square of mixing length to an approximation for eddy viscosity, Equation 4.38, for a thin shear layer. When applied to the TKE transport equation above, the mixing length is a decent guess for turbulent length scale assuming that the ratio of TKE production to dissipation is constant. van Driest[161] observed that Prandtl’s mixing length model ”represents

mean fully developed flow near a wall", but fully developed motion does not exist adjacent to the wall. A damping function for turbulent length scale was proposed by van Driest to account for flow changes adjacent to the wall. A modern empirical formulation for approximating the mixing length was adapted from Li's work[162] on annular sector ducts which was derived from Nukuradse type pipe flow mixing length expressions.[163] This empirically derived mixing length formula combines the use of a radial coordinate and the van Driest damping function to create a model particular to annular fluid domains. For the purposes of this study, the turbulent length scale was calculated as a scalar in the $\mathbf{CC}$ vector space using the local radial distance to the nearest stator or rotor surface to obtain the y^+ value.

$$\mu_t = \rho \left| \overline{\frac{\partial u}{\partial y}} \right| \ell_t^2 \tag{4.38}$$

$$u^+ = \frac{1}{\kappa} \ln y^+ + C^+ \tag{4.39}$$

$$y^+ = \frac{y}{\mu} \sqrt{\rho \tau_{wall}} \tag{4.40}$$

$$u^+ = \frac{u}{u_f} = u \sqrt{\frac{\rho}{\tau_{wall}}} \tag{4.41}$$

$$C^+ \approx 5 \qquad \kappa \approx 0.4 \tag{4.42}$$

$$\ell_{i,k}^t = \delta_{i,k} \left(1 - e^{-\left(\frac{\min\left(y_{i,k}^{+,R}, y_{i,k}^{+,S}\right)}{A^+} \right)^n} \right)^m \tag{4.43}$$

$$\kappa = 0.4 \qquad A^+ = 18 \qquad n = 1 \qquad m = 2.1 \tag{4.44}$$

To calculate the y+ value for each node in the domain, it is first necessary to calculate the wall shear stress, this shear stress is proportional to the characteristic viscosity and the derivative of the axial-circumferential velocity with respect to the radial distance to the wall, Equation 4.45. When modeling turbulent flow, the wall shear stress can also be proportional to the turbulent kinetic energy and fluid density near the wall.[164] It then becomes necessary to determine whether to use the laminar or turbulent relationships for wall shear stress and to modify wall boundary conditions so that the tensor divergence of viscosity and velocity gradient takes the turbulent behavior into account near the wall.

The discrete form of the laminar shear stress in Equation 4.45 is given by Equation 4.48 for i

locations at 0,1 and $N_\chi, N_{\chi+1}$, and the discrete form of the derived local node y+ value and turbulent length scale is given by Equations 4.49 and 4.66. Local laminar y+ values are calculated with the local wall shear stress of the same axial location. Note that the discrete wall shear is calculated on the boundary and not the cell center where TKE is stored, while the y+ values are also stored in the cell centers. However, as long as the y+ value is below ≈ 10, there is negligible difference between deriving this shear stress at the first node inside the domain or on the rotor boundary directly due to the linear nature of the velocity profile in the inner shear layer.[6]

$$\tau^{\chi wall} = \mu_c \frac{\partial U_{equiv}}{\partial r} = \mu_c \left[\left(\frac{\partial v}{\partial r} \right)^2 + \left(\frac{\partial w}{\partial r} \right)^2 \right]^{\frac{1}{2}} \tag{4.45}$$

$$\tau^S_{N_\chi+\frac{1}{2},k} \approx \mu_c \left[4 \left(\frac{v_{N_\chi+1,k} - v_{N_\chi,k}}{\Delta\chi_{N_\chi} + \Delta\chi_{N_\chi+1}} \right)^2 + \left(\frac{w_{N_\chi+1,n} + w_{N_\chi+1,n-1} - w_{N_\chi,n} - w_{N_\chi,n-1}}{\Delta\chi_{N_\chi} + \Delta\chi_{N_\chi+1}} \right)^2 \right]^{\frac{1}{2}} \tag{4.46}$$

$$y^{+,S}_{i,k} = \frac{(R_S - \chi_i)}{\mu_c} \sqrt{\rho_c \tau^S_{N_\chi+\frac{1}{2},k,k}} \tag{4.47}$$

$$\tau^R_{\frac{1}{2},k} \approx \mu_c \left[4 \left(\frac{v_{1,k} - v_{0,k}}{\Delta\chi_0 + \Delta\chi_1} \right)^2 + \left(\frac{w_{1,n} + w_{1,n-1} - w_{0,n} + w_{0,n-1}}{\Delta\chi_0 + \Delta\chi_1} \right)^2 \right]^{\frac{1}{2}} \tag{4.48}$$

$$y^{+,R}_{i,k} = \frac{(\chi_i - R_R)}{\mu_c} \sqrt{\rho_c \tau^R_{\frac{1}{2},k}} \tag{4.49}$$

If the y+ is higher and the first node exists in the log-law of the wall shear region, the friction velocity and associated wall shear stress are calculated using the method of Lauder and Spalding.[164] The friction velocity is given by Equation 4.50 and converted to wall shear stress and y+ value through Equations 4.53 and 4.40. The friction velocities, wall shear stress components, and y+ values are caluclated locally and individually for each wall and each velocity component direction. To accomplish the component direction split for turbulent friction velocity, the total friction velocity predicted using turbulent kinetic energy is split by a scaling factor related to the local near-wall velocity component scales, Equation 4.51. The localized component wall shear stresses are then split according to Equation 4.54.

$$u_\ell = \left(0.3 k^\ell \right)^{\frac{1}{2}} \tag{4.50}$$

$$
\begin{aligned}
C_{\chi,k}^{\theta,S} &= \frac{v_{N_\chi,k}^2}{v_{N_\chi,k}^2 + \left(\frac{w_{N_\chi,n}+w_{N_\chi 1,n-1}}{2}\right)^2} \\
C_{\chi,k}^{z,S} &= \frac{\left(\frac{w_{N_\chi,n}+w_{N_\chi 1,n-1}}{2}\right)^2}{v_{N_\chi,k}^2 + \left(\frac{w_{N_\chi,n}+w_{N_\chi 1,n-1}}{2}\right)^2} \\
C_{\chi,k}^{\theta,R} &= \frac{v_{1,k}^2}{v_{1,k}^2 + \left(\frac{w_{1,n}+w_{1,n-1}}{2}\right)^2} \\
C_{\chi,k}^{z,R} &= \frac{\left(\frac{w_{1,n}+w_{1,n-1}}{2}\right)^2}{v_{1,k}^2 + \left(\frac{w_{1,n}+w_{1,n-1}}{2}\right)^2}
\end{aligned}
\tag{4.51}
$$

$$
\begin{aligned}
v_{\chi,k}^{\ell,S} &= \left(0.3 k_{N_\chi,k}^{t} C_{\chi,k}^{\theta,S}\right)^{\frac{1}{2}} \\
w_{\chi,k}^{\ell,S} &= \left(0.3 k_{N_\chi,k}^{t} C_{\chi,k}^{z,S}\right)^{\frac{1}{2}} \\
v_{\chi,k}^{\ell,R} &= \left(0.3 k_{1,k}^{t} C_{\chi,k}^{\theta,R}\right)^{\frac{1}{2}} \\
w_{\chi,k}^{\ell,R} &= \left(0.3 k_{1,k}^{t} C_{\chi,k}^{z,R}\right)^{\frac{1}{2}}
\end{aligned}
\tag{4.52}
$$

$$
\begin{aligned}
\tau_{N_\chi+\frac{1}{2},k}^{S} &= \rho_{N_\chi,k}\left[\left(v_{\chi,k}^{\ell,S}\right)^2 + \left(w_{\chi,k}^{\ell,S}\right)^2\right] \\
\tau_{\frac{1}{2},k}^{R} &= \rho_{1,k}\left[\left(v_{\chi,k}^{\ell,R}\right)^2 + \left(w_{\chi,k}^{\ell,R}\right)^2\right]
\end{aligned}
\tag{4.53}
$$

$$
\begin{aligned}
\tau_{N_\chi+\frac{1}{2},k}^{\theta,S} &= v_{\chi,k}^{\ell,S}\left(\rho_{N_\chi,k}\tau^S\right)^{\frac{1}{2}} \\
\tau_{N_\chi+\frac{1}{2},k}^{z,S} &= w_{\chi,k}^{\ell,S}\left(\rho_{N_\chi,k}\tau^S\right)^{\frac{1}{2}} \\
\tau_{\frac{1}{2},k}^{\theta,R} &= v^{\ell,R}\left(\rho_{1,k}\tau_{\frac{1}{2},k}^{R}\right)^{\frac{1}{2}} \\
\tau_{\frac{1}{2},k}^{z,R} &= w_{\chi,k}^{\ell,R}\left(\rho_{1,k}\tau_{\frac{1}{2},k}^{R}\right)^{\frac{1}{2}}
\end{aligned}
\tag{4.54}
$$

If the flow is found to be turbulent, Reynolds Number above 850, the local y+ is calculated on each wall as turbulent. The Lauder and Spalding turbulent wall shear stress calculation works better for y+ values solidly in the log-law region (> 30), so the average y+ value is taken. If the average y+ along the wall is below 30, the wall shear stress and y+ values are calculated with the next axial row of nodes that occurs radially away from the wall. This radial shift of wall adjacent nodes is repeated until either the wall distance is greater than 10% of the clearance, or the y+ value is greater than 30. This prevents the turbulent shear predictions from being invalid due to nodes

occuring in the viscous sublayer region when the mesh grid is fine.

While the wall shear stress was calculated accordingly, the effects of any additional shear due to turbulence must be passed into the tensor divergence operator. To accomplish this, the wall boundary condtions for axial and circumferential velocity were changed from homogeneoush Dirichlet, no-slip, to Neumann boundaries defined by the laminar gradients needed to produce the appropriate turbulent wall shear stress. To do this by finite difference, the discrete finite difference equation for wall shear stress is first equated to the wall shear stress defined by the wall functions, Equations 4.55a and 4.59a.

From Appendix D, the gradient of velocity with respect to radial dimension is given by Equation 4.55a and relates to wall shear stress by Equation 4.55b.

$$\mathscr{G}^{\chi}\left(v^0\right)^{Wall} = \frac{1}{\chi}\frac{\partial}{\partial\chi}\left(\chi v^0\right) - \frac{v^0}{\chi} \tag{4.55a}$$

$$\left(\tau_{\ell,\mathbf{k}}^{\theta\chi}\right)^{Wall} = \mu\left[\frac{1}{\chi}\frac{\partial}{\partial\chi}\left(\chi v^0\right) - \frac{v^0}{\chi}\right] \tag{4.55b}$$

In comparison the Neumann boundary condition for circumferential velocity from Appendix C is related to the inner product summation of vorticity over the **FC** and **EC** vector spaces. For convenience these equations are provided below in Equations 4.56 to 4.57.

$$\begin{aligned}\frac{\partial v}{\partial\chi} &= \left(\frac{1}{\chi}\frac{\partial\left(\chi v\right)}{\partial\chi} - \frac{v}{\chi}\right)_{\ell,k} \\ &= 4\frac{1}{\chi_{i+1}+\chi_i}\frac{\chi_{i+1}v^0_{i+1,k} - \chi_i v^0_{i,k}}{\Delta\chi_i + \Delta\chi_{i+1}} - \frac{v^0_{i+1,k}+v^0_{i,k}}{\chi_i+\chi_{i+1}}\end{aligned} \tag{4.56}$$

$$\begin{aligned}\frac{\partial}{\partial\chi}\left(\chi v\right)_{\frac{1}{2},k} &\approx 2\frac{\chi_1 v_{1,k} - \chi_0 v_{0,k}}{\Delta\chi_1 + \Delta\chi_0} \\ v_{0,k} &\approx \frac{\chi_1}{\chi_0}v^0_{1,k} - \frac{1}{\chi_0}\frac{\left(\Delta\chi_1+\Delta\chi_0\right)}{2}\frac{\partial}{\partial\chi}\left(\chi v\right)_{\frac{1}{2},k} \\ v_{N_{\chi+1},k} &\approx \frac{\chi_{N_\chi}}{\chi_{N_{\chi+1}}}v^0_{N_\chi,k} + \frac{1}{\chi_{N_{\chi+1}}}\frac{\left(\Delta\chi_1+\Delta\chi_0\right)}{2}\frac{\partial}{\partial\chi}\left(\chi v\right)_{N_\chi+\frac{1}{2},k}\end{aligned} \tag{4.57}$$

Based on these discrete boundary conditions integral to the mimmetic method, it is convenient to re-cast the wall shear stress in terms of $\frac{\partial}{\partial\chi}\left(\chi v\right)$ as seen below. The relationship is first presented as a continuous equation and then a discrete form for each of the Rotor and Stator walls. Equation 4.58d shows the continuous relationship in dimensional form, which is then adjusted to non-dimensional form in Equation 4.58e.

$$\left(\tau_{\ell,\mathbf{k}}^{\theta\chi}\right)_{Dim}^{Wall} = \mu\left[\frac{1}{r}\frac{\partial}{\partial r}\left(rv_{Dim}^{0}\right) - \frac{v_{Dim}^{0}}{r}\right] \tag{4.58a}$$

$$\frac{\partial}{\partial r}\left(rv^{0}\right) = \frac{r}{\mu}\left(\tau_{\ell,\mathbf{k}}^{\theta\chi}\right)_{Dim}^{Wall} + v_{Dim}^{0} \tag{4.58b}$$

$$\frac{U_c L_c}{L_c}\frac{\partial}{\partial\chi}\left(\chi v^{0}\right) = L_c\rho U_c^2\frac{\chi}{\mu}\left(\tau_{\ell,\mathbf{k}}^{\theta\chi}\right)^{Wall} + U_c v^{0} \tag{4.58c}$$

$$\frac{\partial}{\partial\chi}\left(\chi v^{0}\right) = \chi\frac{\rho U_c L_c}{\mu}\left(\tau_{\ell,\mathbf{k}}^{\theta\chi}\right)^{Wall} + v^{0} \tag{4.58d}$$

$$\frac{\partial}{\partial\chi}\left(\chi v^{0}\right) = \overline{Re_{\ell,k}^{t}}^{\chi}\,\chi\left(\tau_{\ell,\mathbf{k}}^{\theta\chi}\right)^{Wall} + v^{0} \tag{4.58e}$$

$$\begin{aligned}
\frac{\partial}{\partial\chi}\left(\chi v^{0}\right)_{\frac{1}{2},k} &\approx \overline{Re_{\frac{1}{2},k}^{t}}^{\chi}\,\chi_{\frac{1}{2}}\frac{\left(\tau_{\frac{1}{2},\mathbf{k}}^{\theta\chi}\right)_{Dim}^{Rotor}}{\rho U_c^2} + v_{\frac{1}{2},k}^{0} \\
\frac{\partial}{\partial\chi}\left(\chi v^{0}\right)_{N_\chi+\frac{1}{2},k} &\approx \overline{Re_{N_\chi+\frac{1}{2},k}^{t}}^{\chi}\,\chi_{N_\chi+\frac{1}{2}}\frac{\left(\tau_{\mathbf{N}_\chi+\frac{1}{2},\mathbf{k}}^{\theta\chi}\right)_{Dim}^{Stator}}{\rho U_c^2} + v_{N_\chi+\frac{1}{2},k}^{0}
\end{aligned} \tag{4.58f}$$

Similarly to the previous equations for circumferential velocity, it is convenient to re-cast the axial-radial wall shear stress in terms of a Neumann boundary condition.

$$\rho U_c^2\left(\tau_{\ell,\mathbf{n}}^{\mathbf{z}\chi}\right)^{Wall} = \mu\frac{\partial w}{\partial\chi}\frac{U_c}{L_c} \tag{4.59a}$$

$$\frac{\partial w}{\partial\chi} = \overline{Re_{\ell,n}^{t}}^{\chi z}\frac{\left(\tau_{\ell,\mathbf{n}}^{\mathbf{z}\chi}\right)_{Dim}^{Wall}}{\rho U_c^2} \tag{4.59b}$$

$$\frac{\partial}{\partial\chi}(w)_{\frac{1}{2},k} = \overline{Re_{\frac{1}{2},n}^{t}}^{\chi z}\frac{\left(\tau_{\frac{1}{2},\mathbf{n}}^{\mathbf{z}\chi}\right)_{Dim}^{Rotor}}{\rho U_c^2} \tag{4.59c}$$

$$\frac{\partial}{\partial\chi}(w)_{N_\chi+\frac{1}{2},k} = \overline{Re_{N_\chi+\frac{1}{2},n}^{t}}^{\chi z}\frac{\left(\tau_{\mathbf{N}_\chi+\frac{1}{2},\mathbf{n}}^{\mathbf{z}\chi}\right)_{Dim}^{Stator}}{\rho U_c^2} \tag{4.59d}$$

In comparison the Neumann boundary condition for axial velocity is as follows:

$$\begin{aligned}
w_{0,n} &\approx w_{1,n} - \frac{\Delta\chi_1 + \Delta\chi_0}{2}\frac{\partial}{\partial\chi}(w)_{\frac{1}{2},k} \\
w_{N_{\chi+1},n} &\approx w_{N_\chi,n} + \frac{\Delta\chi_{N_\chi+1} + \Delta\chi_{N_\chi}}{2}\frac{\partial}{\partial\chi}(w)_{N_\chi+\frac{1}{2},k}
\end{aligned} \tag{4.60}$$

The turbulent length scale is then calcualted using the maximum value of local shear stress, the rotor or stator value at that axial node, to define the baseline local mixing length scale, δ_k, of Equation 4.65.

$$y_{i,k} = r_{i,k} - R_R \qquad y_k^{mid} = r_k^{mid} - R_R \qquad y_k^{om} = R_S - r_k^{mid} \tag{4.61}$$

$$b_1 = 0.14\frac{y_k^{om}}{y_k^{mid}} \qquad b_2 = 2b_1 - 0.5\kappa_i \qquad b_3 = 0.5\kappa_i - b_1 \tag{4.62}$$

$$\Lambda_k = \frac{r_k^{mid}}{R_S} \qquad \kappa_i = \kappa\frac{R_S}{R_R\left(\Lambda_k - 1\right)}\left[\frac{\left(\frac{R_S}{R_R}\right)^2 - \Lambda_k^2}{\frac{R_S}{R_R}\left(\Lambda_k^2 - 1\right)}\right]^{\frac{1}{2}} \tag{4.63}$$

$$r_k^{mid} = \frac{\Delta\chi_{N_\chi}\tau_{wall,S}^{0.5} + \Delta\chi_1\tau_{wall,R}^{0.5}}{\tau_{wall,S}^{0.5} + \tau_{wall,R}^{0.5}} \tag{4.64}$$

$$\delta_{i,k} = \begin{cases} \delta_{i,k}^{in} = \left[b_1 - b_2\left(1 - \frac{y_{i,k}}{y_k^{mid}}\right)^2 - b_3\left(1 - \frac{y_{i,k}}{y_k^{mid}}\right)^4\right] y_m & r_{i,k} \le r_k^{mid} \\ \delta_{i,k}^{out} = \left[0.14 - \frac{0.08}{\left(y_k^{om}\right)^2}\left(y_{i,k} - y_k^{mid}\right)^2 - \frac{0.06}{\left(y_k^{om}\right)^4}\left(y_{i,k} - y_k^{mid}\right)^4\right] y_k^{om} & r_{i,k} > r_k^{mid} \end{cases} \tag{4.65}$$

$$\ell_{i,k}^t = \mathbf{min}\left(\delta_{i,k}, 0.15H^0\right)\left(1 - e^{-\left(\frac{\mathbf{min}\left(y_{i,k}^{+,R}, y_{i,k}^{+,S}\right)}{18}\right)}\right)^{2.1} \tag{4.66}$$

4.3 Solution of the TKE Transport Equations by Numerical Iteration

Like the RANS momentum and mass conservation equations discussed in the previous chapter, the TKE transport equation has been discretized spatially using the MFD method to be conservative and stable. To maintain stability over time-stepping and to more closely link the iteration in velocity and pressure to the TKE iteration, the TKE transport equation is also discretized in time using a semi-implicit midpoint method and the same time step as the RANS equations.

$$\begin{aligned}\mathrm{St}\frac{\partial k_t}{\partial t}+\vec{u}_s^0\cdot\mathbf{G}_s^0\left(k_t\right)=&\left[\frac{2}{\mathrm{Re}_t}\underline{\underline{\mathbf{E}}}\right]_{qs}\otimes\mathscr{G}_s\vec{u}_q^0-C_D\frac{k^{\frac{3}{2}}}{\ell_t}\\&+\mathbf{D}_s^0\left[\left(\frac{1}{\mathrm{Re}_c}+\frac{1}{\mathrm{Re}_t}\right)\mathbf{G}_s^0\left(k_t\right)\right]\end{aligned}\tag{4.67}$$

$$k_t^{g+\frac{1}{2}}=\frac{1}{2}\left(k_t^g+k_t^{g+1}\right)\tag{4.68}$$

$$\begin{aligned}\mathrm{St}\frac{k_t^{g+1}-k_t^g}{\Delta\tau}+\frac{1}{2}\vec{u}_s^0\cdot\mathbf{G}_s^0\left(k_t^g+k_t^{g+1}\right)=&\left[\frac{2}{\mathrm{Re}_t^g}\underline{\underline{\mathbf{E}}}\right]_{qs}\otimes\mathscr{G}_s\vec{u}_q^0-C_D\frac{k^{\frac{3}{2},g}}{\ell_t}\\&+\frac{1}{2}\mathbf{D}_s^0\left[\left(\frac{1}{\mathrm{Re}_c}+\frac{1}{\mathrm{Re}_t^g}\right)\mathbf{G}_s^0\left(k_t^g+k_t^{g+1}\right)\right]\end{aligned}\tag{4.69}$$

$$\begin{aligned}&k_t^{g+1}-k_t^g+\frac{1}{2}\frac{\Delta\tau}{\mathrm{St}}\vec{u}_s^0\cdot\mathbf{G}_s^0\left(k_t^g\right)\\&\quad+\frac{1}{2}\frac{\Delta\tau}{\mathrm{St}}\vec{u}_s^0\cdot\mathbf{G}_s^0\left(k_t^{g+1}\right)=\frac{\Delta\tau}{\mathrm{St}}\left[\frac{2}{\mathrm{Re}_t^g}\underline{\underline{\mathbf{E}}}\right]_{qs}\otimes\mathscr{G}_s\vec{u}_q^0-\frac{\Delta\tau}{\mathrm{St}}C_D\frac{k^{\frac{3}{2},g}}{\ell_t}\\&\qquad+\frac{1}{2}\frac{\Delta\tau}{\mathrm{St}}\mathbf{D}_s^0\left[\left(\frac{1}{\mathrm{Re}_c}+\frac{1}{\mathrm{Re}_t^g}\right)\mathbf{G}_s^0\left(k_t^g\right)\right]\\&\qquad+\frac{1}{2}\frac{\Delta\tau}{\mathrm{St}}\mathbf{D}_s^0\left[\left(\frac{1}{\mathrm{Re}_c}+\frac{1}{\mathrm{Re}_t^g}\right)\mathbf{G}_s^0\left(k_t^{g+1}\right)\right]\end{aligned}\tag{4.70}$$

$$\begin{aligned}&k_t^{g+1}+\frac{1}{2}\frac{\Delta\tau}{\mathrm{St}}\left\{\vec{u}_s^0\cdot\mathbf{G}_s^0\left(k_t^{g+1}\right)\right.\\&\left.-\mathbf{D}_s^0\left[\left(\frac{1}{\mathrm{Re}_c}+\frac{1}{\mathrm{Re}_t^g}\right)\mathbf{G}_s^0\left(k_t^{g+1}\right)\right]\right\}_{\underline{\underline{\mathbf{A}}}^t}=k_t^g-\frac{1}{2}\frac{\Delta\tau}{\mathrm{St}}\left\{\vec{u}_s^0\cdot\mathbf{G}_s^0\left(k_t^g\right)-\mathbf{D}_s^0\left[\left(\frac{1}{\mathrm{Re}_c}+\frac{1}{\mathrm{Re}_t^g}\right)\mathbf{G}_s^0\left(k_t^g\right)\right]\right\}_{\underline{\underline{\mathbf{A}}}^t}\\&\qquad+\frac{\Delta\tau}{\mathrm{St}}\left\{-\vec{u}_s^0\cdot\mathbf{G}_s^0\left(k_t^g\right)+\mathbf{D}_s^0\left[\left(\frac{1}{\mathrm{Re}_c}+\frac{1}{\mathrm{Re}_t^g}\right)\mathbf{G}_s^0\left(k_t^g\right)\right]\right.\\&\qquad\left.+\left[\frac{2}{\mathrm{Re}_t^g}\underline{\underline{\mathbf{E}}}\right]_{qs}\otimes\mathscr{G}_s\vec{u}_q^0-C_D\frac{k^{\frac{3}{2},g}}{\ell_t}\right\}_{\underline{\mathbf{b}}_{\mathbf{0}}^t}\end{aligned}\tag{4.71}$$

$$\underline{\underline{\mathbf{A}}}^{t}\left(\vec{u^{0}}_{s}^{g}\right) = \vec{u}_{s}^{0} \cdot \mathbf{G}_{s}^{0}\left(k_{t}^{g+1}\right) - \mathbf{D}_{s}^{0}\left[\left(\frac{1}{\mathrm{Re}_{c}} + \frac{1}{\mathrm{Re}_{t}^{g}}\right)\mathbf{G}_{s}^{0}\left(k_{t}^{g+1}\right)\right] \tag{4.72}$$

$$\begin{aligned}\underline{\mathbf{b_0}}^{t}\left(\vec{u^{0}}_{s}^{g}, k_{t}^{g}\right) = &-\left(\vec{u}_{s}^{0}\right)_{BC} \cdot \mathbf{G}_{s}^{0}\left(k_{t}^{g}\right)_{BC} + \mathbf{D}_{s}^{0}\left[\left(\frac{1}{\mathrm{Re}_{c}} + \frac{1}{\mathrm{Re}_{t}^{g}}\right)\mathbf{G}_{s}^{0}\left(k_{t}^{g}\right)\right]_{BC} \\ &+ \left[\frac{2}{\mathrm{Re}_{t}^{g}}\underline{\underline{\mathbf{E}}}\right]^{qs} \otimes \mathscr{G}_{s}\vec{u}_{q}^{0} - C_{D}\frac{k^{\frac{3}{2},g}}{\ell_{t}}\end{aligned} \tag{4.73}$$

$$\left[\underline{\underline{\mathbf{I}}}^{t} + \frac{1}{2}\frac{\Delta\tau}{\mathrm{St}}\underline{\underline{\mathbf{A}}}^{t}\left(\vec{u^{0}}_{s}^{g}\right)\right]k_{t}^{g+1} = \left[\underline{\underline{\mathbf{I}}}^{t} - \frac{1}{2}\frac{\Delta\tau}{\mathrm{St}}\underline{\underline{\mathbf{A}}}^{t}\left(\vec{u^{0}}_{s}^{g}\right)\right]k_{t}^{g} + \frac{\Delta\tau}{\mathrm{St}}\underline{\mathbf{b_0}}^{t}\left(\vec{u^{0}}_{s}^{g}, k_{t}^{g}\right) \tag{4.74}$$

$$\begin{aligned}k_{t}^{g+1} = &\left[\underline{\underline{\mathbf{I}}}^{t} + \frac{1}{2}\frac{\Delta\tau}{\mathrm{St}}\underline{\underline{\mathbf{A}}}^{t}\left(\vec{u^{0}}_{s}^{g}\right)\right]^{-1} \\ &\left\{\left[\underline{\underline{\mathbf{I}}}^{t} - \frac{1}{2}\frac{\Delta\tau}{\mathrm{St}}\underline{\underline{\mathbf{A}}}^{t}\left(\vec{u^{0}}_{s}^{g}\right)\right]k_{t}^{g} + \frac{\Delta\tau}{\mathrm{St}}\underline{\mathbf{b_0}}^{t}\left(\vec{u^{0}}_{s}^{g}, k_{t}^{g}\right)\right\}\end{aligned} \tag{4.75}$$

Chapter 5

Annular Pressure Seal Validation Cases for Seal2D

The full 2D seal code was tested against liquid seal geometries and operating cases from the literature for the zeroth-order concentric solution and the first-order rotordynamic coefficient prediction using both the hybrid bulk-flow method and the 2D first-order solution method. No gas seals were tested in this study as the code is currently for incompressible flows only. The uncertainty bars generated for figures in the following results were calculated using Richardson extrapolation[165] typically using the two finest meshes tested.

The first-order solution of the 2D momentum equations, and the hybrid bulk-flow method employed, require an additional set of 4 first-order axial boundary conditions (real and imaginary velocities at the inlet and outlet). These boundary conditions are not known. Instead they were estimated by minimization of an optimization objective function that compares the sum of the Seal2d first-order pressure solutions at the inlet and exit boundaries to the first-order pressures calculated based on the inlet/exit loss coefficients specified as input and the previous velocity guess. The relationship between velocities, first-order pressure, and loss/recovery coefficients is given in Section 3.7 The 4-dimensional optimization is then performed using a modified Nelder-Mead simplex algorithm based on a combination of the algorithms presented by Gao *et. al.* (2012),[166] Jalaeian-F (2012),[167] and Fajfar *et. al.* (2019).[168] The modifications are selected to improve the robustness of the standard downhill simplex algorithm by introducting perturbations to avoid the

simplex becoming lower-dimensional and to introduce a ”drunkard’s walk” randomness to avoid getting stuck in local minima. There is currently no additional calculation to determine appropriate inlet loss or exit recovery coefficients in this work.

The employed Nelder-Mead simplex algorithm follows the procedure below:

1. Randomly select five sets of axial velocity boundary conditions to form a simplex.
2. Solve the first-order momentum equations (hybrid bulk-flow or 2D) to the required resolution for each new point.
3. Sort the points according to optimization function.
4. Calculate the centroid of the simplex formed by the five best cases.
5. Perform a transformation on the simplex based on the extra point’s value and relative location.
    - If the simplex volume is within error margins or the optimization function is minimized to the given residual: End optimization with the current best point of the simplex.
    - If optimization step count is modulo 20: Randomly select a new point within the allowed values.
    - If the last point generated a new minimum of the optimization function: Perform a reflection of the simplex to move downhill in the appropriate direction.
    - If the last point was a reflection and generated a new minimum: Perform an expansion of the simplex in the same direction as the last reflection.
    - If the last step was a reflection or expansion and the generated objective function value is worse than the existing points in the simplex: Perform an outer contraction of the reflected or expanded simplex in the samre direction as the reflection or expansion.
    - If the last step was a reflection or expansion the generated objective function value is better than some of the existing points in the simplex: Perform an inner contraction of the simplex prior to the reflection or expansion, but along the same direction.
    - Otherwise: Shrink the simplex from a corner node.
6. Take the new simplex point and loop to step 2.

5.1 Case 1: San Andres 2018

For the first test case, an oil seal from San Andres[169] was selected for the simulation of a purely laminar flow. The work of San Andres has flows with axial Reynolds Numbers less than 50 and circumferential Reynolds Numbers under 350.

Table 5.1: Laminar seal case study definition

Variable	**Units**	**Symbol**	San Andres (2018)[169]
Length	mm	L_S	46
Clearance	mm	H^0	0.203
Radius	mm	R_S	63.5
Eccentricity	-	H^1	0.0203
Radial Cell Count	-	Nr	16 to 44
Axial Cell Count	-	Nr	250 to 2,400
Total Cell Count	-	Nr	4,000 to 66,000
Viscosity	Pa · s	μ	0.0108
Density	$\frac{\mathrm{kg}}{\mathrm{m}^3}$	ρ	828.124
Pre-Swirl	-	Pr	0
Rotor Speed	RPM	ω	0 to 3,500
Inlet Loss Coef.	-	ζ_I	0.01
Exit Recovery Coef.	-	ζ_E	0.01
Radial Vel.	$\frac{\mathrm{m}}{\mathrm{s}}$	u_W	0
		$\frac{\partial u_E^0}{\partial z}$	0
		u_S	0
		u_N	0
Angular Vel.	$\frac{\mathrm{m}}{\mathrm{s}}$	v_W	$\mathrm{Pr} \cdot \omega R_S$
		$\frac{\partial v_E^0}{\partial z}$	0
		v_S	ωR_S
		v_N	0
Axial Vel.	$\frac{\mathrm{m}}{\mathrm{s}}$	w_W	≈ 1
		$\frac{\partial w_E^0}{\partial z}$	0
		w_S	0
		w_N	0
TKE	$\left(\frac{\mathrm{m}}{\mathrm{s}}\right)^2$	k_W	0
		$\frac{\partial k_E}{\partial z}$	0
		$\frac{\partial k_S}{\partial \chi}$	0
		$\frac{\partial k_N}{\partial \chi}$	0

5.1.1 Zeroth-order Solution: Concentric Cylinders

The zeroth-order solution for an annular seal from bulk-flow typically provides leakage and power loss. In this case, the code takes an average axial velocity across the seal inlet plane, which sets the leakage by mass conservation. Thus the reported output for comparison with the work of San Andres (2018)[169] is the pressure drop across the seal length instead. The experiment of San Andres (2018)[169] is performed with a fixed pressure drop of 1.5 bar (or 1.50E5 Pa) and the seal code predicted pressure drop is shown in Figure 5.1. The percent difference between predicted and experimental values for pressure drop across the seal is 3.6 % and the uncertainty from Richardson extrapolation[165] is 1.3E-3 %.

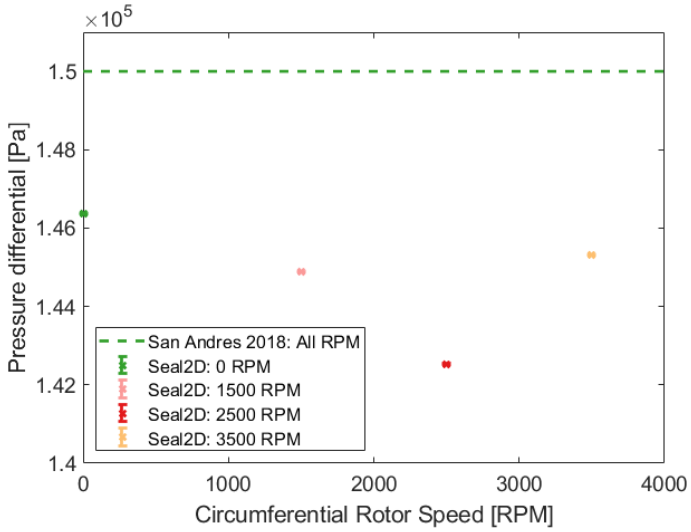

Figure 5.1: Calculated vs. experimental pressure drop across a laminar seal

5.1.2 First-order Equation Simulation Results - Eccentric Annular Region

The laminar first-order rotordynamic coefficients from the work of San Andres (2018)[169] are shown in Table 5.2 along with the coefficients predicted by the hybrid bulk-flow method and the 2D first-order solution. The normal and tangential forces divided by eccentricity from the hybrid-bulk flow method are plotted, in Figures 5.2 and 5.3 respectively, against the whirl frequency and the polynomial expressions equivalent to the vibration equations of Section 2.1. The polynomial regression models for the rotordynamic coefficients do not show a good linearity with R^2 values of

0.318 and 0.12 for the normal and tangential directions respectively. This indicates a lot of noise or uncertainty in the first-order solution for both calculation methods when applied to the laminar flow of San Andres' oil seal. The error may related to the optimization search routine to determine the first-order axial velocity boundary conditions finding many local minima or to the accuracy of the loss coefficients selected for these test cases. Alternatively, the issue may be due to the rapid increase in circumferential velocity from the zero pre-swirl not being sufficiently smoothly modeled with the axial grid resolutions tested for the San Andres seal test cases.

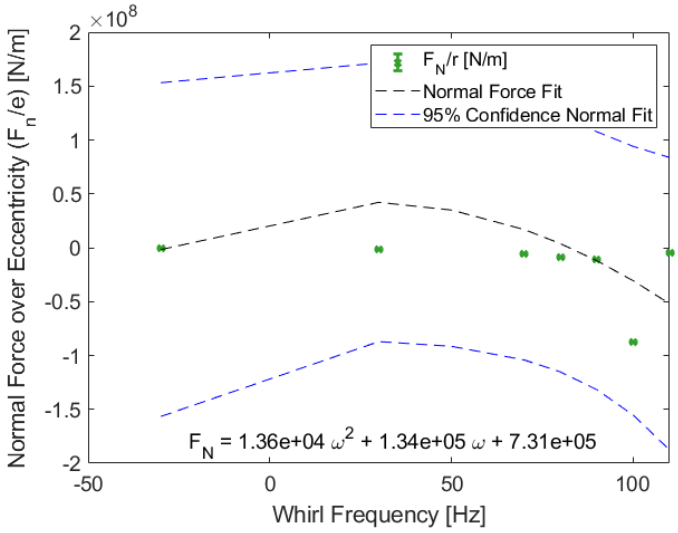

Figure 5.2: San Andres (2018)[169] polynomial fit for hybrid-bulk first-order results: Normal direction

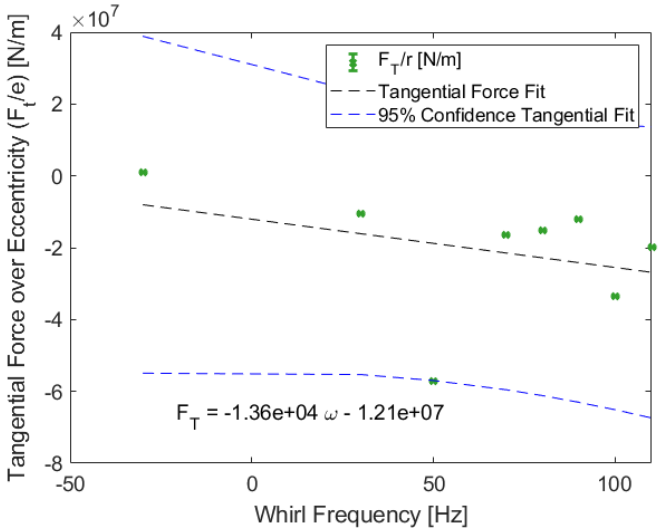

Figure 5.3: San Andres (2018)[169] polynomial fit for hybrid-bulk first-order results: Tangential direction

Table 5.2: Case 1: Laminar rotordynamic coefficients

Variable	**Units**	**Symbol**	San Andres (2018)[169]	Hybrid Code	2D Code
Direct Stiffness	$\mathrm{N/m}$	K_{xx}	3.69E4	7.30E5	7.46E3
Cross-Coupled Stiffness	$\mathrm{N/m}$	K_{xy}	3.70E6	1.20E7	2.68E6
Direct Damping	$\mathrm{N \cdot s/m}$	C_{xx}	2.00E4	1.34E5	2.08E4
Cross-Coupled Damping	$\mathrm{N \cdot s/m}$	C_{xy}	-	1.36E4	1.88E2
Direct Mass	kg	M_{xx}	231	1.36E4	187

5.2 Case 2: Jolly *et. al.* 2018

The second test case was selected as an opposite extreme, Jolly *et. al.* (2018)[170] is characterized by high speed liquid flow at axial Reynolds Numbers of approximately 23,000 and circumferential Reynolds numbers between 0 and 96,000.

Table 5.3: Turbulent seal case study definition

Variable	**Units**	**Symbol**	Jolly *et. al.* (2018)[170]
Length	mm	L_S	150
Clearance	mm	H^0	0.57
Radius	mm	R_S	120
Eccentricity	-	H^1	0.0285
Radial Cell Count	-	Nr	16 to 28
Axial Cell Count	-	Nr	400 to 650
Total Cell Count	-	Nr	6,400 to 18,200
Viscosity	Pa · s	μ	6.53E-4
Density	$\frac{\mathrm{kg}}{\mathrm{m}^3}$	ρ	992.617
Pre-Swirl	-	Pr	0
Rotor Speed	RPM	ω	0 to 2,000
Inlet Loss Coef.	-	ζ_I	0.735
Exit Recovery Coef.	-	ζ_E	1.51
Radial Vel.	$\frac{\mathrm{m}}{\mathrm{s}}$	u_W	0
		$\frac{\partial u_E^0}{\partial z}$	0
		u_S	0
		u_N	0
Angular Vel.	$\frac{\mathrm{m}}{\mathrm{s}}$	v_W	$\mathrm{Pr} \cdot \omega R_S$
		$\frac{\partial v_E^0}{\partial z}$	0
		v_S	ωR_S
		v_N	0
Axial Vel.	$\frac{\mathrm{m}}{\mathrm{s}}$	w_W	8.42 to 13.78
		$\frac{\partial w_E^0}{\partial z}$	0
		w_S	0
		w_N	0
TKE	$\left(\frac{\mathrm{m}}{\mathrm{s}}\right)^2$	k_W	$0.1\left(v_W^2 + w_W^2\right)^{\frac{1}{2}}$
		$\frac{\partial k_E}{\partial z}$	0
		$\frac{\partial k_S}{\partial \chi}$	0
		$\frac{\partial k_N}{\partial \chi}$	0

5.2.1 Zeroth-order Solution: Concentric Cylinders

The leakage from Jolly *et. al.*[170] is again set by the specified average inlet axial velocity for this work. Instead the goal is to match the pressure differential across the seal. Figure 5.4 shows the pressure differential predicted by the zeroth-order solution to the 2D annular seal code. Meshes were tested from 6,400 to 18,200 cells, with the full code solutions becoming less accurate (predicting higher pressure) with increasing mesh density. This is likely due to the nature of the turbulent wall functions used to predict wall shear stress requiring higher y+ values and the limits of a coarse mesh in a radially small clearance region. The updates to the turbulent wall functions to draw information from cells located further into the domain from the walls, partially resolve this issue, but not consistently for every case. The 2,000 RPM test case from Jolly *et. al.*[170] was simulated using ANSYS CFX for the concentric seal with mesh densities ranging from 28,000 to 78,000 elements. The eddy viscosity was then exported and interpolated into the 2-D seal code using radial basis functions.[171] The 2-D Seal code was run without the turbuelent kinetic energy transport equation, using the imported eddy viscosity instead, at mesh densities from 12,100 to 27,500 cells to establish the mesh independence of the modified wall function method stand-alone. Figure 5.5 shows the simulated pressure differential results from the 2-D seal code with a 0.84% Richardson extrapolation error.[165] Thus the remaining mesh independence issues are related to the iteration between the wall function generated shear stress and the turbulent kinetic energy transport equations.

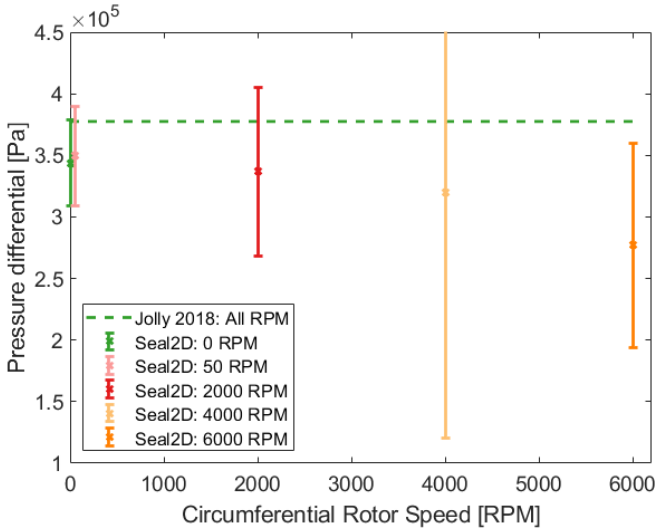

Figure 5.4: Calculated vs. experimental pressure drop across the turbulent seal from Jolly *et. al.* (2018)[170]

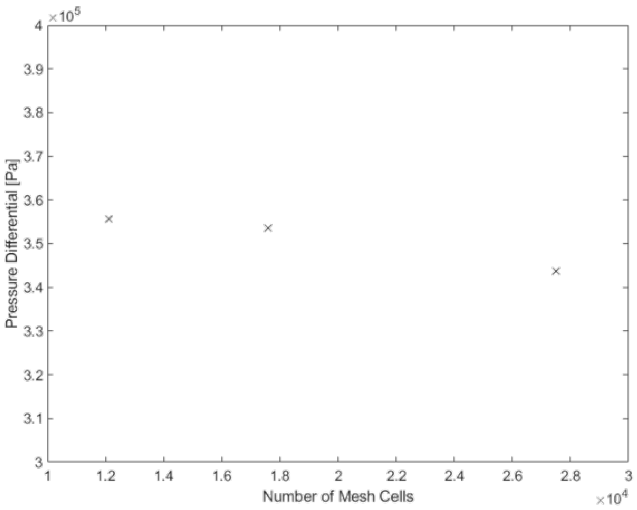

Figure 5.5: Calculated vs. experimental pressure drop across the turbulent seal from Jolly *et. al.* (2018)[170]

5.2.2 First-order Equation Simulation Results - Eccentric Annular Region

Jolly *et. al.*[170] provides an oportunity to compare qualitative pressure profile contours as well as the rotordynamic coefficients. Figure 5.6 shows the first-order pressure profile unwrapped circumferentially from the seal's rotor surface for the Jolly seal geometry at a stationary rotor speed with inlet loss coefficient of 0 and exit recovery coefficient of 0.8. The right side shows in grey-scale the pressure profile provided in Jolly *et. al.*,[170] while the left side shows the pressure profile from the 2D first-order solution. The first order solutions are heavily dependent on the selected loss and recovery coefficients at the inlet and outlet. Future versions of the 2-D code will eliminate this dependence by modeling the upstream and downstream regions of the seal as well. The quantitative values of the contours in Figure 5.6 are approximately the same between the 2-D seal code and the results from Jolly *et. al.*,[170] along with qualitative contour shapes that show the same flow profiles. Similarly, Figure 5.7 shows a set of pressure profiles at 6,000 RPM with inlet loss coefficient of 0 and exit recovery coefficient of 1. While the magnitude of the pressure peaks and valleys are different between the 2-D code and Jolly *et. al.*,[170] the contours remain approximately the same in shape at the 6,000 RPM rotor speed. The magnitude difference can be attributed to

inaccurate estimation of the loss and recovery coefficients, or to the mesh dependence seen in the concentric solution.

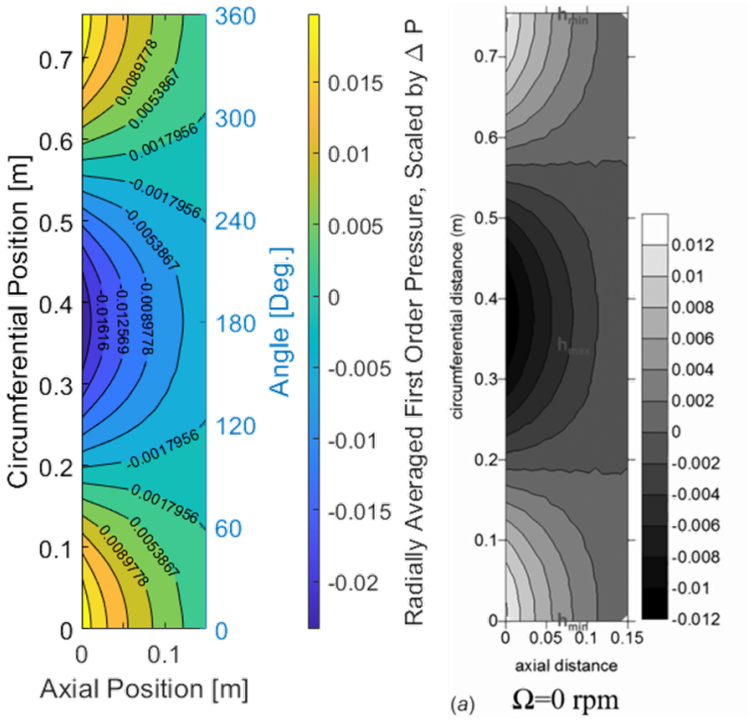

Figure 5.6: first-order pressure profile at 0 RPM rotor speed: Seal2D (left) Jolly *et. al.* (2018)[170] (right)

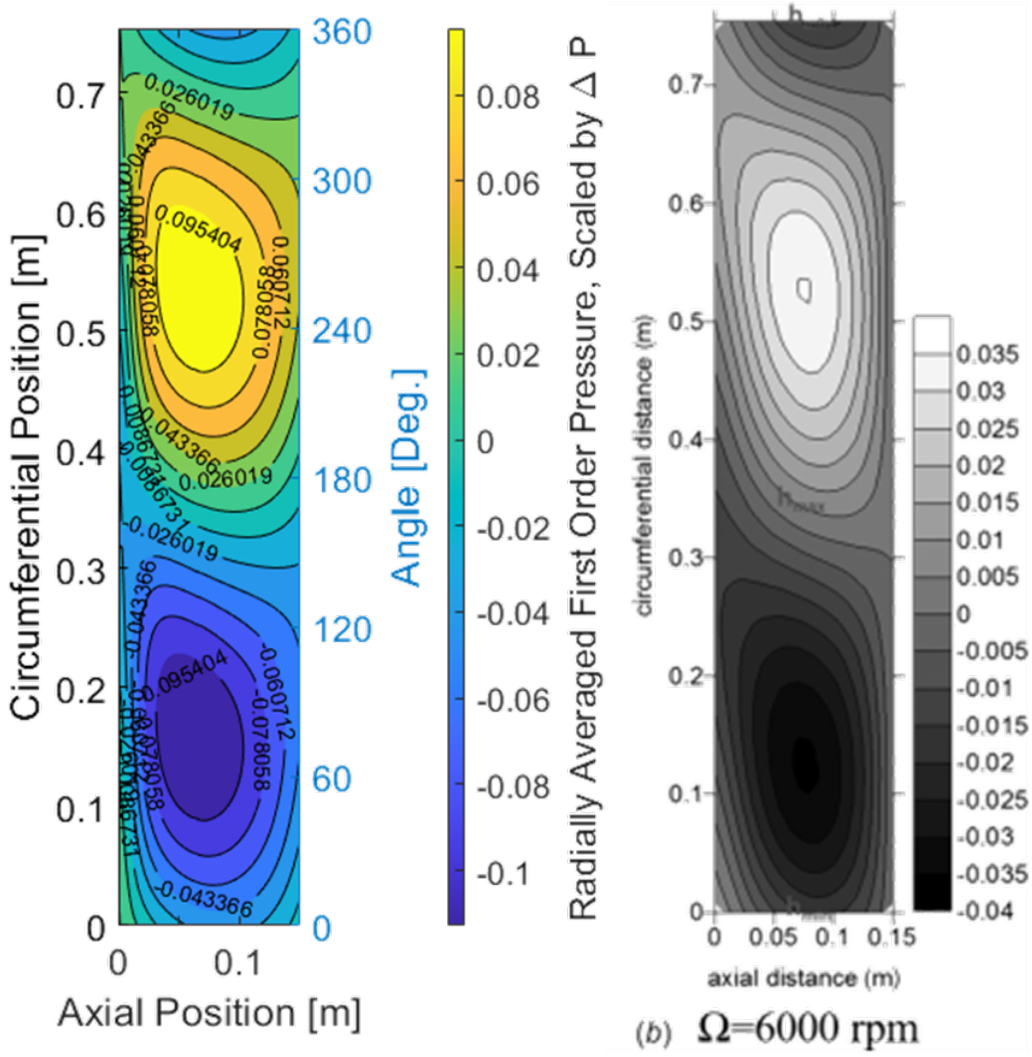

Figure 5.7: first-order pressure profile at 6,000 RPM rotor speed: Seal2D (left) Jolly *et. al.* (2018)[170] (right)

The turbulent first-order rotordynamic coefficients for the seal from Jolly *et. al.* (2018)[170] are given in Table 5.4. The force regression analysis plots for the hybrid and 2D momentum equations are given by Figures 5.8 to 5.11. It can be seen that the regression fit is smoother and more accurate for the hybrid force solution than the 2D solution. The additional noise in the first order solution of the 2-D code is possibly attributable to the mesh dependence issues with the concentric solution compounding with the 2-D perturbation. Without an upstream region or equivalent additional calculation, both solutions are still rather dependent on the inlet and exit loss coefficients specified by the user. Figure 5.12 shows the dimensionless stiffness coefficient profile against rotor speed. Both the hybrid and 2D versions of the code give rotordynamic stiffness coefficients that are within a reasonable range of the experimental values, and showing the appropriate trends, when a good loss coefficient is input. However, it is clear in Figure 5.13 that the dimensionless damping profile is less accurate to the experimental results, though still showing qualitatively similar trends for the 2-D code.

Table 5.4: Case 2: Turbulent rotordynamic coefficients

Variable	**Units**	**Symbol**	Jolly (2018)[170]	Hybrid Code	2D Code
Direct Stiffness	$\mathrm{N/m}$	K_{xx}	7.76E6	1.07E7	6.52E6
Cross-Coupled Stiffness	$\mathrm{N/m}$	K_{xy}	2.65E7	3.45E7	3.29E7
Direct Damping	$\mathrm{N \cdot s/m}$	C_{xx}	1.40E5	1.34E5	6.38E3
Cross-Coupled Damping	$\mathrm{N \cdot s/m}$	C_{xy}	1.20E5	1.00E5	2.84E4
Direct Mass	kg	M_{xx}	-	1.60E2	0

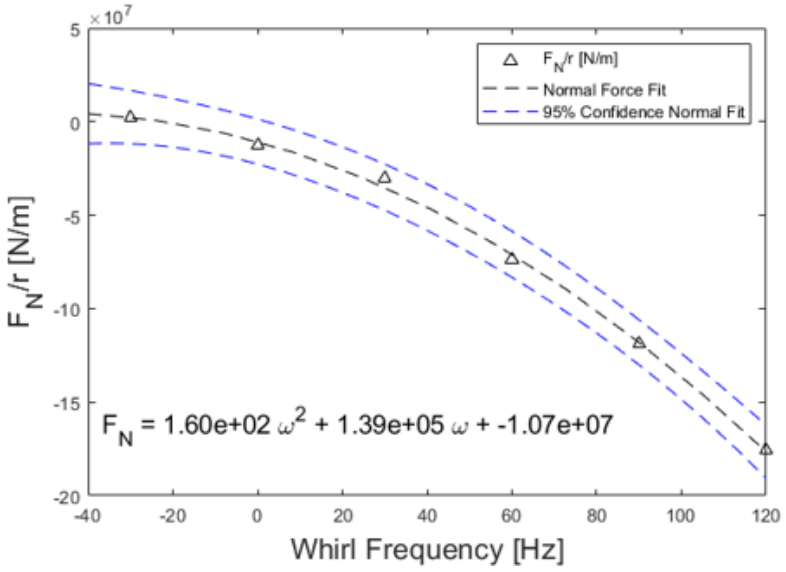

Figure 5.8: Jolly *et. al.* (2018)[170] polynomial fit for hybrid-bulk first-order results: Normal direction

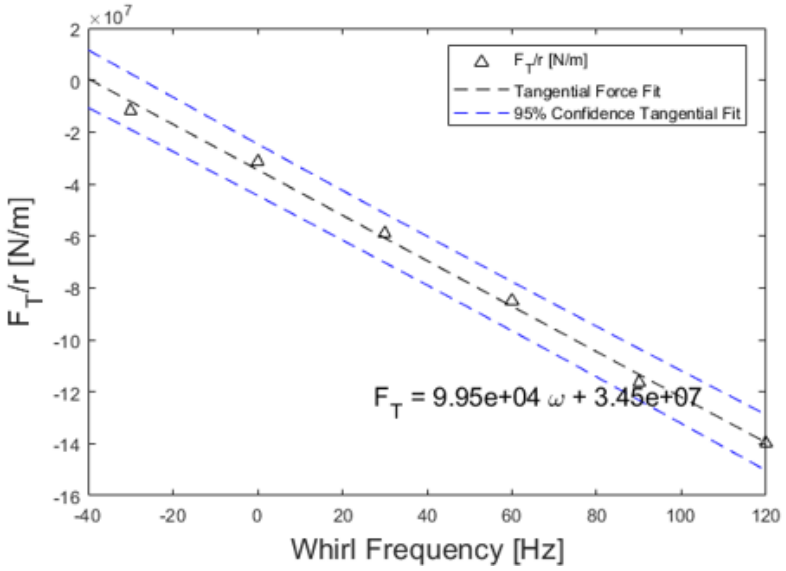

Figure 5.9: Jolly *et. al.* (2018)[170] polynomial fit for hybrid-bulk first-order results: Tangential direction

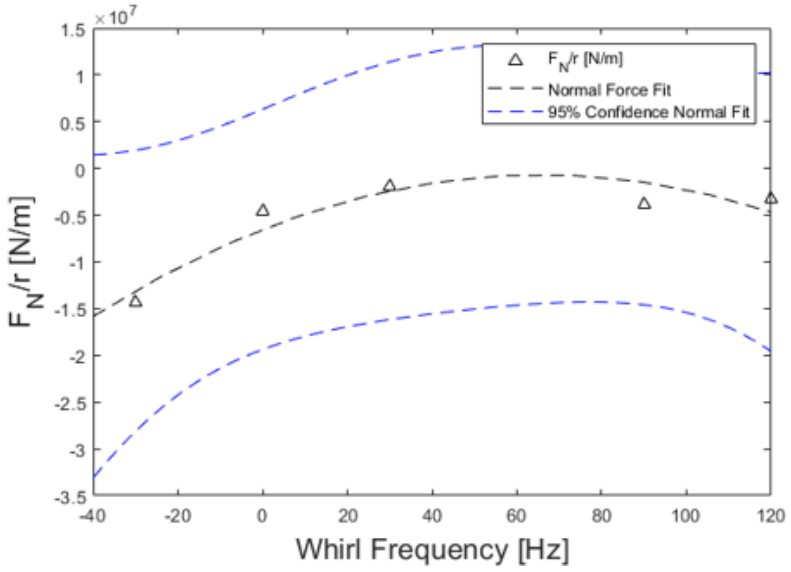

Figure 5.10: Jolly *et. al.*[170] polynomial fit for 2D first-order results: Normal direction

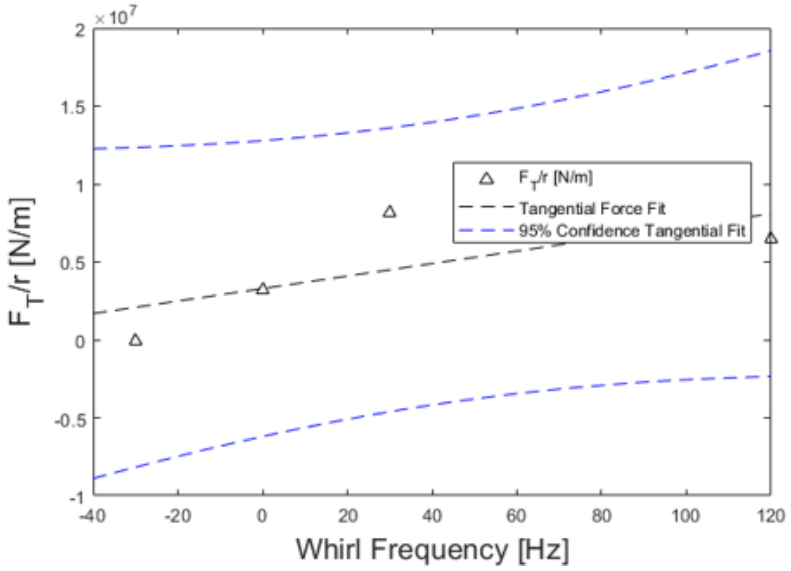

Figure 5.11: Jolly *et. al.*[170] polynomial fit for 2D first-order results: Tangential direction

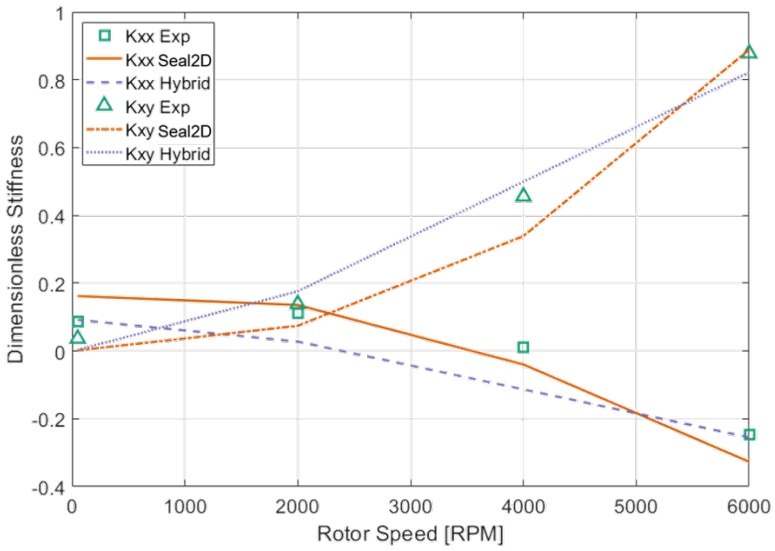

Figure 5.12: Jolly *et. al.*[170] dimensionless stiffness profile.

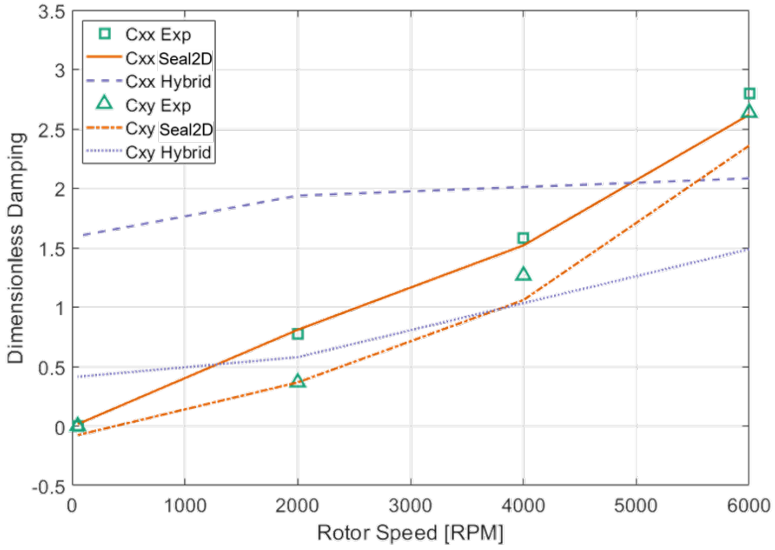

Figure 5.13: Jolly *et. al.*[170] dimensionless damping profile

Chapter 6

Conclusions

The zeroth-order, concentric, solution to the simulation of annular pressure seals was accomplished with a mimetic finite difference method approach to the RANS momentum and mass conservation equations and the Prandtl one-equation turbulence model. The error bars from Richardson extrapolation in Figure 5.4 indicate a significant mesh dependence for the full code, but an imported eddy viscosity profile removes this issue. Further debugging is necessary to integrate the modified Spalding wall functions with the chosen turbulence model. The Prandtl one-equation turbulence model provides quantitatively and qualitatively reasonable profiles when similarly run with fixed velocities. As previously discussed, annular pressure seals have not been modeled with a 2-D axial-radial grid method since the work of Dietzen *et. al.*[36] in 1987 despite the benefits of this method falling between the two modernly accepted approaches in computational cost, engineer set-up time, and engineer training required. The novel applications included herein are the application of many various modern coding and optimization techniques to a mimetic finite difference implementation of both the RANS momentum equations and a selected turbulence model. While work has been done using the mimetic finite difference method with a cylindrical coordinate system on the Navier-Stokes equations, the author has found no works that apply the mimetic finite difference method to a similarly perturbed solution of the RANS equations to the 2-D axial-radial grid for annular pressure seals. Mimetic methods and the shift matrix coding techniques are valuable due to their spatially and transiently stable nature and computational efficiency. Similarly, no work has been done to apply the mimetic finite difference method to the solution of turbulence models with conservation equations in concert to the RANS equations. Neither has the Prandtl one-equation been previously

applied to the simulation of annular pressure seal flows, with or without the specific modifications to length scale and wall function calculation in this work.

The first-order solutions, both hybrid-bulk flow and 2D momentum equation, provide a qualitatively and quantitatively reasonable pressure profile generated circumferentially around the seal due to eccentric whirl and the rotordynamic coefficients that are based on that pressure profile. The first-order pressure profiles and rotordynamic coefficients remain heavily dependent on the loss and recovery coefficients for the inlet and exit of the seal at this time, but this can easily be overcome with future updates to the 2-D and hybrid codes. Both versions of the first-order codes result in rotordynamic coefficients that fall within a reasonable range when an appropriate pair of loss coefficients are selected. However, the hybrid bulk-flow code results in less accurate prediction of damping coefficients, while having a slightly more accurate prediction of cross-coupled stiffness coefficients. The hybrid bulk-flow method is reasonably succesfull on its own, but can be better applied to improve the convergence of the 2-D first order code by providing more accurate initial conditions and initial first-order axial velocity boundary condition guesses. Further debugging of the full zeroth-order code and adjustments to the turbulence model will fine tune the results of both the hybrid and 2-D first-order codes. As discussed above with the 2-D code, the hybrid bulk-flow approach has not been applied to labyrinth seals since Athavale *et. al.* in 1996,[41] though more modern attempts have been made at hybrid methods for hole-pattern seals.

While the 2-D axial-radial grid approach to modeling annular pressure seals is not new, it has been largely neglected in modern literature. The code(s) developed in this work are computationally efficient, parallelized, and capable of being run on computing clusters. The development goals have been met in terms of accuracy, engineer set-up time, and solution time to allow industrial researchers to design seals specific to individual applications with large scale optimization studies on a reasonable time scale.

6.1 Expected Publications

This work will be split into two primary publications. The first publication will consist of the zeroth-order solution methodology and turbulence implementation. The second publication will discuss the first-order solution results with both the hybrid-bulk flow and 2D first-order momentum equations. Additional publications will also be created, but require content discussed in the following section on future work.

6.1.1 Mimetic Finite Difference Implementation of Turbulence In Concentric Annuli

This work will be published in the Journal of Computational Physics. This journal has an impact factor of 3.553 (in 2020), and is appropriate for the discussion of the novel numerical methodology and turbulence application due to the similarity with prior publications in the same journal by Oud.[91]

The abstract for this publication is below: Turbulent incompressible flow through a concentric annular region is modeled numerically with mimetic finite difference (MFD) techniques and the Prandtl One-Equation eddy viscosity turbulence model. The numerical model consists of three Reynolds-Averaged Navier-Stokes (RANS) momentum equations, a mass conservation equation, a turbulent kinetic energy (TKE) conservation equation, and an empirical model for turbulent mixing length. These equation are solved with mimetic discrete operators on an axial-radial staggered grid discretization of a concentric annular flow domain. The work demonstrates the application of MFD methods to eddy viscosity turbulence models with conservation equations. While MFD methods are widely applied to computational fluid dynamics (CFD) in the literature, the author is not aware of any attempts to apply them to turbulence modeling. The resulting analysis code is then validated against annular pressure seal data from the literature.

6.1.2 Mimetic Finite Difference Annular Seal Modeling in 2-D and Hybrid Bulk Flow

The first-order results and discussion will be published in the ASME Journal of Gas Turbines and Power after submission to the ASME Turbomachinery Exposition conference of 2023. This journal was selected due to ROMAC's prior experience with the associated conference.

The abstract for this publication is below: Annular pressure seals are employed in turbomachinery systems to limit the leakage of working fluid between pressure stages. The seal consists of a

thin annular clearance region which lowers leakage with a small cross-sectional area and viscous pressure losses. Modern analysis techniques of such seals tend to fall into two categories. Either the seal model is greatly simplified through assumptions and application of empirical factors, or the seal is modeled using 3-D CFD techniques in generalized fluid dynamics codes. The method of simplification is referred to as “Bulk Flow” analysis due to the use of radially averaged “bulk” values for flow variables. These 1-D bulk flow equations can be solved rapidly at the expense of accuracy, the use of empirical factors, and flexibility in seal geometry types. This work applied a 2-D grid axial-radial grid with a memetic finite difference scheme to strike a balance between the 1-D bulk flow method and 3-D generalized CFD. The 0th and 1st order solution of the geometrically perturbed and incompressible cylindrical Reynolds Averaged Navier-Stokes (RANS) equations were solved to model the seal’s eccentric annular region with an assumed small and circular whirl orbit. Turbulence was modeled with both Reichardt’s zero-equation and Prandtl’s one-equation models for comparison. The 0th order solution provided the user with leakage results, wall shear stress, and initial pressure differential estimates. The 1st-order solution refined the pressure differential estimate and models the circumferential variation to obtain rotordynamic coefficients from multiple whirl speed cases. The rotordynamic coefficients predictions from the perturbed 2D finite difference code were then compared to a 1st-order hybrid CFD-bulk flow method and experimental studies on smooth annular seals from the literature.

6.2 Recommendations for Future Work

The initial goals for further code development consist of additional validation and comparison to the literature and commercial CFD software. The author has requested electronic data for the first-order unwrapped pressure profiles from Jolly *et. al.*,[170] shown in Figures 5.6 and 5.7. A direct numerical comparison of the first-order pressures will allow for further fine-tuning of the 2-D and hybrid codes and a quantification of the first-order solution’s relative accuracy. Both the first-order pressure profiles and rotordynamic coefficients will then be additionally compared to traditional bulk-flow and full 3-D commmercial CFD eccentric simulations for the test cases presented. Then an additional test case will be added from the work of Kaneko *et. al.*[172] that consists of a water seal with axial Reynolds number of 5,000 and circumferential Reynolds numbers ranging from 0 to

4,000 to cover the lower speed turbulent flow range. These additional validation steps will be taken prior to submission of the expected publications from this dissertation.

Outside of code validation, one of the easiest code updates to apply consists of modifying the code to allow compressible flow cases. Due to the spatially conservative construction of the finite difference equations employed in this work, it is likely that the only changes necessary to the momentum and mass conservation equations would be the inclusion of a localized fluid molecular viscosity translated to a local baseline Reynolds number for each node that is updated based on the solution of additional equations for energy conservation or equations of state. The remaining categories of future work can be broken into two approaches. The first category is to allow generalized seal geometry and boundary conditions so that seals can be optimized for specific tasks or more varieties of seals can be investigated. The second category is the investigation and comparison of alternate turbulence models and wall functions for various geometries and operating conditions.

6.2.1 Generalized Geometry

The potential approaches to generalize the geometry for a finite diference CFD code consist of the following options:

- Using a rectangular mesh grid, remove cells outside the seal domain and adjust the boundary handling functions to deal with multiple faces in each boundary direction.
- Link multiple rectangular domains together at adjoining faces to create a multi-domain finite difference method.
- Adjust the fintie difference mimetic operators to apply to an unstructured mesh.
- Apply an immersed boundary method[173] of pseduo wall forces between grid elements to model irregular rotor and stator surfaces.
- Convert the mimetic operators to the finite element method with an unstructured mesh grid.

Each of these options has positive and negative points associated. The first two options are likely the simplest to implement, but would be most restricting on the potential geometries to

model. The user would be restricted to geometries that can be mapped onto quadrilateral grids. Allowing an unstructured grid with mimetic finite difference operators would require additional matrix inversion operations to automatically calculate the adjoint discrete vector and tensor operators, thus increasing the computaitonal cost as the trade-off for flexibility. Employing the immersed boundary method[173] would likely be the most computationally efficient method while retaining the finite difference nature of the code to minimize time to modify and test new code. The last option of switching from fintie difference to finite element methods would allow similar flexibility for geometries, but would sacrifice some of the stability of the mimetic finite difference method and requrie extensive researcher time.

6.2.2 Turbulence Modeling

Future work related to modeling turbulence in the 2D annular seal code consists of testing multiple turbulence models of zero, one, and two conservation equations; or testing the application of different wall functions.

The primary options used for turubulence modeling of annular seals include variations on the $k-\epsilon$ 2 equation model (for $y+$ values > 30) and SST $k-\Omega$ 2 equation model (for $y+$ values < 30).[123] Additional alternative turbulence models of potential interest are:

- Cebeci-Smith empirical model
- Baldwin-Lomax empirical model
- $\frac{1}{2}$ equation model of Johnson *et. al.*
- Spalart-Allmaras 2-equation turbulence model

Another publication could investigate the differences in usage of smooth and non-smooth wall functions or wall functions that account for the circumferential curvature of the seal.

Appendix A

Non-dimensionalization and Reynolds Averaging

As discussed in Section 2.4.1, the mass conservation and Incompressible Navier-Stokes momentum conservation equations are frequently Reynolds Averaged to introduce turbulence modeling corrections for high Reynolds Number flows. This averaging results in the Reynolds Averaged Navier-Stokes (RANS) equations that include a Reynolds Stress Tensor to model local time fluctuating turbulence. In this work, and many from the literature, the Reynolds Stress Tensor is approximated though application of artificial Eddy Viscosity that modifies the diffusion of velocity through the domain. The RANS equations with eddy viscosity modification are given below in Equation A.2, wher each $*$'d variable represents a flow variable with physical dimension. Compressible flow is similarly managed through Favre Averaging over fluid mass.

$$\underline{\underline{\mathbf{E}}}^* = \frac{1}{2}\left[\nabla^* \otimes \vec{u}^* + (\nabla^* \otimes \vec{u}^*)^T\right] \tag{A.1}$$

$$\frac{\partial\left(\rho\vec{u}^*\right)}{\partial t^*} + \rho\vec{u}^* \cdot \nabla^* \otimes \vec{u}^* = -\nabla^* P^* + \nabla^* \cdot \left[\mu\left(2\underline{\underline{\mathbf{E}}}^* - \frac{2}{3}\left[\nabla^* \cdot \vec{u}^*\right]\mathbf{I}\right) + 2\mu^t \underline{\underline{\mathbf{E}}}^* - \frac{2}{3}\rho k^* \cdot \mathbf{I}\right] \tag{A.2}$$

$$k^* = \frac{1}{2}u^{*\prime}u^{*\prime} \tag{A.3}$$

When performing numerical analysis of the partial differential equations it is common to non-dimensionalize them. Non-dimensionalization of the equations allows the researcher to more directly view the relative strength of contribution from different physical effects, levels the scaling of terms to prevent poor matrix conditioning, and exhibits the characteristic properties of the

fluid system. Non-dimensionalization has an additional benefit to the numerical stability of a system of equations because it typically helps to manage the condition number of the matrices by bounding the scale of the numbers involved. All non-dimensionalization is based on the idea that an equation representing physical effects must have consistent units within and between each term of the equations. In this case the momentum, mass, and energy conservation in the Navier-Stokes equations each have consistent units within each conservation. The continuity or mass conservation equation has units of $\left[ms^{-1}\right]\,[m] = \left[s^{-1}\right]$, momentum conservation has units of force, and energy conservation typically has units of temperature (though sometimes other units are used). Thus each piece of a physically meaningful equation can be gathered into dimensionless Π groups, so called from the Buckingham π theorem, where the number of dimensionless π's is based on the number of variables minus the number of physical dimensions involved. In the case of the Navier-Stokes equations there are seven basic variables contributing to the change in momentum: position, velocity, density, viscosity, pressure, force and duration. These variables are based on physical dimensions of length, time and mass. This suggests that there should be 4 dimensionless paramters as coefficients for the non-dimensionalized variables. To determine these Π groups, one first takes each physical dimension and obtains scaling parameters to non-dimensionalize them, these scaling parameters are given in Table A.1. Note that while all of the phyiscal dimensions must be represented in these scaling parameters, it is not necessary for the scaling parameters to contain *only* the physical dimension.

Table A.1: Non-dimensional Scaling Parameters

Variable	Scaling Parameter	Physical Dimensions	SI Units
Position	$L_c = 2H^0$	L	[m]
Velocity	$U_c = max\,(u, w, v)_{BC}$	LT^{-1}	$\left[\frac{m}{s}\right]$
Pressure	ΔP_c	$ML^{-1}T^{-2}$	$\left[\frac{kg}{ms^2}\right]$
Frequency	f	T^{-1}	$\left[\frac{1}{s}\right]$

The equations are then re-written by defining non-dimensional variables, Equation A.4, in terms of the dimensional variables and the scaling factors and substituting these non-dimensional variables into the original equation with the equivalent change of variables operations. The original RANS momentum equation in vector form is Equation A.2 and the substition is performed in Equation A.5. In between steps, the body force is neglected as it is not used in this body of work,

this also means that one of the Π groups will not be discussed further as it, the Froude Number, relates to the scaling of this body force by gravitational acceleration. Every term of Equation A.5 has dimensions of $\left[mL^{-2}t^{-2}\right]$ so multiplying through by $\frac{L_c}{\rho_c U_c^2}$ non-dimensionalizes the whole equation. Note that to preserve compressibility, the division is in terms of a characteristic density rather than the actual density at each point.

$$\vec{r} = \frac{\vec{r}^*}{2H^0} \tag{A.4a}$$

$$\vec{u} = \frac{\vec{U}^*}{U_c} \tag{A.4b}$$

$$\vec{\nabla} = 2H^0 \vec{\nabla}^* \tag{A.4c}$$

$$t = \cancel{f}t^* = \Omega t^* \tag{A.4d}$$

$$P = \frac{P^* - P_{Ref.}}{\Delta P_c} \tag{A.4e}$$

Note that the time non-dimensionalization is based on the whirl speed, Ω rather than the rotor speed, ω. This is because the expression in the exponent of the perturbation term, $\imath\,(\Omega t^* + \theta)$ is already non-dimensional with a $\frac{1}{s} \times s$. This results in the first order equation having a Strouhal number based on the whirl speed while the rotor speed contributions come from the zeroth order velocity and pressure terms. The exponent of the perturbation then becomes simply $\imath\,(t + \theta)$. For model simplicity, the Strouhal number was folded into the discrete time step when performing the numerical calculations.

$$\cancel{f}U_c \frac{\partial\,(\rho\vec{u})}{\partial t} + \frac{U_c^2}{L_c}\rho\vec{u}\cdot\nabla\otimes\vec{u} = -\frac{\Delta P_c}{L_c}\nabla P + \frac{1}{L_c}\nabla\cdot\left[\frac{U_c}{L_c}\mu\left(2\underline{\underline{\mathbf{E}}} - \frac{2}{3}\left[\nabla\cdot\vec{u}\right]\mathbf{I}\right) + \frac{U_c}{L_c}2\mu^t\underline{\underline{\mathbf{E}}} - U_c^2\frac{2}{3}\rho k\cdot\mathbf{I}\right] \tag{A.5}$$

$$\frac{L_c\cancel{f}}{U_c}\frac{\partial\vec{u}}{\partial t} + \vec{u}\cdot\nabla\otimes\vec{u} = -\frac{\Delta P_c}{\rho_c U_c^2}\nabla P + \frac{1}{\rho_c L_c U_c}\nabla\cdot\left[\mu\left(2\underline{\underline{\mathbf{E}}} - \frac{2}{3}\left[\nabla\cdot\vec{u}\right]\mathbf{I}\right) + 2\mu^t\underline{\underline{\mathbf{E}}} - \frac{2}{3}k\cdot\mathbf{I}\right] \tag{A.6}$$

$$\frac{L_c\Omega}{U_c}\frac{\partial\vec{u}}{\partial t} + \vec{u}\cdot\nabla\otimes\vec{u} = -\,\mathrm{Eu}\nabla P + \nabla\cdot\left[\frac{1}{\mathrm{Re}}\left(2\underline{\underline{\mathbf{E}}} - \frac{2}{3}\cancel{[\nabla\cdot\vec{u}]\mathbf{I}}\right) + 2\frac{1}{\mathrm{Re}^t}\underline{\underline{\mathbf{E}}} - \frac{2}{3}k\cdot\mathbf{I}\right] \tag{A.7}$$

$$\mathrm{St}\frac{\partial\vec{u}}{\partial t} + \vec{u}\cdot\nabla\otimes\vec{u} = -\,\mathrm{Eu}\nabla P + \nabla\cdot\left[2\left(\frac{1}{\mathrm{Re}} + \frac{1}{\mathrm{Re}^t}\right)\underline{\underline{\mathbf{E}}} - \frac{2}{3}k\cdot\mathbf{I}\right] \tag{A.8}$$

From left to right, the non-dimensional Π group coefficients in A.7 are identified as the Strouhal Number on the time derivative, the Euler Number on the pressure gradient, and the Reynolds Number on the viscous diffusion terms, seen combined in A.8. When dealing with the incompressible

form of the equations, the ρ's are removed as the characteristic ρ_c is equivalent to the instantaneous ρ. Also, choose $\Delta P_c = \rho_c U_c^2$ so that the Euler Number becomes one.

$$\mathrm{St}\frac{\partial \vec{u}}{\partial t} + \vec{u}\cdot\nabla\otimes\vec{u} = -\nabla P + \nabla\cdot\left[2\left(\frac{1}{\mathrm{Re}} + \frac{1}{\mathrm{Re}^t}\right)\underline{\underline{\mathbf{E}}} - \frac{2}{3}k\cdot\mathbf{I}\right] \tag{A.9}$$

Convert the components of the Navier-Stokes Equations into first order vector operation form to allow conjugate vector operators that reverse the vector space translation.

$$\begin{aligned}\vec{u}\cdot\nabla\otimes\vec{u} &= (\vec{u}\cdot\nabla)\,\vec{u}\\ &= (\nabla\times\vec{u})\times\vec{u} + \frac{1}{2}\nabla(\vec{u}\cdot\vec{u})\\ &= N(\vec{u}) + \frac{1}{2}\nabla(\vec{u}\cdot\vec{u})\end{aligned} \tag{A.10}$$

$$\nabla P^T = \frac{1}{2}\nabla(\vec{u}\cdot\vec{u}) + \nabla P \tag{A.11}$$

$$\begin{aligned}\nabla^2\vec{u} &= \nabla\cancel{(\nabla\cdot\vec{u})} - \nabla\times\nabla\times\vec{u}\\ &= -\nabla\times\nabla\times\vec{u}\\ &= -C\left[\overline{C}(\vec{u})\right]\end{aligned} \tag{A.12}$$

$$\mathrm{St}\frac{\partial\vec{u}}{\partial t} + (\nabla\times\vec{u})\times\vec{u} + \frac{1}{2}\nabla(\vec{u}\cdot\vec{u}) = -\nabla P + \frac{1}{\mathrm{Re}}\{-\nabla\times\nabla\times\vec{u}\} + \nabla\cdot\left[2\frac{1}{\mathrm{Re}^t}\underline{\underline{\mathbf{E}}} - \frac{2}{3}k\cdot\mathbf{I}\right] \tag{A.13}$$

$$\begin{aligned}\frac{\partial(\vec{u})}{\partial t} &= \frac{\partial\vec{u}}{\partial t} + \frac{\partial\chi}{\partial t}\frac{\partial\vec{u}}{\partial\chi}\\ &= i\varepsilon\vec{u}^1 + i\varepsilon(R_S-\chi)\frac{\partial\vec{u}^0}{\partial\chi}\end{aligned} \tag{A.14}$$

$$\begin{aligned}i\varepsilon\mathrm{St}\vec{u}^1 + i\varepsilon\mathrm{St}(R_S-\chi)\frac{\partial\vec{u}^0}{\partial\chi} + \mathbf{N}(\vec{u}) &= -\overline{\mathbf{G}}\left(P^{Total}\right) - \frac{1}{\mathrm{Re}}\frac{1}{\mathrm{Re}}\mathbf{C}\overline{\mathbf{C}}(\vec{u}) + \overline{\mathscr{D}}\left[2\frac{1}{\mathrm{Re}^t}\underline{\underline{\mathbf{E}}} - \frac{2}{3}k\cdot\mathbf{I}\right]\\ i\varepsilon\mathrm{St}\vec{u}^1 &= -i\varepsilon\mathrm{St}(R_S-\chi)\frac{\partial\vec{u}^0}{\partial\chi} - \mathbf{N}(\vec{u})\\ &\quad - \overline{\mathbf{G}}\left(P^{Total}\right) - \frac{1}{\mathrm{Re}}\mathbf{C}\overline{\mathbf{C}}(\vec{u})\\ &\quad + \overline{\mathscr{D}}\left[2\frac{1}{\mathrm{Re}^t}\underline{\underline{\mathbf{E}}} - \frac{2}{3}k\cdot\mathbf{I}\right]\end{aligned} \tag{A.15}$$

$$\underline{\underline{\mathbf{E}}} = \frac{1}{2}\left[\mathscr{G}(\vec{u}) + \mathscr{G}^T(\vec{u})\right] \tag{A.16}$$

$$\begin{aligned}\mathbf{N}(\vec{u}) &= (\nabla \times \vec{u}) \times \vec{u} \\ &= \begin{bmatrix} \omega w - \zeta v \\ \zeta u - \eta w \\ \eta v - \omega u \end{bmatrix}\end{aligned} \tag{A.17}$$

$$\begin{aligned}\nabla P^T &= \overline{\mathbf{G}}\left(P^T\right) \\ &= \begin{bmatrix} \frac{\partial P^T}{\partial r} \\ \frac{\partial P^T}{\partial \theta} \\ \frac{\partial P^T}{\partial z} \end{bmatrix}\end{aligned} \tag{A.18}$$

$$\begin{aligned}\mathbf{C}\overline{\mathbf{C}}(\vec{u}) &= \nabla \times \nabla \times \vec{u} \\ &= \nabla \times \vec{\omega} \\ &= \begin{bmatrix} \frac{1}{r}\frac{\partial \zeta}{\partial \theta} - \frac{\partial \omega}{\partial z} \\ \frac{\partial \eta}{\partial z} - \frac{\partial \zeta}{\partial r} \\ \frac{1}{r}\left(\frac{\partial (r\omega)}{\partial r} - \frac{\partial \eta}{\partial r}\right) \end{bmatrix}\end{aligned} \tag{A.19}$$

$$\begin{aligned}\overline{\mathbf{C}}(\vec{u}) &= \vec{\omega} \\ &= \begin{bmatrix} \frac{1}{r}\frac{\partial w}{\partial \theta} - \frac{\partial v}{\partial z} \\ \frac{\partial u}{\partial z} - \frac{\partial w}{\partial r} \\ \frac{1}{r}\left(\frac{\partial (rv)}{\partial r} - \frac{\partial u}{\partial r}\right) \end{bmatrix}\end{aligned} \tag{A.20}$$

$$\mathscr{D}\left(\underline{\underline{\sigma}}\right) = \nabla \cdot \underline{\underline{\sigma}} \tag{A.21}$$

$$\mathscr{G}(\vec{u}) = \nabla \otimes \vec{u} \tag{A.22}$$

The Prandtl one-equation turbulence model is given by Equation A.24.[123] In this kinetic energy transport equation, every term has the units of $\left[\frac{L^2}{t^3}\right]$. The equation is non-dimensionalized by applying a multiple of $\frac{L_c}{U_c^3}$ to each term to obtain Equation A.27. The specific turbulent kinetic energy (TKE), TKE per fluid density, is non-dimensionalized by the square of the characteristic velocity

scaling parameter. Similarly, the Kolmogrov length is scaled by the characteristic length used in the Reynolds number calculation. The turbulent eddy viscosity μ_t is approximated by Equation A.26 in dimensional form. When non-dimensionalized turbulent Reynolds number corresponding to the eddy viscosity is given by Equation A.30, note that the σ_k scaling parameter is typically assumed to be equal to one.

$$k_t^* = k_t U_c^2 \tag{A.23}$$

$$\frac{\partial k_t^*}{\partial t} + \left(\vec{u}_s^* \cdot \nabla_s^* k_t^*\right) = \underline{\underline{\tau}}_{qs} \otimes \frac{U_c}{L_c}\left(\nabla_s^* \otimes \vec{u}_q^*\right) - C_D \frac{k_t^{*\frac{3}{2}}}{\ell_t^*} + \nabla_s^* \cdot \left[\frac{1}{\rho_0}\left(\mu_0 + \frac{\mu_t}{\sigma_k}\right)\nabla_s^* k_t^*\right] \tag{A.24}$$

$$\begin{aligned} \underline{\underline{\tau}}_{qs} &= \left[\frac{2\mu_t}{\rho_0}\underline{\underline{\mathbf{E}}} - \frac{2}{3}k_t^* \delta_{qs}\right]_{qs} \\ \Rightarrow \underline{\underline{\tau}}_{qq} &= 2k^* \end{aligned} \tag{A.25}$$

$$\mu_t = \rho_c k_t^{*\frac{1}{2}} \ell_t^* = \rho_c \left(k_t^{\frac{1}{2}} U_c\right)(\ell_t L_c) \tag{A.26}$$

$$\begin{aligned} U_c^2 f \frac{\partial k_t}{\partial t} + \frac{U_c^3}{L_c}\left(\vec{u}_s \cdot \nabla_s k_t\right) = &\left[2U_c L_c k_t^{\frac{1}{2}} \ell_t \frac{U_c}{L_c}\underline{\underline{\mathbf{E}}} - U_c^2 \frac{2}{3} k_t \delta_{qs}\right]_{qs} \otimes \frac{U_c}{L_c}\left(\nabla_s \otimes \vec{u}_q\right) \\ &- \frac{U_c^3}{L_c} C_D \frac{k_t^{\frac{3}{2}}}{\ell_t} + \frac{1}{L_c}\nabla_s \cdot \left[\frac{1}{\rho_0}\left(\mu_0 + \frac{\mu_t}{\sigma_k}\right)\frac{U_c^2}{L_c}\nabla_s k_t\right] \end{aligned} \tag{A.27}$$

$$\begin{aligned} \frac{L_c}{U_c^3} U_c^2 f \frac{\partial k_t}{\partial t} + \frac{L_c}{U_c^3}\frac{U_c^3}{L_c}\left(\vec{u}_s \cdot \nabla_s k_t\right) = &\frac{L_c}{U_c^3}\left[2U_c L_c k_t^{\frac{1}{2}} \ell_t \frac{U_c}{L_c}\underline{\underline{\mathbf{E}}} - U_c^2 \frac{2}{3} k_t \delta_{qs}\right]_{qs} \otimes \frac{U_c}{L_c}\left(\nabla_s \otimes \vec{u}_q\right) \\ &- \frac{L_c}{U_c^3}\frac{U_c^3}{L_c} C_D \frac{k_t^{\frac{3}{2}}}{\ell_t} + \frac{L_c}{U_c^3}\frac{1}{L_c}\nabla_s \cdot \left[\frac{1}{\rho_0}\left(\mu_0 + \frac{\mu_t}{\sigma_k}\right)\frac{U_c^2}{L_c}\nabla_s k_t\right] \end{aligned} \tag{A.28}$$

$$\begin{aligned} f\frac{L_c}{U_c}\frac{\partial k_t}{\partial t} + \left(\vec{u}_s \cdot \nabla_s k_t\right) = &\left[2k_t^{\frac{1}{2}} \ell_t \underline{\underline{\mathbf{E}}} - \frac{2}{3} k_t \delta_{qs}\right]_{qs} \otimes \left(\nabla_s \otimes \vec{u}_q\right) \\ &- C_D \frac{k_t^{\frac{3}{2}}}{\ell_t} + \frac{1}{\rho_c L_c U_c}\nabla_s \cdot \left[\left(\mu_0 + \frac{\mu_t}{\sigma_k}\right)\nabla_s k_t\right] \end{aligned} \tag{A.29}$$

$$\frac{1}{\mathrm{Re}_t} = \frac{\mu_t}{\rho_c L_c U_c} = \frac{\rho_c k_t^{*\frac{1}{2}} \ell_t^*}{\rho_c L_c U_c} = k_t^{\frac{1}{2}} \ell_t \tag{A.30}$$

$$\begin{aligned} \mathrm{St}\frac{\partial k_t}{\partial t} + \left(\vec{u}_s \cdot \nabla_s k_t\right) = &\left[\frac{1}{\mathrm{Re}_t}\left\{\nabla_s \vec{u}_q + \left(\nabla_q \vec{u}_s\right)^T\right\} - \frac{2}{3} k_t \delta_{qs}\right]_{qs} \otimes \left(\nabla_s \otimes \vec{u}_q\right) \\ &- C_D \frac{k_t^{\frac{3}{2}}}{\ell_t} + \nabla_s \cdot \left[\left(\frac{1}{\mathrm{Re}_c} + \frac{1}{\sigma_k \mathrm{Re}_t}\right)\nabla_s k_t\right] \end{aligned} \tag{A.31}$$

Appendix B

Discrete Mimetic Operator Derivation: Divergence & Adjoint Gradient

Divergenc and gradient are vector calculus operators that act on variables that represent field values. The divergence operator acts on a vector field to calculate the scalar outward flux density of a differential volume. For the purposes of this study, the divergence operator ($\mathbf{D}_{\mathbf{FC}\rightarrow\mathbf{CC}}$) is a primary discrete operator and represents the mass conservation part of the Navier-Stokes equation. $\mathbf{D}_{\mathbf{FC}\rightarrow\mathbf{CC}}$ will act on the velocity vector components stored in the face centered (**FC**) vector space and translate it to a scalar value held in the cell centered (**CC**) nodal vector space.[91,115] The **CC** vector space stores flow variables such as pressure, viscosity, density, turbulent kinetic energy and turbulent kinetic energy dissipation. The derived operator based on $\mathbf{D}_{\mathbf{FC}\rightarrow\mathbf{CC}}$ must act as translation opposite to it, going from the **CC** vector space to the face centered space. This derived operator acts as the gradient of pressure, determining the vector rate of change of a scalar field, and is represented by $\overline{\mathbf{G}}_{\mathbf{CC}\rightarrow\mathbf{FC}}$.[88,91,117]

B.1 Divergence Operator, $\mathbf{D}_{\mathbf{FC}\rightarrow\mathbf{CC}}\left(\vec{u}\right) = \nabla\cdot\vec{u}$

The divergence operator is defined in a continuous invariant space using Equation B.1.

$$\nabla\cdot\vec{u} \equiv \lim_{V\rightarrow 0}\frac{1}{V}\oint_{V}\langle\vec{u},\hat{n}\rangle\ dS \tag{B.1}$$

The $\langle \vec{u}, \hat{n} \rangle$ is the inner product of the velocity vector field and the outward normal to the boundary S of volume V, inner product being a generalization of dot product that reduces a pair of vector/tensor objects to scalar through multiplication and summation. The discrete vector operator for divergence is constructed by performing a finite volume analysis of the integral in Equation B.1. As each velocity vector component exists in the center of a single cell face's outward normal direction, it is convenient to assume that vector component value for the entire cell face of a given cylindrical shell element. Equation B.2 is the divergence primary operator definition in standard cylindrical coordinates.

$$\begin{aligned} \mathbf{D}_{\mathbf{FC}\rightarrow\mathbf{CC}}\left(\vec{u}\right) = & \frac{1}{r_i \Delta r_i \Delta\theta \Delta z_k} \left[\Delta\theta \Delta z_k \left(r_\ell u_{\ell,k} - r_{\ell-1} u_{\ell-1,k}\right)\right. \\ & \left. + \Delta r_i \Delta z_k \left(v_{i,m,k} - v_{i,m-1,k}\right) + r_i \Delta r_i \Delta\theta \left(w_{i,n} - w_{i,n-1}\right)\right] \\ = & \frac{\left(r_\ell u_{\ell,k} - r_{\ell-1} u_{\ell-1,k}\right)}{r_i \Delta r_i} + \frac{\left(v_{i,m,k} - v_{i,m-1,k}\right)}{r_i \Delta\theta} + \frac{\left(w_{i,n} - w_{i,n-1}\right)}{\Delta z_k} \end{aligned} \tag{B.2}$$

This standard cylindrical coordinate operator is transformed for annular seal analysis by substitution and chain rule to the eccentrically perturbed coordinate system. This variable transformation changes the radial and circumferential terms, but leaves the axial terms in the same form. The resulting primary discrete operator is given by Equation B.3. The $\frac{1}{r_i}$ and $\frac{1}{\Delta r_i}$ terms are approximated by Taylor series to avoid ending with perturbation parameters in the denominator which would later prevent the first order terms from having the same scales of ε. The circumferential derivative has also replaced by a discrete equivalent that includes the effects of the perturbed variable transformation and chain rule.

$$\begin{aligned} \mathbf{D}_{\mathbf{FC}\rightarrow\mathbf{CC}}\left(\vec{u}\right) = 0 = & \frac{1}{\chi_i} \frac{\chi_\ell u^0_{\ell,k} - \chi_{\ell-1} u^0_{\ell-1,k}}{\Delta\chi_i} \left(1+\varepsilon\right) \\ & + \varepsilon \frac{1}{\chi_i} \frac{\left[\chi_\ell u^1_{\ell,k} + \left(R_S - \chi_\ell\right) u^0_{\ell,k}\right] - \left[\chi_{\ell-1} u^1_{\ell-1,k} + \left(R_S - \chi_{\ell-1}\right) u^0_{\ell-1,k}\right]}{\Delta\chi_i} \\ & - \varepsilon \frac{\left(R_S - \chi_i\right)}{\chi_i^2} \frac{\chi_\ell u^0_{\ell,k} - \chi_{\ell-1} u^0_{\ell-1,k}}{\Delta\chi_i} \\ & + \imath\varepsilon \frac{1}{\chi_i} \left[v^1_{i,k} + 2\left(R_S - \chi_i\right) \frac{v^0_{i+1,k} - v^0_{i-1,k}}{\Delta\chi_{i+1} + 2\Delta\chi_i + \Delta\chi_{i-1}}\right] \\ & + \frac{w^0_{i,n} - w^0_{i,n-1}}{\Delta z_k} + \varepsilon \frac{w^1_{i,n} - w^1_{i,n-1}}{\Delta z_k} \end{aligned} \tag{B.3}$$

B.2 Discrete Divergence Operator, Zeroth Order: $\mathbf{D}^0(\vec{u})$

$$\mathbf{D}^{\mathbf{0}}_{\mathbf{FC\to CC}}(\vec{u}) = 0 = \frac{1}{\chi_i}\frac{\chi_\ell u^0_{\ell,k} - \chi_{\ell-1}u^0_{\ell-1,k}}{\Delta\chi_i} + \frac{w^0_{i,n} - w^0_{i,n-1}}{\Delta z_k} \tag{B.4}$$

B.3 Discrete Divergence Operator, First Order: $\mathbf{D}^1(\vec{u})$

$$\begin{aligned}\mathbf{D}^{\mathbf{1}}_{\mathbf{FC\to CC}}(\vec{u}) = 0 =& \frac{1}{\chi_i}\frac{\chi_\ell u^0_{\ell,k} - \chi_{\ell-1}u^0_{\ell-1,k}}{\Delta\chi_i} + \frac{1}{\chi_i}\frac{(R_S - \cancel{\chi_\ell})\,u^0_{\ell,k} - (R_S - \cancel{\chi_{\ell-1}})\,u^0_{\ell-1,k}}{\Delta\chi_i}\\ &- \frac{(R_S - \cancel{\chi_i})}{\chi_i^2}\frac{\chi_\ell u^0_{\ell,k} - \chi_{\ell-1}u^0_{\ell-1,k}}{\Delta\chi_i} + \frac{1}{\chi_i}\frac{\chi_\ell u^1_{\ell,k} - \chi_{\ell-1}u^1_{\ell-1,k}}{\Delta\chi_i}\\ &+ \imath\frac{1}{\chi_i}\left[v^1_{i,k} + 2(R_S - \chi_i)\frac{v^0_{i+1,k} - v^0_{i-1,k}}{\Delta\chi_{i+1} + 2\Delta\chi_i + \Delta\chi_{i-1}}\right] + \frac{w^1_{i,n} - w^1_{i,n-1}}{\Delta z_k}\end{aligned} \tag{B.5}$$

B.3.1 Discrete Divergence Operator, Real First Order: $\mathbf{D}^R(\vec{u})$

$$\begin{aligned}\mathbf{D}^{\mathbf{R}}_{\mathbf{FC\to CC}}(\vec{u}) = 0 =& \frac{1}{\chi_i}\frac{\chi_\ell u^0_{\ell,k} - \chi_{\ell-1}u^0_{\ell-1,k}}{\Delta\chi_i} + \frac{R_S}{\chi_i}\frac{u^0_{\ell,k} - u^0_{\ell-1,k}}{\Delta\chi_i}\\ &- \frac{R_S}{\chi_i^2}\frac{\chi_\ell u^0_{\ell,k} - \chi_{\ell-1}u^0_{\ell-1,k}}{\Delta\chi_i} + \frac{1}{\chi_i}\frac{\chi_\ell u^R_{\ell,k} - \chi_{\ell-1}u^R_{\ell-1,k}}{\Delta\chi_i}\\ &- \frac{1}{\chi_i}v^I_{i,k} + \frac{w^R_{i,n} - w^R_{i,n-1}}{\Delta z_k}\end{aligned} \tag{B.6}$$

B.3.2 Discrete Divergence Operator, Imaginary First Order: $\mathbf{D}^I(\vec{u})$

$$\begin{aligned}\mathbf{D}^{\mathbf{I}}_{\mathbf{FC\to CC}}(\vec{u}) = 0 =& \frac{1}{\chi_i}\frac{\chi_\ell u^I_{\ell,k} - \chi_{\ell-1}u^I_{\ell-1,k}}{\Delta\chi_i}\\ &+ \frac{1}{\chi_i}\left[v^R_{i,k} + 2(R_S - \chi_i)\frac{v_{i+1,k} - v_{i-1,k}}{\Delta\chi_{i+1} + 2\Delta\chi_i + \Delta\chi_{i-1}}\right] + \frac{w^I_{i,n} - w^I_{i,n-1}}{\Delta z_k}\end{aligned} \tag{B.7}$$

B.4 Derivation of the Adjoint Gradient Operator, $\overline{\mathbf{G}}_{\mathbf{CC}\rightarrow\mathbf{FC}}$

Using the support operator method, the adjoint gradient operator ($\overline{\mathbf{G}}_{\mathbf{CC}\rightarrow\mathbf{FC}}$) must be constructed as the negative conjugate of the divergence operators. The adjoint discrete gradient operator must map between vector spaces in a reverse of the discrete divergence operator.[116,117] The discrete gradient operator maps from the cell centered vector space (**CC**) to the face centered vector space (**FC**). The construction of the paired support operators enforces the properties and identities of the vector calculus operations involved.[88,116] Equation B.8 describes the relationship between these paired operators and is based on integration by parts from the Gauss-Green Divergence Theorem. Notice, the RHS of this relationship covers directly including boundary conditions into the discretization and will be discussed later in Sections B.5 and C.3.[88,146]

$$\int_{\mathscr{V}} \overline{\mathbf{G}}_{CC\rightarrow FC}\left(P\right)\cdot\vec{u}\,d\mathscr{V}+\int_{\mathscr{V}} P\,\mathbf{D}\left(\vec{u}\right)\,d\mathscr{V}=\oint_{\mathscr{S}} P\left(\vec{u}\cdot\hat{n}\right)\,d\mathscr{S} \tag{B.8}$$

For any given cells within the domain, the volume integral must apply discretely, so for grid locations that are not bordering the domain Equations B.11 and B.10 apply.

$$\int_{\mathscr{V}} \overline{\mathbf{G}}\left(P\right)\cdot\vec{u}\,d\mathscr{V}=-\int_{\mathscr{V}} P\,\mathbf{D}\left(\vec{u}\right)\,d\mathscr{V} \tag{B.9}$$

$$\left\langle\overline{\mathbf{G}}\left(P\right),\vec{u}\right\rangle_{\mathbf{FC}}=-\left\langle\overline{P},\mathbf{D}\left(\vec{u}\right)\right\rangle_{\mathbf{CC}} \tag{B.10}$$

The inner product is a generalized dot product that measures the magnitude of the inner space between the contributing terms. As a magnitude, a complex conjugate must be used on each side to ensure that it continues to work with the complex valued perturbed flow variables. One of the scalars or vectors in the inner product space is selected to be the complex conjugate, and the other term must be conjugate for the different inner product space. The gradient operator and the inner product relationship is developed by selecting an arbitrary internal cell (i,k) and collecting all contributions to that cell's degrees of freedom by including the **FC** vector space contributions from neighboring cells. As a gradient, the neighboring cells in each coordinate direction will contribute to the terms that must equal the divergence in our arbitrarily chosen **CC** vector space cell of i,k.[91] Notice that the velocities are shown unperturbed and the circumferential derivative is given as an

operator, otherwise it is impossible to directly equate the operators for divergence and gradient as the circumferential derivative operator results only in first order values for the derivative of θ. Similarly, the equations are maintained in their un-expanded form without any higher order ε terms removed to maintain the possibility of equating the operators. This means that the operators will not be perfectly adjoint in the long run, but the error should be no worse than that included inherently in the perturbation method.

$$\begin{aligned}\left\langle \overline{P}, \mathbf{D}\left(\vec{u}\right)\right\rangle_{\mathbf{CC(i,k)}} = \Bigg\langle \overline{P_{i,k}}\left(\chi_i + \varepsilon\left[R_S - \chi_i\right]\right)\Delta\chi_i\left(1-\varepsilon\right)\Delta\theta\Delta z_k \Bigg\{ \\ \left[\frac{1}{\chi_i} - \varepsilon\frac{\left(R_S-\chi_i\right)}{\chi_i^2}\right]\left(1+\varepsilon\right)\frac{\left[\chi_\ell + \varepsilon\left(R_S-\chi_\ell\right)\right]\left[u^0_{\ell,k} + \varepsilon u^1_{\ell,k}\right]}{\Delta\chi_i} \\ - \left[\frac{1}{\chi_i} - \varepsilon\frac{\left(R_S-\chi_i\right)}{\chi_i^2}\right]\left(1+\varepsilon\right)\frac{\left[\chi_{\ell-1} + \varepsilon\left(R_S-\chi_{\ell-1}\right)\right]\left[u^0_{\ell-1,k} + \varepsilon u^1_{\ell-1,k}\right]}{\Delta\chi_i} \\ + \left[\frac{1}{\chi_i} - \varepsilon\frac{\left(R_S-\chi_i\right)}{\chi_i^2}\right]\left[\imath\varepsilon v^1_{i,k} + 2\imath\varepsilon\left(R_S-\chi\right)\frac{v^0_{i+1,k} - v^0_{i-1,k}}{\Delta\chi_{i+1} + 2\Delta\chi_i + \Delta\chi_{i-1}}\right] \\ + \frac{w^0_{i,n} - w^0_{i,n-1}}{\Delta z_k} + \varepsilon\frac{w^1_{i,n} - w^1_{i,n-1}}{\Delta z_k}\Bigg\}\Bigg\rangle_{\mathbf{CC(i,k)}}\end{aligned} \tag{B.11}$$

Begin with radial terms only from the Divergence inner product for cells (i) and (i+1), with extra Δ's canceled as appropriate because they will be in the conjugate gradient inner product also. The product of $\left(1-\varepsilon\right)\left(1+\varepsilon\right)$ can be left out at this step as it results in $\left(1+\varepsilon^2 h^2\right)$ and the squared perturbation parameters are dropped.

$$
\begin{aligned}
&\left\langle \overline{P}\,\mathbf{D}\left(\vec{u}\right)\right\rangle_{\mathbf{CC(i,k)}} + \left\langle \overline{P}\,\mathbf{D}\left(\vec{u}\right)\right\rangle_{\mathbf{CC(i+1,k)}} = \\
&\qquad \overline{P_{i,k}}\left[\chi_i + \varepsilon\left(R_S - \chi_i\right)\right]\Delta\chi_i \Bigg\{ \\
&\qquad \left[\frac{1}{\chi_i} - \varepsilon\frac{\left(R_S - \chi_i\right)}{\chi_i^2}\right](1+\varepsilon)\,\frac{\left[\chi_\ell + \varepsilon\left(R_S - \chi_\ell\right)\right]u_{\ell,k}}{\Delta\chi_i} \\
&\qquad - \left[\frac{1}{\chi_i} - \varepsilon\frac{\left(R_S - \chi_i\right)}{\chi_i^2}\right](1+\varepsilon)\,\frac{\left[\chi_{\ell-1} + \varepsilon\left(R_S - \chi_{\ell-1}\right)\right]u_{\ell-1,k}}{\Delta\chi_i}\Bigg\} \\
&\qquad + \overline{P_{i+1,k}}\left[\chi_{i+1} + \varepsilon\left(R_S - \chi_{i+1}\right)\right]\Delta\chi_{i+1} \Bigg\{ \\
&\qquad \left[\frac{1}{\chi_{i+1}} - \varepsilon\frac{\left(R_S - \chi_{i+1}\right)}{\chi_{i+1}^2}\right](1+\varepsilon)\,\frac{\left[\chi_{\ell+1} + \varepsilon\left(R_S - \chi_{\ell+1}\right)\right]u_{\ell+1,k}}{\Delta\chi_{i+1}} \\
&\qquad - \left[\frac{1}{\chi_{i+1}} - \varepsilon\frac{\left(R_S - \chi_{i+1}\right)}{\chi_{i+1}^2}\right](1+\varepsilon)\,\frac{\left[\chi_\ell + \varepsilon\left(R_S - \chi_\ell\right)\right]u_{\ell,k}}{\Delta\chi_{i+1}}\Bigg\}
\end{aligned}
\tag{B.12}
$$

Collect $u_{\ell,k}$ terms in the gradient inner product space to match with the divergence terms.

$$
\begin{aligned}
\left(-\left\langle \overline{\mathbf{G}}\left(P\right)\cdot\vec{u}\right\rangle_{\mathbf{FC,cell(i,k)}}\right)_{u_{\ell,k}} &= \left(\left\langle \overline{P}\,\mathbf{D}\left(\vec{u}\right)\right\rangle_{\mathbf{CC(i,k)}} + \left\langle \overline{P}\,\mathbf{D}\left(\vec{u}\right)\right\rangle_{\mathbf{CC(i+1,k)}}\right)_{u_{\ell,k}} = \\
&\qquad \overline{P_{i,k}}\left[\chi_i + \varepsilon\left(R_S - \chi_i\right)\right]\Delta\chi_i\,(1+\varepsilon)\Bigg\{ \\
&\qquad \left[\frac{1}{\chi_i} - \varepsilon\frac{\left(R_S - \chi_i\right)}{\chi_i^2}\right]\frac{\left[\chi_\ell + \varepsilon\left(R_S - \chi_\ell\right)\right]u_{\ell,k}}{\Delta\chi_i}\Bigg\} \\
&\qquad + \overline{P_{i+1,k}}\left[\chi_{i+1} + \varepsilon\left(R_S - \chi_{i+1}\right)\right]\Delta\chi_{i+1}\,(1+\varepsilon)\Bigg\{ \\
&\qquad - \left[\frac{1}{\chi_{i+1}} - \varepsilon\frac{\left(R_S - \chi_{i+1}\right)}{\chi_{i+1}^2}\right]\frac{\left[\chi_\ell + \varepsilon\left(R_S - \chi_\ell\right)\right]u_{\ell,k}}{\Delta\chi_{i+1}}\Bigg\}
\end{aligned}
\tag{B.13}
$$

$$
\begin{aligned}
\left(-\left\langle \overline{\mathbf{G}}\left(P\right)\cdot\vec{u}\right\rangle_{\mathbf{FC,cell(i,k)}}\right)_{u_{\ell,k}} &= -\frac{\Delta\chi_i}{2}\left\{\left[\chi_\ell + \varepsilon\left(R_S - \chi_\ell\right)\right]u_{\ell,k}\overline{\mathbf{G}_{\mathbf{CC}\to\mathbf{FC}}\chi}P_{i,k}\right\} \\
&\qquad - \frac{\Delta\chi_{i+1}}{2}\left\{\left[\chi_\ell + \varepsilon\left(R_S - \chi_\ell\right)\right]u_{\ell,k}\overline{\mathbf{G}_{\mathbf{CC}\to\mathbf{FC}}\chi}P_{i,k}\right\}
\end{aligned}
\tag{B.14}
$$

$$
\begin{aligned}
-\frac{1}{2}\left(\Delta\chi_i+\Delta\chi_{i+1}\right)\Big\{&\cancel{\left[\chi_\ell+\varepsilon\left(R_S-\chi_\ell\right)\right]}\cancel{u_{\ell,k}}\overline{\mathbf{G}_{\mathbf{CC}\rightarrow\mathbf{FC}}}_{\chi}P_{i,k}\Big\}=\\
&\overline{P_{i,k}}\left[\chi_i+\varepsilon\left(R_S-\chi_i\right)\right]\cancel{\Delta\chi_i}\left(1+\varepsilon\right)\Bigg\{\\
&\left[\frac{1}{\chi_i}-\varepsilon\frac{\left(R_S-\chi_i\right)}{\chi_i^2}\right]\frac{\cancel{\left[\chi_\ell+\varepsilon\left(R_S-\chi_\ell\right)\right]}\cancel{u_{\ell,k}}}{\cancel{\Delta\chi_i}}\Bigg\}\\
&+\overline{P_{i+1,k}}\left[\chi_{i+1}+\varepsilon\left(R_S-\chi_{i+1}\right)\right]\cancel{\Delta\chi_{i+1}}\left(1+\varepsilon\right)\Bigg\{\\
&-\left[\frac{1}{\chi_{i+1}}-\varepsilon\frac{\left(R_S-\chi_{i+1}\right)}{\chi_{i+1}^2}\right]\frac{\cancel{\left[\chi_\ell+\varepsilon\left(R_S-\chi_\ell\right)\right]}\cancel{u_{\ell,k}}}{\cancel{\Delta\chi_{i+1}}}\Bigg\}
\end{aligned}
\tag{B.15}
$$

$$
\begin{aligned}
\overline{\mathbf{G}}_{\chi}\left(P\right)=\frac{\partial P_{\ell,k}}{\partial\chi}=\frac{2\left(1+\varepsilon\right)}{\Delta\chi_i+\Delta\chi_{i+1}}\Bigg\{&\overline{P_{i+1,k}}\left[\chi_{i+1}+\varepsilon\left(R_S-\chi_{i+1}\right)\right]\left[\frac{1}{\chi_{i+1}}-\varepsilon\frac{\left(R_S-\chi_{i+1}\right)}{\chi_{i+1}^2}\right]\\
&-\overline{P_{i,k}}\left[\chi_i+\varepsilon\left(R_S-\chi_i\right)\right]\left[\frac{1}{\chi_i}-\varepsilon\frac{\left(R_S-\chi_i\right)}{\chi_i^2}\right]\Bigg\}
\end{aligned}
\tag{B.16}
$$

At this step the higher order ε terms are discarded to obtain the final discrete radial gradient operator. This operator is the equivalent of a standard finite difference estimation of the radial pressure derivative, but with the nodal pressure values scaled by the difference between the true radial location and the approximated inverse radial location.

$$
\begin{aligned}
\overline{\mathbf{G}}_{\chi}\left(P\right)=\frac{\partial P_{\ell,k}}{\partial\chi}=\frac{2\left(1+\varepsilon\right)}{\Delta\chi_i+\Delta\chi_{i+1}}\Bigg\{&P_{i+1,k}^0\chi_{i+1}\frac{1}{\chi_{i+1}}-P_{i,k}^0\chi_i\frac{1}{\chi_i}\\
&-\varepsilon P_{i+1,k}^0\chi_{i+1}\frac{\left(R_S-\chi_{i+1}\right)}{\chi_{i+1}^2}+\varepsilon P_{i+1,k}^0\left(R_S-\chi_{i+1}\right)\frac{1}{\chi_{i+1}}\\
&+\varepsilon P_{i,k}^0\chi_i\frac{\left(R_S-\chi_i\right)}{\chi_i^2}-\varepsilon P_{i,k}^0\left(R_S-\chi_i\right)\frac{1}{\chi_i}\\
&+\varepsilon\overline{P_{i+1,k}^1}\chi_{i+1}\frac{1}{\chi_{i+1}}-\varepsilon\overline{P_{i,k}^1}\chi_i\frac{1}{\chi_i}\Bigg\}
\end{aligned}
\tag{B.17}
$$

$$
\begin{aligned}
\overline{\mathbf{G}}_{\chi}\left(P\right)=\frac{\partial P_{\ell,k}}{\partial\chi}=\frac{2\left(1+\varepsilon\right)}{\Delta\chi_i+\Delta\chi_{i+1}}\Big\{&P_{i+1,k}^0-P_{i,k}^0\\
&-\varepsilon P_{i+1,k}^0\frac{\left(R_S-\chi_{i+1}\right)}{\chi_{i+1}}+\varepsilon P_{i+1,k}^0\frac{\left(R_S-\chi_{i+1}\right)}{\chi_{i+1}}\\
&+\varepsilon P_{i,k}^0\frac{\left(R_S-\chi_i\right)}{\chi_i}-\varepsilon P_{i,k}^0\frac{\left(R_S-\chi_i\right)}{\chi_i}\\
&+\varepsilon\overline{P_{i+1,k}^1}-\varepsilon\overline{P_{i,k}^1}\Big\}
\end{aligned}
\tag{B.18}
$$

$$
\overline{\mathbf{G}}_{\chi}\left(P\right)=\frac{\partial P_{\ell,k}}{\partial\chi}=\frac{2}{\Delta\chi_i+\Delta\chi_{i+1}}\left\{P_{i+1,k}^0-P_{i,k}^0+\varepsilon\overline{P_{i+1,k}^1}-\varepsilon\overline{P_{i,k}^1}\right\}\left(1+\varepsilon\right)
\tag{B.19}
$$

Next, perform a similar analysis for the circumferential terms of the inner product equivalence. Select cells (i-1,k), (i,k), and (i+1,k) for analysis as they all contain $v_{i,k}$ terms due to the radial derivative in $\frac{\partial}{\partial\theta}$ term. Note the truncation of higher order ε terms.

$$\begin{aligned}
&\left(\left\langle \overline{P}\,\mathbf{D}\left(\vec{u}\right)\right\rangle_{\mathbf{CC(i-1,k)}} + \left\langle \overline{P}\,\mathbf{D}\left(\vec{u}\right)\right\rangle_{\mathbf{CC(i,k)}} + \left\langle \overline{P}\,\mathbf{D}\left(\vec{u}\right)\right\rangle_{\mathbf{CC(i+1,k)}}\right)_{\theta} = \\
&\quad \overline{P_{i-1,k}}\left[\chi_{i-1} + \cancel{\varepsilon\left(R_S - \chi_{i-1}\right)}\right]\Delta\chi_{i-1}\Delta\theta\Delta z_k\left(1-\varepsilon\right)\Bigg\{ \\
&\qquad \left[\frac{1}{\chi_{i-1}} - \varepsilon\frac{\cancel{\left(R_S - \chi_{i-1}\right)}}{\chi_{i-1}^2}\right]\left[\imath\varepsilon v_{i-1,k}^1 + 2\imath\varepsilon\left(R_S-\chi\right)\frac{v_{i,k}^0 - v_{i-2,k}^0}{\Delta\chi_i + 2\Delta\chi_{i-1} + \chi_{i-2}}\right]\Bigg\} \\
&\quad + \overline{P_{i,k}}\left[\chi_i + \cancel{\varepsilon\left(R_S - \chi_i\right)}\right]\Delta\chi_i\Delta\theta\Delta z_k\left(1-\varepsilon\right)\Bigg\{ \\
&\qquad \left[\frac{1}{\chi_i} - \varepsilon\frac{\cancel{\left(R_S - \chi_i\right)}}{\chi_i^2}\right]\left[\imath\varepsilon v_{i,k}^1 + 2\imath\varepsilon\left(R_S-\chi\right)\frac{v_{i+1,k}^0 - v_{i-1,k}^0}{\Delta\chi_{i+1} + 2\Delta\chi_i + \chi_{i-1}}\right]\Bigg\} \\
&\quad + \overline{P_{i+1,k}}\left[\chi_{i+1} + \cancel{\varepsilon\left(R_S - \chi_{i+1}\right)}\right]\Delta\chi_{i+1}\Delta\theta\Delta z_k\left(1-\varepsilon\right)\Bigg\{ \\
&\qquad \left[\frac{1}{\chi_{i+1}} - \varepsilon\frac{\cancel{\left(R_S - \chi_{i+1}\right)}}{\chi_{i+1}^2}\right]\left[\imath\varepsilon v_{i+1,k}^1 + 2\imath\varepsilon\left(R_S-\chi\right)\frac{v_{i+2,k}^0 - v_{i,k}^0}{\Delta\chi_{i+2} + 2\Delta\chi_{i+1} + \chi_i}\right]\Bigg\}
\end{aligned} \tag{B.20}$$

Collect only the coefficients of $v_{i,k}$ to equate to the gradient operator inner product since the circumferential derivative is a known function of θ at any given node.

$$\begin{aligned}
\left(-\left\langle \overline{\mathbf{G}}\left(P\right)\cdot\vec{u}\right\rangle_{\mathbf{FC}}\right)_{v_{i,k}} &= \left(\left\langle \overline{P}\,\mathbf{D}\left(\vec{u}\right)\right\rangle_{\mathbf{CC(i-1,k)}} + \left\langle \overline{P}\,\mathbf{D}\left(\vec{u}\right)\right\rangle_{\mathbf{CC(i,k)}} + \left\langle \overline{P}\,\mathbf{D}\left(\vec{u}\right)\right\rangle_{\mathbf{CC(i+1,k)}}\right)_{v_{i,k}} = \\
&\quad + \overline{P_{i-1,k}}\chi_{i-1}\Delta\chi_{i-1}\Delta\theta\Delta z_k\left(1-\varepsilon\right)\Bigg\{ \\
&\qquad \frac{1}{\chi_{i-1}}\left[2\imath\varepsilon\left(R_S-\chi\right)\frac{v_{i,k}^0}{\Delta\chi_i + 2\Delta\chi_{i-1} + \chi_{i-2}}\right]\Bigg\} \\
&\quad + \overline{P_{i,k}}\chi_i\Delta\chi_i\Delta\theta\Delta z_k\left(1-\varepsilon\right)\frac{1}{\chi_i}\imath\varepsilon v_{i,k}^1 \\
&\quad - \overline{P_{i+1,k}}\chi_{i+1}\Delta\chi_{i+1}\Delta\theta\Delta z_k\left(1-\varepsilon\right)\Bigg\{ \\
&\qquad \frac{1}{\chi_{i+1}}\left[2\imath\varepsilon\left(R_S-\chi\right)\frac{v_{i,k}^0}{\Delta\chi_{i+2} + 2\Delta\chi_{i+1} + \chi_i}\right]\Bigg\}
\end{aligned} \tag{B.21}$$

$$\left(\left\langle \overline{\mathbf{G}}\left(P\right)\cdot\vec{u}\right\rangle_{\mathbf{FC,cell(i,k)}}+\left\langle \vec{\mathbf{G}}\left(P\right)\cdot\vec{u}\right\rangle_{\mathbf{FC,cell(i,j+1,k)}}\right)_{v_{i,k}}$$
$$=\frac{\Delta\chi_i\Delta\theta\Delta z_k\left(1-\varepsilon\right)}{2}\left[\chi_i+\varepsilon\left(R_S-\chi_i\right)\right]\left\{\overbrace{v_{i,k}\left(\overline{\mathbf{G}}_\theta\left(P\right)\right)_m}^{i,k}+\overbrace{v_{i,k}\left(\overline{\mathbf{G}}_\theta\left(P\right)\right)_m}^{i,j+1,k}\right\} \tag{B.22}$$

The Δ and $(1-\varepsilon)$ terms cancel.

$$\begin{aligned}&\overline{P_{i-1,k}}\chi_{i-1}\Delta\chi_{i-1}\left\{\frac{1}{\chi_{i-1}}\left[2\imath\varepsilon\left(R_S-\chi\right)\frac{v_{i,k}^0}{\Delta\chi_i+2\Delta\chi_{i-1}+\Delta\chi_{i-2}}\right]\right\}\\&+\overline{P_{i,k}}\chi_i\Delta\chi_i\frac{1}{\chi_i}\imath\varepsilon v_{i,k}^1\\&-\overline{P_{i+1,k}}\chi_{i+1}\Delta\chi_{i+1}\left\{\frac{1}{\chi_{i+1}}\left[2\imath\varepsilon\left(R_S-\chi\right)\frac{v_{i,k}^0}{\Delta\chi_{i+2}+2\Delta\chi_{i+1}+\Delta\chi_i}\right]\right\}\\&=-\Delta\chi_i\left[\chi_i+\cancel{\varepsilon\left(R_S-\chi_i\right)}\right]v_{i,k}\overline{\mathbf{G}}_\theta\left(P\right)\end{aligned} \tag{B.23}$$

$$\begin{aligned}&-\frac{\cancel{\chi_{i-1}}\Delta\chi_{i-1}}{\chi_i\Delta\chi_i}\left\{\frac{1}{\cancel{\chi_{i-1}}}\left[2\imath\varepsilon\left(R_S-\chi\right)\frac{\overline{P_{i-1,k}}^0}{\Delta\chi_i+2\Delta\chi_{i-1}+\Delta\chi_{i-2}}\right]\right\}\\&-\frac{\chi_i\Delta\cancel{\chi_i}}{\cancel{\chi_i}\Delta\chi_i}\frac{1}{\chi_i}\imath\varepsilon\overline{P_{i,k}}^1\\&+\frac{\cancel{\chi_{i+1}}\Delta\chi_{i+1}}{\chi_i\Delta\chi_i}\left\{\frac{1}{\cancel{\chi_{i+1}}}\left[2\imath\varepsilon\left(R_S-\chi\right)\frac{\overline{P_{i+1,k}}^0}{\Delta\chi_{i+2}+2\Delta\chi_{i+1}+\Delta\chi_i}\right]\right\}\\&=\overline{\mathbf{G}}_\theta\left(P\right)\end{aligned} \tag{B.24}$$

The obtained circumferential scalar gradient operator, Equation B.24, is maintained with a nominal circumferential derivative of the first order pressure while the additional chain rule term is defined with a non-standard finite difference where nodal zeroth-order pressure values are scaled by the difference between the true radial location and the approximated inverse radial location along with a differential area that includes the surrounding cells. Note that the derived gradient operator is the conjugate and the pressure terms used at this step are complex conjugates of pressure, only relevant for the first order pressure terms.

$$\begin{aligned}\overline{\mathbf{G}}_\theta\left(P\right)=&-\frac{\imath\varepsilon}{\chi_i}\overline{P_{i,k}^1}+2\imath\varepsilon\frac{\Delta\chi_{i+1}}{\Delta\chi_i}\frac{\left(R_S-\chi_{i+1}\right)}{\chi_i}\frac{P_{i+1,k}^0}{\Delta\chi_{i+2}+2\Delta\chi_{i+1}+\Delta\chi_i}\\&-2\imath\varepsilon\frac{\Delta\chi_{i-1}}{\Delta\chi_i}\frac{\left(R_S-\chi_{i-1}\right)}{\chi_i}\frac{P_{i-1,k}^0}{\Delta\chi_i+2\Delta\chi_{i-1}+\Delta\chi_{i-2}}\end{aligned} \tag{B.25}$$

As previously discussed, the axial component of gradient is unaffected by the variable change except the first order term being a complex conjugate. Thus the whole discrete support operator for gradient, Equation B.27 is obtained by combining Equations B.17, B.25, and B.26. It is then split into zeroth and first order perturbation components as with the divergence operator.

$$\begin{aligned}\overline{\mathbf{G}}_{\mathbf{z}}(P) &= 2\frac{P_{i,k+1}-P_{i,k}}{\Delta z_k+\Delta z_{k+1}} \\ &= 2\frac{P^0_{i,k+1}-P^0_{i,k}}{\Delta z_k+\Delta z_{k+1}} + 2\varepsilon\frac{\overline{P^1_{i+1,k}}-\overline{P^1_{i,k}}}{\Delta z_k+\Delta z_{k+1}}\end{aligned} \tag{B.26}$$

$$\begin{bmatrix}\left(\overline{\mathbf{G}}_{\chi}P\right)_{\ell,k}\\ \left(\overline{\mathbf{G}}_{\theta}P\right)_{i,k}\\ \left(\overline{\mathbf{G}}_{\mathbf{z}}P\right)_{i,n}\end{bmatrix} = \begin{bmatrix} 2\frac{P^0_{i+1,k}-P^0_{i,k}}{\Delta\chi_i+\Delta\chi_{i+1}}(1+\varepsilon) + 2\varepsilon\frac{\overline{P^1_{i+1,k}}-\overline{P^1_{i,k}}}{\Delta\chi_i+\Delta\chi_{i+1}} \\ \varepsilon\frac{-P^I_{i,k}-\imath P^R_{i,k}}{\chi_i}+2\imath\varepsilon\frac{\Delta\chi_{i+1}}{\Delta\chi_i}\frac{(R_S-\chi_{i+1})}{\chi_i}\frac{P^0_{i+1,k}}{\Delta\chi_{i+2}+2\Delta\chi_{i+1}+\Delta\chi_i} \\ \quad -2\imath\varepsilon\frac{\Delta\chi_{i-1}}{\Delta\chi_i}\frac{(R_S-\chi_{i-1})}{\chi_i}\frac{P^0_{i-1,k}}{\Delta\chi_i+2\Delta\chi_{i-1}+\Delta\chi_{i-2}} \\ 2\frac{P^0_{i,k+1}-P^0_{i,k}}{\Delta z_k+\Delta z_{k+1}}+2\varepsilon\frac{\overline{P^1_{i+1,k}}-\overline{P^1_{i,k}}}{\Delta z_k+\Delta z_{k+1}}\end{bmatrix} \tag{B.27}$$

B.4.1 Discrete Conjugate Gradient Operator, Zeroth Order: $\overline{\mathbf{G}}^0(P)$

$$\begin{bmatrix}\left(\mathbf{G}_{\chi}P\right)^0_{\ell,k}\\ \left(\mathbf{G}_{\theta}P\right)^0_{i,k}\\ \left(\mathbf{G}_{z}P\right)^0_{i,n}\end{bmatrix} = \begin{bmatrix}2\frac{P^0_{i+1,k}-P^0_{i,k}}{\Delta\chi_i+\Delta\chi_{i+1}}\\ 0\\ 2\frac{P^0_{i,k+1}-P^0_{i,k}}{\Delta z_k+\Delta z_{k+1}}\end{bmatrix} \tag{B.28}$$

B.4.2 Discrete Conjugate Gradient Operator, First Order: $\overline{\mathbf{G}}^1(P)$

$$\begin{bmatrix}\left(\overline{\mathbf{G}}_{\chi}P\right)^1_{\ell,k}\\ \left(\overline{\mathbf{G}}_{\theta}P\right)^1_{i,k}\\ \left(\overline{\mathbf{G}}_{\mathbf{z}}P\right)^1_{i,n}\end{bmatrix} = \begin{bmatrix} 2\frac{P^0_{i+1,k}-P^0_{i,k}}{\Delta\chi_i+\Delta\chi_{i+1}}+2\frac{\overline{P^1_{i+1,k}}-\overline{P^1_{i,k}}}{\Delta\chi_i+\Delta\chi_{i+1}} \\ \frac{-P^I_{i,k}-\imath P^R_{i,k}}{\chi_i}+2\imath\frac{\Delta\chi_{i+1}}{\Delta\chi_i}\frac{(R_S-\chi_{i+1})}{\chi_i}\frac{P^0_{i+1,k}}{\Delta\chi_{i+2}+2\Delta\chi_{i+1}+\Delta\chi_i} \\ \quad -2\imath\frac{\Delta\chi_{i-1}}{\Delta\chi_i}\frac{(R_S-\chi_{i-1})}{\chi_i}\frac{P^0_{i-1,k}}{\Delta\chi_i+2\Delta\chi_{i-1}+\Delta\chi_{i-2}} \\ 2\frac{\overline{P^1_{i+1,k}}-\overline{P^1_{i,k}}}{\Delta z_k+\Delta z_{k+1}}\end{bmatrix} \tag{B.29}$$

Discrete Conjugate Gradient Operator, Real First Order: $\overline{\mathbf{G}}^{R}\,(P)$

$$\begin{bmatrix} \left(\overline{\mathbf{G}}_{\chi}P\right)^{R}_{\ell,k} \\ \left(\overline{\mathbf{G}}_{\theta}P\right)^{R}_{i,k} \\ \left(\overline{\mathbf{G}}_{\mathbf{z}}P\right)^{R}_{i,n} \end{bmatrix} = \begin{bmatrix} 2\dfrac{P^{0}_{i+1,k}-P^{0}_{i,k}}{\Delta\chi_i+\Delta\chi_{i+1}} + 2\dfrac{P^{R}_{i+1,k}-P^{R}_{i,k}}{\Delta\chi_i+\Delta\chi_{i+1}} \\ -\dfrac{P^{I}_{i,k}}{\chi_i} \\ 2\frac{P^{R}_{i+1,k}-P^{R}_{i,k}}{\Delta z_k+\Delta z_{k+1}} \end{bmatrix} \tag{B.30}$$

Discrete Conjugate Gradient Operator, Imaginary First Order: $\overline{\mathbf{G}}^{I}\,(P)$

$$\begin{bmatrix} \left(\overline{\mathbf{G}}_{\chi}P\right)^{I}_{\ell,k} \\ \left(\overline{\mathbf{G}}_{\theta}P\right)^{I}_{i,k} \\ \left(\overline{\mathbf{G}}_{\mathbf{z}}P\right)^{I}_{i,n} \end{bmatrix} = \begin{bmatrix} -2\dfrac{P^{I}_{i+1,k}-P^{I}_{i,k}}{\Delta\chi_i+\Delta\chi_{i+1}} \\ -\dfrac{P^{R}_{i,k}}{\chi_i} + 2\dfrac{\Delta\chi_{i+1}}{\Delta\chi_i}\dfrac{(R_S-\chi_{i+1})}{\chi_i}\dfrac{P^{0}_{i+1,k}}{\Delta\chi_{i+2}+2\Delta\chi_{i+1}+\Delta\chi_i} \\ \qquad -2\dfrac{\Delta\chi_{i-1}}{\Delta\chi_i}\dfrac{(R_S-\chi_{i-1})}{\chi_i}\dfrac{P^{0}_{i-1,k}}{\Delta\chi_i+2\Delta\chi_{i-1}+\Delta\chi_{i-2}} \\ -2\frac{P^{I}_{i+1,k}-P^{I}_{i,k}}{\Delta z_k+\Delta z_{k+1}} \end{bmatrix} \tag{B.31}$$

B.5 Boundary Conditions from Conjugate Gradient Operator

Currently the mimetic discretizations of divergence and gradient operators, establilshed in Seciton B.4, use data that is entirely within the domain or on the domain's boundary, except for the circumferential gradient of pressure. The circumferential momentum equiation requires a pressure gradient calculation at every cell location in the domain causing i+1 adn i-1 indices to extend out of the domain on the rotor and stator boundaries. This means that the rotor and stator boundaries require their ghost cells to have defined pressures. This pressure value is not obvious, but a value consistent with the physics of the problem and the discretization can be obtained through application of standard no-penetration and no-slip wall boundary conditions.

To obtain a consistent ghost cell value for pressure, the conjugate gradient operator can be used to determine the radial gradient at the $\ell = 0$ $\left(i = \frac{1}{2}\right)$ and $\ell = N_{\chi}$ $\left(i = N_{\chi} + \frac{1}{2}\right)$. If this gradient is set equal to zero, the values for the ghost cells can be directly determined using Equations B.32 and B.33.

$$\begin{gathered}\overline{\mathbf{G}}_{\chi}\left(P\right)_{\frac{1}{2},k}=0=\frac{2}{\Delta\chi_0+\Delta\chi_{i+1}}\left\{P^0_{1,k}-P^0_{0,k}+\varepsilon P^1_{1,k}-\varepsilon P^1_{0,k}\right\}\\ P^0_{0,k}+\varepsilon P^1_{0,k}=P^0_{1,k}+\varepsilon P^1_{1,k}\end{gathered} \tag{B.32}$$

$$\begin{gathered}\overline{\mathbf{G}}_{\chi}\left(P\right)_{N_\chi+\frac{1}{2},k}=0=\frac{2}{\Delta\chi_i+\Delta\chi_{i+1}}\left\{P^0_{N_\chi+1,k}-P^0_{N_\chi,k}+\varepsilon P^1_{N_\chi+1,k}-\varepsilon P^1_{N_\chi,k}\right\}\\ P^0_{N_\chi+1,k}+\varepsilon P^1_{N_\chi+1,k}=P^0_{N_\chi,k}+\varepsilon P^1_{N_\chi,k}\end{gathered} \tag{B.33}$$

By extending the divergence operator to the boundary using the identity given by Equation B.8, the value of the pressure on the boundary can be calculated from the values within the domain. This is not strictly necessary, since the radial gradient of pressure along the radial boundaries is zero, the value on the boundary is approximately equal to the value of the first cell center within the domain.

Appendix C

Discrete Mimetic Operator Derivation: Curl & Adjoint Curl

Curl is a vector calculus operator used to calculate the rate of rotation in a vector field. Two sequentially applied curl operators, are related by vector identity to the laplacian. This work employs the curl operator and its adjoint discrete operator to calculate the laplacian of the velocity vector field and thus the flow diffusion. This means that the curl and adjoint curl operators must respectively end and start in the face centered $(\mathbf{FC})$ so that they can be used in the Navier-Stokes momentum equations for each coordinate direction. As the curl vector operator, results in a vector as well, the intermediate vector space must have individual locations for each vector component like the $\mathbf{FC}$. This transitional vector space that the curl operators map to and from is located on the edge center, $(\mathbf{FC})$ of each positive cell face. The primary operator curl, $\mathbf{C}(\vec{u})$, is chosen to translate from the $\mathbf{EC}$ vector space to the $\mathbf{FC}$ vector space based on the equivalent similar work done by Oud[91] and the review of Lipnikov.[88] The adjoint curl, $\overline{\mathbf{C}}(\vec{u})$, performs the translation in reverse from $\mathbf{FC}$ to $\mathbf{EC}$ and represents the vorticity vector field of the fluid flow.

C.1 Curl Operator, $\mathbf{C}_{\mathbf{EC}\rightarrow\mathbf{FC}}(\vec{\omega}) = \nabla \times \vec{\omega}$

The coordinate invariant definition of curl in a continuous vector field is given by Equation C.1.[88,115,174] The left surface integral is performed over the positive outward normal face of a given cell in each axial direction and the right line integral is performed around the perimeter of each positive face.

So, $\hat{t}$ is a unit vector directed tangentially along the face perimeter in a standard right hand rule orientation. $\vec{\omega}$ is the $\mathbf{EC}$ vector space projection of the flow vorticity vector. Operating on the $\mathbf{EC}$ vector space, this definition is particular to the primary discrete curl operator.

$$\begin{aligned} \int_S \mathbf{C}_{\mathbf{EC}\to\mathbf{FC}}\left(\vec{\omega}_{\mathbf{EC}}\right)\cdot\hat{n}dS &= \oint_\ell \vec{\omega}_{\mathbf{EC}}\cdot\hat{t}d\ell \\ \left\langle\vec{n},\mathbf{C}_{\mathbf{EC}\to\mathbf{FC}}\left(\vec{\omega}_{\mathbf{EC}}\right)\right\rangle &= \lim_{S\to 0}\frac{1}{S}\oint_S\left\langle\vec{\omega}_{\mathbf{EC}},\hat{t}\right\rangle d\ell \end{aligned} \tag{C.1}$$

The discrete curl vector operator is formed by discrete integration at each $\mathbf{EC}$ location on the outward normal faces defined around $\mathbf{FC}$. Oud[91] defines this discrete operator in cylindrical coordinates using Equation C.2. For convenience, the discrete circumferential derivatives from Oud's equations are replaced in advance by the circumferential partial derivative as this is known due to the geometric perturbation and assumed perturbation form of each variable's solution. Note carefully the different usage of r_ℓ and r_i depending on the radial location of the vector component in the $\mathbf{FC}$ vector space.

$$\mathbf{C}_{\mathbf{EC}\to\mathbf{FC}}\left(\vec{\omega}_{\mathbf{EC}}\right)=\nabla\times\vec{\omega}=\begin{bmatrix}C\left(\vec{\omega}\right)_{\ell,k}\\ C\left(\vec{\omega}\right)_{i,k}\\ C\left(\vec{\omega}\right)_{i,n}\end{bmatrix}=\begin{bmatrix}\frac{1}{r}\frac{\partial\zeta}{\partial\theta}-\frac{\partial\omega}{\partial z}\\ \frac{\partial\eta}{\partial z}-\frac{\partial\zeta}{\partial r}\\ \frac{1}{r}\left[\frac{\partial(r\omega)}{\partial r}-\frac{\partial\eta}{\partial\theta}\right]\end{bmatrix}=\begin{bmatrix}\frac{1}{r_\ell}\left(\frac{\partial\zeta}{\partial\theta}\right)_{\ell,k}-\frac{\omega_{\ell,n}-\omega_{\ell,n-1}}{\Delta z_k}\\ \frac{\eta_{i,n}-\eta_{i,n-1}}{\Delta z_k}-\frac{\zeta_{\ell,k}-\zeta_{\ell-1,k}}{\Delta r_i}\\ \frac{1}{r_i}\left[\frac{r_\ell\omega_{\ell,n}-r_{\ell-1}\omega_{\ell-1,n}}{\Delta r_i}-\left(\frac{\partial\eta}{\partial\theta}\right)_{i,n}\right]\end{bmatrix} \tag{C.2}$$

Equation C.2 is adapted for this work by translation to the geometrically perturbed coordinate system through substitution and the chain rule resulting in Equation C.3. As with the discrete divergence operator, inverse radii are approximated through Taylor series to avoid perturbation parameters in the denominator. Equation C.3 is the form that will be needed to construct the adjoint support operator for curl.

$$\mathbf{C_{EC\rightarrow FC}}\left(\vec{\omega}\right) = \begin{bmatrix} C\left(\vec{\omega}\right)_{\ell,k} \\ C\left(\vec{\omega}\right)_{i,k} \\ C\left(\vec{\omega}\right)_{i,n} \end{bmatrix} = \begin{bmatrix} \left[\frac{1}{\chi_\ell} - \varepsilon\frac{(R_S-\chi_\ell)}{\chi_\ell^2}\right]\left[i\varepsilon\zeta^1_{\ell,k} + i\varepsilon\left(R_S-\chi_\ell\right)\frac{\zeta^0_{\ell+1,k}-\zeta^0_{\ell-1,k}}{\Delta\chi_i+\Delta\chi_{i+1}}\right] \\ \qquad\qquad - \frac{\omega_{\ell,n}-\omega_{\ell,n-1}}{\Delta z_k} \\ \hdashline \frac{\eta_{i,n}-\eta_{i,n-1}}{\Delta z_k} - \frac{\zeta_{\ell,k}-\zeta_{\ell-1,k}}{\Delta\chi_i}\frac{1}{1-\varepsilon} \\ \hdashline \left[\frac{1}{\chi_i} - \varepsilon\frac{(R_S-\chi_i)}{\chi_i^2}\right]\Bigg\{ \\ \quad \frac{\left[\chi_\ell+\varepsilon(R_S-\chi_\ell)\right]\omega_{\ell,n}}{\Delta\chi_i}(1+\varepsilon) \\ \quad - \frac{\left[\chi_{\ell-1}+\varepsilon(R_S-\chi_{\ell-1})\right]\omega_{\ell-1,n}}{\Delta\chi_i}(1+\varepsilon) \\ \quad - \left[i\varepsilon\eta^1_{i,n} + 2i\varepsilon\left(R_S-\chi_i\right)\frac{\eta^0_{i+1,n}-\eta^0_{i-1,n}}{\Delta\chi_{i-1}+2\Delta\chi_i+\Delta\chi_{i+1}}\right]\Bigg\} \end{bmatrix} \tag{C.3}$$

To complete the primary operator, before moving on to the support operator, the perturbed flow variables are substituted and higher order powers of the perturbation variables are discarded to result in Equation C.4. This equation is then split into its zeroth and first order perturbation terms for usage in the numerical code.

$$\mathbf{C_{EC\rightarrow FC}}\left(\vec{\omega}\right) = \begin{bmatrix} C\left(\vec{\omega}\right)_{\ell,k} \\ C\left(\vec{\omega}\right)_{i,k} \\ C\left(\vec{\omega}\right)_{i,n} \end{bmatrix} = \begin{bmatrix} \left[\frac{1}{\chi_\ell} - \varepsilon\frac{(R_S-\chi_\ell)}{\chi_\ell^2}\right]\left[i\varepsilon\zeta^1_{\ell,k} + i\varepsilon\left(R_S-\chi_\ell\right)\frac{\zeta^0_{\ell+1,k}-\zeta^0_{\ell-1,k}}{\Delta\chi_i+\Delta\chi_{i+1}}\right] \\ \qquad\qquad - \frac{\omega^0_{\ell,n}-\omega^0_{\ell,n-1}}{\Delta z_k} - \varepsilon\frac{\omega^1_{\ell,n}-\omega^1_{\ell,n-1}}{\Delta z_k} \\ \hdashline \frac{\eta^0_{i,n}-\eta^0_{i,n-1}}{\Delta z_k} + \varepsilon\frac{\eta^1_{i,n}-\eta^1_{i,n-1}}{\Delta z_k} \\ \quad - \left(\frac{\zeta^0_{\ell,k}-\zeta^0_{\ell-1,k}}{\Delta\chi_i} + \varepsilon\frac{\zeta^1_{\ell,k}-\zeta^1_{\ell-1,k}}{\Delta\chi_i}\right)(1+\varepsilon) \\ \hdashline \left[\frac{1}{\chi_i} - \varepsilon\frac{(R_S-\chi_i)}{\chi_i^2}\right]\Bigg\{ \\ \quad \frac{\left[\chi_\ell+\varepsilon(R_S-\chi_\ell)\right]\left[\omega^0_{\ell,n}+\varepsilon\omega^1_{\ell,n}\right]}{\Delta\chi_i}(1+\varepsilon) \\ \quad - \frac{\left[\chi_{\ell-1}+\varepsilon(R_S-\chi_{\ell-1})\right]\left[\omega^0_{\ell-1,n}+\varepsilon\omega^1_{\ell-1,n}\right]}{\Delta\chi_i}(1+\varepsilon) \\ \quad - \left[i\varepsilon\eta^1_{i,n} + 2i\varepsilon\left(R_S-\chi\right)\frac{\eta^0_{i+1,n}-\eta^0_{i-1,n}}{\Delta\chi_{i-1}+2\Delta\chi_i+\Delta\chi_{i+1}}\right]\Bigg\} \end{bmatrix} \tag{C.4}$$

C.1.1 Discrete Primary Curl Operator, Zeroth Order: $\mathbf{C}^0\left(\vec{\omega}\right)$

$$\mathbf{C}^0_{\mathbf{EC}\rightarrow\mathbf{FC}}\left(\vec{\omega}\right) = \begin{bmatrix} C\left(\vec{\omega}\right)^0_{\ell,k} \\ C\left(\vec{\omega}\right)^0_{i,k} \\ C\left(\vec{\omega}\right)^0_{i,n} \end{bmatrix} = \begin{bmatrix} -\dfrac{\omega^0_{\ell,n}-\omega^0_{\ell,n-1}}{\Delta z_k} \\ \dfrac{\eta^0_{i,n}-\eta^0_{i,n-1}}{\Delta z_k} - \dfrac{\zeta^0_{\ell,k}-\zeta^0_{\ell-1,k}}{\Delta\chi_i} \\ \dfrac{1}{\chi_i}\dfrac{\chi_\ell\omega^0_{\ell,n}-\chi_{\ell-1}\omega^0_{\ell-1,n}}{\Delta\chi_i} \end{bmatrix} \tag{C.5}$$

C.1.2 Discrete Primary Curl Operator, First Order: $\mathbf{C}^1\left(\vec{\omega}\right)$

$$\mathbf{C}^1_{\mathbf{EC}\rightarrow\mathbf{FC}}\left(\vec{\omega}\right) = \begin{bmatrix} C\left(\vec{\omega}\right)^1_{\ell,k} \\ C\left(\vec{\omega}\right)^1_{i,k} \\ C\left(\vec{\omega}\right)^1_{i,n} \end{bmatrix} = \begin{bmatrix} \dfrac{1}{\chi_\ell}\left[\imath\zeta^1_{\ell,k}+\imath\left(R_S-\chi_\ell\right)\dfrac{\zeta^0_{\ell+1,k}-\zeta^0_{\ell-1,k}}{\Delta\chi_i+\Delta\chi_{i+1}}\right] - \dfrac{\omega^1_{\ell,n}-\omega^1_{\ell,n-1}}{\Delta z_k} \\ \dfrac{\eta^1_{i,n}-\eta^1_{i,n-1}}{\Delta z_k} - \left(\dfrac{\zeta^0_{\ell,k}-\zeta^0_{\ell-1,k}}{\Delta\chi_i}+\dfrac{\zeta^1_{\ell,k}-\zeta^1_{\ell-1,k}}{\Delta\chi_i}\right) \\ \begin{aligned} &\frac{1}{\chi_i}\frac{\chi_\ell\omega^0_{\ell,n}-\chi_{\ell-1}\omega^0_{\ell-1,n}}{\Delta\chi_i} \\ &-\frac{(R_S-\cancel{\chi_i})}{\chi_i^2}\frac{\chi_\ell\omega^0_{\ell,n}-\chi_{\ell-1}\omega^0_{\ell-1,n}}{\Delta\chi_i} \\ &+\frac{1}{\chi_i}\frac{(R_S-\cancel{\chi_\ell})\omega^0_{\ell,n}-(R_S-\cancel{\chi_{\ell-1}})\omega^0_{\ell-1,n}}{\Delta\chi_i} \\ &+\frac{1}{\chi_i}\frac{\chi_\ell\omega^1_{\ell,n}-\chi_{\ell-1}\varepsilon\omega^1_{\ell-1,n}}{\Delta\chi_i} \\ &-\frac{1}{\chi_i}\left[\imath\eta^1_{i,n}+2\imath\left(R_S-\chi\right)\frac{\eta^0_{i+1,n}-\eta^0_{i-1,n}}{\Delta\chi_{i-1}+2\Delta\chi_i+\Delta\chi_{i+1}}\right] \end{aligned} \end{bmatrix} \tag{C.6}$$

$$\mathbf{C}^1_{\mathbf{EC}\rightarrow\mathbf{FC}} = \begin{bmatrix} C\left(\vec{\omega}\right)^1_{\ell,k} \\ C\left(\vec{\omega}\right)^1_{i,k} \\ C\left(\vec{\omega}\right)^1_{i,n} \end{bmatrix} = \begin{bmatrix} \dfrac{1}{\chi_\ell}\left[\imath\zeta^1_{\ell,k}+\imath\left(R_S-\chi_\ell\right)\dfrac{\zeta^0_{\ell+1,k}-\zeta^0_{\ell-1,k}}{\Delta\chi_i+\Delta\chi_{i+1}}\right] - \dfrac{\omega^1_{\ell,n}-\omega^1_{\ell,n-1}}{\Delta z_k} \\ \dfrac{\eta^1_{i,n}-\eta^1_{i,n-1}}{\Delta z_k} - \left(\dfrac{\zeta^0_{\ell,k}-\zeta^0_{\ell-1,k}}{\Delta\chi_i}+\dfrac{\zeta^1_{\ell,k}-\zeta^1_{\ell-1,k}}{\Delta\chi_i}\right) \\ \begin{aligned} &\frac{1}{\chi_i}\frac{\chi_\ell\omega^0_{\ell,n}-\chi_{\ell-1}\omega^0_{\ell-1,n}}{\Delta\chi_i} - \frac{R_S}{\chi_i^2}\frac{\chi_\ell\omega^0_{\ell,n}-\chi_{\ell-1}\omega^0_{\ell-1,n}}{\Delta\chi_i} \\ &+\frac{R_S}{\chi_i}\frac{\omega^0_{\ell,n}-\omega^0_{\ell-1,n}}{\Delta\chi_i}+\frac{1}{\chi_i}\frac{\chi_\ell\omega^1_{\ell,n}-\chi_{\ell-1}\omega^1_{\ell-1,n}}{\Delta\chi_i} \\ &-\frac{1}{\chi_i}\left[\imath\eta^1_{i,n}+2\imath\left(R_S-\chi\right)\frac{\eta^0_{i+1,n}-\eta^0_{i-1,n}}{\Delta\chi_{i-1}+2\Delta\chi_i+\Delta\chi_{i+1}}\right] \end{aligned} \end{bmatrix} \tag{C.7}$$

Discrete Primary Curl Operator, Real First Order: $\mathbf{C}^{R}\left(\vec{\omega}\right)$

$$\mathbf{C}^{R}_{\mathbf{EC}\rightarrow\mathbf{FC}}=\begin{bmatrix} C\left(\vec{\omega}\right)^{R}_{\ell,k} \\ C\left(\vec{\omega}\right)^{R}_{i,k} \\ C\left(\vec{\omega}\right)^{R}_{i,n} \end{bmatrix}=\begin{bmatrix} -\dfrac{1}{\chi_{\ell}}\zeta^{I}_{\ell,k}-\dfrac{\omega^{R}_{\ell,n}-\omega^{R}_{\ell,n-1}}{\Delta z_{k}} \\ \dfrac{\eta^{R}_{i,n}-\eta^{R}_{i,n-1}}{\Delta z_{k}}-\left(\dfrac{\zeta^{0}_{\ell,k}-\zeta^{0}_{\ell-1,k}}{\Delta\chi_{i}}+\dfrac{\zeta^{R}_{\ell,k}-\zeta^{R}_{\ell-1,k}}{\Delta\chi_{i}}\right) \\ \dfrac{1}{\chi_{i}}\dfrac{\chi_{\ell}\omega^{0}_{\ell,n}-\chi_{\ell-1}\omega^{0}_{\ell-1,n}}{\Delta\chi_{i}}-\dfrac{R_{S}}{\chi^{2}_{i}}\dfrac{\chi_{\ell}\omega^{0}_{\ell,n}-\chi_{\ell-1}\omega^{0}_{\ell-1,n}}{\Delta\chi_{i}} \\ \quad+\dfrac{R_{S}}{\chi_{i}}\dfrac{\omega^{0}_{\ell,n}-\omega^{0}_{\ell-1,n}}{\Delta\chi_{i}}+\dfrac{1}{\chi_{i}}\dfrac{\chi_{\ell}\omega^{R}_{\ell,n}-\chi_{\ell-1}\omega^{R}_{\ell-1,n}}{\Delta\chi_{i}}+\dfrac{1}{\chi_{i}}\eta^{I}_{i,n} \end{bmatrix} \tag{C.8}$$

Discrete Primary Curl Operator, Imaginary First Order: $\mathbf{C}^{I}\left(\vec{\omega}\right)$

$$\mathbf{C}^{I}_{\mathbf{EC}\rightarrow\mathbf{FC}}=\begin{bmatrix} C\left(\vec{\omega}\right)^{I}_{\ell,k} \\ C\left(\vec{\omega}\right)^{I}_{i,j+\frac{1}{2},k} \\ C\left(\vec{\omega}\right)^{I}_{i,n} \end{bmatrix}=\begin{bmatrix} \dfrac{1}{\chi_{\ell}}\left[\zeta^{R}_{\ell,k}+\left(R_{S}-\chi_{\ell}\right)\dfrac{\zeta^{0}_{\ell+1,k}-\zeta^{0}_{\ell-1,k}}{\Delta\chi_{i}+\Delta\chi_{i+1}}\right]-\dfrac{\omega^{I}_{\ell,n}-\omega^{I}_{\ell,n-1}}{\Delta z_{k}} \\ \dfrac{\eta^{I}_{i,n}-\eta^{I}_{i,n-1}}{\Delta z_{k}}-\dfrac{\zeta^{I}_{\ell,k}-\zeta^{I}_{\ell-1,k}}{\Delta\chi_{i}} \\ \dfrac{1}{\chi_{i}}\dfrac{\chi_{\ell}\omega^{I}_{\ell,n}-\chi_{\ell-1}\varepsilon\omega^{I}_{\ell-1,n}}{\Delta\chi_{i}} \\ \quad-\dfrac{1}{\chi_{i}}\left[\eta^{R}_{i,n}+2\left(R_{S}-\chi\right)\dfrac{\eta^{0}_{i+1,n}-\eta^{0}_{i-1,n}}{\Delta\chi_{i-1}+2\Delta\chi_{i}+\Delta\chi_{i+1}}\right] \end{bmatrix} \tag{C.9}$$

C.2 Derivation of the Adjoint Curl Operator, $\overline{\mathbf{C}}_{\mathbf{FC}\rightarrow\mathbf{EC}}$

Like the adjoint discrete gradient operator constructed in the previous chapter, the adjoint operator to the discrete curl operator must translate between vector spaces in reverse of the primary operator. The primary curl operator was selected to map $\mathbf{EC} \rightarrow \mathbf{FC}$, so it's adjoint pair will map $\mathbf{FC} \rightarrow \mathbf{EC}$. The primary operator supports the construction of its discrete adjoint through the vector calculus identity given in Equation C.10.[117] The volume integrals correspond to inner products of each vector and operator combination, while the surface integral is applied to extend the operators to the domain boundary to meet the specified boundary conditions. When the grid is rectangular, the surface integral on the LHS is zero by definition of the velocities since the velocity vectors are parallel to the outward normals of the boundary. For any vector space locations within the domain, the identity relationship must be enforced, so by collecting the primary operator terms that contain a given vector $\vec{\omega}_{\mathbf{EC}}$ at one vector location in the $\mathbf{EC}$ vector space, it is possible to derive the operator to define the adjoint curl mapping. Using the inner product to define this relationship, Equation C.11 must hold for all internal nodes.

$$\int_{\mathscr{V}} \mathbf{C}_{\mathbf{EC}\rightarrow\mathbf{FC}}\left(\vec{\omega}\right) \cdot \vec{u}\, d\mathscr{V} = \int_{\mathscr{V}} \vec{\omega} \cdot \overline{\mathbf{C}}_{\mathbf{FC}\rightarrow\mathbf{EC}}\left(\vec{u}\right)\, d\mathscr{V} - \oint_{\mathscr{S}} \vec{\omega} \cdot \left(\hat{n} \times \vec{u}\right)\, d\mathscr{S} \tag{C.10}$$

$$\left\langle \Delta\mathscr{V}\, \mathbf{C}_{\mathbf{EC}\rightarrow\mathbf{FC}}\left(\vec{\omega}\right), \overline{\vec{u}} \right\rangle_{\mathbf{FC}} = \left\langle \Delta\mathscr{V}\, \overline{\vec{\omega}}, \overline{\mathbf{C}}_{\mathbf{FC}\rightarrow\mathbf{EC}}\left(\vec{u}\right) \right\rangle_{\mathbf{EC}} \tag{C.11}$$

Recall that the adjoint curl operator defines vorticity, so $\eta_{i,n}$, $\omega_{\ell,n}$, and $\zeta_{\ell,k}$ correspond to the individual vector components of the adjoint curl operator: $\overline{\mathbf{C}}\left(\vec{u}\right)_{i,n}$, $\overline{\mathbf{C}}\left(\vec{u}\right)_{\ell,n}$, and $\overline{\mathbf{C}}\left(\vec{u}\right)_{\ell,k}$. Oud's work[91] defines the inner product on the $\mathbf{FC}$ and $\mathbf{EC}$ vector spaces for cylindrical coordinates. The equivalent inner products for the 2-D grid in this work are given by Equations 3.18 and 3.19. The following equations apply that definition with a coordinate change to define the components of inner product at a given vector space location $\underline{I}$ that corresponds to the faces or edges of cell (i,k). First the LHS of C.11 is defined with Equation C.12, and equated with Equation C.14, then the linear operator can be determined through algebraic manipulation.

$$\begin{aligned}\left\langle \mathbf{C}_{\mathbf{EC}\rightarrow\mathbf{FC}}\left(\vec{\omega}\right),\vec{\overline{u}}\right\rangle_{FC} \equiv \sum_{(i,k)} \frac{\Delta\chi_i\left(1-\varepsilon\right)\Delta\theta\Delta z_k}{2}\Bigg\{ & \\ & \left[\chi_{\ell-1}+\varepsilon\left(R_S-\chi_{\ell-1}\right)\right]\overline{u}_{\ell-1,k}\mathbf{C}_{\chi_{\ell-1}} \\ & +\left[\chi_{\ell}+\varepsilon\left(R_S-\chi_{\ell}\right)\right]\overline{u}_{\ell,k}\mathbf{C}_{\chi_{\ell}} \\ & +2\left[\chi_i+\varepsilon\left(R_S-\chi_i\right)\right]\overline{v}_{i,k}\mathbf{C}_{\theta_j} \\ & +\left[\chi_i+\varepsilon\left(R_S-\chi_i\right)\right]\left[\overline{w}_{i,n-1}\mathbf{C}_{z_{n-1}}+\overline{w}_{i,n}\mathbf{C}_{z_n}\right]\Bigg\}\end{aligned} \tag{C.12}$$

$$\mathbf{C}_{\chi_{\ell-1}} = \mathscr{f}\left(\zeta_{\ell-2,k},\zeta_{\ell-1,k},\zeta_{\ell,k},\omega_{\ell-1,n-1},\omega_{\ell-1,n}\right) \tag{C.13a}$$

$$\mathbf{C}_{\chi_{\ell}} = \mathscr{f}\left(\zeta_{\ell-1,k},\zeta_{\ell,k},\zeta_{\ell+1,k},\omega_{\ell,n-1},\omega_{\ell,n}\right) \tag{C.13b}$$

$$\mathbf{C}_{\chi_{\theta_j}} = \mathscr{f}\left(\eta_{i,n-1},\eta_{i,n},\zeta_{\ell-1,k},\zeta_{\ell,k}\right) \tag{C.13c}$$

$$\mathbf{C}_{\chi_{z_{n-1}}} = \mathscr{f}\left(\omega_{\ell-1,n-1},\omega_{\ell,n-1},\eta_{i-1,n-1},\eta_{i,n-1},\eta_{i+1,n-1}\right) \tag{C.13d}$$

$$\mathbf{C}_{\chi_{z_n}} = \mathscr{f}\left(\omega_{\ell-1,n},\omega_{\ell,n},\eta_{i-1,n},\eta_{i,n},\eta_{i+1,n}\right) \tag{C.13e}$$

$$\begin{aligned}\left\langle \vec{\omega},\overline{\mathbf{C}}\left(\vec{u}\right)\right\rangle_{EC} \equiv \sum_{(i,k)} \frac{\Delta\chi_i\left(1-\varepsilon\right)\Delta\theta\Delta z_k}{2}\Bigg\{ & \\ & \left[\chi_i+\varepsilon\left(R_S-\chi_i\right)\right]\left[\eta_{i,n-1}\overline{\mathbf{C}}_{\theta_j,z_{n-1}}+\eta_{i,n}\overline{\mathbf{C}}_{\theta_j,z_n}\right] \\ & +\left[\chi_{\ell-1}+\varepsilon\left(R_S-\chi_{\ell-1}\right)\right]\frac{\omega_{\ell-1,n-1}\overline{\mathbf{C}}_{\chi_{\ell-1},z_{n-1}}+\omega_{\ell-1,n}\overline{\mathbf{C}}_{\chi_{\ell-1},z_n}}{2} \\ & +\left[\chi_{\ell}+\varepsilon\left(R_S-\chi_{\ell}\right)\right]\frac{\omega_{\ell,n-1}\overline{\mathbf{C}}_{\chi_{\ell},z_{n-1}}+\omega_{\ell,n}\overline{\mathbf{C}}_{\chi_{\ell},z_n}}{2} \\ & +\frac{\chi_i+\chi_{i-1}+\varepsilon\left(2R_S-\chi_i-\chi_{i-1}\right)}{2}\zeta_{\ell-1,k}\overline{\mathbf{C}}_{\chi_{\ell-1},\theta_j} \\ & +\frac{\chi_i+\chi_{i+1}+\varepsilon\left(2R_S-\chi_i-\chi_{i+1}\right)}{2}\zeta_{\ell,k}\overline{\mathbf{C}}_{\chi_{\ell},\theta_j}\Bigg\}\end{aligned} \tag{C.14}$$

Collecting all contributions for $\eta_{i,n}$ in both inner product spaces spans $\mathbf{FC}$ and $\mathbf{EC}$ locations corresponding to cells (i,k),(i,k+1), (i+1,k), (i+1,k+1), (i-1,k), and (i-1,k+1). The i+1 and i-1 cells are included due to the expansion of dependence caused by the circumferential derivative of η requiring extra radial locations for the $\frac{\partial r}{\partial\theta}\frac{\partial\eta}{\partial r}$ term. To fit the equation on the page, the radii in the 1+1 and 1-1 terms were combined to cancel each other out in advance.

$$
\begin{aligned}
&\left\langle \mathbf{C}, \overline{\vec{u}} \right\rangle_{FC} |_{\eta_{i,n}} = \\
&\frac{\Delta\chi_{i-1}\,(1-\varepsilon)\,\Delta\theta\Delta z_k}{2}\left\{ \left[\chi_{i-1}+\varepsilon\,(R_S-\chi_{i-1})\right]\left[\overline{w_{i-1,n}}\mathbf{C}_{z_n}\left(\eta_{i-2,n},\eta_{i-1,n},\eta_{i,n}\right)\right]\right\}(i-1,k)\\
&+\frac{\Delta\chi_{i}\,(1-\varepsilon)\,\Delta\theta\Delta z_k}{2}\left\{ \begin{array}{l} 2\left[\chi_{i}+\varepsilon\,(R_S-\chi_{i})\right]\overline{v_{i,k}}\mathbf{C}_{\theta_j}\left(\eta_{i,n-1},\eta_{i,n}\right)\\ +\left[\chi_{i}+\varepsilon\,(R_S-\chi_{i})\right]\left[\overline{w_{i,n}}\mathbf{C}_{z_n}\left(\eta_{i-1,n},\eta_{i,n},\eta_{i+1,n}\right)\right]\end{array}\right\}(i,k)\\
&+\frac{\Delta\chi_{i+1}\,(1-\varepsilon)\,\Delta\theta\Delta z_k}{2}\left\{ \left[\chi_{i+1}+\varepsilon\,(R_S-\chi_{i+1})\right]\left[\overline{w_{i+1,n}}\mathbf{C}_{z_n}\left(\eta_{i,n},\eta_{i+1,n},\eta_{i+2,n}\right)\right]\right\}(i+1,k)\\
&+\frac{\Delta\chi_{i-1}\,(1-\varepsilon)\,\Delta\theta\Delta z_{k+1}}{2}\left\{ \left[\chi_{i-1}+\varepsilon\,(R_S-\chi_{i-1})\right]\left[\overline{w_{i-1,n}}\mathbf{C}_{z_n}\left(\eta_{i-2,n},\eta_{i-1,n},\eta_{i,n}\right)\right]\right\}(i-1,k+1)\\
&+\frac{\Delta\chi_{i}\,(1-\varepsilon)\,\Delta\theta\Delta z_{k+1}}{2}\left\{ \begin{array}{l} +2\left[\chi_{i}+\varepsilon\,(R_S-\chi_{i})\right]\overline{v_{i,k+1}}\mathbf{C}_{\theta_j}\left(\eta_{i,n},\eta_{i,n+1}\right)\\ +\left[\chi_{i}+\varepsilon\,(R_S-\chi_{i})\right]\left[\overline{w_{i,n}}\mathbf{C}_{z_n}\left(\eta_{i-1,n},\eta_{i,n},\eta_{i+1,n}\right)\right]\end{array}\right\}(i,k+1)\\
&+\frac{\Delta\chi_{i+1}\,(1-\varepsilon)\,\Delta\theta\Delta z_{k+1}}{2}\left\{ \left[\chi_{i+1}+\varepsilon\,(R_S-\chi_{i+1})\right]\left[\overline{w_{i+1,n}}\mathbf{C}_{z_n}\left(\eta_{i,n},\eta_{i+1,n},\eta_{i+2,n}\right)\right]\right\}(i+1,k+1)
\end{aligned}
\tag{C.15}
$$

$$
\begin{aligned}
&\left\langle \vec{\omega}, \overline{\mathbf{C}}\left(\vec{u}\right)\right\rangle_{EC} |_{\eta_{i,n}} = \\
&+\frac{\Delta\chi_{i}\,(1-\varepsilon)\,\Delta\theta\Delta z_k}{2}\left\{ \left[\chi_{i}+\varepsilon\,(R_S-\chi_{i})\right]\left[\eta_{i,n-1}\overline{\mathbf{C}}_{\theta_j,z_{n-1}}+\eta_{i,n}\overline{\mathbf{C}}_{\theta_j,z_n}\right]\right\}(i,k)\\
&+\frac{\Delta\chi_{i}\,(1-\varepsilon)\,\Delta\theta\Delta z_{k+1}}{2}\left\{ \left[\chi_{i}+\varepsilon\,(R_S-\chi_{i})\right]\left[\eta_{i,n}\overline{\mathbf{C}}_{\theta_j,z_n}+\eta_{i,n+1}\overline{\mathbf{C}}_{\theta_j,z_{n+1}}\right]\right\}(i,k+1)
\end{aligned}
\tag{C.16}
$$

$$
\begin{aligned}
&\frac{\Delta\chi_{i-1}}{\Delta\chi_i}\frac{[\chi_{i-1}+\varepsilon\left(R_S-\chi_{i-1}\right)]}{[\chi_i+\varepsilon\left(R_S-\chi_i\right)]}\left[\overline{w_{i-1,n}}\mathbf{C}_{z_n}\left(\eta_{i-2,n},\eta_{i-1,n},\eta_{i,n}\right)\right]\\
&+\left[\overline{w_{i,n}}\mathbf{C}_{z_n}\left(\eta_{i-1,n},\eta_{i,n},\eta_{i+1,n}\right)\right]\\
&+\frac{1}{(\Delta z_k+\Delta z_{k+1})}\Bigg\{\\
&\qquad+2\Delta z_k\overline{v_{i,k}}\mathbf{C}_{\theta_j}\left(\eta_{i,n},\eta_{i,n+1}\right)\\
&\qquad+2\Delta z_{k+1}\overline{v_{i,k+1}}\mathbf{C}_{\theta_j}\left(\eta_{i,n},\eta_{i,n+1}\right)\Bigg\}\\
&+\frac{\Delta\chi_{i+1}}{\Delta\chi_i}\frac{[\chi_{i+1}+\varepsilon\left(R_S-\chi_{i+1}\right)]}{[\chi_i+\varepsilon\left(R_S-\chi_i\right)]}\left[\overline{w_{i+1,n}}\mathbf{C}_{z_n}\left(\eta_{i,n},\eta_{i+1,n},\eta_{i+2,n}\right)\right]\\
&=\eta_{i,n}\,\overline{\mathbf{C}}_{\theta_j,z_n}
\end{aligned}
\tag{C.17}
$$

Equating the inner products, canceling like terms, and combining the Δz terms in the LHS leads to Equation C.17. Substituting the primary curl operator into Equation C.17 leads to Equation C.19.

$$
\begin{aligned}
&-\frac{\Delta\chi_{i-1}}{\Delta\chi_i}\frac{w^0_{i-1,n}}{[\chi_i+\varepsilon\left(R_S-\chi_i\right)]}\left[2\imath\varepsilon\left(R_S-\chi_{i-1}\right)\frac{1}{\Delta\chi_{i-2}+2\Delta\chi_{i-1}+\Delta\chi_i}\right]\\
&-\frac{\imath\varepsilon}{[\chi_i+\varepsilon\left(R_S-\chi_i\right)]}\overline{w^1_{i,n}}+\frac{1}{(\Delta z_k+\Delta z_{k+1})}\left\{2\Delta z_k\overline{v_{i,k}}\frac{1}{\Delta z_k}-2\Delta z_{k+1}\overline{v_{i,k+1}}\frac{1}{\Delta z_{k+1}}\right\}\\
&+\frac{\Delta\chi_{i+1}}{\Delta\chi_i}\frac{w^0_{i+1,n}}{[\chi_i+\varepsilon\left(R_S-\chi_i\right)]}\left[2\imath\varepsilon\left(R_S-\chi_{i+1}\right)\frac{1}{\Delta\chi_i+2\Delta\chi_{i+1}+\Delta\chi_{i+2}}\right]\\
&=\overline{\mathbf{C}}_{\theta_j,z_n}
\end{aligned}
\tag{C.18}
$$

$$
\begin{aligned}
\overline{\mathbf{C}}_{\theta_j,z_n}=\overline{\eta_{i,n}}=&-\frac{1}{\chi_i}\imath\varepsilon\overline{w^1_{i,n}}-2\frac{\overline{v_{i,k+1}}-\overline{v_{i,k}}}{\Delta z_k+\Delta z_{k+1}}\\
&+2\imath\varepsilon\frac{\Delta\chi_{i+1}}{\chi_i\Delta\chi_i}\left[\frac{\left(R_S-\chi_{i+1}\right)w^0_{i+1,n}}{\Delta\chi_i+2\Delta\chi_{i+1}+\Delta\chi_{i+2}}\right]\\
&-2\imath\varepsilon\frac{\Delta\chi_{i-1}}{\chi_i\Delta\chi_i}\left[\frac{\left(R_S-\chi_{i-1}\right)w^0_{i-1,n}}{\Delta\chi_{i-2}+2\Delta\chi_{i-1}+\Delta\chi_i}\right]
\end{aligned}
\tag{C.19}
$$

Here the flow variables are expanded into their perturbed forms and the higher order ϵh terms are removed. Note that this formulation is similar to that of Oud,[91] with the substitution of the known circumferential derivative and the addition of the $\frac{\partial r}{\partial\theta}\frac{\partial w}{\partial r}$ terms.

$$
\begin{aligned}
\overline{\eta_{i,n}}=&-\frac{1}{\chi_i}\imath\varepsilon\overline{w^1_{i,n}}+2\imath\varepsilon\frac{\Delta\chi_{i+1}}{\chi_i\Delta\chi_i}\left[\frac{\left(R_S-\chi_{i+1}\right)w^0_{i+1,n}}{\Delta\chi_i+2\Delta\chi_{i+1}+\Delta\chi_{i+2}}\right]-2\imath\varepsilon\frac{\Delta\chi_{i-1}}{\chi_i\Delta\chi_i}\left[\frac{\left(R_S-\chi_{i-1}\right)w^0_{i-1,n}}{\Delta\chi_{i-2}+2\Delta\chi_{i-1}+\Delta\chi_i}\right]\\
&-2\frac{v^0_{i,k+1}-v^0_{i,k}}{\Delta z_k+\Delta z_{k+1}}-2\varepsilon\frac{\overline{v^1_{i,k+1}}-\overline{v^1_{i,k}}}{\Delta z_k+\Delta z_{k+1}}
\end{aligned}
\tag{C.20}
$$

Next gather the $\omega_{\ell,n}$ terms in each inner product from cells (i,k), (i+1,k), (i,k+1), and (i+1,k+1).

$$
\begin{aligned}
&\left\langle \mathbf{C}, \overline{\vec{u}} \right\rangle_{FC} |_{\omega_{\ell,n}} = \\
&\left.\begin{aligned}
&\frac{\Delta\chi_i\,(1-\varepsilon)\,\Delta\theta\Delta z_k}{2}\Big(\\
&\quad + [\chi_\ell + \varepsilon\,(R_S - \chi_\ell)]\,\overline{u_{\ell,k}}\mathbf{C}_{\chi_\ell}\left(\omega_{\ell,n-1},\, \omega_{\ell,n}\right) \\
&\quad + [\chi_i + \varepsilon\,(R_S - \chi_i)]\left[\overline{w_{i,n}}\mathbf{C}_{z_n}\left(\omega_{\ell-1,n},\, \omega_{\ell,n}\right)\right]\Big)
\end{aligned}\right\}(i,k) \\
&+\left.\begin{aligned}
&\frac{\Delta\chi_{i+1}\,(1-\varepsilon)\,\Delta\theta\Delta z_k}{2}\Big(\\
&\quad + [\chi_\ell + \varepsilon\,(R_S - \chi_\ell)]\,\overline{u_{\ell,k}}\mathbf{C}_{\chi_\ell}\left(\omega_{\ell,n-1},\, \omega_{\ell,n}\right) \\
&\quad + [\chi_{i+1} + \varepsilon\,(R_S - \chi_{i+1})]\left[\overline{w_{i+1,n}}\mathbf{C}_{z_n}\left(\omega_{\ell,n},\omega_{\ell+1,n}\right)\right]\Big)
\end{aligned}\right\}(i+1,k) \\
&\quad +\left.\begin{aligned}
&\frac{\Delta\chi_i\,(1-\varepsilon)\,\Delta\theta\Delta z_{k+1}}{2}\Big(\\
&\quad + [\chi_\ell + \varepsilon\,(R_S - \chi_\ell)]\,\overline{u_{\ell,k+1}}\mathbf{C}_{\chi_\ell}\left(\omega_{\ell,n},\omega_{\ell,n+1}\right) \\
&\quad + [\chi_i + \varepsilon\,(R_S - \chi_i)]\left[\overline{w_{i,n}}\mathbf{C}_{z_n}\left(\omega_{\ell-1,n},\, \omega_{\ell,n}\right)\right]\Big)
\end{aligned}\right\}(i,k+1) \\
&+\left.\begin{aligned}
&\frac{\Delta\chi_{i+1}\,(1-\varepsilon)\,\Delta\theta\Delta z_{k+1}}{2}\Big(\\
&\quad + [\chi_\ell + \varepsilon\,(R_S - \chi_\ell)]\,\overline{u_{\ell,k+1}}\mathbf{C}_{\chi_\ell}\left(\omega_{\ell,n},\omega_{\ell,n+1}\right) \\
&\quad + [\chi_{i+1} + \varepsilon\,(R_S - \chi_{i+1})]\left[\overline{w_{i+1,n}}\mathbf{C}_{z_n}\left(\omega_{\ell,n},\omega_{\ell+1,n}\right)\right]\Big)
\end{aligned}\right\}(i+1,k+1)
\end{aligned}
\tag{C.21}
$$

$$
\begin{aligned}
&\left\langle \vec{\omega}, \overline{\mathbf{C}}\,(\vec{u}) \right\rangle_{EC} |_{\omega_{\ell,n}} = \\
&\left.\frac{\Delta\chi_i\,(1-\varepsilon)\,\Delta\theta\Delta z_k}{2}\,[\chi_\ell + \varepsilon\,(R_S - \chi_\ell)]\,\frac{\omega_{\ell,n}}{2}\overline{\mathbf{C}}_{\chi_\ell,z_n}\right\}(i,k) \\
&+\left.\frac{\Delta\chi_{i+1}\,(1-\varepsilon)\,\Delta\theta\Delta z_k}{2}\,[\chi_\ell + \varepsilon\,(R_S - \chi_\ell)]\,\frac{\omega_{\ell,n}}{2}\overline{\mathbf{C}}_{\chi_\ell,z_n}\right\}(i+1,k) \\
&+\left.\frac{\Delta\chi_i\,(1-\varepsilon)\,\Delta\theta\Delta z_k}{2}\,[\chi_\ell + \varepsilon\,(R_S - \chi_\ell)]\,\frac{\omega_{\ell,n}}{2}\overline{\mathbf{C}}_{\chi_\ell,z_n}\right\}(i,k+1) \\
&+\left.\frac{\Delta\chi_{i+1}\,(1-\varepsilon)\,\Delta\theta\Delta z_{k+1}}{2}\,[\chi_\ell + \varepsilon\,(R_S - \chi_\ell)]\,\frac{\omega_{\ell,n}}{2}\overline{\mathbf{C}}_{\chi_\ell,z_n}\right\}(i+1,k+1)
\end{aligned}
\tag{C.22}
$$

$$
\begin{aligned}
&\frac{2}{\Delta z_k + \Delta z_{k+1}} \Big[\Delta z_k \overline{u_{\ell,k}} \mathbf{C}_{\chi_\ell} \left(\omega_{\ell,n-1}, \omega_{\ell,n} \right) \\
&\qquad + \Delta z_{k+1} \overline{u_{\ell,k+1}} \mathbf{C}_{\chi_\ell} \left(\omega_{\ell,n}, \omega_{\ell,n+1} \right) \Big] \\
&+ \frac{2}{\Delta \chi_i + \Delta \chi_i} \Big\{ \Delta \chi_i \frac{[\chi_i + \varepsilon (R_S - \chi_i)]}{[\chi_\ell + \varepsilon (R_S - \chi_\ell)]} \left[\overline{w_{i,n}} \mathbf{C}_{z_n} \left(\omega_{\ell-1,n}, \omega_{\ell,n} \right) \right] \\
&\qquad + \Delta \chi_{i+1} \frac{[\chi_{i+1} + \varepsilon (R_S - \chi_{i+1})]}{[\chi_\ell + \varepsilon (R_S - \chi_\ell)]} \left[\overline{w_{i+1,n}} \mathbf{C}_{z_n} \left(\omega_{\ell,n}, \omega_{\ell+1,n} \right) \right] \Big\} \\
&= \omega_{\ell,n} \overline{\mathbf{C}}_{\chi_\ell, z_n}
\end{aligned}
\tag{C.23}
$$

$$
\begin{aligned}
&\frac{2}{\Delta z_k + \Delta z_{k+1}} \left[-\Delta z_k \overline{u_{\ell,k}} \frac{1}{\Delta z_k} + \Delta z_{k+1} \overline{u_{\ell,k+1}} \frac{1}{\Delta z_{k+1}} \right] \\
&+ \frac{2}{\Delta \chi_i + \Delta \chi_i} \left[\Delta \chi_i \overline{w_{i,n}} \frac{1}{\Delta \chi_i} (1 + \varepsilon) - \Delta \chi_{i+1} \overline{w_{i+1,n}} \frac{1}{\Delta \chi_{i+1}} (1 + \varepsilon) \right] \\
&= \overline{\mathbf{C}}_{\chi_\ell, z_n}
\end{aligned}
\tag{C.24}
$$

Again the flow variables are expanded into their perturbed forms and the higher order ϵh terms are removed. This is also similar to the form of Oud's ω vorticity term, with the difference being the complex conjugates in the first order components.

$$
\begin{aligned}
\overline{\mathbf{C}}_{\chi_\ell, z_n} = \overline{\omega_{\ell,n}} = &2 \frac{u^0_{\ell,k+1} - u^0_{\ell,k}}{\Delta z_k + \Delta z_{k+1}} + 2\varepsilon \frac{\overline{u^1_{\ell,k+1}} - \overline{u^1_{\ell,k}}}{\Delta z_k + \Delta z_{k+1}} \\
&- 2 \frac{w^0_{i+1,n} - w^0_{i,n}}{\Delta \chi_i + \Delta \chi_i} - 2\varepsilon \frac{w^0_{i+1,n} - w^0_{i,n}}{\Delta \chi_i + \Delta \chi_i} - 2\varepsilon \frac{\overline{w^1_{i+1,n}} - \overline{w^1_{i,n}}}{\Delta \chi_i + \Delta \chi_i}
\end{aligned}
\tag{C.25}
$$

Next the $\zeta_{\ell,k}$ terms in each inner product were gathered from cells (i,k), (i+1,k), (i-1,k) and (i+2,k).

$$\begin{aligned}
&\left\langle \mathbf{C}, \vec{\overline{u}} \right\rangle_{FC} |_{\zeta_{\ell,k}} = \\
&\frac{\Delta\chi_{i-1}\,(1-\varepsilon)\,\Delta\theta\Delta z_k}{2}\left[\chi_{\ell-1}+\varepsilon\,(R_S-\chi_{\ell-1})\right]\overline{u_{\ell-1,k}}\mathbf{C}_{\chi_{\ell-1}}\left(\zeta_{\ell-2,k},\zeta_{\ell-1,k},\boxed{\zeta_{\ell,k}}\right)\Bigg\}(i-1,k)\\
&\quad+\frac{\Delta\chi_i\,(1-\varepsilon)\,\Delta\theta\Delta z_k}{2}\Bigg\{\\
&\qquad\left[\chi_{\ell-1}+\varepsilon\,(R_S-\chi_{\ell-1})\right]\overline{u_{\ell-1,k}}\mathbf{C}_{\chi_{\ell-1}}\left(\zeta_{\ell-2,k},\zeta_{\ell-1,k},\boxed{\zeta_{\ell,k}}\right)\\
&\qquad+\left[\chi_{\ell}+\varepsilon\,(R_S-\chi_{\ell})\right]\overline{u_{\ell,k}}\mathbf{C}_{\chi_{\ell}}\left(\zeta_{\ell-1,k},\boxed{\zeta_{\ell,k}},\zeta_{\ell+1,k}\right)\\
&\qquad+2\left[\chi_i+\varepsilon\,(R_S-\chi_i)\right]\overline{v_{i,k}}\mathbf{C}_{\theta_j}\left(\zeta_{\ell-1,k},\boxed{\zeta_{\ell,k}}\right)\Bigg\}\Bigg\}(i,k)\\
&\quad+\frac{\Delta\chi_{i+1}\,(1-\varepsilon)\,\Delta\theta\Delta z_k}{2}\Bigg\{\\
&\qquad\left[\chi_{\ell}+\varepsilon\,(R_S-\chi_{\ell})\right]\overline{u_{\ell,k}}\mathbf{C}_{\chi_{\ell}}\left(\zeta_{\ell-1,k},\boxed{\zeta_{\ell,k}},\zeta_{\ell+1,k}\right)\\
&\qquad+\left[\chi_{\ell+1}+\varepsilon\,(R_S-\chi_{\ell+1})\right]\overline{u_{\ell+1,k}}\mathbf{C}_{\chi_{\ell+1}}\left(\boxed{\zeta_{\ell,k}},\zeta_{\ell+1,k},\zeta_{\ell+2,k}\right)\\
&\qquad+2\left[\chi_{i+1}+\varepsilon\,(R_S-\chi_{i+1})\right]\overline{v_{i+1,k}}\mathbf{C}_{\theta_j}\left(\boxed{\zeta_{\ell,k}},\zeta_{\ell+1,k}\right)\Bigg\}\Bigg\}(i+1,k)\\
&+\frac{\Delta\chi_{i+2}\,(1-\varepsilon)\,\Delta\theta\Delta z_k}{2}\left[\chi_{\ell+1}+\varepsilon\,(R_S-\chi_{\ell+1})\right]\overline{u_{\ell+1,k}}\mathbf{C}_{\chi_{\ell+1}}\left(\boxed{\zeta_{\ell,k}},\zeta_{\ell+1,k},\zeta_{\ell+2,k}\right)\Bigg\}(i+2,k)
\end{aligned}\tag{C.26}$$

$$\begin{aligned}
&\left\langle \vec{\omega}, \overline{\mathbf{C}}\,(\vec{u}) \right\rangle_{EC} = \\
&\quad+\frac{\Delta\chi_i\,(1-\varepsilon)\,\Delta\theta\Delta z_k}{2}\frac{\chi_i+\chi_{i+1}+\varepsilon\,(2R_S-\chi_i-\chi_{i+1})}{2}\zeta_{\ell,k}\overline{\mathbf{C}}_{\chi_\ell,\theta_j}\Bigg\}(i,k)\\
&+\frac{\Delta\chi_{i+1}\,(1-\varepsilon)\,\Delta\theta\Delta z_k}{2}+\frac{\chi_i+\chi_{i+1}+\varepsilon\,(2R_S-\chi_i-\chi_{i+1})}{2}\zeta_{\ell,k}\overline{\mathbf{C}}_{\chi_\ell,\theta_j}\Bigg\}(i+1,k)
\end{aligned}\tag{C.27}$$

$$
\begin{aligned}
&2\frac{\Delta\chi_{i-1}}{\Delta\chi_i+\Delta\chi_{i+1}}\frac{\chi_{\ell-1}+\varepsilon\left(R_S-\chi_{\ell-1}\right)}{\chi_i+\chi_{i+1}+\varepsilon\left(2R_S-\chi_i-\chi_{i+1}\right)}\overline{u_{\ell-1,k}}\mathbf{C}_{\chi_{\ell-1}}\left(\zeta_{\ell-2,k},\zeta_{\ell-1,k},\zeta_{\ell,k}\right)\\
&+\frac{\Delta\chi_i}{\Delta\chi_i+\Delta\chi_{i+1}}\frac{2}{\chi_i+\chi_{i+1}+\varepsilon\left(2R_S-\chi_i-\chi_{i+1}\right)}\Big\{\\
&\quad\left[\chi_{\ell-1}+\varepsilon\left(R_S-\chi_{\ell-1}\right)\right]\overline{u_{\ell-1,k}}\mathbf{C}_{\chi_{\ell-1}}\left(\zeta_{\ell-2,k},\zeta_{\ell-1,k},\zeta_{\ell,k}\right)\\
&\quad+\left[\chi_\ell+\varepsilon\left(R_S-\chi_\ell\right)\right]\overline{u_{\ell,k}}\mathbf{C}_{\chi_\ell}\left(\zeta_{\ell-1,k},\zeta_{\ell,k},\zeta_{\ell+1,k}\right)\\
&\quad+2\left[\chi_i+\varepsilon\left(R_S-\chi_i\right)\right]\overline{v_{i,k}}\mathbf{C}_{\theta_j}\left(\zeta_{\ell-1,k},\zeta_{\ell,k}\right)\Big\}\\
&+\frac{\Delta\chi_{i+1}}{\Delta\chi_i+\Delta\chi_{i+1}}\frac{2}{\chi_i+\chi_{i+1}+\varepsilon\left(2R_S-\chi_i-\chi_{i+1}\right)}\Big\{\\
&\quad+\left[\chi_\ell+\varepsilon\left(R_S-\chi_\ell\right)\right]\overline{u_{\ell,k}}\mathbf{C}_{\chi_\ell}\left(\zeta_{\ell-1,k},\zeta_{\ell,k},\zeta_{\ell+1,k}\right)\\
&\quad+\left[\chi_{\ell+1}+\varepsilon\left(R_S-\chi_{\ell+1}\right)\right]\overline{u_{\ell+1,k}}\mathbf{C}_{\chi_{\ell+1}}\left(\zeta_{\ell,k},\zeta_{\ell+1,k},\zeta_{\ell+2,k}\right)\\
&\quad+2\left[\chi_{i+1}+\varepsilon\left(R_S-\chi_{i+1}\right)\right]\overline{v_{i+1,k}}\mathbf{C}_{\theta_j}\left(\zeta_{\ell,k},\zeta_{\ell+1,k}\right)\Big\}\\
&+2\frac{\Delta\chi_{i+2}}{\Delta\chi_i+\Delta\chi_{i+1}}\frac{\chi_{\ell+1}+\varepsilon\left(R_S-\chi_{\ell+1}\right)}{\chi_i+\chi_{i+1}+\varepsilon\left(2R_S-\chi_i-\chi_{i+1}\right)}\overline{u_{\ell+1,k}}\mathbf{C}_{\chi_{\ell+1}}\left(\zeta_{\ell,k},\zeta_{\ell+1,k},\zeta_{\ell+2,k}\right)\\
&=\zeta_{\ell,k}\overline{\mathbf{C}}_{\chi_\ell,\theta_j}
\end{aligned}
\tag{C.28}
$$

To ensure the equation is more readable, r and $\frac{1}{r}$ terms are canceled as the curl operator is substituted into the next equation. Even when the $\frac{1}{r}$ term is taylor approximated, the resulting error from the cancelation is a second order ε term and thus discarded.

$$
\begin{aligned}
&+2\frac{\Delta\chi_{i-1}}{\Delta\chi_i+\Delta\chi_{i+1}}\frac{1}{\chi_i+\chi_{i+1}+\varepsilon\left(2R_S-\chi_i-\chi_{i+1}\right)}u^0_{\ell-1,k}\frac{\imath\varepsilon\left(R_S-\chi_{\ell-1}\right)}{\Delta\chi_{i-1}+\Delta\chi_i}\\
&+\frac{\Delta\chi_i}{\Delta\chi_i+\Delta\chi_{i+1}}\frac{2}{\chi_i+\chi_{i+1}+\varepsilon\left(2R_S-\chi_i-\chi_{i+1}\right)}\Big\{+\imath\varepsilon\overline{u^1_{\ell,k}}\\
&\quad+u^0_{\ell-1,k}\imath\varepsilon\left(R_S-\chi_{\ell-1}\right)\frac{1}{\Delta\chi_{i-1}+\Delta\chi_i}\\
&\quad-2\left[\chi_i+\varepsilon\left(R_S-\chi_i\right)\right]\overline{v_{i,k}}\frac{1}{\Delta\chi_i}\left(1+\varepsilon\right)\Big\}\\
&+\frac{\Delta\chi_{i+1}}{\Delta\chi_i+\Delta\chi_{i+1}}\frac{2}{\chi_i+\chi_{i+1}+\varepsilon\left(2R_S-\chi_i-\chi_{i+1}\right)}\Big\{+\imath\varepsilon\overline{u^1_{\ell,k}}\\
&\quad-u^0_{\ell+1,k}\imath\varepsilon\left(R_S-\chi_{\ell+1}\right)\frac{1}{\Delta\chi_{i+1}+\Delta\chi_{i+2}}\\
&\quad+2\left[\chi_{i+1}+\varepsilon\left(R_S-\chi_{i+1}\right)\right]\overline{v_{i+1,k}}\frac{1}{\Delta\chi_{i+1}}\left(1+\varepsilon\right)\Big\}\\
&-2\frac{\Delta\chi_{i+2}}{\Delta\chi_i+\Delta\chi_{i+1}}\frac{1}{\chi_i+\chi_{i+1}+\varepsilon\left(2R_S-\chi_i-\chi_{i+1}\right)}u^0_{\ell+1,k}\imath\varepsilon\left(R_S-\chi_{\ell+1}\right)\frac{1}{\Delta\chi_{i+1}+\Delta\chi_{i+2}}\\
&=\overline{\mathbf{C}}_{\chi_\ell,\theta_j}
\end{aligned}
\tag{C.29}
$$

$$
\begin{aligned}
&\frac{2}{\chi_i+\chi_{i+1}+\varepsilon\left(2R_S-\chi_i-\chi_{i+1}\right)}\left\{+\imath\varepsilon\overline{u^1_{\ell,k}}\right.\\
&\quad-\frac{\imath\varepsilon}{\Delta\chi_i+\Delta\chi_{i+1}}\left[u^0_{\ell+1,k}\left(R_S-\chi_{\ell+1}\right)\frac{\Delta\chi_{i+1}+\cancel{\Delta\chi_{i+2}}}{\cancel{\Delta\chi_{i+1}+\Delta\chi_{i+2}}}\right.\\
&\quad\left.\left.-u^0_{\ell-1,k}\left(R_S-\chi_{\ell-1}\right)\frac{\Delta\chi_i+\cancel{\Delta\chi_{i-1}}}{\cancel{\Delta\chi_{i-1}}+\Delta\chi_i}\right]\right\}\\
&-\frac{4}{\chi_i+\chi_{i+1}+\varepsilon\left(2R_S-\chi_i-\chi_{i+1}\right)}\frac{\left[\chi_i+\varepsilon\left(R_S-\chi_i\right)\right]\overline{v_{i,k}}}{\Delta\chi_i+\Delta\chi_{i+1}}\left(1+\varepsilon\right)\\
&+\frac{4}{\chi_i+\chi_{i+1}+\varepsilon\left(2R_S-\chi_i-\chi_{i+1}\right)}\frac{\left[\chi_{i+1}+\varepsilon\left(R_S-\chi_{i+1}\right)\right]\overline{v_{i+1,k}}}{\Delta\chi_i+\Delta\chi_{i+1}}\left(1+\varepsilon\right)\\
&=\overline{\mathbf{C}}_{\chi_\ell,\theta_j}
\end{aligned}
\tag{C.30}
$$

Each nominal velocity was substituted with zeroth and first order perturbation components and simplifed to remove higher powers of ε.

$$
\begin{aligned}
\overline{\mathbf{C}}_{\chi_\ell,\theta_j}&=\overline{\zeta_{\ell,k}}\\
&=\frac{2}{\chi_{i+1}+\chi_i+\varepsilon\left(2R_S-\chi_i-\chi_{i+1}\right)}\left\{\right.\\
&\qquad 2\frac{\left[\chi_{i+1}+\varepsilon\left(R_S-\chi_{i+1}\right)\right]\overline{v_{i+1,k}}-\left[\chi_i+\varepsilon\left(R_S-\chi_i\right)\right]\overline{v_{i,k}}}{\Delta\chi_i+\Delta\chi_{i+1}}\left(1+\varepsilon\right)\\
&\qquad\left.-\left[-\imath\varepsilon\overline{u^1_{\ell,k}}+\imath\varepsilon\frac{\left(R_S-\chi_{\ell+1}\right)u^0_{\ell+1,k}-\left(R_S-\chi_{\ell-1}\right)u^0_{\ell-1,k}}{\Delta\chi_i+\Delta\chi_{i+1}}\right]\right\}
\end{aligned}
\tag{C.31}
$$

$$
\begin{aligned}
\overline{\left[\overline{\mathbf{C}}\left(\vec{u}\right)\right]_{\ell,k}}&=\overline{\zeta^0_{\ell,k}+\varepsilon\zeta^1_{\ell,k}}\\
&=4\frac{1}{\chi_{i+1}+\chi_i}\frac{\chi_{i+1}v^0_{i+1,k}-\chi_iv^0_{i,k}}{\Delta\chi_i+\Delta\chi_{i+1}}\left(1+\varepsilon\right)+4\varepsilon\frac{1}{\chi_{i+1}+\chi_i}\frac{\chi_{i+1}\overline{v^1_{i+1,k}}-\chi_i\overline{v^1_{i,k}}}{\Delta\chi_i+\Delta\chi_{i+1}}\\
&\quad+4\varepsilon\frac{R_S}{\chi_{i+1}+\chi_i}\frac{v^0_{i+1,k}-v^0_{i,k}}{\Delta\chi_i+\Delta\chi_{i+1}}-4\varepsilon\frac{1}{\cancel{\chi_{i+1}+\chi_i}}\frac{\cancel{\chi_{i+1}v^0_{i+1,k}-\chi_iv^0_{i,k}}}{\Delta\chi_i+\Delta\chi_{i+1}}\\
&\quad-4\varepsilon\frac{2R_S}{\left(\chi_{i+1}+\chi_i\right)^2}\frac{\chi_{i+1}v^0_{i+1,k}-\chi_iv^0_{i,k}}{\Delta\chi_i+\Delta\chi_{i+1}}+4\varepsilon\frac{1}{\cancel{\chi_{i+1}+\chi_i}}\frac{\cancel{\chi_{i+1}v^0_{i+1,k}-\chi_iv^0_{i,k}}}{\Delta\chi_i+\Delta\chi_{i+1}}\\
&\quad+2\frac{1}{\chi_{i+1}+\chi_i}\left\{\imath\varepsilon\overline{u^1_{\ell,k}}-\imath\varepsilon\frac{\left(R_S-\chi_{\ell+1}\right)u^0_{\ell+1,k}-\left(R_S-\chi_{\ell-1}\right)u^0_{\ell-1,k}}{\Delta\chi_i+\Delta\chi_{i+1}}\right\}\\
&=4\frac{1}{\chi_{i+1}+\chi_i}\frac{\chi_{i+1}v^0_{i+1,k}-\chi_iv^0_{i,k}}{\Delta\chi_i+\Delta\chi_{i+1}}\left(1+\varepsilon\right)+4\varepsilon\frac{1}{\chi_{i+1}+\chi_i}\frac{\chi_{i+1}\overline{v^1_{i+1,k}}-\chi_i\overline{v^1_{i,k}}}{\Delta\chi_i+\Delta\chi_{i+1}}\\
&\quad+4\varepsilon\frac{R_S}{\chi_{i+1}+\chi_i}\frac{v^0_{i+1,k}-v^0_{i,k}}{\Delta\chi_i+\Delta\chi_{i+1}}-8\varepsilon\frac{R_S}{\left(\chi_{i+1}+\chi_i\right)^2}\frac{\chi_{i+1}v^0_{i+1,k}-\chi_iv^0_{i,k}}{\Delta\chi_i+\Delta\chi_{i+1}}\\
&\quad-\frac{2}{\chi_{i+1}+\chi_i}\left[-\imath\varepsilon\overline{u^1_{\ell,k}}+\imath\varepsilon\frac{\left(R_S-\chi_{\ell+1}\right)u^0_{\ell+1,k}-\left(R_S-\chi_{\ell-1}\right)u^0_{\ell-1,k}}{\Delta\chi_i+\Delta\chi_{i+1}}\right]
\end{aligned}
\tag{C.32}
$$

C.2.1 Conjugate Curl Operator: $\overline{\mathrm{C}}\left(\vec{u}\right) = \nabla \times \vec{u}$

$$\left[\overline{\mathrm{C}}\left(\vec{u}\right)\right] = \begin{bmatrix} \eta_{i,n} \\ \omega_{\ell,n} \\ \zeta_{\ell,k} \end{bmatrix} \equiv \begin{bmatrix} \frac{1}{r}\frac{\partial w}{\partial \theta} - \frac{\partial v}{\partial z} \\ \frac{\partial u}{\partial z} - \frac{\partial w}{\partial r} \\ \frac{1}{r}\frac{\partial (rv)}{\partial r} - \frac{1}{r}\frac{\partial u}{\partial \theta} \end{bmatrix} \tag{C.33}$$

$$\left[\overline{\mathrm{C}}\left(\vec{u}\right)\right] = \begin{bmatrix} \overline{\eta_{i,n}} \\ \overline{\omega_{\ell,n}} \\ \overline{\zeta_{\ell,k}} \end{bmatrix} = \begin{bmatrix} \frac{1}{\chi_i}\varepsilon\left(-w^I_{i,n} - \imath w^R_{i,n}\right) + 2\imath\varepsilon\frac{\Delta\chi_{i+1}}{\chi_i\Delta\chi_i}\left[\frac{\left(R_S-\chi_{i+1}\right)w^0_{i+1,n}}{\Delta\chi_i + 2\Delta\chi_{i+1} + \Delta\chi_{i+2}}\right] \\ \quad -2\imath\varepsilon\frac{\Delta\chi_{i-1}}{\chi_i\Delta\chi_i}\left[\frac{\left(R_S-\chi_{i-1}\right)w^0_{i-1,n}}{\Delta\chi_{i-2} + 2\Delta\chi_{i-1} + \Delta\chi_i}\right] \\ \quad -2\frac{v^0_{i,k+1} - v^0_{i,k}}{\Delta z_k + \Delta z_{k+1}} - 2\varepsilon\frac{\overline{v^1_{i,k+1}} - \overline{v^1_{i,k}}}{\Delta z_k + \Delta z_{k+1}} \\ \hline 2\frac{u^0_{\ell,k+1} - u^0_{\ell,k}}{\Delta z_k + \Delta z_{k+1}} + 2\varepsilon\frac{\overline{u^1_{\ell,k+1}} - \overline{u^1_{\ell,k}}}{\Delta z_k + \Delta z_{k+1}} \\ \quad -2\frac{w^0_{i+1,n} - w^0_{i,n}}{\Delta\chi_{i+1} + \Delta\chi_i} - 2\varepsilon\frac{w^0_{i+1,n} - w^0_{i,n}}{\Delta\chi_{i+1} + \Delta\chi_i} - 2\varepsilon\frac{\overline{w^1_{i+1,n}} - \overline{w^1_{i,n}}}{\Delta\chi_{i+1} + \Delta\chi_i} \\ \hline 4\frac{1}{\chi_{i+1} + \chi_i}\frac{\chi_{i+1}v^0_{i+1,k} - \chi_i v^0_{i,k}}{\Delta\chi_i + \Delta\chi_{i+1}}\left(1+\varepsilon\right) + 4\varepsilon\frac{1}{\chi_{i+1} + \chi_i}\frac{\chi_{i+1}\overline{v^1_{i+1,k}} - \chi_i\overline{v^1_{i,k}}}{\Delta\chi_i + \Delta\chi_{i+1}} \\ \quad + 4\varepsilon\frac{R_S}{\chi_{i+1} + \chi_i}\frac{v^0_{i+1,k} - v^0_{i,k}}{\Delta\chi_i + \Delta\chi_{i+1}} - 8\varepsilon\frac{R_S}{\left(\chi_{i+1} + \chi_i\right)^2}\frac{\chi_{i+1}v^0_{i+1,k} - \chi_i v^0_{i,k}}{\Delta\chi_i + \Delta\chi_{i+1}} \\ \quad -\frac{2}{\chi_{i+1} + \chi_i}\left[\varepsilon\left(-u^I_{\ell,k} - \imath u^R_{\ell,k}\right) + \imath\varepsilon\frac{\left(R_S-\chi_{\ell+1}\right)u^0_{\ell+1,k} - \left(R_S-\chi_{\ell-1}\right)u^0_{\ell-1,k}}{\Delta\chi_i + \Delta\chi_{i+1}}\right] \end{bmatrix} \tag{C.34}$$

C.2.2 Conjugate Curl Operator, Zeroth Order: $\overline{\mathrm{C}^0}\left(\vec{u}\right)$

$$\left[\overline{\mathrm{C}}^0\left(\vec{u}\right)\right] = \begin{bmatrix} \eta^0_{i,n} \\ \omega^0_{\ell,n} \\ \zeta^0_{\ell,k} \end{bmatrix} = \begin{bmatrix} -2\frac{v^0_{i,k+1} - v^0_{i,k}}{\Delta z_k + \Delta z_{k+1}} \\ 2\frac{u^0_{\ell,k+1} - u^0_{\ell,k}}{\Delta z_k + \Delta z_{k+1}} - 2\frac{w^0_{i+1,n} - w^0_{i,n}}{\Delta\chi_{i+1} + \Delta\chi_i} \\ \frac{4}{\chi_{i+1} + \chi_i}\frac{\chi_{i+1}v^0_{i+1,k} - \chi_i v^0_{i,k}}{\Delta\chi_i + \Delta\chi_{i+1}} \end{bmatrix} \tag{C.35}$$

C.2.3 Conjugate Curl Operator, First Order: $\overline{\mathrm{C}^1}\left(\vec{u}\right)$

$$\overline{\mathbf{C}}^1\left(\vec{u}\right)=\begin{bmatrix}\overline{\eta}^1_{i,n}\\ \overline{\omega}^1_{\ell,n}\\ \overline{\zeta}^1_{\ell,k}\end{bmatrix}=\begin{bmatrix}\frac{1}{\chi_i}\left(-w^I_{i,n}-\imath w^R_{i,n}\right)+2\imath\frac{\Delta\chi_{i+1}}{\chi_i\Delta\chi_i}\left[\frac{\left(R_S-\chi_{i+1}\right)w^0_{i+1,n}}{\Delta\chi_i+2\Delta\chi_{i+1}+\Delta\chi_{i+2}}\right] \\ -2\imath\frac{\Delta\chi_{i-1}}{\chi_i\Delta\chi_i}\left[\frac{\left(R_S-\chi_{i-1}\right)w^0_{i-1,n}}{\Delta\chi_{i-2}+2\Delta\chi_{i-1}+\Delta\chi_i}\right]-2\frac{\overline{v^1_{i,k+1}}-\overline{v^1_{i,k}}}{\Delta z_k+\Delta z_{k+1}} \\ 2\frac{\overline{u^1_{\ell,k+1}}-\overline{u^1_{\ell,k}}}{\Delta z_k+\Delta z_{k+1}}-2\frac{w^0_{i+1,n}-w^0_{i,n}}{\Delta\chi_{i+1}+\Delta\chi_i}-2\frac{\overline{w^1_{i+1,n}}-\overline{w^1_{i,n}}}{\Delta\chi_{i+1}+\Delta\chi_i} \\ \frac{4}{\chi_{i+1}+\chi_i}\frac{\chi_{i+1}v^0_{i+1,k}-\chi_iv^0_{i,k}}{\Delta\chi_i+\Delta\chi_{i+1}}+\frac{4}{\chi_{i+1}+\chi_i}\frac{\chi_{i+1}\overline{v^1_{i+1,k}}-\chi_i\overline{v^1_{i,k}}}{\Delta\chi_i+\Delta\chi_{i+1}} \\ +4\frac{R_S}{\chi_{i+1}+\chi_i}\frac{v^0_{i+1,k}-v^0_{i,k}}{\Delta\chi_i+\Delta\chi_{i+1}}-8\frac{R_S}{\left(\chi_{i+1}+\chi_i\right)^2}\frac{\chi_{i+1}v^0_{i+1,k}-\chi_iv^0_{i,k}}{\Delta\chi_i+\Delta\chi_{i+1}} \\ -\frac{2}{\chi_{i+1}+\chi_i}\left[\varepsilon\left(-u^I_{\ell,k}-\imath u^R_{\ell,k}\right)+\imath\varepsilon\frac{\left(R_S-\chi_{\ell+1}\right)u^0_{\ell+1,k}-\left(R_S-\chi_{\ell-1}\right)u^0_{\ell-1,k}}{\Delta\chi_i+\Delta\chi_{i+1}}\right]\end{bmatrix} \tag{C.36}$$

Conjugate Curl Operator, Real First Order: $\overline{\mathbf{C}^R}\left(\vec{u}\right)$

$$\overline{\mathbf{C}}^R\left(\vec{u}\right)=\begin{bmatrix}\overline{\eta}^R_{i,n}\\ \overline{\omega}^R_{\ell,n}\\ \overline{\zeta}^R_{\ell,k}\end{bmatrix}=\begin{bmatrix}-\frac{1}{\chi_i}w^I_{i,n}-2\frac{v^R_{i,k+1}-v^R_{i,k}}{\Delta z_k+\Delta z_{k+1}}\\ 2\frac{u^R_{\ell,k+1}-u^R_{\ell,k}}{\Delta z_k+\Delta z_{k+1}}-2\frac{w^0_{i+1,n}-w^0_{i,n}}{\Delta\chi_{i+1}+\Delta\chi_i}-2\frac{w^R_{i+1,n}-w^R_{i,n}}{\Delta\chi_{i+1}+\Delta\chi_i}\\ \frac{4}{\chi_{i+1}+\chi_i}\frac{\chi_{i+1}v^0_{i+1,k}-\chi_i v^0_{i,k}}{\Delta\chi_i+\Delta\chi_{i+1}}+\frac{4}{\chi_{i+1}+\chi_i}\frac{\chi_{i+1}v^R_{i+1,k}-\chi_i v^R_{i,k}}{\Delta\chi_i+\Delta\chi_{i+1}}\\ \quad+4\frac{R_S}{\chi_{i+1}+\chi_i}\frac{v^0_{i+1,k}-v^0_{i,k}}{\Delta\chi_i+\Delta\chi_{i+1}}-8\frac{R_S}{(\chi_{i+1}+\chi_i)^2}\frac{\chi_{i+1}v^0_{i+1,k}-\chi_i v^0_{i,k}}{\Delta\chi_i+\Delta\chi_{i+1}}+\frac{2}{\chi_{i+1}+\chi_i}u^I_{\ell,k}\end{bmatrix} \tag{C.37}$$

Conjugate Curl Operator, Imaginary First Order: $\overline{\mathbf{C}^I}\left(\vec{u}\right)$

$$\overline{\mathbf{C}}^I\left(\vec{u}\right)=\begin{bmatrix}\overline{\eta}^I_{i,n}\\ \overline{\omega}^I_{\ell,n}\\ \overline{\zeta}^I_{\ell,k}\end{bmatrix}=\begin{bmatrix}-\frac{1}{\chi_i}w^R_{i,n}+2\frac{\Delta\chi_{i+1}}{\chi_i\Delta\chi_i}\left[\frac{\left(R_S-\chi_{i+1}\right)w^0_{i+1,n}}{\Delta\chi_i+2\Delta\chi_{i+1}+\Delta\chi_{i+2}}\right]\\ \quad-2\frac{\Delta\chi_{i-1}}{\chi_i\Delta\chi_i}\left[\frac{\left(R_S-\chi_{i-1}\right)w^0_{i-1,n}}{\Delta\chi_{i-2}+2\Delta\chi_{i-1}+\Delta\chi_i}\right]+2\frac{v^I_{i,k+1}-v^I_{i,k}}{\Delta z_k+\Delta z_{k+1}}\\ -2\frac{u^I_{\ell,k+1}-u^I_{\ell,k}}{\Delta z_k+\Delta z_{k+1}}+2\frac{w^I_{i+1,n}-w^I_{i,n}}{\Delta\chi_{i+1}+\Delta\chi_i}\\ -\frac{4}{\chi_{i+1}+\chi_i}\frac{\chi_{i+1}v^I_{i+1,k}-\chi_i v^I_{i,k}}{\Delta\chi_i+\Delta\chi_{i+1}}\\ \quad-\frac{2}{\chi_{i+1}+\chi_i}\left\{-u^R_{\ell,k}+\frac{\left(R_S-\chi_{\ell+1}\right)u^0_{\ell+1,k}-\left(R_S-\chi_{\ell-1}\right)u^0_{\ell-1,k}}{\Delta\chi_i+\Delta\chi_{i+1}}\right\}\end{bmatrix} \tag{C.38}$$

C.3 Boundary Conditions for Velocity and Vorticity from Discrete Curl Operators

The discretizations of the curl operators that have been created are mimetic for infinite domains. However, any turbomachinery flow analsyis is within a finite domain. These finite domain boundaries are given Dirichlet, Neumann, or Robin boundary conditions based on the flow physics, but the boundary conditions also have to be applied within the context of the grid and DVTC operators to maintian the mimetic identities. This is in contrast to a direct linear interpolation of the boundary values to the boundary nodes, though the ideas are not incompatibile with correctly chosen interpolation methods. As the divergence and gradient operators only employ nodes that are directly on the boundaries or in the cell centers, the context for the velocity boundary conditions comes from the curl operators. Particularly of interest, the η and ζ vorticities' derivatives in the circumferential direction require these vorticities be calcualted at the ghost and boundary nodes of the rotor and stator boundaries. This becomes problematic because the conjugate curl operator that defines η and ζ would then require information for w and u velocities, respectively, outside the domain and single layer of ghost cells in the radial direction. Thus, the first boundary definition to address is how to select values for those second layer ghost cell velocities or calculate vorticities or velocities along the boundaries that are consistent with the mimetic scheme.

Starting with the rotor boundary, the inner product contribution for the first radial layer of cells, $i = N_\chi$, within the domain is written to collect the $\zeta_{\ell,k} = \zeta_{N_\chi+\frac{1}{2},k}$ vorticity terms in Equation C.39. Unlike Equations C.26 and C.27, the inner product formulation does not include cells (i+1,k) or (i+2,k) because it represents the volume integral over the fluid domian domain of the inner product space. This exclusion of cells outside the domain is only a workable method of directly determining homogeneous boundary conditions due to the discrete volume integral not containing points on the wall for every velocity in this discretization. However, the derived homogeneous boundaries can then suggest the form of non-homogeneous boundary values.

$$\begin{aligned}
&\frac{\Delta\chi_{N_\chi}\left(1-\varepsilon\right)\Delta\theta\Delta z_k}{2}\frac{\chi_{N_\chi}+\chi_{N_\chi+1}+\varepsilon\left(2R_S-\chi_{N_\chi}-\chi_{N_\chi+1}\right)}{2}\zeta_{N_\chi+\frac{1}{2},k}\overline{\mathbf{C}}^{\zeta}_{\chi_{N_\chi},\theta_j}\Bigg\}(N_\chi,k)=\\
&\frac{\Delta\chi_{N_\chi-1}\left(1-\varepsilon\right)\Delta\theta\Delta z_k}{2}\chi_{N_\chi-\frac{1}{2}}\overline{u}_{N_\chi-\frac{1}{2},k}\mathbf{C}^{\omega,\zeta}_{\chi_{N_\chi-1}}\left(\zeta_{N_\chi-1\frac{1}{2},k},\zeta_{N_\chi-\frac{1}{2},k},\zeta_{N_\chi+\frac{1}{2},k}\right)\Bigg\}(N_\chi-1,k)\\
&\quad+\frac{\Delta\chi_{N_\chi}\left(1-\varepsilon\right)\Delta\theta\Delta z_k}{2}\Bigg\{\\
&\qquad+\chi_{N_\chi-\frac{1}{2}}\overline{u}_{N_\chi-\frac{1}{2},k}\mathbf{C}^{\omega,\zeta}_{\chi_{\ell-1}}\left(\zeta_{N_\chi-1\frac{1}{2},k},\zeta_{N_\chi-\frac{1}{2},k},\zeta_{N_\chi+\frac{1}{2},k}\right)\\
&\qquad+\chi_{\ell N_\chi}\overline{u}_{N_\chi+\frac{1}{2},k}\mathbf{C}^{\omega,\zeta}_{\chi_{N_\chi}}\left(\zeta_{N_\chi-1,k},\zeta_{N_\chi+\frac{1}{2},k},\zeta_{N_\chi+1\frac{1}{2},k}\right)\\
&\qquad+2\left[\chi_{N_\chi}+\varepsilon\left(R_S-\chi_{N_\chi}\right)\right]\overline{v}_{N_\chi,k}\mathbf{C}^{\eta,\zeta}_{\theta_j}\left(\zeta_{N_\chi-\frac{1}{2},k},\zeta_{N_\chi+\frac{1}{2},k}\right)\Bigg\}\Bigg\}(N_\chi,k)
\end{aligned}\tag{C.39}$$

$$\begin{aligned}
&+2\frac{\Delta\chi_{N_\chi-1}}{\Delta\chi_{N_\chi}}\frac{1}{\chi_{N_\chi}+\chi_{N_\chi+1}+\varepsilon\left(2R_S-\chi_{N_\chi}-\chi_{N_\chi+1}\right)}u^0_{N_\chi-\frac{1}{2},k}\frac{\imath\varepsilon\left(R_S-\chi_{N_\chi-\frac{1}{2}}\right)}{\Delta\chi_{N_\chi-1}+\Delta\chi_i}\\
&+\frac{\Delta\chi_{N_\chi}}{\Delta\chi_{N_\chi}}\frac{2}{\chi_{N_\chi}+\chi_{N_\chi+1}+\varepsilon\left(2R_S-\chi_{N_\chi}-\chi_{N_\chi+1}\right)}\Bigg\{+\imath\varepsilon\overline{u}^1_{N_\chi+\frac{1}{2},k}\\
&\qquad+u^0_{N_\chi-\frac{1}{2},k}\imath\varepsilon\left(R_S-\chi_{N_\chi-\frac{1}{2}}\right)\frac{1}{\Delta\chi_{N_\chi-1}+\Delta\chi_{N_\chi}}\\
&\qquad-2\left[\chi_{N_\chi}+\varepsilon\left(R_S-\chi_{N_\chi}\right)\right]\overline{v}_{N_\chi,k}\frac{1}{\Delta\chi_{N_\chi}}\left(1+\varepsilon\right)\Bigg\}\\
&=\overline{\mathbf{C}}^{\zeta}_{\chi_\ell,\theta_j}
\end{aligned}\tag{C.40}$$

$$\begin{aligned}
\overline{\zeta_{N_\chi+\frac{1}{2},k}}=&-\frac{4\left[\chi_{N_\chi}+\varepsilon\left(R_S-\chi_{N_\chi}\right)\right]}{\chi_{N_\chi}+\chi_{N_\chi+1}+\varepsilon\left(2R_S-\chi_{N_\chi}-\chi_{N_\chi+1}\right)}\frac{\overline{v}_{N_\chi,k}}{\Delta\chi_{N_\chi}}\left(1+\varepsilon\right)+\frac{2}{\chi_{N_\chi}+\chi_{N_\chi+1}}\imath\varepsilon\overline{u}^1_{N_\chi+\frac{1}{2},k}\\
&+2\imath\varepsilon\frac{\left(R_S-\chi_{N_\chi-\frac{1}{2}}\right)}{\chi_{N_\chi}+\chi_{N_\chi+1}}\frac{u^0_{N_\chi-\frac{1}{2},k}}{\Delta\chi_{N_\chi}}
\end{aligned}\tag{C.41}$$

A similar expression can be derived for $\omega_{\ell,n}$ and $\eta_{i,n}$. However, the ω vorticity component does not have any variable transformed circumferential derivatives to make it more complicated than the boundary conditions derived by Oud[91] aside from the perterbation of the velocities involved. The η voriticity component does have an additional circumferential derivative, however the axial velocity ghost cells also have to meet the requirements of ω so there is no need to specifically derive separate radial boundaries for axial velocity from η. The remaining boundaries velocities for velocities in their own component directions, *i.e.* radial velocity in the radial direction, have trivial derivations for Dirichlet boundary types since the **FC** vector space exists on the rotor and stator

surfaces for radial velocity and on the inlet and outlet surfaces for the axial velocity. The Neumann type BC's for any velocity and boundary can be derived by setting the vorticity component related to that velocity and surface to be zero.

C.3.1 South (Rotor Surface) and North (Stator Surface) Boundaries

Applying the no penetration and no slip condition, $u_{\frac{1}{2},k}$ must have a homogeneous Dirichlet boundary condition for the entire rotor and stator surfaces. The circumferential derivative of the radial velocity's first order component goes to zero also along the walls plus the $\frac{\partial r}{\partial \theta}\frac{\partial}{\partial r}$ term. The required ghost cell for radial velocity can be obtained from setting Equation C.41 equal to the standard ζ vorticity definition from Equation C.34 and equate the radial velocity components of the equations. This results in a ghost cell dirichlet value, Equation C.44, for radial velocity necessary when calculating ζ directly on the walls. The equivalent ghost cell value on the Rotor wall surface is given by Equation C.45. Both of these radial velocity ghost cells are the equivalent of a standard mirrored boundary condition across the wall. The homogeneous Neumann boundary condition is obtained from the radial derivative defined by the divergence operator in Equation B.3. This results in Equation C.46.

$$+2\frac{1}{\chi_{N_\chi+1}+\chi_{N_\chi}}\left\{\cancel{i\varepsilon u^1_{N_\chi+\frac{1}{2},k}}+i\varepsilon\frac{\left(R_S-\chi_{N_\chi+1\frac{1}{2}}\right)u^0_{N_\chi+1\frac{1}{2},k}-\left(R_S-\chi_{N_\chi-\frac{1}{2}}\right)u^0_{N_\chi-\frac{1}{2},k}}{\Delta\chi_{N_\chi}+\Delta\chi_{N_\chi+1}}\right\}= \tag{C.42}$$
$$-\cancel{\frac{2}{\chi_{N_\chi}+\chi_{N_\chi+1}}i\varepsilon u^1_{N_\chi+\frac{1}{2},k}}+2\frac{i\varepsilon}{\chi_{N_\chi}+\chi_{N_\chi+1}}\left(R_S-\chi_{N_\chi-\frac{1}{2}}\right)\frac{u^0_{N_\chi-\frac{1}{2},k}}{\Delta\chi_i}$$

$$\frac{\left(R_S-\chi_{N_\chi+1\frac{1}{2}}\right)u^0_{N_\chi+1\frac{1}{2},k}}{\Delta\chi_{N_\chi}+\Delta\chi_{N_\chi+1}}=+\left(R_S-\chi_{N_\chi-\frac{1}{2}}\right)\frac{u^0_{N_\chi-\frac{1}{2},k}}{\Delta\chi_i}+\frac{\left(R_S-\chi_{N_\chi-\frac{1}{2}}\right)u^0_{N_\chi-\frac{1}{2},k}}{\Delta\chi_{N_\chi}+\Delta\chi_{N_\chi+1}} \tag{C.43}$$

$$u^0_{N_\chi+1\frac{1}{2},k}=\frac{\left(R_S-\chi_{N_\chi-\frac{1}{2}}\right)}{\left(R_S-\chi_{N_\chi+1\frac{1}{2}}\right)}\left[+\frac{\Delta\chi_{N_\chi}+\Delta\chi_{N_\chi+1}}{\Delta\chi_{N_\chi}}+1\right]u^0_{N_\chi-\frac{1}{2},k} \tag{C.44}$$

$$u^0_{-\frac{1}{2},k}=\frac{\left(R_S-\chi_{\frac{1}{2}}\right)}{\left(R_S-\chi_{-\frac{1}{2}}\right)}\left[+\frac{\Delta\chi_0+\Delta\chi_1}{\Delta\chi_0}+1\right]u^0_{\frac{1}{2},k} \tag{C.45}$$

$$
\begin{aligned}
u_{\frac{1}{2},k} &\approx \frac{\chi_{1+\frac{1}{2}}}{\chi_{\frac{1}{2}}} u^0_{1+\frac{1}{2},k} + \varepsilon \frac{\chi_{1+\frac{1}{2}}}{\chi_{\frac{1}{2}}} u^1_{1+\frac{1}{2},k} + \varepsilon \left(1 - \frac{\chi_{1+\frac{1}{2}}}{\chi_{\frac{1}{2}}}\right) \frac{R_S}{\chi_{\frac{1}{2}}} u^0_{1+\frac{1}{2},k} \\
&\quad - \left[\frac{1}{\chi_{\frac{1}{2}}} - \varepsilon \frac{R_S - \chi_{\frac{1}{2}}}{\chi^2_{\frac{1}{2}}}\right] \Delta\chi_1 \frac{\partial}{\partial\chi} (\chi u)_{\frac{1}{2},k} \\
u_{N_\chi+\frac{1}{2},k} &\approx \frac{\chi_{N_\chi-\frac{1}{2}}}{\chi_{N_{\chi+\frac{1}{2}}}} u^0_{N_\chi-\frac{1}{2},k} + \varepsilon \frac{\chi_{N_\chi-\frac{1}{2}}}{\chi_{N_{\chi+\frac{1}{2}}}} u^1_{N_\chi-\frac{1}{2},k} + \varepsilon \left(1 - \frac{\chi_{N_\chi-\frac{1}{2}}}{\chi_{N_{\chi+\frac{1}{2}}}}\right) \frac{R_S}{\chi_{N_{\chi+\frac{1}{2}}}} u^0_{N_\chi-\frac{1}{2},k} \\
&\quad + \left[\frac{1}{\chi_{N_{\chi+\frac{1}{2}}}} - \varepsilon \frac{R_S - \chi_{N_{\chi+\frac{1}{2}}}}{\chi^2_{N_{\chi+\frac{1}{2}}}}\right] \Delta\chi_{N_\chi} \frac{\partial}{\partial\chi} (\chi u)_{N_{\chi+\frac{1}{2}},k}
\end{aligned}
\tag{C.46}
$$

The stator wall ghost cell boundary condition for circumferential velocity is also obtained from the wall surface conjugate vorticity using Equation C.47 and the original definition of $\overline{\zeta}$. The resulting boundary condition is given by Equation C.49 and shows ghost cell boundary condition assuming that there is no contribution, and therefore no work, from outside the face centered nodes in the domain, i.e. no wall velocity. It is then noted that the ghost cell value, $v_{N_\chi,k}$, is equivalent to a reflection ghost boundary condition obtained by Taylor approximation of the stator surface speed based on the radial derivative defined in the conjugate curl operator's $\overline{\zeta}$ term with a zero rotor wall velocity. This equivalence is shown in Equation C.50. Note that the first order component of the ghost boundary value is still a *complex conjugate* of the circumferential velocity's first order value. However, this complex conjugate does not actually change the assigned boundary value as there are no additional i multiples to change the sign from the RHS to LHS.

$$
\begin{aligned}
\overline{\zeta_{N_\chi+\frac{1}{2},k}}^v &= -\frac{\cancel{4}\left[\chi_{N_\chi} + \varepsilon\left(R_S - \chi_{N_\chi}\right)\right]}{\chi_{N_\chi} + \chi_{N_\chi+1} + \varepsilon\left(2R_S - \chi_{N_\chi} - \chi_{N_\chi+1}\right)} \frac{1}{\Delta\chi_{N_\chi}} \cancel{(1+\varepsilon)} \left[v^0_{N_\chi,k} + \varepsilon\overline{v^1_{N_\chi,k}}\right] \\
&= \frac{2}{\cancel{\chi_{N_\chi+1} + \chi_{N_\chi} + \varepsilon\left(2R_S - \chi_{N_\chi} - \chi_{N_\chi+1}\right)}} \Bigg\{ \\
&\qquad \cancel{2} \frac{\left[\chi_{N_\chi+1} + \varepsilon\left(R_S - \chi_{N_\chi+1}\right)\right]\overline{v_{N_\chi+1,k}} - \left[\chi_{N_\chi} + \varepsilon\left(R_S - \chi_{N_\chi}\right)\right]\overline{v_{N_\chi,k}}}{\Delta\chi_{N_\chi} + \Delta\chi_{N_\chi+1}} \cancel{(1+\varepsilon)} \Bigg\}
\end{aligned}
\tag{C.47}
$$

$$
\begin{aligned}
\overline{\zeta_{N_\chi+\frac{1}{2},k}}^v &= -\left[\chi_{N_\chi} + \varepsilon\left(R_S - \chi_{N_\chi}\right)\right] \frac{1}{\Delta\chi_{N_\chi}} \left[v^0_{N_\chi,k} + \varepsilon\overline{v^1_{N_\chi,k}}\right] \\
&= \frac{\left[\chi_{N_\chi+1} + \varepsilon\left(R_S - \chi_{N_\chi+1}\right)\right]\overline{v_{N_\chi+1,k}} - \left[\chi_{N_\chi} + \varepsilon\left(R_S - \chi_{N_\chi}\right)\right]\overline{v_{N_\chi,k}}}{\Delta\chi_{N_\chi} + \Delta\chi_{N_\chi+1}}
\end{aligned}
\tag{C.48}
$$

$$
\begin{aligned}
v^0_{N_\chi+1,k} + \varepsilon\overline{v^1_{N_\chi+1,k}} = \\
- \frac{\left[\chi_{N_\chi} + \varepsilon\left(R_S - \chi_{N_\chi}\right)\right]}{\left[\chi_{N_\chi+1} + \varepsilon\left(R_S - \chi_{N_\chi+1}\right)\right]} \frac{\Delta\chi_{N_\chi+1}}{\Delta\chi_{N_\chi}} \left[v^0_{N_\chi,k} + \varepsilon\overline{v^1_{N_\chi,k}}\right]
\end{aligned}
\tag{C.49}
$$

$$
\begin{aligned}
0 &\approx \left(r_{N_\chi} v_{N_\chi,k}\right) + \Delta r \frac{\partial}{\partial r}\left(rv\right)_{N_\chi+\frac{1}{2},k} \\
0 &\approx r_{N_\chi}\overline{v_{N_\chi,k}} + \frac{\Delta\chi_{N_\chi}}{\Delta\chi_{N_\chi} + \Delta\chi_{N_\chi+1}}\left[r_{N_\chi+1}\overline{v_{N_\chi+1,k}} - r_{N_\chi}\overline{v_{N_\chi,k}}\right] \\
v^0_{N_\chi+1,k} + \varepsilon\overline{v^1_{N_\chi+1,k}} &\approx - \frac{\left[\chi_{N_\chi} + \varepsilon\left(R_S - \chi_{N_\chi}\right)\right]}{\left[\chi_{N_\chi+1} + \varepsilon\left(R_S - \chi_{N_\chi+1}\right)\right]} \frac{\Delta\chi_{N_\chi+1}}{\Delta\chi_{N_\chi}} \left[v^0_{N_\chi,k} + \varepsilon\overline{v^1_{N_\chi,k}}\right] \\
v^0_{N_\chi+1,k} &\approx - \frac{\chi_{N_\chi}}{\chi_{N_\chi+1}} \frac{\Delta\chi_{N_\chi+1}}{\Delta\chi_{N_\chi}} v^0_{N_\chi,k} \\
\overline{v^1_{N_\chi+1,k}} &\approx - \frac{\Delta\chi_{N_\chi+1}}{\Delta\chi_{N_\chi}} \left[\frac{R_S}{\chi_{N_\chi+1}}\left(1 - \frac{\chi_{N_\chi}}{\chi_{N_\chi+1}}\right) v^0_{N_\chi,k} + \frac{\chi_{N_\chi}}{\chi_{N_\chi+1}}\overline{v^1_{N_\chi,k}}\right]
\end{aligned}
\tag{C.50}
$$

A zero wall speed is fine for the stator surface, but it is a trivial case in turbomachinery analysis for the rotor surface, $i = \frac{1}{2}$. It is necessary to obtain a relationship for the ghost cell boundary value that allows a non-zero wall speed. As previously noted, the originally derived boundary for circumferential velocity is equivalent to a Taylor series approximation using the combined rv as the expanded variable with a radial derivative approximation. The ghost cell value for a moving rotor surface is provided in Equation C.51. A similar ghost cell value can be derived for a moving stator, but is not presented in this work.

$$
\begin{aligned}
\left(r_{\frac{1}{2}} v_{\frac{1}{2},k}\right) &\approx \left(r_1 v_{1,k}\right) - \Delta r \frac{\partial}{\partial r}\left(rv\right)_{\frac{1}{2},k} \\
r_{\frac{1}{2}} \overline{v_{\frac{1}{2},k}} &\approx r_1 \overline{v_{1,k}} - \frac{\Delta\chi_1}{\Delta\chi_1 + \Delta\chi_0}\left[r_1 \overline{v_{1,k}} - r_0 \overline{v_{0,k}}\right] \\
\overline{v_{0,k}} &\approx \frac{r_1}{r_0}\overline{v_{1,k}}\left(1 - \frac{\Delta\chi_1 + \Delta\chi_0}{\Delta\chi_1}\right) + \frac{\Delta\chi_1 + \Delta\chi_0}{\Delta\chi_1}\frac{r_{\frac{1}{2}}}{r_0}\overline{v_{\frac{1}{2},k}} \\
\overline{v_{0,k}} &\approx -\frac{\Delta\chi_0}{\Delta\chi_1}\frac{r_1}{r_0}\overline{v_{1,k}} + \left(1 + \frac{\Delta\chi_0}{\Delta\chi_1}\right)\frac{r_{\frac{1}{2}}}{r_0}\overline{v_{\frac{1}{2},k}} \\
v^0_{0,k} + \varepsilon\overline{v^1_{0,k}} &\approx \left[\frac{1}{\chi_0} - \varepsilon\frac{(R_S - \chi_0)}{\chi_0^2}\right]\left\{-\left[\chi_1 + \varepsilon\left(R_S - \chi_1\right)\right]\frac{\Delta\chi_0}{\Delta\chi_1}\left[v^0_{0,k} + \varepsilon\overline{v^1_{0,k}}\right]\right. \\
&\qquad \left. + \left[\frac{\chi_1 + \chi_0}{2} + \varepsilon\frac{2R_S - \chi_1 - \chi_0}{2}\right]\left(1 + \frac{\Delta\chi_0}{\Delta\chi_1}\right)\left[v^0_{\frac{1}{2},k} + \varepsilon\overline{v^1_{\frac{1}{2},k}}\right]\right\} \\
v^0_{0,k} &\approx -\frac{\chi_1}{\chi_0}\frac{\Delta\chi_0}{\Delta\chi_1}v^0_{1,k} + \frac{\chi_1 + \chi_0}{2\chi_0}\left(1 + \frac{\Delta\chi_0}{\Delta\chi_1}\right)v^0_{\frac{1}{2},k} \\
\overline{v^1_{0,k}} &\approx -\frac{\Delta\chi_0}{\Delta\chi_1}\left[\frac{R_S}{\chi_0}\left(1 - \frac{\chi_1}{\chi_0}\right)v^0_{1,k} + \frac{\chi_1}{\chi_0}\overline{v^1_{1,k}}\right] \\
&\qquad + \left(1 + \frac{\Delta\chi_0}{\Delta\chi_1}\right)\left[\frac{R_S}{\chi_0}\left(1 - \frac{\chi_1 + \chi_0}{2\chi_0}\right)v^0_{\frac{1}{2},k} + \frac{1}{\chi_0}\frac{\chi_1 + \chi_0}{2}\overline{v^1_{\frac{1}{2},k}}\right]
\end{aligned}
\tag{C.51}
$$

$$
\begin{aligned}
\frac{\partial}{\partial\chi}\left(\chi v\right)_{\frac{1}{2},k} &\approx 2\frac{\left[\chi_1 + \varepsilon\left(R_S - \chi_1\right)\right]v_{1,k} - \left[\chi_0 + \varepsilon\left(R_S - \chi_0\right)\right]v_{0,k}}{\Delta\chi_1 + \Delta\chi_0} \\
v_{0,k} &\approx \left[\frac{1}{\chi_0} - \varepsilon\frac{R_S - \chi_0}{\chi_0^2}\right]\left(\left[\chi_1 + \varepsilon\left(R_S - \chi_1\right)\right]v_{1,k} - \frac{(\Delta\chi_1 + \Delta\chi_0)}{2}\frac{\partial}{\partial\chi}\left(\chi v\right)_{\frac{1}{2},k}\right) \\
&\approx \frac{\chi_1}{\chi_0}v^0_{1,k} + \varepsilon\left(1 - \frac{\chi_1}{\chi_0}\right)\frac{R_S}{\chi_0}v^0_{1,k} + \varepsilon\frac{\chi_1}{\chi_0}v^1_{1,k} \\
&\qquad - \left[\frac{1}{\chi_0} - \varepsilon\frac{R_S - \chi_0}{\chi_0^2}\right]\frac{(\Delta\chi_1 + \Delta\chi_0)}{2}\frac{\partial}{\partial\chi}\left(\chi v\right)_{\frac{1}{2},k} \\
v_{N_{\chi+1},k} &\approx \left[\frac{1}{\chi_{N_{\chi+1}}} - \varepsilon\frac{R_S - \chi_{N_{\chi+1}}}{\chi^2_{N_{\chi+1}}}\right]\left(\left[\chi_{N_\chi} + \varepsilon\left(R_S - \chi_{N_\chi}\right)\right]v_{N_\chi,k} + \frac{(\Delta\chi_1 + \Delta\chi_0)}{2}\frac{\partial}{\partial\chi}\left(\chi v\right)_{N_\chi+\frac{1}{2},k}\right) \\
&\approx \frac{\chi_{N_\chi}}{\chi_{N_{\chi+1}}}v^0_{N_\chi,k} + \varepsilon\left(1 - \frac{\chi_{N_\chi}}{\chi_{N_{\chi+1}}}\right)\frac{R_S}{\chi_{N_{\chi+1}}}v^0_{N_\chi,k} + \varepsilon\frac{\chi_{N_\chi}}{\chi_{N_{\chi+1}}}v^1_{N_\chi,k} \\
&\qquad + \left[\frac{1}{\chi_{N_{\chi+1}}} - \varepsilon\frac{R_S - \chi_{N_{\chi+1}}}{\chi^2_{N_{\chi+1}}}\right]\frac{(\Delta\chi_1 + \Delta\chi_0)}{2}\frac{\partial}{\partial\chi}\left(\chi v\right)_{N_\chi+\frac{1}{2},k}
\end{aligned}
\tag{C.52}
$$

It can be demonstrated that the same procedure performed for the η vorticity terms and the axial velocity second layer ghost cells, results in the same outcome. The second layer of ghost cells is assumed to have a zero valued velocity and the first layer of ghost cells can be assigned by linear interpolation through Taylor series approximation using the directional derivatives defined in the derived conjugate curl operators of Equation C.34. These inerpolations to the boundary are equivalent to the simpler boundaries assumed in Oud's work[91] when the boundary is homogeneous

and the rotor eccentricity is assumed zero (collapsing the perturbed coordinate system back to standard cylindrical).

The rotor/stator ghost cell values for Dirichlet axial velocity are defined in Equation C.53 based on ω's radial derivative component in Equation C.34. Neumann BC's for the same surfaces are given by Equation C.59. Obviously, for nearly all cases the axial rotor and stator boundaries will have a homogeneous dirichlet BC, the fully boundary forms are included for completeness and in case of modeling upstream/downstream conditions or slip along the walls.

$$
\begin{aligned}
\left(w_{i-\frac{1}{2},k}\right) &\approx \left(w_{i,k}\right) - \Delta r \frac{\partial}{\partial r}\left(w\right)_{\frac{1}{2},k} \\
w_{R,k} &\approx w_{1,k} - \frac{\Delta\chi_1}{2}\left(1-\varepsilon\right)\left[2\frac{w_{1,n}-w_{0,n}}{\left(\Delta\chi_1+\Delta\chi_0\right)\left(1-\varepsilon\right)}\right] \\
\frac{w_{0,n}}{\Delta\chi_1+\Delta\chi_0} &\approx \frac{w_{1,n}}{\Delta\chi_1+\Delta\chi_0} + \frac{1}{\Delta\chi_1}\left(w_{R,k}-w_{1,k}\right) \\
w_{0,n} &\approx -\frac{\Delta\chi_0}{\Delta\chi_1}w_{1,n} + \left(1+\frac{\Delta\chi_0}{\Delta\chi_1}\right)w_{R,k} \\
w^0_{0,n}+\varepsilon w^1_{0,n} &\approx -\frac{\Delta\chi_0}{\Delta\chi_1}\left(w^0_{1,n}+\varepsilon w^1_{1,n}\right) + \left(1+\frac{\Delta\chi_0}{\Delta\chi_1}\right)\left(w^0_{R,k}+\varepsilon w^1_{R,k}\right) \\
w_{N_{\chi+1},n} &\approx -\frac{\Delta\chi_{N_{\chi+1}}}{\Delta\chi_{N_\chi}}w_{N_\chi,n} + \left(1+\frac{\Delta\chi_{N_{\chi+1}}}{\Delta\chi_{N_\chi}}\right)w_{S,k} \\
w^0_{N_{\chi+1},n}+\varepsilon w^1_{N_{\chi+1},n} &\approx -\frac{\Delta\chi_{N_{\chi+1}}}{\Delta\chi_{N_\chi}}\left(w^0_{N_\chi,n}+\varepsilon w^1_{N_\chi,n}\right) + \left(1+\frac{\Delta\chi_{N_{\chi+1}}}{\Delta\chi_{N_\chi}}\right)\left(w^0_{S,k}+\varepsilon w^1_{S,k}\right)
\end{aligned}
\tag{C.53}
$$

$$
\begin{aligned}
\left(w_{i-\frac{1}{2},n}\right) &\approx \left(w_{i,n}\right) - \Delta r \frac{\partial}{\partial r}\left(w\right)_{\frac{1}{2},n} \\
\frac{\partial}{\partial r}\left(w\right)_{\frac{1}{2},n} &\approx \frac{w_{1,n}-w_{0,n}}{\left(\Delta\chi_1+\Delta\chi_0\right)} \\
w_{0,n} &\approx w_{1,n} - \left(\Delta\chi_1+\Delta\chi_0\right)\frac{\partial}{\partial r}\left(w\right)_{\frac{1}{2},n} \\
w_{N_{\chi+1},n} &\approx w_{N_\chi,n} + \left(\Delta\chi_1+\Delta\chi_0\right)\frac{\partial}{\partial r}\left(w\right)_{N_\chi+\frac{1}{2},n}
\end{aligned}
\tag{C.54}
$$

C.3.2 West (Inlet) and East (Outlet) Boundaries

The axial derivative components in the ω and η vorticities from the derived conjugate curl operator are used to calculate consistent ghost node values for the East and West boundaries of radial and circumferential velocities respectively. The ghost cell values for Dirichlet and Neumann boundaries of Radial velocity are given by Equations C.55 and C.56, while the circumferential ghost cell values are given by C.57 and C.58. As with the radial velocity and the rotor/stator boundaries, the east/west

boundaries for axial velocity are trivial when a Dirichlet condition is used. Equation C.59 provides the appropriate boundary cell value for a Neumann condition on the axial velocity.

$$\begin{aligned} u_{\ell,W} &\approx u_{\ell,1} - \frac{\Delta z_1}{2}\frac{\partial u_{\ell,\frac{1}{2}}}{\partial z} \\ &\approx u_{\ell,1} - \frac{\Delta z_1}{2} 2\frac{u_{\ell,1} - u_{\ell,0}}{\Delta z_1 + \Delta z_0} \\ u_{\ell,0} &\approx -\frac{\Delta z_0}{\Delta z_1} u_{\ell,1} + \left(1 + \frac{\Delta z_0}{\Delta z_1}\right) u_{\ell,W} \\ u_{\ell,N_z+1} &\approx -\frac{\Delta z_{N_z+1}}{\Delta z_{N_z}} u_{\ell,N_z} + \left(1 + \frac{\Delta z_{N_z+1}}{\Delta z_{N_z}}\right) u_{\ell,E} \end{aligned} \tag{C.55}$$

$$\begin{aligned} \frac{\partial u_{\ell,\frac{1}{2}}}{\partial z} &\approx \frac{u_{\ell,1} - u_{\ell,0}}{\Delta z_1 + \Delta z_0} \\ u_{\ell,0} &\approx u_{\ell,1} - (\Delta z_1 + \Delta z_0)\frac{\partial u_{\ell,W}}{\partial z} \\ u_{\ell,N_z+1} &\approx u_{\ell,N_z} + \left(\Delta z_{N_z} + \Delta z_{N_z+1}\right)\frac{\partial u_{\ell,E}}{\partial z} \end{aligned} \tag{C.56}$$

$$\begin{aligned} v_{i,W} &\approx v_{i,1} - \frac{\Delta z_1}{2}\frac{\partial v_{i,\frac{1}{2}}}{\partial z} \\ &\approx v_{i,1} - \frac{\Delta z_1}{2} 2\frac{v_{i,1} - v_{i,0}}{\Delta z_1 + \Delta z_0} \\ v_{i,0} &\approx -\frac{\Delta z_0}{\Delta z_1} v_{i,1} + \left(1 + \frac{\Delta z_0}{\Delta z_1}\right) v_{i,W} \\ v_{i,N_z+1} &\approx -\frac{\Delta z_{N_z+1}}{\Delta z_{N_z}} v_{i,N_z} + \left(1 + \frac{\Delta z_{N_z+1}}{\Delta z_{N_z}}\right) v_{i,E} \end{aligned} \tag{C.57}$$

$$\begin{aligned} \frac{\partial v_{i,\frac{1}{2}}}{\partial z} &\approx \frac{v_{i,1} - v_{i,0}}{\Delta z_1 + \Delta z_0} \\ v_{i,0} &\approx v_{i,1} - (\Delta z_1 + \Delta z_0)\frac{\partial v_{i,W}}{\partial z} \\ v_{i,N_z+1} &\approx v_{i,N_z} + \left(\Delta z_{N_z} + \Delta z_{N_z+1}\right)\frac{\partial v_{i,E}}{\partial z} \end{aligned} \tag{C.58}$$

$$\begin{aligned} \frac{\partial w_{i,1}}{\partial z} &\approx \frac{w_{i,1+\frac{1}{2}} - w_{i,\frac{1}{2}}}{\Delta z_1} \\ w_{i,\frac{1}{2}} &\approx w_{i,1+\frac{1}{2}} - \Delta z_1 \frac{\partial w_{i,W}}{\partial z} \\ w_{i,N_z+\frac{1}{2}} &\approx w_{i,N_z-\frac{1}{2}} + \Delta z_{N_z}\frac{\partial w_{i,E}}{\partial z} \end{aligned} \tag{C.59}$$

Appendix D

Discrete Mimetic Operator Derivation: Tensor Gradient & Divergence

The DVTC for tensor operators functioned the same way as those for vector operators. A primary operator was selected, in this case the tensor gradient operator. This tensor gradient operator was derived from the coordinate invariant definition of the partial gradients using Equation D.1. Acting on the vector valued velocity stored in the cell face centered locations to produce a 3 by 3 tensor of velocity gradients; and based on the relationship between the tensor gradient (Equation D.2a), the strain rate tensor (Equation D.2b), and the spin tensor (Equation D.2d); it was clear that the tensor gradient terms in the off-diagonals are stored in the $\mathbf{EC}$ vector space. Similarly, since the relationship between strain tensor and vector divergence is given by Equation D.3, the diagonal terms were stored in the $\mathbf{CC}$ vector space. Note that the coordinate invariant definition of the gradient operator here does *not* match the equivalent derivatives obtained in the derived support operator for vorticity due to the adjoint conjugate nature of the derived operators.

$$\int_L \frac{\partial \vec{u}}{\partial \tau} dL = \int_L \mathscr{G}\left(\vec{u}\right) \cdot \tau dL = \vec{u}\left(\mathbf{r}_2\right) - \vec{u}\left(\mathbf{r}_1\right) \tag{D.1}$$

$$\underline{\underline{\nabla}}\vec{u} = \underline{\underline{\mathbf{E}}} + \underline{\underline{\mathbf{\Omega}}} = \begin{bmatrix} \left(\frac{1}{r}\frac{\partial(ru)}{\partial r} - \frac{u}{r}\right)_{i,k} & \left(\frac{1}{r}\frac{\partial u}{\partial \theta} - \frac{v}{r}\right)_{\ell,k} & \left(\frac{\partial u}{\partial z}\right)_{\ell,n} \\ \left(\frac{1}{r}\frac{\partial(rv)}{\partial r} - \frac{v}{r}\right)_{\ell,k} & \left(\frac{1}{r}\frac{\partial v}{\partial \theta} + \frac{u}{r}\right)_{i,k} & \left(\frac{\partial v}{\partial z}\right)_{i,n} \\ \left(\frac{\partial w}{\partial r}\right)_{\ell,n} & \left(\frac{1}{r}\frac{\partial w}{\partial \theta}\right)_{i,n} & \left(\frac{\partial w}{\partial z}\right)_{i,k} \end{bmatrix} \tag{D.2a}$$

$$\underline{\underline{\mathbf{E}}} = \frac{1}{2}\left[\nabla\vec{u} + \left(\nabla\vec{u}\right)^T\right] = \frac{1}{2}\begin{bmatrix} 2\left(\frac{1}{r}\frac{\partial(ru)}{\partial r} - \frac{u}{r}\right)_{i,k} & \frac{1}{r}\left(\frac{\partial u}{\partial\theta} + \frac{\partial(rv)}{\partial r} - 2v\right)_{\ell,k} & \left(\frac{\partial u}{\partial z} + \frac{\partial w}{\partial r}\right)_{\ell,n} \\ \frac{1}{r}\left(\frac{\partial u}{\partial\theta} + \frac{\partial(rv)}{\partial r} - 2v\right)_{\ell,k} & 2\left(\frac{1}{r}\frac{\partial v}{\partial\theta} + \frac{u}{r}\right)_{i,k} & \left(\frac{\partial v}{\partial z} + \frac{1}{r}\frac{\partial w}{\partial\theta}\right)_{i,n} \\ \left(\frac{\partial u}{\partial z} + \frac{\partial w}{\partial r}\right)_{\ell,n} & \left(\frac{\partial v}{\partial z} + \frac{1}{r}\frac{\partial w}{\partial\theta}\right)_{i,n} & 2\left(\frac{\partial w}{\partial z}\right)_{i,k} \end{bmatrix} \tag{D.2b}$$

$$\underline{\underline{\mathbf{\Omega}}} = \frac{1}{2}\left[\nabla\vec{u} - \left(\nabla\vec{u}\right)^T\right] = \frac{1}{2}\begin{bmatrix} 0 & -\zeta_{\ell,k} & \omega_{\ell,n} \\ \zeta_{\ell,k} & 0 & -\eta_{i,n} \\ -\omega_{\ell,n} & \eta_{i,n} & 0 \end{bmatrix} \tag{D.2c}$$

$$= \frac{1}{2}\begin{bmatrix} 0 & \left(\frac{1}{r}\frac{\partial u}{\partial\theta} - \frac{1}{r}\frac{\partial(rv)}{\partial r}\right)_{\ell,k} & \left(\frac{\partial u}{\partial z} - \frac{\partial w}{\partial r}\right)_{\ell,n} \\ \left(\frac{1}{r}\frac{\partial(rv)}{\partial r} - \frac{1}{r}\frac{\partial u}{\partial\theta}\right)_{\ell,k} & 0 & \left(\frac{\partial v}{\partial z} - \frac{1}{r}\frac{\partial w}{\partial\theta}\right)_{i,n} \\ \left(\frac{\partial w}{\partial r} - \frac{\partial u}{\partial z}\right)_{\ell,n} & \left(\frac{1}{r}\frac{\partial w}{\partial\theta} - \frac{\partial v}{\partial z}\right)_{i,n} & 0 \end{bmatrix} \tag{D.2d}$$

$$tr\left(\mathbf{E}\right) = \nabla\cdot\vec{u} = \left(\frac{1}{r}\frac{\partial\left(ru\right)}{\partial r} - \frac{u}{r}\right)_{i,k} + \left(\frac{\partial v}{\partial\theta} + \frac{u}{r}\right)_{i,k} + \left(\frac{\partial w}{\partial z}\right)_{i,k} = 0 \tag{D.3}$$

D.1 Discrete Tensor Gradient Operator, $\underline{\underline{\mathscr{G}}}_s\left(\vec{u}_q\right)$

Applying Equation D.1, the discrete derivatives from Appendix B, and Section 3.1 to the tensor decomposition and trace definitions of the velocity gradient tensor allowed for the construction of the discrete tensor gradient operator for velocity. The discrete divergence operator from Equation B.5 was split into each of the three diagonal terms representing the tangential gradients. Note that special attention needs to be given to the tangential velocity gradient of the radial velocity because the divergence operator is in conservative form, combining the radial gradient into a single term rather than the expanded form of Equation D.4. To maintain consistency of Equation D.3, the radial gradient term's form is not changed and instead the additional $\frac{u}{r}$ term is subracted from the radial gradient of radial velocity and added to the circumferential gradient of circumferential velocity. This fraction of radial velocity and radial position is of course averaged by a simple linear interpolation as seen with the convection terms in Section 3.6.3. The resulting discretized derivatives and averages of velocity are given in Equations D.6 to D.8. Equation D.9 shows the effect of these chain rule changes on the tensor gradient as a whole.

$$\frac{1}{r}\frac{\partial\left(ru\right)}{\partial r} = \frac{\partial u}{\partial r} + \frac{u}{r} \tag{D.4}$$

$$\frac{1}{r}\frac{\partial\left(ru\right)}{\partial r}-\frac{\partial u}{\partial r}=\frac{u}{r} \tag{D.5}$$

$$\begin{aligned}&\frac{1}{\chi_i}\frac{\chi_\ell u^0_{\ell,k}-\chi_{\ell-1}u^0_{\ell-1,k}}{\Delta\chi_i}\left(1+\varepsilon\right)-\varepsilon\frac{\left(R_S-\chi_i\right)}{\chi_i^2}\frac{\chi_\ell u^0_{\ell,k}-\chi_{\ell-1}u^0_{\ell-1,k}}{\Delta\chi_i}\\&+\varepsilon\frac{1}{\chi_i}\frac{\left[\chi_\ell u^1_{\ell,k}+\left(R_S-\chi_\ell\right)u^0_{\ell,k}\right]-\left[\chi_{\ell-1}u^1_{\ell-1,k}+\left(R_S-\chi_{\ell-1}\right)u^0_{\ell-1,k}\right]}{\Delta\chi_i}\\&-\frac{u^0_{\ell,k}-u^0_{\ell-1,k}}{\Delta\chi_i}\left(1+\varepsilon\right)-\varepsilon\frac{u^1_{\ell,k}-u^1_{\ell-1,k}}{\Delta\chi_i}=\left[\frac{1}{\chi_i}-\varepsilon\frac{\left(R_S-\chi_i\right)}{\chi_i^2}\right]\overline{u}_{i,k}\end{aligned} \tag{D.6}$$

$$\begin{aligned}\overline{u}_{i,k}=&\frac{u^0_{\ell,k}+u^0_{\ell-1,k}}{2}+\varepsilon\frac{u^1_{\ell,k}+u^1_{\ell-1,k}}{2}\\\frac{\overline{u}_{i,k}}{r_i}\approx&\left[\frac{1}{\chi_i}-\varepsilon\frac{\left(R_S-\chi_i\right)}{\chi_i^2}\right]\frac{u^0_{\ell,k}+u^0_{\ell-1,k}}{2}+\varepsilon\frac{u^1_{\ell,k}+u^1_{\ell-1,k}}{2\chi_i}\end{aligned} \tag{D.7}$$

$$\begin{aligned}\overline{v}_{\ell,k}=&\frac{v^0_{i+1,k}+v^0_{i,k}}{2}+\varepsilon\frac{v^1_{i+1,k}+v^1_{i,k}}{2}\\2\frac{\overline{v}_{\ell,k}}{r_i+r_{i+1}}\approx&\frac{v^0_{i+1,k}+v^0_{i,k}}{\chi_i+\chi_{i+1}}-\varepsilon\frac{\left(2R_S-\chi_i-\chi_{i+1}\right)}{\left(\chi_i+\chi_{i+1}\right)^2}\left(v^0_{i+1,k}+v^0_{i,k}\right)+\varepsilon\frac{v^1_{i+1,k}+v^1_{i,k}}{\chi_i+\chi_{i+1}}\end{aligned} \tag{D.8}$$

$$\nabla\vec{u}=\begin{bmatrix}\left(\frac{1}{\chi}\frac{\partial(\chi u)}{\partial\chi}\left[1+\varepsilon\right]-\frac{u}{\chi}\right)_{i,k} & \left(\frac{1}{\chi}\frac{\partial u}{\partial\theta}-\frac{v}{\chi}\right)_{\ell,k} & \left(\frac{\partial u}{\partial z}\right)_{\ell,n}\\\left(\frac{1}{\chi}\frac{\partial(\chi v)}{\partial\chi}\left[1+\varepsilon\right]-\frac{v}{\chi}\right)_{\ell,k} & \left(\frac{1}{\chi}\frac{\partial v}{\partial\theta}+\frac{u}{\chi}\right)_{i,k} & \left(\frac{\partial v}{\partial z}\right)_{i,n}\\\left(\frac{\partial w}{\partial\chi}\left[1+\varepsilon\right]\right)_{\ell,n} & \left(\frac{1}{\chi}\frac{\partial w}{\partial\theta}\right)_{i,n} & \left(\frac{\partial w}{\partial z}\right)_{i,k}\end{bmatrix} \tag{D.9}$$

$$\left(\frac{1}{\chi}\frac{\partial\left(\chi u\right)}{\partial\chi}\left[1+\varepsilon\right]-\frac{u}{\chi}\right)_{i,k}=\frac{1}{\chi_i}\frac{\chi_\ell u^0_{\ell,k}-\chi_{\ell-1}u^0_{\ell-1,k}}{\Delta\chi_i}\left(1+\varepsilon\right)-\varepsilon\frac{\left(R_S-\chi_i\right)}{\chi_i^2}\frac{\chi_\ell u^0_{\ell,k}-\chi_{\ell-1}u^0_{\ell-1,k}}{\Delta\chi_i}$$
$$+\varepsilon\frac{1}{\chi_i}\frac{\left[\chi_\ell u^1_{\ell,k}+\left(R_S-\chi_\ell\right)u^0_{\ell,k}\right]-\left[\chi_{\ell-1}u^1_{\ell-1,k}+\left(R_S-\chi_{\ell-1}\right)u^0_{\ell-1,k}\right]}{\Delta\chi_i} \tag{D.10a}$$
$$-\left[\frac{1}{\chi_i}-\varepsilon\frac{\left(R_S-\chi_i\right)}{\chi_i^2}\right]\frac{u^0_{\ell,k}+u^0_{\ell-1,k}}{2}-\varepsilon\frac{u^1_{\ell,k}+u^1_{\ell-1,k}}{2\chi_i}$$

$$\left(\frac{1}{\chi}\frac{\partial u}{\partial\theta}-\frac{v}{\chi}\right)_{\ell,k}=\frac{2}{\chi_{i+1}+\chi_i}\left\{\imath\varepsilon u^1_{\ell,k}+\imath\varepsilon\frac{\left(R_S-\chi_{\ell+1}\right)u^0_{\ell+1,k}-\left(R_S-\chi_{\ell-1}\right)u^0_{\ell-1,k}}{\Delta\chi_i+\Delta\chi_{i+1}}\right\} \tag{D.10b}$$
$$-\frac{v^0_{i+1,k}+v^0_{i,k}}{\chi_i+\chi_{i+1}}+\varepsilon\frac{\left(2R_S-\chi_i-\chi_{i+1}\right)}{\left(\chi_i+\chi_{i+1}\right)^2}\left(v^0_{i+1,k}+v^0_{i,k}\right)-\varepsilon\frac{v^1_{i+1,k}+v^1_{i,k}}{\chi_i+\chi_{i+1}}$$

$$\left(\frac{\partial u}{\partial z}\right)_{\ell,n}=2\frac{u^0_{\ell,k+1}-u^0_{\ell,k}}{\Delta z_k+\Delta z_{k+1}}+2\varepsilon\frac{u^1_{\ell,k+1}-u^1_{\ell,k}}{\Delta z_k+\Delta z_{k+1}} \tag{D.10c}$$

$$\left(\frac{1}{\chi}\frac{\partial\left(\chi v\right)}{\partial\chi}\left[1+\varepsilon\right]-\frac{v}{\chi}\right)_{\ell,k}=4\frac{1}{\chi_{i+1}+\chi_i}\frac{\chi_{i+1}v^0_{i+1,k}-\chi_i v^0_{i,k}}{\Delta\chi_i+\Delta\chi_{i+1}}\left(1+\varepsilon\right)+4\varepsilon\frac{1}{\chi_{i+1}+\chi_i}\frac{\chi_{i+1}v^1_{i+1,k}-\chi_i v^1_{i,k}}{\Delta\chi_i+\Delta\chi_{i+1}}$$
$$+4\varepsilon\frac{R_S}{\chi_{i+1}+\chi_i}\frac{v^0_{i+1,k}-v^0_{i,k}}{\Delta\chi_i+\Delta\chi_{i+1}}-8\varepsilon\frac{R_S}{\left(\chi_{i+1}+\chi_i\right)^2}\frac{\chi_{i+1}v^0_{i+1,k}-\chi_i v^0_{i,k}}{\Delta\chi_i+\Delta\chi_{i+1}} \tag{D.10d}$$
$$-\frac{v^0_{i+1,k}+v^0_{i,k}}{\chi_i+\chi_{i+1}}+\varepsilon\frac{\left(2R_S-\chi_i-\chi_{i+1}\right)}{\left(\chi_i+\chi_{i+1}\right)^2}\left(v^0_{i+1,k}+v^0_{i,k}\right)-\varepsilon\frac{v^1_{i+1,k}+v^1_{i,k}}{\chi_i+\chi_{i+1}}$$

$$\left(\frac{1}{\chi}\frac{\partial v}{\partial\theta}+\frac{u}{\chi}\right)_{i,k}=\imath\varepsilon\frac{1}{\chi_i}\left[v^1_{i,m,k}+2\left(R_S-\chi_i\right)\frac{v^0_{i+1,m,k}-v^0_{i-1,m,k}}{\Delta\chi_{i+1}+2\Delta\chi_i+\Delta\chi_{i-1}}\right] \tag{D.10e}$$
$$+\left[\frac{1}{\chi_i}-\varepsilon\frac{\left(R_S-\chi_i\right)}{\chi_i^2}\right]\frac{u^0_{\ell,k}+u^0_{\ell-1,k}}{2}+\varepsilon\frac{u^1_{\ell,k}+u^1_{\ell-1,k}}{2\chi_i}$$

$$\left(\frac{\partial v}{\partial z}\right)_{i,n}=2\frac{v^0_{i,k+1}-v^0_{i,k}}{\Delta z_k+\Delta z_{k+1}}+2\varepsilon\frac{v^1_{i,k+1}-v^1_{i,k}}{\Delta z_k+\Delta z_{k+1}} \tag{D.10f}$$

$$\left(\frac{\partial w}{\partial\chi}\left[1+\varepsilon\right]\right)_{\ell,n}=2\frac{w^0_{i+1,n}-w^0_{i,n}}{\Delta\chi_{i+1}+\Delta\chi_i}+2\varepsilon\frac{w^0_{i+1,n}-w^0_{i,n}}{\Delta\chi_{i+1}+\Delta\chi_i}+2\varepsilon\frac{w^1_{i+1,n}-w^1_{i,n}}{\Delta\chi_{i+1}+\Delta\chi_i} \tag{D.10g}$$

$$\left(\frac{1}{\chi}\frac{\partial w}{\partial\theta}\right)_{i,n}=\frac{1}{\chi_i}\imath\varepsilon w^1_{i,n}$$
$$+2\imath\varepsilon\frac{\Delta\chi_{i+1}}{\chi_i\Delta\chi_i}\left[\frac{\left(R_S-\chi_{i+1}\right)w^0_{i+1,n}}{\Delta\chi_i+2\Delta\chi_{i+1}+\Delta\chi_{i+2}}\right]-2\imath\varepsilon\frac{\Delta\chi_{i-1}}{\chi_i\Delta\chi_i}\left[\frac{\left(R_S-\chi_{i-1}\right)w^0_{i-1,n}}{\Delta\chi_{i-2}+2\Delta\chi_{i-1}+\Delta\chi_i}\right] \tag{D.10h}$$

$$\left(\frac{\partial w}{\partial z}\right)_{i,k}=\frac{w^0_{i,k,n}-w^0_{i,k,n-1}}{\Delta z_k}+\varepsilon\frac{w^1_{i,k,n}-w^1_{i,k,n-1}}{\Delta z_k} \tag{D.10i}$$

D.2 Discrete Strain Rate Tensor: $\underline{\underline{E}}$

The discrete strain rate tensor is composed from the gradient tensor as seen in the previous section's Equation D.2b. All of the discrete operators are known, so $\mathbf{E}$ is constructed term by term in Equation D.11. Note that there are only 6 terms because the strain rate tensor is symmetric. This also negates the need to distinguish between $\mathbf{Div}\,(\sigma)$ and $\nabla\cdot\sigma$ which are related through the transpose of σ. For completness, the following section defines the discrete tensor divergence as $\mathbf{Div}\,(\sigma)$.

$$\begin{aligned}\mathbf{E}^{\chi\chi}_{\mathbf{i,k}} =&\frac{1}{\chi_i}\frac{\chi_\ell u^0_{\ell,k}-\chi_{\ell-1}u^0_{\ell-1,k}}{\Delta\chi_i}(1+\varepsilon)-\varepsilon\frac{(R_S-\chi_i)}{\chi_i^2}\frac{\chi_\ell u^0_{\ell,k}-\chi_{\ell-1}u^0_{\ell-1,k}}{\Delta\chi_i}\\&+\varepsilon\frac{1}{\chi_i}\frac{\left[\chi_\ell u^1_{\ell,k}+(R_S-\chi_\ell)\,u^0_{\ell,k}\right]-\left[\chi_{\ell-1}u^1_{\ell-1,k}+(R_S-\chi_{\ell-1})\,u^0_{\ell-1,k}\right]}{\Delta\chi_i}\\&-\left[\frac{1}{\chi_i}-\varepsilon\frac{(R_S-\chi_i)}{\chi_i^2}\right]\frac{u^0_{\ell,k}+u^0_{\ell-1,k}}{2}-\varepsilon\frac{u^1_{\ell,k}+u^1_{\ell-1,k}}{2\chi_i}\end{aligned}\tag{D.11a}$$

$$\begin{aligned}\mathbf{E}^{\theta\theta}_{\mathbf{i,k}} =&\varepsilon\frac{1}{\chi_i}\left[\left(-v^I_{i,m,k}+\imath v^R_{i,m,k}\right)+2\imath\,(R_S-\chi_i)\,\frac{v^0_{i+1,m,k}-v^0_{i-1,m,k}}{\Delta\chi_{i+1}+2\Delta\chi_i+\chi_{i-1}}\right]\\&+\left[\frac{1}{\chi_i}-\varepsilon\frac{(R_S-\chi_i)}{\chi_i^2}\right]\frac{u^0_{\ell,k}+u^0_{\ell-1,k}}{2}+\varepsilon\frac{u^1_{\ell,k}+u^1_{\ell-1,k}}{2\chi_i}\end{aligned}\tag{D.11b}$$

$$\mathbf{E}^{\mathbf{zz}}_{\mathbf{i,k}} =\frac{w^0_{i,k,n}-w^0_{i,k,n-1}}{\Delta z_k}+\varepsilon\frac{w^1_{i,k,n}-w^1_{i,k,n-1}}{\Delta z_k}\tag{D.11c}$$

$$\begin{aligned}\mathbf{E}^{\chi\theta}_{\ell,\mathbf{k}} =&\frac{1}{\chi_{i+1}+\chi_i}\left\{\varepsilon\left(-u^I_{\ell,k}+\imath u^R_{\ell,k}\right)+\imath\varepsilon\frac{(R_S-\chi_{\ell+1})\,u^0_{\ell+1,k}-(R_S-\chi_{\ell-1})\,u^0_{\ell-1,k}}{\Delta\chi_i+\Delta\chi_{i+1}}\right\}\\&+2\frac{1}{\chi_{i+1}+\chi_i}\frac{\chi_{i+1}v^0_{i+1,k}-\chi_i v^0_{i,k}}{\Delta\chi_i+\Delta\chi_{i+1}}(1+\varepsilon)+2\varepsilon\frac{1}{\chi_{i+1}+\chi_i}\frac{\chi_{i+1}v^1_{i+1,k}-\chi_i v^1_{i,k}}{\Delta\chi_i+\Delta\chi_{i+1}}\\&+2\varepsilon\frac{R_S}{\chi_{i+1}+\chi_i}\frac{v^0_{i+1,k}-v^0_{i,k}}{\Delta\chi_i+\Delta\chi_{i+1}}-4\varepsilon\frac{R_S}{(\chi_{i+1}+\chi_i)^2}\frac{\chi_{i+1}v^0_{i+1,k}-\chi_i v^0_{i,k}}{\Delta\chi_i+\Delta\chi_{i+1}}\\&-\frac{v^0_{i+1,k}+v^0_{i,k}}{\chi_i+\chi_{i+1}}+\varepsilon\frac{(2R_S-\chi_i-\chi_{i+1})}{(\chi_i+\chi_{i+1})^2}\left(v^0_{i+1,k}+v^0_{i,k}\right)-\varepsilon\frac{v^1_{i+1,k}+v^1_{i,k}}{\chi_i+\chi_{i+1}}\end{aligned}\tag{D.11d}$$

$$\begin{aligned}\mathbf{E}^{\theta\mathbf{z}}_{\mathbf{i,n}} =&\frac{v^0_{i,k+1}-v^0_{i,k}}{\Delta z_k+\Delta z_{k+1}}+\varepsilon\frac{v^1_{i,k+1}-v^1_{i,k}}{\Delta z_k+\Delta z_{k+1}}\\&+\frac{1}{2\chi_i}\varepsilon\left(-w^I_{i,n}+\imath w^R_{i,n}\right)\\&+\imath\varepsilon\frac{\Delta\chi_{i+1}}{\chi_i\Delta\chi_i}\left[\frac{(R_S-\chi_{i+1})\,w^0_{i+1,n}}{\Delta\chi_i+2\Delta\chi_{i+1}+\Delta\chi_{i+2}}\right]-\imath\varepsilon\frac{\Delta\chi_{i-1}}{\chi_i\Delta\chi_i}\left[\frac{(R_S-\chi_{i-1})\,w^0_{i-1,n}}{\Delta\chi_{i-2}+2\Delta\chi_{i-1}+\Delta\chi_i}\right]\end{aligned}\tag{D.11e}$$

$$\begin{aligned}\mathbf{E}^{\mathbf{z}\chi}_{\ell,\mathbf{n}} =& \frac{u^0_{\ell,k+1}-u^0_{\ell,k}}{\Delta z_k+\Delta z_{k+1}}+\varepsilon\frac{u^1_{\ell,k+1}-u^1_{\ell,k}}{\Delta z_k+\Delta z_{k+1}}\\ &+\frac{w^0_{i+1,n}-w^0_{i,n}}{\Delta\chi_{i+1}+\Delta\chi_i}+\varepsilon\frac{w^0_{i+1,n}-w^0_{i,n}}{\Delta\chi_{i+1}+\Delta\chi_i}+\varepsilon\frac{w^1_{i+1,n}-w^1_{i,n}}{\Delta\chi_{i+1}+\Delta\chi_i}\end{aligned} \tag{D.11f}$$

D.2.1 Zeroth Order Discrete Strain Rate Tensor Operator: $\underline{\underline{E}}^0(\vec{u})$

$$\left(\mathbf{E}^{\chi\chi}_{\mathbf{i},\mathbf{k}}\right)^0 = \frac{1}{\chi_i}\frac{\chi_\ell u^0_{\ell,k}-\chi_{\ell-1}u^0_{\ell-1,k}}{\Delta\chi_i}-\frac{1}{\chi_i}\frac{u^0_{\ell,k}+u^0_{\ell-1,k}}{2} \tag{D.12a}$$

$$\left(\mathbf{E}^{\theta\theta}_{\mathbf{i},\mathbf{k}}\right)^0 = \frac{1}{\chi_i}\frac{u^0_{\ell,k}+u^0_{\ell-1,k}}{2} \tag{D.12b}$$

$$\left(\mathbf{E}^{\mathbf{zz}}_{\mathbf{i},\mathbf{k}}\right)^0 = \frac{w^0_{i,k,n}-w^0_{i,k,n-1}}{\Delta z_k} \tag{D.12c}$$

$$\left(\mathbf{E}^{\chi\theta}_{\ell,\mathbf{k}}\right)^0 = \frac{2}{\chi_{i+1}+\chi_i}\frac{\chi_{i+1}v^0_{i+1,k}-\chi_i v^0_{i,k}}{\Delta\chi_i+\Delta\chi_{i+1}}-\frac{v^0_{i+1,k}+v^0_{i,k}}{\chi_i+\chi_{i+1}} \tag{D.12d}$$

$$\left(\mathbf{E}^{\theta\mathbf{z}}_{\mathbf{i},\mathbf{n}}\right)^0 = \frac{v^0_{i,k+1}-v^0_{i,k}}{\Delta z_k+\Delta z_{k+1}} \tag{D.12e}$$

$$\left(\mathbf{E}^{\mathbf{z}\chi}_{\ell,\mathbf{n}}\right)^0 = \frac{u^0_{\ell,k+1}-u^0_{\ell,k}}{\Delta z_k+\Delta z_{k+1}}+\frac{w^0_{i+1,n}-w^0_{i,n}}{\Delta\chi_{i+1}+\Delta\chi_i} \tag{D.12f}$$

D.2.2 First Order Discrete Strain Rate Tensor Operator: $\underline{\underline{E}}^1(\vec{u})$

$$\begin{aligned}\left(\mathbf{E}^{\chi\chi}_{\mathbf{i},\mathbf{k}}\right)^1 =& \frac{1}{\chi_i}\frac{\chi_\ell u^0_{\ell,k}-\chi_{\ell-1}u^0_{\ell-1,k}}{\Delta\chi_i}-\frac{(R_S-\chi_i)}{\chi_i^2}\frac{\chi_\ell u^0_{\ell,k}-\chi_{\ell-1}u^0_{\ell-1,k}}{\Delta\chi_i}\\ &+\frac{1}{\chi_i}\frac{\left[\chi_\ell u^1_{\ell,k}+(R_S-\chi_\ell)\,u^0_{\ell,k}\right]-\left[\chi_{\ell-1}u^1_{\ell-1,k}+(R_S-\chi_{\ell-1})\,u^0_{\ell-1,k}\right]}{\Delta\chi_i}\\ &+\frac{(R_S-\chi_i)}{\chi_i^2}\frac{u^0_{\ell,k}+u^0_{\ell-1,k}}{2}-\frac{u^1_{\ell,k}+u^1_{\ell-1,k}}{2\chi_i}\end{aligned} \tag{D.13a}$$

$$\begin{aligned}\left(\mathbf{E}^{\theta\theta}_{\mathbf{i},\mathbf{k}}\right)^1 =& \frac{1}{\chi_i}\left[\left(-v^I_{i,m,k}+\dot{\imath}v^R_{i,m,k}\right)+2\dot{\imath}\,(R_S-\chi_i)\,\frac{v^0_{i+1,m,k}-v^0_{i-1,m,k}}{\Delta\chi_{i+1}+2\Delta\chi_i+\chi_{i-1}}\right]\\ &-\frac{(R_S-\chi_i)}{\chi_i^2}\frac{u^0_{\ell,k}+u^0_{\ell-1,k}}{2}+\frac{u^1_{\ell,k}+u^1_{\ell-1,k}}{2\chi_i}\end{aligned} \tag{D.13b}$$

$$\left(\mathbf{E}^{\mathbf{zz}}_{\mathbf{i},\mathbf{k}}\right)^1 = \frac{w^1_{i,k,n}-w^1_{i,k,n-1}}{\Delta z_k} \tag{D.13c}$$

$$\begin{aligned}\left(\mathbf{E}_{\ell,\mathbf{k}}^{\chi\theta}\right)^{1} =&\frac{1}{\chi_{i+1}+\chi_i}\left\{\left(-u_{\ell,k}^{I}+\imath u_{\ell,k}^{R}\right)+\imath\frac{\left(R_S-\chi_{\ell+1}\right)u_{\ell+1,k}^{0}-\left(R_S-\chi_{\ell-1}\right)u_{\ell-1,k}^{0}}{\Delta\chi_i+\Delta\chi_{i+1}}\right\}\\&+2\frac{1}{\chi_{i+1}+\chi_i}\frac{\chi_{i+1}v_{i+1,k}^{0}-\chi_i v_{i,k}^{0}}{\Delta\chi_i+\Delta\chi_{i+1}}+2\frac{1}{\chi_{i+1}+\chi_i}\frac{\chi_{i+1}v_{i+1,k}^{1}-\chi_i v_{i,k}^{1}}{\Delta\chi_i+\Delta\chi_{i+1}}\\&+2\frac{R_S}{\chi_{i+1}+\chi_i}\frac{v_{i+1,k}^{0}-v_{i,k}^{0}}{\Delta\chi_i+\Delta\chi_{i+1}}-4\frac{R_S}{\left(\chi_{i+1}+\chi_i\right)^2}\frac{\chi_{i+1}v_{i+1,k}^{0}-\chi_i v_{i,k}^{0}}{\Delta\chi_i+\Delta\chi_{i+1}}\\&+\frac{\left(2R_S-\chi_i-\chi_{i+1}\right)}{\left(\chi_i+\chi_{i+1}\right)^2}\left(v_{i+1,k}^{0}+v_{i,k}^{0}\right)-\frac{v_{i+1,k}^{1}+v_{i,k}^{1}}{\chi_i+\chi_{i+1}}\end{aligned}\tag{D.13d}$$

$$\begin{aligned}\left(\mathbf{E}_{\mathbf{i},\mathbf{n}}^{\theta\mathbf{z}}\right)^{1} =&\frac{v_{i,k+1}^{1}-v_{i,k}^{1}}{\Delta z_k+\Delta z_{k+1}}+\frac{1}{2\chi_i}\left(-w_{i,n}^{I}+\imath w_{i,n}^{R}\right)\\&+\imath\frac{\Delta\chi_{i+1}}{\chi_i\Delta\chi_i}\left[\frac{\left(R_S-\chi_{i+1}\right)w_{i+1,n}^{0}}{\Delta\chi_i+2\Delta\chi_{i+1}+\Delta\chi_{i+2}}\right]-\imath\frac{\Delta\chi_{i-1}}{\chi_i\Delta\chi_i}\left[\frac{\left(R_S-\chi_{i-1}\right)w_{i-1,n}^{0}}{\Delta\chi_{i-2}+2\Delta\chi_{i-1}+\Delta\chi_i}\right]\end{aligned}\tag{D.13e}$$

$$\left(\mathbf{E}_{\ell,\mathbf{n}}^{\mathbf{z}\chi}\right)^{1} =\frac{u_{\ell,k+1}^{1}-u_{\ell,k}^{1}}{\Delta z_k+\Delta z_{k+1}}+\frac{w_{i+1,n}^{0}-w_{i,n}^{0}}{\Delta\chi_{i+1}+\Delta\chi_i}+\frac{w_{i+1,n}^{1}-w_{i,n}^{1}}{\Delta\chi_{i+1}+\Delta\chi_i}\tag{D.13f}$$

Real First Order Discrete Strain Rate Tensor Operator: $\underline{\underline{E}}^{R}\left(\vec{u}\right)$

$$\begin{aligned}\left(\mathbf{E}_{\mathbf{i},\mathbf{k}}^{\chi\chi}\right)^{R} =&\frac{1}{\chi_i}\frac{\chi_\ell u_{\ell,k}^{0}-\chi_{\ell-1}u_{\ell-1,k}^{0}}{\Delta\chi_i}-\frac{\left(R_S-\chi_i\right)}{\chi_i^2}\frac{\chi_\ell u_{\ell,k}^{0}-\chi_{\ell-1}u_{\ell-1,k}^{0}}{\Delta\chi_i}\\&+\frac{1}{\chi_i}\frac{\left[\chi_\ell u_{\ell,k}^{R}+\left(R_S-\chi_\ell\right)u_{\ell,k}^{0}\right]-\left[\chi_{\ell-1}u_{\ell-1,k}^{R}+\left(R_S-\chi_{\ell-1}\right)u_{\ell-1,k}^{0}\right]}{\Delta\chi_i}\\&+\frac{\left(R_S-\chi_i\right)}{\chi_i^2}\frac{u_{\ell,k}^{0}+u_{\ell-1,k}^{0}}{2}-\frac{u_{\ell,k}^{R}+u_{\ell-1,k}^{R}}{2\chi_i}\end{aligned}\tag{D.14a}$$

$$\left(\mathbf{E}_{\mathbf{i},\mathbf{k}}^{\theta\theta}\right)^{R} =-\frac{1}{\chi_i}v_{i,m,k}^{I}-\frac{\left(R_S-\chi_i\right)}{\chi_i^2}\frac{u_{\ell,k}^{0}+u_{\ell-1,k}^{0}}{2}+\frac{u_{\ell,k}^{R}+u_{\ell-1,k}^{R}}{2\chi_i}\tag{D.14b}$$

$$\left(\mathbf{E}_{\mathbf{i},\mathbf{k}}^{\mathbf{zz}}\right)^{R} =\frac{w_{i,k,n}^{R}-w_{i,k,n-1}^{R}}{\Delta z_k}\tag{D.14c}$$

$$\begin{aligned}\left(\mathbf{E}_{\ell,\mathbf{k}}^{\chi\theta}\right)^{R} =&-\frac{1}{\chi_{i+1}+\chi_i}u_{\ell,k}^{I}\\&+2\frac{1}{\chi_{i+1}+\chi_i}\frac{\chi_{i+1}v_{i+1,k}^{0}-\chi_i v_{i,k}^{0}}{\Delta\chi_i+\Delta\chi_{i+1}}+2\frac{1}{\chi_{i+1}+\chi_i}\frac{\chi_{i+1}v_{i+1,k}^{R}-\chi_i v_{i,k}^{R}}{\Delta\chi_i+\Delta\chi_{i+1}}\\&+2\frac{R_S}{\chi_{i+1}+\chi_i}\frac{v_{i+1,k}^{0}-v_{i,k}^{0}}{\Delta\chi_i+\Delta\chi_{i+1}}-4\frac{R_S}{\left(\chi_{i+1}+\chi_i\right)^2}\frac{\chi_{i+1}v_{i+1,k}^{0}-\chi_i v_{i,k}^{0}}{\Delta\chi_i+\Delta\chi_{i+1}}\\&+\frac{\left(2R_S-\chi_i-\chi_{i+1}\right)}{\left(\chi_i+\chi_{i+1}\right)^2}\left(v_{i+1,k}^{0}+v_{i,k}^{0}\right)-\frac{v_{i+1,k}^{R}+v_{i,k}^{R}}{\chi_i+\chi_{i+1}}\end{aligned}\tag{D.14d}$$

$$\left(\mathbf{E}_{\mathbf{i},\mathbf{n}}^{\theta\mathbf{z}}\right)^{R} =\frac{v_{i,k+1}^{R}-v_{i,k}^{R}}{\Delta z_k+\Delta z_{k+1}}-\frac{1}{2\chi_i}w_{i,n}^{I}\tag{D.14e}$$

$$\left(\mathbf{E}^{\mathbf{z}\chi}_{\ell,\mathbf{n}}\right)^{R} = \frac{u^{R}_{\ell,k+1} - u^{R}_{\ell,k}}{\Delta z_k + \Delta z_{k+1}} + \frac{w^{0}_{i+1,n} - w^{0}_{i,n}}{\Delta\chi_{i+1} + \Delta\chi_i} + \frac{w^{R}_{i+1,n} - w^{R}_{i,n}}{\Delta\chi_{i+1} + \Delta\chi_i} \tag{D.14f}$$

Imaginary First Order Discrete Strain Rate Tensor Operator: $\underline{\underline{E}}^{I}\left(\vec{u}\right)$

$$\left(\mathbf{E}^{\chi\chi}_{\mathbf{i},\mathbf{k}}\right)^{I} = \frac{1}{\chi_i}\frac{\chi_\ell u^{I}_{\ell,k} - \chi_{\ell-1}u^{I}_{\ell-1,k}}{\Delta\chi_i} - \frac{u^{I}_{\ell,k} + u^{I}_{\ell-1,k}}{2\chi_i} \tag{D.15a}$$

$$\left(\mathbf{E}^{\theta\theta}_{\mathbf{i},\mathbf{k}}\right)^{I} = \frac{1}{\chi_i}\left[v^{R}_{i,m,k} + 2\left(R_S - \chi_i\right)\frac{v^{0}_{i+1,m,k} - v^{0}_{i-1,m,k}}{\Delta\chi_{i+1} + 2\Delta\chi_i + \chi_{i-1}}\right] + \frac{u^{I}_{\ell,k} + u^{I}_{\ell-1,k}}{2\chi_i} \tag{D.15b}$$

$$\left(\mathbf{E}^{\mathbf{zz}}_{\mathbf{i},\mathbf{k}}\right)^{I} = \frac{w^{I}_{i,k,n} - w^{I}_{i,k,n-1}}{\Delta z_k} \tag{D.15c}$$

$$\begin{aligned}\left(\mathbf{E}^{\chi\theta}_{\ell,\mathbf{k}}\right)^{I} = &\frac{1}{\chi_{i+1} + \chi_i}\left\{u^{R}_{\ell,k} + \frac{\left(R_S - \chi_{\ell+1}\right)u^{0}_{\ell+1,k} - \left(R_S - \chi_{\ell-1}\right)u^{0}_{\ell-1,k}}{\Delta\chi_i + \Delta\chi_{i+1}}\right\} \\ &+ 2\frac{1}{\chi_{i+1} + \chi_i}\frac{\chi_{i+1}v^{I}_{i+1,k} - \chi_i v^{I}_{i,k}}{\Delta\chi_i + \Delta\chi_{i+1}} - \frac{v^{I}_{i+1,k} + v^{I}_{i,k}}{\chi_i + \chi_{i+1}}\end{aligned} \tag{D.15d}$$

$$\begin{aligned}\left(\mathbf{E}^{\theta\mathbf{z}}_{\mathbf{i},\mathbf{n}}\right)^{I} = &\frac{v^{I}_{i,k+1} - v^{I}_{i,k}}{\Delta z_k + \Delta z_{k+1}} + \frac{1}{2\chi_i}w^{R}_{i,n} \\ &+ \frac{\Delta\chi_{i+1}}{\chi_i\Delta\chi_i}\left[\frac{\left(R_S - \chi_{i+1}\right)w^{0}_{i+1,n}}{\Delta\chi_i + 2\Delta\chi_{i+1} + \Delta\chi_{i+2}}\right] - \frac{\Delta\chi_{i-1}}{\chi_i\Delta\chi_i}\left[\frac{\left(R_S - \chi_{i-1}\right)w^{0}_{i-1,n}}{\Delta\chi_{i-2} + 2\Delta\chi_{i-1} + \Delta\chi_i}\right]\end{aligned} \tag{D.15e}$$

$$\left(\mathbf{E}^{\mathbf{z}\chi}_{\ell,\mathbf{n}}\right)^{I} = \frac{u^{I}_{\ell,k+1} - u^{I}_{\ell,k}}{\Delta z_k + \Delta z_{k+1}} + \frac{w^{I}_{i+1,n} - w^{I}_{i,n}}{\Delta\chi_{i+1} + \Delta\chi_i} \tag{D.15f}$$

D.3 Derivation of Discrete Tensor Divergence Operator, $\underline{\underline{\mathscr{D}}}_{,s}\left(\sigma_{\mathbf{qs}}\right)$

Like in Appendix B, the support operator method is used to construct an adjoint pair to the primary operator. However, for the tensor operators, the gradient operator is the primary and the tensor divergence is it's adjoint support operator. Equation D.17 is the tensor equivalent to the inner product relationship of Equation B.10. Note that here the tensor gradient terms of the inner product are summed as $\mathbf{EC}$ and $\mathbf{CC}$ to properly represent a discrete integration over a given cell centered on (i,k) due to the vector space locations that store the tensor gradient values. The tensor divergence is stored in the $\mathbf{FC}$ vector space as it must be incorporated directly into the conservation of momentum equations that are solved in the $\mathbf{FC}$ vector space. The inner products on the left and right hand

sides of Equation D.17 are then summed three times by collecting all terms that contain a single value of each of the three velocity components. This is analagous to steps performed in Sections B.4 and C.2, where each direction component of the tensor divergence in the $\mathbf{FC}$ vector space will be solved through the collection of the inner product terms that contain a single value of component velocity.

$$\sigma^{\mathbf{qs}} = \begin{bmatrix} \sigma^{\chi\chi}_{\mathbf{i},\mathbf{k}} & \sigma^{\chi\theta}_{\ell,\mathbf{k}} & \sigma^{\chi\mathbf{z}}_{\ell,\mathbf{n}} \\ \sigma^{\theta\chi}_{\ell,\mathbf{k}} & \sigma^{\theta\theta}_{\mathbf{i},\mathbf{k}} & \sigma^{\theta\mathbf{z}}_{\mathbf{i},\mathbf{n}} \\ \sigma^{\mathbf{z}\chi}_{\ell,\mathbf{n}} & \sigma^{\mathbf{z}\theta}_{\mathbf{i},\mathbf{n}} & \sigma^{\mathbf{zz}}_{\mathbf{i},\mathbf{k}} \end{bmatrix} \tag{D.16}$$

$$\left\langle \overline{\sigma^{\mathbf{qs}}}, \mathscr{G}^{\mathbf{s}}\left(\vec{u}^{q}\right)\right\rangle_{\mathbf{CC+EC}} = -\left\langle \overline{\mathscr{D}^{\mathbf{s}}}\left(\sigma^{\mathbf{qs}}\right), \vec{u}_{q}\right\rangle_{\mathbf{FC}} \tag{D.17}$$

$$
\begin{aligned}
\left\langle \overline{\sigma^{\mathbf{qs}}}, \mathscr{G}^{\mathbf{q},\mathbf{s}} \right\rangle \equiv \sum_{(i,k)} & \left[\chi_i + \varepsilon\left(R_S - \chi_i\right)\right] \Delta\chi_i \left(1-\varepsilon\right) \Delta\theta \Delta z_k \\
& \left[\overline{\sigma^{\chi\chi}} \mathscr{G}^{\mathbf{u},\chi}\left(u_{\ell-1}, \boxed{u_\ell}\right) + \overline{\sigma^{\theta\theta}} \mathscr{G}^{\mathbf{v},\theta}\left(u_{\ell-1}, \boxed{u_\ell}, v_{i-1}, \boxed{v_i}, v_{i+1}\right) \right. \\
& \left. + \overline{\sigma^{\mathbf{zz}}} \mathscr{G}^{\mathbf{w},\mathbf{z}}\left(w_{n-1}, \boxed{w_n}\right) \right]_{i,k} \\
& + \frac{\Delta\chi_i \left(1-\varepsilon\right) \Delta\theta \Delta z_k}{2} \Bigg\{ \\
& \left[\chi_i + \varepsilon\left(R_S - \chi_i\right)\right] \\
& \left[\left\{ \overline{\sigma^{\theta\mathbf{z}}} \mathscr{G}^{\mathbf{v},\mathbf{z}}\left(v_{k-1}, \boxed{v_k}\right) + \overline{\sigma^{\mathbf{z}\theta}} \mathscr{G}^{\mathbf{w},\theta}\left(w_{i-1,n-1}, w_{i,n-1}, w_{i+1,n-1}\right) \right\}_{i,n-1} \right. \\
& \left. + \left\{ \overline{\sigma^{\theta\mathbf{z}}} \mathscr{G}^{\mathbf{v},\mathbf{z}}\left(\boxed{v_k}, v_{k+1}\right) + \overline{\sigma^{\mathbf{z}\theta}} \mathscr{G}^{\mathbf{w},\theta}\left(w_{i-1,n}, \boxed{w_{i,n}}, w_{i+1,n}\right) \right\}_{i,n} \right] \\
& + \left[\chi_{\ell-1} + \varepsilon\left(R_S - \chi_{\ell-1}\right)\right] \\
& \left[\frac{\overline{\sigma^{\chi\mathbf{z}}} \mathscr{G}^{\mathbf{u},\mathbf{z}}\left(u_{\ell-1,k-1}, u_{\ell-1,k}\right) + \overline{\sigma^{\mathbf{z}\chi}} \mathscr{G}^{\mathbf{w},\chi}\left(w_{i-1,n-1}, w_{i,n-1}\right)}{2}_{\ell-1,n-1} \right. \\
& \left. + \frac{\overline{\sigma^{\chi\mathbf{z}}} \mathscr{G}^{\mathbf{u},\mathbf{z}}\left(u_{\ell-1,k}, u_{\ell-1,k+1}\right) + \overline{\sigma^{\mathbf{z}\chi}} \mathscr{G}^{\mathbf{w},\chi}\left(w_{i-1,n}, \boxed{w_{i,n}}\right)}{2}_{\ell-1,n} \right] \\
& + \left[\chi_\ell + \varepsilon\left(R_S - \chi_\ell\right)\right] \\
& \left[\frac{\overline{\sigma^{\chi\mathbf{z}}} \mathscr{G}^{\mathbf{u},\mathbf{z}}\left(u_{\ell,k-1}, \boxed{u_{\ell,k}}\right) + \overline{\sigma^{\mathbf{z}\chi}} \mathscr{G}^{\mathbf{w},\chi}\left(w_{i,n-1}, w_{i+1,n-1}\right)}{2}_{\ell,n-1} \right. \\
& \left. + \frac{\overline{\sigma^{\chi\mathbf{z}}} \mathscr{G}^{\mathbf{u},\mathbf{z}}\left(\boxed{u_{\ell,k}}, u_{\ell,k+1}\right) + \overline{\sigma^{\mathbf{z}\chi}} \mathscr{G}^{\mathbf{w},\chi}\left(\boxed{w_{i,n}}, w_{i+1,n}\right)}{2}_{\ell,n} \right] \\
& + \frac{\chi_i + \chi_{i-1} + \varepsilon\left(2R_S - \chi_i - \chi_{i-1}\right)}{2} \\
& \left\{ \overline{\sigma^{\chi\theta}} \mathscr{G}^{\mathbf{u},\theta}\left(u_{\ell-2}, u_{\ell-1}, \boxed{u_\ell}, v_{i-1,k}, \boxed{v_{i,k}}\right) + \overline{\sigma^{\theta\chi}} \mathscr{G}^{\mathbf{v},\chi}\left(v_{i-1}, \boxed{v_i}\right) \right\}_{\ell-1,k} \\
& + \frac{\chi_i + \chi_{i+1} + \varepsilon\left(2R_S - \chi_i - \chi_{i+1}\right)}{2} \\
& \left\{ \overline{\sigma^{\chi\theta}} \mathscr{G}^{\mathbf{u},\theta}\left(u_{\ell-1}, \boxed{u_\ell}, u_{\ell+1}, \boxed{v_{i,k}}, v_{i+1,k}\right) + \overline{\sigma^{\theta\chi}} \mathscr{G}^{\mathbf{v},\chi}\left(\boxed{v_i}, v_{i+1}\right) \right\}_{\ell,k} \Bigg\}
\end{aligned}
\tag{D.18}
$$

$$\begin{aligned}\left\langle \overline{\mathscr{D}^{\mathbf{qs,s}}}\left(\sigma^{\mathbf{qs}}\right), \vec{u}_q \right\rangle \equiv \sum_{(i,k)} \frac{\Delta\chi_i \left(1-\varepsilon\right) \Delta\theta \Delta z_k}{2} \Big\{ \\ \left[\chi_{\ell-1} + \varepsilon\left(R_S - \chi_{\ell-1}\right)\right] \overline{\mathscr{D}^{,\chi}{}_{\ell-1,k}} u_{\ell-1,k} \\ + \left[\chi_{\ell} + \varepsilon\left(R_S - \chi_{\ell}\right)\right] \overline{\mathscr{D}^{,\chi}{}_{\ell,k}}\, u_{\ell,k} \\ + 2\left[\chi_i + \varepsilon\left(R_S - \chi_i\right)\right] \overline{\mathscr{D}^{,\theta}{}_{i,k}}\, v_{i,k} \\ + \left[\chi_i + \varepsilon\left(R_S - \chi_i\right)\right] \left[\overline{\mathscr{D}^{,\mathbf{z}}{}_{i,n-1}} w_{i,n-1} + \overline{\mathscr{D}^{,\mathbf{z}}{}_{i,n}}\, w_{i,n}\right] \Big\}\end{aligned} \tag{D.19}$$

D.3.1 Collect Radial Discrete Tensor Divergence Terms in Inner Product

Begining by collecting all inner product contributions that contain $u_{\ell,k}$ from cells (i,k) and (i+1,k) of the $\mathbf{FC}$ inner product space of the RHS; and cells (i,k-1), (i+1,k-1), (i-1,k), (i,k), (i+1,k), (i+2,k), (i,k+1), and (i+1,k+1) from the $\mathbf{CC}$ and $\mathbf{EC}$ inner product spaces of the LHS.

$$\begin{aligned}\left\langle \overline{\mathscr{D}^{\mathbf{qs,s}}}\left(\sigma^{\mathbf{qs}}\right), \vec{u}_q \right\rangle|_{u_{\ell,k}} = \\ \frac{\Delta\chi_i \left(1-\varepsilon\right) \Delta z_k}{2} \left[\chi_{\ell} + \varepsilon\left(R_S - \chi_{\ell}\right)\right] \overline{\mathscr{D}^{,\chi}{}_{\ell,k}}\, u_{\ell,k} \Big\} (i,k) \\ + \frac{\Delta\chi_{i+1} \left(1-\varepsilon\right) \Delta z_k}{2} \left[\chi_{\ell} + \varepsilon\left(R_S - \chi_{\ell}\right)\right] \overline{\mathscr{D}^{,\chi}{}_{\ell,k}}\, u_{\ell,k} \Big\} (i+1,k) \\ \left\langle \overline{\mathscr{D}^{\mathbf{qs,s}}}\left(\sigma^{\mathbf{qs}}\right), \vec{u}_q \right\rangle|_{u_{\ell,k}} = \\ \frac{\Delta\chi_i + \Delta\chi_{i+1}}{2} \left(1-\varepsilon\right) \Delta z_k \left[\chi_{\ell} + \varepsilon\left(R_S - \chi_{\ell}\right)\right] \overline{\mathscr{D}^{,\chi}{}_{\ell,k}}\, u_{\ell,k}\end{aligned} \tag{D.20}$$

$$
\begin{aligned}
&\left\langle \overline{\sigma^{\mathbf{qs}}}, \mathscr{G}^{\mathbf{q,s}} \right\rangle |_{u_{\ell,k}} = \\
&\left.\begin{aligned}
&\frac{\Delta\chi_i\,(1-\varepsilon)\,\Delta z_{k-1}}{2}\left[\chi_\ell + \varepsilon\,(R_S - \chi_\ell)\right]\frac{\overline{\sigma^{\chi_{\mathbf{z}}}_{\ell,\mathbf{n-1}}}\mathscr{G}^{\mathbf{u,z}}\left(u_{\ell,k-1},\, u_{\ell,k}\right)}{2}\Bigg\}(i,k-1)\\
&+\frac{\Delta\chi_{i+1}\,(1-\varepsilon)\,\Delta z_{k-1}}{2}\left[\chi_\ell + \varepsilon\,(R_S - \chi_\ell)\right]\frac{\overline{\sigma^{\chi_{\mathbf{z}}}_{\ell,\mathbf{n-1}}}\mathscr{G}^{\mathbf{u,z}}\left(u_{\ell,k-1},\, u_{\ell,k}\right)}{2}\Bigg\}(i+1,k-1)\\
&+\frac{\Delta\chi_{i-1}\,(1-\varepsilon)\,\Delta z_k}{2}\frac{\chi_i+\chi_{i-1}+\varepsilon\,(2R_S-\chi_i-\chi_{i-1})}{2}\overline{\sigma^{\chi_\theta}_{\ell-\mathbf{1},\mathbf{k}}}\mathscr{G}^{\mathbf{u},\theta}\left(u_{\ell-2},u_{\ell-1},\,u_\ell\right)\Bigg\}(i-1,k)\\
&\left.\begin{aligned}
&+\left[\chi_i+\varepsilon\,(R_S-\chi_i)\right]\Delta\chi_i\,(1-\varepsilon)\,\Delta z_k\\
&\quad\left[\overline{\sigma^{\chi\chi}_{\mathbf{i},\mathbf{k}}}\mathscr{G}^{\mathbf{u},\chi}\left(u_{\ell-1},\,u_\ell\right)+\overline{\sigma^{\theta\theta}_{\mathbf{i},\mathbf{k}}}\mathscr{G}^{\mathbf{v},\theta}\left(u_{\ell-1},\,u_\ell,v_{i-1},v_i,v_{i+1}\right)\right]\\
&+\frac{\Delta\chi_i\,(1-\varepsilon)\,\Delta z_k}{2}\left[\chi_\ell+\varepsilon\,(R_S-\chi_\ell)\right]\\
&\quad\left[\frac{\overline{\sigma^{\chi_{\mathbf{z}}}_{\ell,\mathbf{n-1}}}\mathscr{G}^{\mathbf{u,z}}\left(u_{\ell,k-1},\,u_{\ell,k}\right)}{2}+\frac{\overline{\sigma^{\chi_{\mathbf{z}}}_{\ell,\mathbf{n}}}\mathscr{G}^{\mathbf{u,z}}\left(u_{\ell,k},\,u_{\ell,k+1}\right)}{2}\right]\\
&+\frac{\Delta\chi_i\,(1-\varepsilon)\,\Delta z_k}{2}\frac{\chi_i+\chi_{i-1}+\varepsilon\,(2R_S-\chi_i-\chi_{i-1})}{2}\overline{\sigma^{\chi_\theta}_{\ell-\mathbf{1},\mathbf{k}}}\mathscr{G}^{\mathbf{u},\theta}\left(u_{\ell-2},u_{\ell-1},\,u_\ell\right)\\
&+\frac{\Delta\chi_i\,(1-\varepsilon)\,\Delta z_k}{2}\frac{\chi_i+\chi_{i+1}+\varepsilon\,(2R_S-\chi_i-\chi_{i+1})}{2}\overline{\sigma^{\chi_\theta}_{\ell,\mathbf{k}}}\mathscr{G}^{\mathbf{u},\theta}\left(u_{\ell-1},\,u_\ell,u_{\ell+1}\right)\Bigg\}(i,k)\\
&\left.\begin{aligned}
&+\left[\chi_{i+1}+\varepsilon\,(R_S-\chi_{i+1})\right]\Delta\chi_{i+1}\,(1-\varepsilon)\,\Delta z_k\\
&\quad\left[\overline{\sigma^{\chi\chi}_{\mathbf{i+1},\mathbf{k}}}\mathscr{G}^{\mathbf{u},\chi}\left(u_\ell,\,u_{\ell+1}\right)+\overline{\sigma^{\theta\theta}_{\mathbf{i+1},\mathbf{k}}}\mathscr{G}^{\mathbf{v},\theta}\left(u_\ell,\,u_{\ell+1},v_{i-1},v_i,v_{i+1}\right)\right]\\
&+\frac{\Delta\chi_{i+1}\,(1-\varepsilon)\,\Delta z_k}{2}\left[\chi_\ell+\varepsilon\,(R_S-\chi_\ell)\right]\\
&\quad\left[\frac{\overline{\sigma^{\chi_{\mathbf{z}}}_{\ell,\mathbf{n-1}}}\mathscr{G}^{\mathbf{u,z}}\left(u_{\ell,k-1},\,u_{\ell,k}\right)}{2}+\frac{\overline{\sigma^{\chi_{\mathbf{z}}}_{\ell,\mathbf{n}}}\mathscr{G}^{\mathbf{u,z}}\left(u_{\ell,k},\,u_{\ell,k+1}\right)}{2}\right]\\
&+\frac{\Delta\chi_{i+1}\,(1-\varepsilon)\,\Delta z_k}{2}\frac{\chi_i+\chi_{i+1}+\varepsilon\,(2R_S-\chi_i-\chi_{i+1})}{2}\overline{\sigma^{\chi_\theta}_{\ell,\mathbf{k}}}\mathscr{G}^{\mathbf{u},\theta}\left(u_{\ell-1},\,u_\ell,u_{\ell+1}\right)\\
&+\frac{\Delta\chi_{i+1}\,(1-\varepsilon)\,\Delta z_k}{2}\frac{\chi_{i+2}+\chi_{i+1}+\varepsilon\,(2R_S-\chi_{i+2}-\chi_{i+1})}{2}\overline{\sigma^{\chi_\theta}_{\ell+\mathbf{1},\mathbf{k}}}\mathscr{G}^{\mathbf{u},\theta}\left(u_\ell,u_{\ell+1},u_{\ell+2}\right)\Bigg\}(i+1,k)\\
&+\frac{\Delta\chi_{i+2}\,(1-\varepsilon)\,\Delta z_k}{2}\frac{\chi_{i+2}+\chi_{i+1}+\varepsilon\,(2R_S-\chi_{i+2}-\chi_{i+1})}{2}\overline{\sigma^{\chi_\theta}_{\ell+\mathbf{1},\mathbf{k}}}\mathscr{G}^{\mathbf{u},\theta}\left(u_\ell,u_{\ell+1},u_{\ell+2}\right)\Bigg\}(i+2,k)\\
&+\frac{\Delta\chi_i\,(1-\varepsilon)\,\Delta z_{k+1}}{2}\left[\chi_\ell+\varepsilon\,(R_S-\chi_\ell)\right]\frac{\overline{\sigma^{\chi_{\mathbf{z}}}_{\ell,\mathbf{n}}}\mathscr{G}^{\mathbf{u,z}}\left(u_{\ell,k},\,u_{\ell,k+1}\right)}{2}\Bigg\}(i,k+1)\\
&+\frac{\Delta\chi_{i+1}\,(1-\varepsilon)\,\Delta z_{k+1}}{2}\left[\chi_\ell+\varepsilon\,(R_S-\chi_\ell)\right]\frac{\overline{\sigma^{\chi_{\mathbf{z}}}_{\ell,\mathbf{n}}}\mathscr{G}^{\mathbf{u,z}}\left(u_{\ell,k},\,u_{\ell,k+1}\right)}{2}\Bigg\}(i+1,k+1)
\end{aligned}
$$

(D.21)

$$
\begin{aligned}
&-\frac{\Delta\chi_i+\Delta\chi_{i+1}}{2}\Delta z_k\left[\chi_\ell+\varepsilon\left(R_S-\chi_\ell\right)\right]\overline{\mathscr{D}^{,\chi}{}_{\ell,k}}\,u_{\ell,k}=\\
&\frac{\Delta\chi_i+\Delta\chi_{i+1}}{2}\left[\chi_\ell+\varepsilon\left(R_S-\chi_\ell\right)\right]\frac{\Delta z_k+\Delta z_{k-1}}{2}\overline{\sigma^{\chi\mathbf{z}}_{\ell,\mathbf{n-1}}}\mathcal{G}^{\mathbf{u},\mathbf{z}}\left(u_{\ell,k-1},\,u_{\ell,k}\right)\\
&+\frac{\Delta\chi_i+\Delta\chi_{i+1}}{2}\left[\chi_\ell+\varepsilon\left(R_S-\chi_\ell\right)\right]\frac{\Delta z_k+\Delta z_{k+1}}{2}\overline{\sigma^{\chi\mathbf{z}}_{\ell,\mathbf{n}}}\mathcal{G}^{\mathbf{u},\mathbf{z}}\left(u_{\ell,k},u_{\ell,k+1}\right)\\
&+\frac{\Delta\chi_i+\Delta\chi_{i+1}}{2}\Delta z_k\frac{\chi_i+\chi_{i+1}+\varepsilon\left(2R_S-\chi_i-\chi_{i+1}\right)}{2}\overline{\sigma^{\chi\theta}_{\ell,\mathbf{k}}}\mathcal{G}^{\mathbf{u},\theta}\left(u_{\ell-1},\,u_\ell\,,u_{\ell+1}\right)\\
&+\frac{\Delta\chi_{i-1}+\Delta\chi_i}{2}\Delta z_k\frac{\chi_i+\chi_{i-1}}{2}\overline{\sigma^{\chi\theta}_{\ell-\mathbf{1},\mathbf{k}}}\mathcal{G}^{\mathbf{u},\theta}\left(u_{\ell-2},u_{\ell-1},\,u_\ell\,\right)\\
&+\frac{\Delta\chi_{i+1}+\Delta\chi_{i+2}}{2}\Delta z_k\frac{\chi_{i+2}+\chi_{i+1}}{2}\overline{\sigma^{\chi\theta}_{\ell+\mathbf{1},\mathbf{k}}}\mathcal{G}^{\mathbf{u},\theta}\left(u_\ell\,,u_{\ell+1},u_{\ell+2}\right)\\
&+\left[\chi_i+\varepsilon\left(R_S-\chi_i\right)\right]\Delta\chi_i\Delta z_k\overline{\sigma^{\chi\chi}_{\mathbf{i},\mathbf{k}}}\mathcal{G}^{\mathbf{u},\chi}\left(u_{\ell-1},\,u_\ell\,\right)\\
&+\left[\chi_{i+1}+\varepsilon\left(R_S-\chi_{i+1}\right)\right]\Delta\chi_{i+1}\Delta z_k\overline{\sigma^{\chi\chi}_{\mathbf{i+1},\mathbf{k}}}\mathcal{G}^{\mathbf{u},\chi}\left(u_\ell\,,u_{\ell+1}\right)\\
&+\left[\chi_i+\varepsilon\left(R_S-\chi_i\right)\right]\Delta\chi_i\Delta z_k\overline{\sigma^{\theta\theta}_{\mathbf{i},\mathbf{k}}}\mathcal{G}^{\mathbf{v},\theta}\left(u_{\ell-1},\,u_\ell\,,v_{i-1},v_i,v_{i+1}\right)\\
&+\left[\chi_{i+1}+\varepsilon\left(R_S-\chi_{i+1}\right)\right]\Delta\chi_{i+1}\Delta z_k\overline{\sigma^{\theta\theta}_{\mathbf{i+1},\mathbf{k}}}\mathcal{G}^{\mathbf{v},\theta}\left(u_\ell\,,u_{\ell+1},v_{i-1},v_i,v_{i+1}\right)
\end{aligned}
\tag{D.22}
$$

$$
\mathscr{D}^{,\mathbf{r}}\left(\sigma^{qs}\right)\equiv\frac{\partial\sigma^{rr}}{\partial r}+\frac{1}{r}\left[\frac{\partial\sigma^{r\theta}}{\partial\theta}+\sigma^{rr}-\sigma^{\theta\theta}\right]+\frac{\partial\sigma^{rz}}{\partial z}
\tag{D.23}
$$

$$
\begin{aligned}
&\overline{\mathscr{D}^{,\chi}{}_{\ell,k}}=\\
&2\frac{\sigma^{\chi\chi}_{\mathbf{i+1},\mathbf{k}}{}^{0}-\sigma^{\chi\chi0}_{\mathbf{i},\mathbf{k}}}{\Delta\chi_i+\Delta\chi_{i+1}}\left(1+\varepsilon\right)+2\varepsilon\frac{\overline{\sigma^{\chi\chi}_{\mathbf{i+1},\mathbf{k}}{}^{1}}-\overline{\sigma^{\chi\chi1}_{\mathbf{i},\mathbf{k}}}}{\Delta\chi_i+\Delta\chi_{i+1}}\\
&-\frac{\imath\varepsilon}{\chi_\ell}\overline{\sigma^{\chi\theta1}_{\ell,\mathbf{k}}}+\imath\varepsilon\frac{\left(R_S-\chi_\ell\right)}{\chi_\ell}\frac{\sigma^{\chi\theta}_{\ell+\mathbf{1},\mathbf{k}}{}^{0}-\sigma^{\chi\theta}_{\ell-\mathbf{1},\mathbf{k}}{}^{0}}{\Delta\chi_i+\Delta\chi_{i+1}}\\
&+\left[\frac{1}{\chi_\ell}-\varepsilon\frac{\left(R_S-\chi_\ell\right)}{\chi_\ell^2}\right]\left(\frac{\Delta\chi_i\sigma^{\chi\chi0}_{\mathbf{i},\mathbf{k}}+\Delta\chi_{i+1}\sigma^{\chi\chi}_{\mathbf{i+1},\mathbf{k}}{}^{0}}{\Delta\chi_i+\Delta\chi_{i+1}}-\frac{\Delta\chi_i\sigma^{\theta\theta0}_{\mathbf{i},\mathbf{k}}+\Delta\chi_{i+1}\sigma^{\theta\theta}_{\mathbf{i+1},\mathbf{k}}{}^{0}}{\Delta\chi_i+\Delta\chi_{i+1}}\right)\\
&+\frac{\varepsilon}{\chi_\ell}\left(\frac{\Delta\chi_i\overline{\sigma^{\chi\chi1}_{\mathbf{i},\mathbf{k}}}+\Delta\chi_{i+1}\overline{\sigma^{\chi\chi}_{\mathbf{i+1},\mathbf{k}}{}^{1}}}{\Delta\chi_i+\Delta\chi_{i+1}}-\frac{\Delta\chi_i\overline{\sigma^{\theta\theta1}_{\mathbf{i},\mathbf{k}}}+\Delta\chi_{i+1}\overline{\sigma^{\theta\theta}_{\mathbf{i+1},\mathbf{k}}{}^{1}}}{\Delta\chi_i+\Delta\chi_{i+1}}\right)\\
&+\frac{\sigma^{\chi\mathbf{z}}_{\ell,\mathbf{n}}{}^{0}-\sigma^{\chi\mathbf{z}}_{\ell,\mathbf{n-1}}{}^{0}}{\Delta z_k}+\varepsilon\frac{\overline{\sigma^{\chi\mathbf{z}}_{\ell,\mathbf{n}}{}^{1}}-\overline{\sigma^{\chi\mathbf{z}}_{\ell,\mathbf{n-1}}{}^{1}}}{\Delta z_k}
\end{aligned}
\tag{D.24}
$$

D.3.2 Collect Circumferential Discrete Tensor Divergence Terms in Inner Product

Then collect inner product contributions that contain $v_{i,k}$ from cell (i,k) of the $\mathbf{FC}$ inner product space of the RHS; and cells (i,k-1), (i-1,k), (i,k), (i+1,k), and (i,k+1) from the $\mathbf{CC}$ and $\mathbf{EC}$ inner product

spaces of the LHS.

$$
\begin{aligned}
&\left\langle \overline{\sigma^{\mathbf{qs}}}, \mathscr{G}^{\mathbf{q,s}} \right\rangle |_{v_{i,k}} = \\
&\left.\frac{\Delta\chi_i\left(1-\varepsilon\right)\Delta z_{k-1}}{2}\left[\chi_i+\varepsilon\left(R_S-\chi_i\right)\right]\overline{\sigma^{\theta\mathbf{z}}_{\mathbf{i,n-1}}}\mathscr{G}^{\mathbf{v},\mathbf{z}}\left(v_{k-1},\boxed{v_k}\right)\right\}(i,k-1)\\
&\left.\begin{aligned}
&+\left[\chi_{i-1}+\varepsilon\left(R_S-\chi_{i-1}\right)\right]\Delta\chi_{i-1}\left(1-\varepsilon\right)\Delta z_k\overline{\sigma^{\theta\theta}_{\mathbf{i-1,k}}}\mathscr{G}^{\mathbf{v},\theta}\left(u_{\ell-2},u_{\ell-1},v_{i-2},v_{i-1},\boxed{v_i}\right)\\
&+\frac{\Delta\chi_{i-1}\left(1-\varepsilon\right)\Delta z_k}{2}\frac{\chi_i+\chi_{i-1}+\varepsilon\left(2R_S-\chi_i-\chi_{i-1}\right)}{2}\overline{\sigma^{\chi\theta}_{\ell-\mathbf{1,k}}}\mathscr{G}^{\mathbf{u},\theta}\left(v_{i-1},\boxed{v_i}\right)\\
&+\frac{\Delta\chi_{i-1}\left(1-\varepsilon\right)\Delta z_k}{2}\frac{\chi_i+\chi_{i-1}+\varepsilon\left(2R_S-\chi_i-\chi_{i-1}\right)}{2}\overline{\sigma^{\theta\chi}_{\ell-\mathbf{1,k}}}\mathscr{G}^{\mathbf{v},\chi}\left(v_{i-1},\boxed{v_i}\right)
\end{aligned}\right\}(i-1,k)\\
&\left.\begin{aligned}
&+\left[\chi_i+\varepsilon\left(R_S-\chi_i\right)\right]\Delta\chi_i\left(1-\varepsilon\right)\Delta\theta\Delta z_k\overline{\sigma^{\theta\theta}_{\mathbf{i,k}}}\mathscr{G}^{\mathbf{v},\theta}\left(u_{\ell-1},u_\ell,v_{i-1},\boxed{v_i},v_{i+1}\right)\\
&+\frac{\Delta\chi_i\left(1-\varepsilon\right)\Delta\theta\Delta z_k}{2}\left[\chi_i+\varepsilon\left(R_S-\chi_i\right)\right]\\
&\qquad\left[\overline{\sigma^{\theta\mathbf{z}}_{\mathbf{i,n-1}}}\mathscr{G}^{\mathbf{v},\mathbf{z}}\left(v_{k-1},\boxed{v_k}\right)+\overline{\sigma^{\theta\mathbf{z}}_{\mathbf{i,n}}}\mathscr{G}^{\mathbf{v},\mathbf{z}}\left(\boxed{v_k},v_{k+1}\right)\right]\\
&+\frac{\Delta\chi_i\left(1-\varepsilon\right)\Delta\theta\Delta z_k}{2}\frac{\chi_i+\chi_{i-1}+\varepsilon\left(2R_S-\chi_i-\chi_{i-1}\right)}{2}\left\{\overline{\sigma^{\chi\theta}_{\ell-\mathbf{1,k}}}\mathscr{G}^{\mathbf{u},\theta}\left(v_{i-1},\boxed{v_i}\right)\right\}\\
&+\frac{\Delta\chi_i\left(1-\varepsilon\right)\Delta\theta\Delta z_k}{2}\frac{\chi_i+\chi_{i+1}+\varepsilon\left(2R_S-\chi_i-\chi_{i+1}\right)}{2}\left\{\overline{\sigma^{\chi\theta}_{\ell,\mathbf{k}}}\mathscr{G}^{\mathbf{u},\theta}\left(\boxed{v_i},v_{i+1}\right)\right\}\\
&+\frac{\Delta\chi_i\left(1-\varepsilon\right)\Delta\theta\Delta z_k}{2}\frac{\chi_i+\chi_{i-1}+\varepsilon\left(2R_S-\chi_i-\chi_{i-1}\right)}{2}\overline{\sigma^{\theta\chi}_{\ell-\mathbf{1,k}}}\mathscr{G}^{\mathbf{v},\chi}\left(v_{i-1},\boxed{v_i}\right)\\
&+\frac{\Delta\chi_i\left(1-\varepsilon\right)\Delta\theta\Delta z_k}{2}\frac{\chi_i+\chi_{i+1}+\varepsilon\left(2R_S-\chi_i-\chi_{i+1}\right)}{2}\overline{\sigma^{\theta\chi}_{\ell,\mathbf{k}}}\mathscr{G}^{\mathbf{v},\chi}\left(\boxed{v_i},v_{i+1}\right)
\end{aligned}\right\}(i,k)\\
&\left.\begin{aligned}
&+\left[\chi_{i+1}+\varepsilon\left(R_S-\chi_{i+1}\right)\right]\Delta\chi_{i+1}\left(1-\varepsilon\right)\Delta z_k\overline{\sigma^{\theta\theta}_{\mathbf{i+1,k}}}\mathscr{G}^{\mathbf{v},\theta}\left(u_\ell,u_{\ell+1},\boxed{v_i},v_{i+1},v_{i+2}\right)\\
&+\frac{\Delta\chi_{i+1}\left(1-\varepsilon\right)\Delta z_k}{2}\frac{\chi_i+\chi_{i+1}+\varepsilon\left(2R_S-\chi_i-\chi_{i+1}\right)}{2}\overline{\sigma^{\chi\theta}_{\ell,\mathbf{k}}}\mathscr{G}^{\mathbf{u},\theta}\left(\boxed{v_i},v_{i+1}\right)\\
&+\frac{\Delta\chi_{i+1}\left(1-\varepsilon\right)\Delta z_k}{2}\frac{\chi_i+\chi_{i+1}+\varepsilon\left(2R_S-\chi_i-\chi_{i+1}\right)}{2}\overline{\sigma^{\theta\chi}_{\ell,\mathbf{k}}}\mathscr{G}^{\mathbf{v},\chi}\left(\boxed{v_i},v_{i+1}\right)
\end{aligned}\right\}(i+1,k)\\
&\left.+\frac{\Delta\chi_i\left(1-\varepsilon\right)\Delta z_{k+1}}{2}\left[\chi_i+\varepsilon\left(R_S-\chi_i\right)\right]\overline{\sigma^{\theta\mathbf{z}}_{\mathbf{i,n}}}\mathscr{G}^{\mathbf{v},\mathbf{z}}\left(\boxed{v_k},v_{k+1}\right)\right\}(i,k+1)
\end{aligned}
\tag{D.25}
$$

$$
\begin{aligned}
&\left\langle \overline{\mathscr{D}^{\mathbf{qs,s}}}\left(\sigma^{\mathbf{qs}}\right),\vec{u}_q\right\rangle |_{v_{i,k}} = \\
&\left.\Delta\chi_i\left(1-\varepsilon\right)\Delta z_k\left[\chi_i+\varepsilon\left(R_S-\chi_i\right)\right]\overline{\mathscr{D}^{,\theta}}_{i,k}\boxed{v_{i,k}}\right\}(i,k)
\end{aligned}
\tag{D.26}
$$

$$
\mathscr{D}^{,\theta}\left(\sigma^{qs}\right)\equiv\frac{\partial\sigma^{\theta r}}{\partial r}+\frac{1}{r}\left[\frac{\partial\sigma^{\theta\theta}}{\partial\theta}+\sigma^{\theta r}+\sigma^{r\theta}\right]+\frac{\partial\sigma^{\theta z}}{\partial z}
\tag{D.27}
$$

$$
\begin{aligned}
-\overline{\mathscr{D}^{,\theta}}_{i,k}\, v_{i,k} = \\
+\overline{\sigma^{\theta\theta}_{\mathbf{i,k}}}\mathscr{G}^{\mathbf{v},\theta}\left(u_{\ell-1}, u_{\ell}, v_{i-1}, v_i, v_{i+1}\right) \\
+\frac{\chi_{i-1}\Delta\chi_{i-1}}{\Delta\chi_i\chi_i}\overline{\sigma^{\theta\theta}_{\mathbf{i-1,k}}}\mathscr{G}^{\mathbf{v},\theta}\left(u_{\ell-2}, u_{\ell-1}, v_{i-2}, v_{i-1}, v_i\right) \\
+\frac{\chi_{i+1}\Delta\chi_{i+1}}{\Delta\chi_i\chi_i}\overline{\sigma^{\theta\theta}_{\mathbf{i+1,k}}}\mathscr{G}^{\mathbf{v},\theta}\left(u_{\ell}, u_{\ell+1}, v_i, v_{i+1}, v_{i+2}\right) \\
+\frac{\Delta\chi_{i-1}+\Delta\chi_i}{2\Delta\chi_i}\frac{\chi_i+\chi_{i-1}+\varepsilon\left(2R_S-\chi_i-\chi_{i-1}\right)}{2\left[\chi_i+\varepsilon\left(R_S-\chi_i\right)\right]}\overline{\sigma^{\chi\theta}_{\ell-1,\mathbf{k}}}\mathscr{G}^{\mathbf{u},\theta}\left(v_{i-1}, v_i\right) \\
+\frac{\Delta\chi_i+\Delta\chi_{i+1}}{2\Delta\chi_i}\frac{\chi_i+\chi_{i+1}+\varepsilon\left(2R_S-\chi_i-\chi_{i+1}\right)}{2\left[\chi_i+\varepsilon\left(R_S-\chi_i\right)\right]}\overline{\sigma^{\chi\theta}_{\ell,\mathbf{k}}}\mathscr{G}^{\mathbf{u},\theta}\left(v_i, v_{i+1}\right) \\
+\frac{\Delta\chi_{i-1}+\Delta\chi_i}{2\Delta\chi_i}\frac{\chi_i+\chi_{i-1}+\varepsilon\left(2R_S-\chi_i-\chi_{i-1}\right)}{2\left[\chi_i+\varepsilon\left(R_S-\chi_i\right)\right]}\overline{\sigma^{\theta\chi}_{\ell-1,\mathbf{k}}}\mathscr{G}^{\mathbf{v},\chi}\left(v_{i-1}, v_i\right) \\
+\frac{\Delta\chi_{i+1}+\Delta\chi_i}{2\Delta\chi_i}\frac{\chi_i+\chi_{i+1}+\varepsilon\left(2R_S-\chi_i-\chi_{i+1}\right)}{2\left[\chi_i+\varepsilon\left(R_S-\chi_i\right)\right]}\overline{\sigma^{\theta\chi}_{\ell,\mathbf{k}}}\mathscr{G}^{\mathbf{v},\chi}\left(v_i, v_{i+1}\right) \\
+\frac{\Delta z_{k-1}+\Delta z_k}{2\Delta z_k}\overline{\sigma^{\theta\mathbf{z}}_{\mathbf{i,n-1}}}\mathscr{G}^{\mathbf{v},\mathbf{z}}\left(v_{k-1}, v_k\right) \\
+\frac{\Delta z_k+\Delta z_{k+1}}{2\Delta z_k}\overline{\sigma^{\theta\mathbf{z}}_{\mathbf{i,n}}}\mathscr{G}^{\mathbf{v},\mathbf{z}}\left(v_k, v_{k+1}\right)
\end{aligned}
\tag{D.28}
$$

$$
\begin{aligned}
\overline{\mathscr{D}^{,\theta}}_{i,k} = \\
+\frac{{\sigma^{\theta\chi}_{\ell,\mathbf{k}}}^{0}-{\sigma^{\theta\chi}_{\ell-1,\mathbf{k}}}^{0}}{\Delta\chi_i}(1+\varepsilon)+\varepsilon\frac{\overline{\sigma^{\theta\chi}_{\ell,\mathbf{k}}}^{1}-\overline{\sigma^{\theta\chi}_{\ell-1,\mathbf{k}}}^{1}}{\Delta\chi_i}-\imath\varepsilon\frac{\overline{\sigma^{\theta\theta}_{\mathbf{i,k}}}^{1}}{\chi_i} \\
+2\imath\varepsilon\frac{1}{\chi_i}\frac{\Delta\chi_{i+1}}{\Delta\chi_i}\frac{\left(R_S-\chi_{i+1}\right){\sigma^{\theta\theta}_{\mathbf{i+1,k}}}^{0}}{\Delta\chi_{i+2}+2\Delta\chi_{i+1}+\Delta\chi_i}-2\imath\varepsilon\frac{1}{\chi_i}\frac{\Delta\chi_{i-1}}{\Delta\chi_i}\frac{\left(R_S-\chi_{i-1}\right){\sigma^{\theta\theta}_{\mathbf{i-1,k}}}^{0}}{\Delta\chi_i+2\Delta\chi_{i-1}+\Delta\chi_{i-2}} \\
+\left[\frac{1}{\chi_i}-\varepsilon\frac{\left(R_S-\chi_i\right)}{\chi_i^2}\right]\frac{\left(\Delta\chi_{i-1}+\Delta\chi_i\right){\sigma^{\theta\chi}_{\ell-1,\mathbf{k}}}^{0}+\left(\Delta\chi_i+\Delta\chi_{i+1}\right)\sigma^{\theta\chi^0}_{\ell,\mathbf{k}}}{4\Delta\chi_i} \\
+\varepsilon\frac{1}{\chi_i}\frac{\left(\Delta\chi_{i-1}+\Delta\chi_i\right)\overline{\sigma^{\theta\chi}_{\ell-1,\mathbf{k}}}^{1}+\left(\Delta\chi_i+\Delta\chi_{i+1}\right)\overline{\sigma^{\theta\chi}_{\ell,\mathbf{k}}}^{1}}{4\Delta\chi_i} \\
+\left[\frac{1}{\chi_i}-\varepsilon\frac{\left(R_S-\chi_i\right)}{\chi_i^2}\right]\frac{\left(\Delta\chi_{i-1}+\Delta\chi_i\right){\sigma^{\chi\theta}_{\ell-1,\mathbf{k}}}^{0}+\left(\Delta\chi_i+\Delta\chi_{i+1}\right)\sigma^{\chi\theta^0}_{\ell,\mathbf{k}}}{4\Delta\chi_i} \\
+\varepsilon\frac{1}{\chi_i}\frac{\left(\Delta\chi_{i-1}+\Delta\chi_i\right)\overline{\sigma^{\chi\theta}_{\ell-1,\mathbf{k}}}^{1}+\left(\Delta\chi_i+\Delta\chi_{i+1}\right)\overline{\sigma^{\chi\theta^1}_{\ell,\mathbf{k}}}}{4\Delta\chi_i} \\
+\frac{\sigma^{\theta\mathbf{z}^0}_{\mathbf{i,n}}-{\sigma^{\theta\mathbf{z}}_{\mathbf{i,n-1}}}^{0}}{\Delta z_k}+\varepsilon\frac{\overline{\sigma^{\theta\mathbf{z}^1}_{\mathbf{i,n}}}-\overline{\sigma^{\theta\mathbf{z}}_{\mathbf{i,n-1}}}^{1}}{\Delta z_k}
\end{aligned}
\tag{D.29}
$$

D.3.3 Collect Axial Discrete Tensor Divergence Terms in Inner Product

End by collecting inner product contributions that contain $w_{i,n}$ from cells (i,k) and (i,k+1) of the $\mathbf{FC}$ inner product space of the RHS; and cells (i-1,k)2, (i,k)4, (i+1,k)2, (i-1,k+1)2, (i,k+1)4, and (i+1,k+1)2 from the $\mathbf{CC}$ and $\mathbf{EC}$ inner product spaces of the LHS.

$$\begin{aligned}
&\left\langle \overline{\mathscr{D}^{\mathbf{qs,s}}}\left(\sigma^{\mathbf{qs}}\right), \vec{u}_q \right\rangle|_{w_{i,n}} = \\
&\left.\frac{\Delta\chi_i\left(1-\varepsilon\right)\Delta\theta\Delta z_k}{2}\left[\chi_i+\varepsilon\left(R_S-\chi_i\right)\right]\overline{\mathscr{D}^{,\mathbf{z}}}_{i,n}\, w_{i,n}\right\}(i,k) \\
&+\left.\frac{\Delta\chi_i\left(1-\varepsilon\right)\Delta\theta\Delta z_{k+1}}{2}\left[\chi_i+\varepsilon\left(R_S-\chi_i\right)\right]\overline{\mathscr{D}^{,\mathbf{z}}}_{i,n}\, w_{i,n}\right\}(i,k+1) \\
&\left\langle \overline{\mathscr{D}^{\mathbf{qs,s}}}\left(\sigma^{\mathbf{qs}}\right), \vec{u}_q \right\rangle|_{w_{i,n}} = \\
&\Delta\chi_i\left(1-\varepsilon\right)\Delta\theta\frac{\Delta z_k+\Delta z_{k+1}}{2}\left[\chi_i+\varepsilon\left(R_S-\chi_i\right)\right]\overline{\mathscr{D}^{,\mathbf{z}}}_{i,n}\, w_{i,n}
\end{aligned} \tag{D.30}$$

$$
\begin{aligned}
&\left\langle \overline{\sigma^{\mathbf{qs}}}, \mathcal{G}^{\mathbf{q,s}} \right\rangle|_{w_{i,n}} = \\
&\left.\begin{aligned}
&\frac{\Delta\chi_{i-1}(1-\varepsilon)\Delta z_k}{2}\left[\chi_{i-1}+\varepsilon\left(R_S-\chi_{i-1}\right)\right]\left\{\overline{\sigma^{\mathbf{z}\theta}_{\mathbf{i-1,n}}}\mathcal{G}^{\mathbf{w},\theta}\left(w_{i-2,n}, w_{i-1,n}, \boxed{w_{i,n}}\right)\right\} \\
&+\frac{\Delta\chi_{i-1}(1-\varepsilon)\Delta z_k}{2}\left[\chi_{\ell-1}+\varepsilon\left(R_S-\chi_{\ell-1}\right)\right]\frac{\overline{\sigma^{\mathbf{z}\chi}_{\ell-1,\mathbf{n}}}\mathcal{G}^{\mathbf{w},\chi}\left(w_{i-1,n}, \boxed{w_{i,n}}\right)}{2}
\end{aligned}\right\}(i-1,k) \\
&\left.\begin{aligned}
&\left[\chi_i+\varepsilon\left(R_S-\chi_i\right)\right]\Delta\chi_i(1-\varepsilon)\Delta z_k\overline{\sigma^{\mathbf{zz}}_{\mathbf{i,k}}}\mathcal{G}^{\mathbf{w},\mathbf{z}}\left(w_{n-1}, \boxed{w_n}\right) \\
&+\frac{\Delta\chi_i(1-\varepsilon)\Delta z_k}{2}\left[\chi_i+\varepsilon\left(R_S-\chi_i\right)\right]\overline{\sigma^{\mathbf{z}\theta}_{\mathbf{i,n}}}\mathcal{G}^{\mathbf{w},\theta}\left(w_{i-1,n}, \boxed{w_{i,n}}, w_{i+1,n}\right) \\
&+\frac{\Delta\chi_i(1-\varepsilon)\Delta z_k}{2}\left[\chi_{\ell-1}+\varepsilon\left(R_S-\chi_{\ell-1}\right)\right]\frac{\overline{\sigma^{\mathbf{z}\chi}_{\ell-1,\mathbf{n}}}\mathcal{G}^{\mathbf{w},\chi}\left(w_{i-1,n}, \boxed{w_{i,n}}\right)}{2} \\
&+\frac{\Delta\chi_i(1-\varepsilon)\Delta z_k}{2}\left[\chi_{\ell}+\varepsilon\left(R_S-\chi_{\ell}\right)\right]\frac{\overline{\sigma^{\mathbf{z}\chi}_{\ell,\mathbf{n}}}\mathcal{G}^{\mathbf{w},\chi}\left(\boxed{w_{i,n}}, w_{i+1,n}\right)}{2}
\end{aligned}\right\}(i,k) \\
&\left.\begin{aligned}
&+\frac{\Delta\chi_{i+1}(1-\varepsilon)\Delta z_k}{2}\left[\chi_{i+1}+\varepsilon\left(R_S-\chi_{i+1}\right)\right]\left\{\overline{\sigma^{\mathbf{z}\theta}_{\mathbf{i+1,n}}}\mathcal{G}^{\mathbf{w},\theta}\left(\boxed{w_{i,n}}, w_{i+1,n}, w_{i+2,n}\right)\right\} \\
&+\frac{\Delta\chi_{i+1}(1-\varepsilon)\Delta z_k}{2}\left[\chi_{\ell}+\varepsilon\left(R_S-\chi_{\ell}\right)\right]\frac{\overline{\sigma^{\mathbf{z}\chi}_{\ell,\mathbf{n}}}\mathcal{G}^{\mathbf{w},\chi}\left(\boxed{w_{i,n}}, w_{i+1,n}\right)}{2}
\end{aligned}\right\}(i+1,k) \\
&\left.\begin{aligned}
&+\frac{\Delta\chi_{i-1}(1-\varepsilon)\Delta z_{k+1}}{2}\left[\chi_{i-1}+\varepsilon\left(R_S-\chi_{i-1}\right)\right]\left\{\overline{\sigma^{\mathbf{z}\theta}_{\mathbf{i-1,n}}}\mathcal{G}^{\mathbf{w},\theta}\left(w_{i-2,n}, w_{i-1,n}, \boxed{w_{i,n}}\right)\right\} \\
&+\frac{\Delta\chi_{i-1}(1-\varepsilon)\Delta z_{k+1}}{2}\left[\chi_{\ell-1}+\varepsilon\left(R_S-\chi_{\ell-1}\right)\right]\frac{\overline{\sigma^{\mathbf{z}\chi}_{\ell-1,\mathbf{n}}}\mathcal{G}^{\mathbf{w},\chi}\left(w_{i-1,n}, \boxed{w_{i,n}}\right)}{2}
\end{aligned}\right\}(i-1,k+1) \\
&\left.\begin{aligned}
&\left[\chi_i+\varepsilon\left(R_S-\chi_i\right)\right]\Delta\chi_i(1-\varepsilon)\Delta z_{k+1}\overline{\sigma^{\mathbf{zz}}_{\mathbf{i,k+1}}}\mathcal{G}^{\mathbf{w},\mathbf{z}}\left(\boxed{w_n}, w_{n+1}\right) \\
&+\frac{\Delta\chi_i(1-\varepsilon)\Delta z_{k+1}}{2}\left[\chi_i+\varepsilon\left(R_S-\chi_i\right)\right]\overline{\sigma^{\mathbf{z}\theta}_{\mathbf{i,n}}}\mathcal{G}^{\mathbf{w},\theta}\left(w_{i-1,n}, \boxed{w_{i,n}}, w_{i+1,n}\right) \\
&+\frac{\Delta\chi_i(1-\varepsilon)\Delta z_{k+1}}{2}\left[\chi_{\ell-1}+\varepsilon\left(R_S-\chi_{\ell-1}\right)\right]\frac{\overline{\sigma^{\mathbf{z}\chi}_{\ell-1,\mathbf{n}}}\mathcal{G}^{\mathbf{w},\chi}\left(w_{i-1,n}, \boxed{w_{i,n}}\right)}{2} \\
&+\frac{\Delta\chi_i(1-\varepsilon)\Delta z_{k+1}}{2}\left[\chi_{\ell}+\varepsilon\left(R_S-\chi_{\ell}\right)\right]\frac{\overline{\sigma^{\mathbf{z}\chi}_{\ell,\mathbf{n}}}\mathcal{G}^{\mathbf{w},\chi}\left(\boxed{w_{i,n}}, w_{i+1,n}\right)}{2}
\end{aligned}\right\}(i,k+1) \\
&\left.\begin{aligned}
&+\frac{\Delta\chi_{i+1}(1-\varepsilon)\Delta z_{k+1}}{2}\left[\chi_{i+1}+\varepsilon\left(R_S-\chi_{i+1}\right)\right]\left\{\overline{\sigma^{\mathbf{z}\theta}_{\mathbf{i+1,n}}}\mathcal{G}^{\mathbf{w},\theta}\left(\boxed{w_{i,n}}, w_{i+1,n}, w_{i+2,n}\right)\right\} \\
&+\frac{\Delta\chi_{i+1}(1-\varepsilon)\Delta z_{k+1}}{2}\left[\chi_{\ell}+\varepsilon\left(R_S-\chi_{\ell}\right)\right]\frac{\overline{\sigma^{\mathbf{z}\chi}_{\ell,\mathbf{n}}}\mathcal{G}^{\mathbf{w},\chi}\left(\boxed{w_{i,n}}, w_{i+1,n}\right)}{2}
\end{aligned}\right\}(i+1,k+1)
\end{aligned}
\tag{D.31}
$$

$$
\mathscr{D}^{,\mathbf{z}}\left(\sigma^{qs}\right) \equiv \frac{1}{r}\frac{\partial\left(r\sigma^{zr}\right)}{\partial r}+\frac{1}{r}\frac{\partial\sigma^{z\theta}}{\partial\theta}+\frac{\partial\sigma^{zz}}{\partial z} \tag{D.32}
$$

$$
\begin{aligned}
&\overline{\mathscr{D}_{,\mathbf{z}}}_{i,n}\left(\sigma^{qs}\right) = \\
&\frac{1}{\chi_i\Delta\chi_i}\left(\left[\chi_\ell+\varepsilon\left(R_S-\chi_\ell\right)\right]{\sigma^{\mathbf{z}\chi}_{\ell,\mathbf{n}}}^{0}-\left[\chi_{\ell-1}+\varepsilon\left(R_S-\chi_{\ell-1}\right)\right]{\sigma^{\mathbf{z}\chi}_{\ell-\mathbf{1},\mathbf{n}}}^{0}\right) \\
&-\frac{1}{\Delta\chi_i}\varepsilon\frac{\left(R_S-\chi_i\right)}{\chi_i^2}\left(\chi_\ell{\sigma^{\mathbf{z}\chi}_{\ell,\mathbf{n}}}^{0}-\chi_{\ell-1}{\sigma^{\mathbf{z}\chi}_{\ell-\mathbf{1},\mathbf{n}}}^{0}\right) \\
&+\frac{\varepsilon}{\chi_i\Delta\chi_i}\left(\chi_\ell{\sigma^{\mathbf{z}\chi}_{\ell,\mathbf{n}}}^{0}-\chi_{\ell-1}{\sigma^{\mathbf{z}\chi}_{\ell-\mathbf{1},\mathbf{n}}}^{0}\right)+\frac{\varepsilon}{\chi_i\Delta\chi_i}\left(\chi_\ell\overline{\sigma^{\mathbf{z}\chi}_{\ell,\mathbf{n}}}^{1}-\chi_{\ell-1}\overline{\sigma^{\mathbf{z}\chi}_{\ell-\mathbf{1},\mathbf{n}}}^{1}\right) \\
&-\frac{1}{\chi_i}i\varepsilon\overline{\sigma^{\mathbf{z}\theta}_{\mathbf{i},\mathbf{n}}}^{1}+2i\varepsilon\frac{\left(R_S-\chi_i\right)}{\chi_i}\frac{{\sigma^{\mathbf{z}\theta}_{\mathbf{i+1},\mathbf{n}}}^{0}-{\sigma^{\mathbf{z}\theta}_{\mathbf{i-1},\mathbf{n}}}^{0}}{\Delta\chi_{i-1}+2\Delta\chi_i+\Delta\chi_{i+1}} \\
&+2\frac{{\sigma^{\mathbf{zz}}_{\mathbf{i},\mathbf{k+1}}}^{0}-\sigma^{\mathbf{zz}\,0}_{\mathbf{i},\mathbf{k}}}{\Delta z_{k+1}+\Delta z_k}+2\varepsilon\frac{\overline{\sigma^{\mathbf{zz}}_{\mathbf{i},\mathbf{k+1}}}^{1}-\overline{\sigma^{\mathbf{zz}}_{\mathbf{i},\mathbf{k}}}^{1}}{\Delta z_{k+1}+\Delta z_k}
\end{aligned}
\tag{D.33}
$$

D.3.4 Zeroth Order Discrete Tensor Divergence Operator: $\underline{\underline{\mathscr{D}}}^{0}\left(\sigma\right)$

$$
\begin{bmatrix}\mathscr{D}^{\mathbf{0},\chi}{}_{\ell,k}\\ \mathscr{D}^{\mathbf{0},\theta}{}_{i,k}\\ \mathscr{D}^{\mathbf{0},\mathbf{z}}{}_{i,n}\end{bmatrix}=\begin{bmatrix}
2\frac{{\sigma^{\chi\chi}_{\mathbf{i+1},\mathbf{k}}}^{0}-\sigma^{\chi\chi\,0}_{\mathbf{i},\mathbf{k}}}{\Delta\chi_i+\Delta\chi_{i+1}}+\frac{\sigma^{\chi\mathbf{z}\,0}_{\ell,\mathbf{n}}-{\sigma^{\chi\mathbf{z}}_{\ell,\mathbf{n-1}}}^{0}}{\Delta z_k} \\
+\frac{1}{\chi_\ell}\left(\frac{\Delta\chi_i\sigma^{\chi\chi\,0}_{\mathbf{i},\mathbf{k}}+\Delta\chi_{i+1}{\sigma^{\chi\chi}_{\mathbf{i+1},\mathbf{k}}}^{0}}{\Delta\chi_i+\Delta\chi_{i+1}}-\frac{\Delta\chi_i\sigma^{\theta\theta\,0}_{\mathbf{i},\mathbf{k}}+\Delta\chi_{i+1}{\sigma^{\theta\theta}_{\mathbf{i+1},\mathbf{k}}}^{0}}{\Delta\chi_i+\Delta\chi_{i+1}}\right) \\
\hdashline
\frac{\sigma^{\theta\chi\,0}_{\ell,\mathbf{k}}-{\sigma^{\theta\chi}_{\ell-\mathbf{1},\mathbf{k}}}^{0}}{\Delta\chi_i}+\frac{\sigma^{\theta\mathbf{z}\,0}_{\mathbf{i},\mathbf{n}}-{\sigma^{\theta\mathbf{z}}_{\mathbf{i},\mathbf{n-1}}}^{0}}{\Delta z_k} \\
+\frac{1}{\chi_i}\frac{\left(\Delta\chi_{i-1}+\Delta\chi_i\right){\sigma^{\theta\chi}_{\ell-\mathbf{1},\mathbf{k}}}^{0}+\left(\Delta\chi_i+\Delta\chi_{i+1}\right)\sigma^{\theta\chi\,0}_{\ell,\mathbf{k}}}{4\Delta\chi_i} \\
+\frac{1}{\chi_i}\frac{\left(\Delta\chi_{i-1}+\Delta\chi_i\right){\sigma^{\chi\theta}_{\ell-\mathbf{1},\mathbf{k}}}^{0}+\left(\Delta\chi_i+\Delta\chi_{i+1}\right)\sigma^{\chi\theta\,0}_{\ell,\mathbf{k}}}{4\Delta\chi_i} \\
\hdashline
\frac{1}{\chi_i\Delta\chi_i}\left(\chi_\ell{\sigma^{\mathbf{z}\chi}_{\ell,\mathbf{n}}}^{0}-\chi_{\ell-1}{\sigma^{\mathbf{z}\chi}_{\ell-\mathbf{1},\mathbf{n}}}^{0}\right)+2\frac{{\sigma^{\mathbf{zz}}_{\mathbf{i},\mathbf{k+1}}}^{0}-\sigma^{\mathbf{zz}\,0}_{\mathbf{i},\mathbf{k}}}{\Delta z_{k+1}+\Delta z_k}
\end{bmatrix}
\tag{D.34}
$$

D.3.5 First Order Discrete Tensor Divergence Operator: $\underline{\underline{\mathscr{D}}}^{1}\left(\sigma\right)$

The collected first order tensor divergence vector is given below in Equation D.35.

$$
\begin{bmatrix} \overline{\mathscr{D}^{\mathbf{1},\chi}}_{\ell,k} \\ \overline{\mathscr{D}^{\mathbf{1},\theta}}_{i,k} \\ \overline{\mathscr{D}^{\mathbf{1},\mathbf{z}}}_{i,n} \end{bmatrix} =
\begin{bmatrix}
2\dfrac{\sigma^{\chi\chi}{}^{0}_{\mathbf{i+1,k}} - \sigma^{\chi\chi 0}_{\mathbf{i,k}}}{\Delta\chi_i + \Delta\chi_{i+1}} + 2\dfrac{\overline{\sigma^{\chi\chi}{}^{1}_{\mathbf{i+1,k}}} - \overline{\sigma^{\chi\chi 1}_{\mathbf{i,k}}}}{\Delta\chi_i + \Delta\chi_{i+1}} + \dfrac{\overline{\sigma^{\chi\mathbf{z}}{}^{1}_{\ell,\mathbf{n}}} - \overline{\sigma^{\chi\mathbf{z}}{}^{1}_{\ell,\mathbf{n-1}}}}{\Delta z_k} \\
+\dfrac{1}{\chi_\ell}\left(-\sigma^{\chi\theta I}_{\ell,\mathbf{k}} - i\sigma^{\chi\theta R}_{\ell,\mathbf{k}}\right) + i\dfrac{(R_S-\chi_\ell)}{\chi_\ell}\dfrac{\sigma^{\chi\theta}{}^{0}_{\ell+1,\mathbf{k}} - \sigma^{\chi\theta}{}^{0}_{\ell-1,\mathbf{k}}}{\Delta\chi_i + \Delta\chi_{i+1}} \\
-\dfrac{(R_S-\chi_\ell)}{\chi_\ell^2}\left(\dfrac{\Delta\chi_i\sigma^{\chi\chi 0}_{\mathbf{i,k}} + \Delta\chi_{i+1}\sigma^{\chi\chi}{}^{0}_{\mathbf{i+1,k}}}{\Delta\chi_i + \Delta\chi_{i+1}} - \dfrac{\Delta\chi_i\sigma^{\theta\theta 0}_{\mathbf{i,k}} + \Delta\chi_{i+1}\sigma^{\theta\theta}{}^{0}_{\mathbf{i+1,k}}}{\Delta\chi_i + \Delta\chi_{i+1}}\right) \\
+\dfrac{1}{\chi_\ell}\left(\dfrac{\Delta\chi_i\overline{\sigma^{\chi\chi 1}_{\mathbf{i,k}}} + \Delta\chi_{i+1}\overline{\sigma^{\chi\chi}{}^{1}_{\mathbf{i+1,k}}}}{\Delta\chi_i + \Delta\chi_{i+1}} - \dfrac{\Delta\chi_i\overline{\sigma^{\theta\theta 1}_{\mathbf{i,k}}} + \Delta\chi_{i+1}\overline{\sigma^{\theta\theta}{}^{1}_{\mathbf{i+1,k}}}}{\Delta\chi_i + \Delta\chi_{i+1}}\right)
\end{bmatrix}
$$

$$
\begin{bmatrix}
\dfrac{\sigma^{\theta\chi 0}_{\ell,\mathbf{k}} - \sigma^{\theta\chi}{}^{0}_{\ell-1,\mathbf{k}}}{\Delta\chi_i} + \dfrac{\overline{\sigma^{\theta\chi 1}_{\ell,\mathbf{k}}} - \overline{\sigma^{\theta\chi}{}^{1}_{\ell-1,\mathbf{k}}}}{\Delta\chi_i} + \dfrac{\overline{\sigma^{\theta\mathbf{z}1}_{\mathbf{i,n}}} - \overline{\sigma^{\theta\mathbf{z}}{}^{1}_{\mathbf{i,n-1}}}}{\Delta z_k} + \dfrac{1}{\chi_i}\left(-\sigma^{\theta\theta I}_{\mathbf{i,k}} - i\sigma^{\theta\theta R}_{\mathbf{i,k}}\right) \\
+2i\dfrac{1}{\chi_i}\dfrac{\Delta\chi_{i+1}}{\Delta\chi_i}\dfrac{(R_S-\chi_{i+1})\,\sigma^{\theta\theta}{}^{0}_{\mathbf{i+1,k}}}{\Delta\chi_{i+2} + 2\Delta\chi_{i+1} + \Delta\chi_i} - 2i\dfrac{1}{\chi_i}\dfrac{\Delta\chi_{i-1}}{\Delta\chi_i}\dfrac{(R_S-\chi_{i-1})\,\sigma^{\theta\theta}{}^{0}_{\mathbf{i-1,k}}}{\Delta\chi_i + 2\Delta\chi_{i-1} + \Delta\chi_{i-2}} \\
-\dfrac{(R_S-\chi_i)}{\chi_i^2}\dfrac{(\Delta\chi_{i-1}+\Delta\chi_i)\,\sigma^{\theta\chi}{}^{0}_{\ell-1,\mathbf{k}} + (\Delta\chi_i+\Delta\chi_{i+1})\,\sigma^{\theta\chi 0}_{\ell,\mathbf{k}}}{4\Delta\chi_i} \\
+\dfrac{1}{\chi_i}\dfrac{(\Delta\chi_{i-1}+\Delta\chi_i)\,\overline{\sigma^{\theta\chi}{}^{1}_{\ell-1,\mathbf{k}}} + (\Delta\chi_i+\Delta\chi_{i+1})\,\overline{\sigma^{\theta\chi 1}_{\ell,\mathbf{k}}}}{4\Delta\chi_i} \\
-\dfrac{(R_S-\chi_i)}{\chi_i^2}\dfrac{(\Delta\chi_{i-1}+\Delta\chi_i)\,\sigma^{\chi\theta}{}^{0}_{\ell-1,\mathbf{k}} + (\Delta\chi_i+\Delta\chi_{i+1})\,\sigma^{\chi\theta 0}_{\ell,\mathbf{k}}}{4\Delta\chi_i} \\
+\dfrac{1}{\chi_i}\dfrac{(\Delta\chi_{i-1}+\Delta\chi_i)\,\overline{\sigma^{\chi\theta}{}^{1}_{\ell-1,\mathbf{k}}} + (\Delta\chi_i+\Delta\chi_{i+1})\,\overline{\sigma^{\chi\theta 1}_{\ell,\mathbf{k}}}}{4\Delta\chi_i}
\end{bmatrix}
\tag{D.35}
$$

$$
\begin{bmatrix}
\dfrac{1}{\chi_i\Delta\chi_i}\left((R_S-\chi_\ell)\,\sigma^{\mathbf{z}\chi}{}^{0}_{\ell,\mathbf{n}} - (R_S-\chi_{\ell-1})\,\sigma^{\mathbf{z}\chi}{}^{0}_{\ell-1,\mathbf{n}}\right) \\
-\dfrac{1}{\Delta\chi_i}\dfrac{(R_S-\chi_i)}{\chi_i^2}\left(\chi_\ell\sigma^{\mathbf{z}\chi}{}^{0}_{\ell,\mathbf{n}} - \chi_{\ell-1}\sigma^{\mathbf{z}\chi}{}^{0}_{\ell-1,\mathbf{n}}\right) \\
+\dfrac{1}{\chi_i\Delta\chi_i}\left(\chi_\ell\sigma^{\mathbf{z}\chi}{}^{0}_{\ell,\mathbf{n}} - \chi_{\ell-1}\sigma^{\mathbf{z}\chi}{}^{0}_{\ell-1,\mathbf{n}}\right) + \dfrac{1}{\chi_i\Delta\chi_i}\left(\chi_\ell\overline{\sigma^{\mathbf{z}\chi}{}^{1}_{\ell,\mathbf{n}}} - \chi_{\ell-1}\overline{\sigma^{\mathbf{z}\chi}{}^{1}_{\ell-1,\mathbf{n}}}\right) \\
+\dfrac{1}{\chi_i}\left(-\sigma^{\mathbf{z}\theta I}_{\mathbf{i,n}} - \sigma^{\mathbf{z}\theta R}_{\mathbf{i,n}}\right) + 2i\dfrac{(R_S-\chi_i)}{\chi_i}\dfrac{\sigma^{\mathbf{z}\theta}{}^{0}_{\mathbf{i+1,n}} - \sigma^{\mathbf{z}\theta}{}^{0}_{\mathbf{i-1,n}}}{\Delta\chi_{i-1} + 2\Delta\chi_i + \Delta\chi_{i+1}} \\
+2\dfrac{\overline{\sigma^{\mathbf{zz}}{}^{1}_{\mathbf{i,k+1}}} - \overline{\sigma^{\mathbf{zz}\,1}_{\mathbf{i,k}}}}{\Delta z_{k+1} + \Delta z_k}
\end{bmatrix}
$$

Real First Order Discrete Tensor Divergence Operator: $\underline{\underline{\mathscr{D}}}^{R}\left(\sigma\right)$

$$\begin{bmatrix} \overline{\mathscr{D}^{\mathbf{R},\chi}}_{\ell,k} \\ \hdashline \overline{\mathscr{D}^{\mathbf{R},\theta}}_{i,k} \\ \hdashline \overline{\mathscr{D}^{\mathbf{R},\mathbf{z}}}_{i,n} \end{bmatrix} = \begin{bmatrix} 2\dfrac{\sigma^{\chi\chi\ 0}_{\mathbf{i+1,k}}-\sigma^{\chi\chi 0}_{\mathbf{i,k}}}{\Delta\chi_i+\Delta\chi_{i+1}}+2\dfrac{\sigma^{\chi\chi\ R}_{\mathbf{i+1,k}}-\sigma^{\chi\chi R}_{\mathbf{i,k}}}{\Delta\chi_i+\Delta\chi_{i+1}}+\dfrac{\sigma^{\chi\mathbf{z}\ R}_{\ell,\mathbf{n}}-\sigma^{\chi\mathbf{z}\ \ R}_{\ell,\mathbf{n-1}}}{\Delta z_k}-\dfrac{1}{\chi_\ell}\sigma^{\chi\theta I}_{\ell,\mathbf{k}} \\ -\dfrac{(R_S-\chi_\ell)}{\chi_\ell^2}\left(\dfrac{\Delta\chi_i\sigma^{\chi\chi\ 0}_{\mathbf{i,k}}+\Delta\chi_{i+1}\sigma^{\chi\chi\ \ 0}_{\mathbf{i+1,k}}}{\Delta\chi_i+\Delta\chi_{i+1}}-\dfrac{\Delta\chi_i\sigma^{\theta\theta 0}_{\mathbf{i,k}}+\Delta\chi_{i+1}\sigma^{\theta\theta\ \ 0}_{\mathbf{i+1,k}}}{\Delta\chi_i+\Delta\chi_{i+1}}\right) \\ +\dfrac{1}{\chi_\ell}\left(\dfrac{\Delta\chi_i\sigma^{\chi\chi R}_{\mathbf{i,k}}+\Delta\chi_{i+1}\sigma^{\chi\chi\ \ R}_{\mathbf{i+1,k}}}{\Delta\chi_i+\Delta\chi_{i+1}}-\dfrac{\Delta\chi_i\sigma^{\theta\theta R}_{\mathbf{i,k}}+\Delta\chi_{i+1}\sigma^{\theta\theta\ \ R}_{\mathbf{i+1,k}}}{\Delta\chi_i+\Delta\chi_{i+1}}\right) \\ \hdashline \dfrac{\sigma^{\theta\chi 0}_{\ell,\mathbf{k}}-\sigma^{\theta\chi\ \ 0}_{\ell-\mathbf{1,k}}}{\Delta\chi_i}+\dfrac{\sigma^{\theta\chi R}_{\ell,\mathbf{k}}-\sigma^{\theta\chi\ \ R}_{\ell-\mathbf{1,k}}}{\Delta\chi_i}+\dfrac{\sigma^{\theta\mathbf{z}R}_{\mathbf{i,n}}-\sigma^{\theta\mathbf{z}\ \ R}_{\mathbf{i,n-1}}}{\Delta z_k}-\dfrac{1}{\chi_i}\sigma^{\theta\theta I}_{\mathbf{i,k}} \\ -\dfrac{(R_S-\chi_i)}{\chi_i^2}\dfrac{(\Delta\chi_{i-1}+\Delta\chi_i)\,\sigma^{\theta\chi\ \ 0}_{\ell-\mathbf{1,k}}+(\Delta\chi_i+\Delta\chi_{i+1})\,\sigma^{\theta\chi 0}_{\ell,\mathbf{k}}}{4\Delta\chi_i} \\ +\dfrac{1}{\chi_i}\dfrac{(\Delta\chi_{i-1}+\Delta\chi_i)\,\sigma^{\theta\chi\ \ R}_{\ell-\mathbf{1,k}}+(\Delta\chi_i+\Delta\chi_{i+1})\,\sigma^{\theta\chi R}_{\ell,\mathbf{k}}}{4\Delta\chi_i} \\ -\dfrac{(R_S-\chi_i)}{\chi_i^2}\dfrac{(\Delta\chi_{i-1}+\Delta\chi_i)\,\sigma^{\chi\theta\ \ 0}_{\ell-\mathbf{1,k}}+(\Delta\chi_i+\Delta\chi_{i+1})\,\sigma^{\chi\theta 0}_{\ell,\mathbf{k}}}{4\Delta\chi_i} \\ +\dfrac{1}{\chi_i}\dfrac{(\Delta\chi_{i-1}+\Delta\chi_i)\,\sigma^{\chi\theta\ \ R}_{\ell-\mathbf{1,k}}+(\Delta\chi_i+\Delta\chi_{i+1})\,\sigma^{\chi\theta R}_{\ell,\mathbf{k}}}{4\Delta\chi_i} \\ \hdashline \dfrac{1}{\chi_i\Delta\chi_i}\left((R_S-\chi_\ell)\,\sigma^{\mathbf{z}\chi\ 0}_{\ell,\mathbf{n}}-(R_S-\chi_{\ell-1})\,\sigma^{\mathbf{z}\chi\ \ 0}_{\ell-\mathbf{1,n}}\right) \\ -\dfrac{1}{\Delta\chi_i}\dfrac{(R_S-\chi_i)}{\chi_i^2}\left(\chi_\ell\sigma^{\mathbf{z}\chi\ 0}_{\ell,\mathbf{n}}-\chi_{\ell-1}\sigma^{\mathbf{z}\chi\ \ 0}_{\ell-\mathbf{1,n}}\right) \\ +\dfrac{1}{\chi_i\Delta\chi_i}\left(\chi_\ell\sigma^{\mathbf{z}\chi\ 0}_{\ell,\mathbf{n}}-\chi_{\ell-1}\sigma^{\mathbf{z}\chi\ \ 0}_{\ell-\mathbf{1,n}}\right)+\dfrac{1}{\chi_i\Delta\chi_i}\left(\chi_\ell\sigma^{\mathbf{z}\chi\ R}_{\ell,\mathbf{n}}-\chi_{\ell-1}\sigma^{\mathbf{z}\chi\ \ R}_{\ell-\mathbf{1,n}}\right) \\ -\dfrac{1}{\chi_i}\sigma^{\mathbf{z}\theta I}_{\mathbf{i,n}}+2\dfrac{\sigma^{\mathbf{zz}\ \ R}_{\mathbf{i,k+1}}-\sigma^{\mathbf{zz}\ R}_{\mathbf{i,k}}}{\Delta z_{k+1}+\Delta z_k} \end{bmatrix} \tag{D.36}$$

Imaginary First Order Discrete Tensor Divergence Operator: $\underline{\underline{\mathscr{D}}}^{I}(\sigma)$

$$\begin{bmatrix} \overline{\mathscr{D}^{\mathbf{I},\chi}}_{\ell,k} \\ \overline{\mathscr{D}^{\mathbf{I},\theta}}_{i,k} \\ \overline{\mathscr{D}^{\mathbf{I},\mathbf{z}}}_{i,n} \end{bmatrix} = \begin{bmatrix} -2\dfrac{\sigma^{\chi\chi\ I}_{\mathbf{i+1,k}} - \sigma^{\chi\chi I}_{\mathbf{i,k}}}{\Delta\chi_i + \Delta\chi_{i+1}} - \dfrac{\sigma^{\chi\mathbf{z}\ I}_{\ell,\mathbf{n}} - \sigma^{\chi\mathbf{z}\ \ I}_{\ell,\mathbf{n-1}}}{\Delta z_k} \\ -\dfrac{1}{\chi_\ell}\sigma^{\chi\theta R}_{\ell,\mathbf{k}} + \dfrac{(R_S-\chi_\ell)}{\chi_\ell}\dfrac{\sigma^{\chi\theta\ \ 0}_{\ell+1,\mathbf{k}} - \sigma^{\chi\theta\ \ 0}_{\ell-1,\mathbf{k}}}{\Delta\chi_i + \Delta\chi_{i+1}} \\ -\dfrac{1}{\chi_\ell}\left(\dfrac{\Delta\chi_i\sigma^{\chi\chi I}_{\mathbf{i,k}} + \Delta\chi_{i+1}\sigma^{\chi\chi\ \ I}_{\mathbf{i+1,k}}}{\Delta\chi_i + \Delta\chi_{i+1}} - \dfrac{\Delta\chi_i\sigma^{\theta\theta I}_{\mathbf{i,k}} + \Delta\chi_{i+1}\sigma^{\theta\theta\ \ I}_{\mathbf{i+1,k}}}{\Delta\chi_i + \Delta\chi_{i+1}}\right) \end{bmatrix} \\ \begin{bmatrix} -\dfrac{\sigma^{\theta\chi I}_{\ell,\mathbf{k}} - \sigma^{\theta\chi\ \ I}_{\ell-1,\mathbf{k}}}{\Delta\chi_i} - \dfrac{\sigma^{\theta\mathbf{z}I}_{\mathbf{i,n}} - \sigma^{\theta\mathbf{z}\ \ I}_{\mathbf{i,n-1}}}{\Delta z_k} - \dfrac{1}{\chi_i}\sigma^{\theta\theta R}_{\mathbf{i,k}} \\ +2\dfrac{1}{\chi_i}\dfrac{\Delta\chi_{i+1}}{\Delta\chi_i}\dfrac{(R_S-\chi_{i+1})\,\sigma^{\theta\theta\ \ 0}_{\mathbf{i+1,k}}}{\Delta\chi_{i+2}+2\Delta\chi_{i+1}+\Delta\chi_i} - 2\dfrac{1}{\chi_i}\dfrac{\Delta\chi_{i-1}}{\Delta\chi_i}\dfrac{(R_S-\chi_{i-1})\,\sigma^{\theta\theta\ \ 0}_{\mathbf{i-1,k}}}{\Delta\chi_i+2\Delta\chi_{i-1}+\Delta\chi_{i-2}} \\ -\dfrac{1}{\chi_i}\dfrac{(\Delta\chi_{i-1}+\Delta\chi_i)\,\sigma^{\theta\chi\ \ I}_{\ell-1,\mathbf{k}} + (\Delta\chi_i+\Delta\chi_{i+1})\,\sigma^{\theta\chi I}_{\ell,\mathbf{k}}}{4\Delta\chi_i} \\ -\dfrac{1}{\chi_i}\dfrac{(\Delta\chi_{i-1}+\Delta\chi_i)\,\sigma^{\chi\theta\ \ I}_{\ell-1,\mathbf{k}} + (\Delta\chi_i+\Delta\chi_{i+1})\,\sigma^{\chi\theta I}_{\ell,\mathbf{k}}}{4\Delta\chi_i} \end{bmatrix} \\ \begin{bmatrix} -\dfrac{1}{\chi_i\Delta\chi_i}\left(\chi_\ell\sigma^{\mathbf{z}\chi\ I}_{\ell,\mathbf{n}} - \chi_{\ell-1}\sigma^{\mathbf{z}\chi\ \ I}_{\ell-1,\mathbf{n}}\right) \\ -\dfrac{1}{\chi_i}\sigma^{\mathbf{z}\theta R}_{\mathbf{i,n}} + 2\dfrac{(R_S-\chi_i)}{\chi_i}\dfrac{\sigma^{\mathbf{z}\theta\ \ 0}_{\mathbf{i+1,n}} - \sigma^{\mathbf{z}\theta\ \ 0}_{\mathbf{i-1,n}}}{\Delta\chi_{i-1}+2\Delta\chi_i+\Delta\chi_{i+1}} \\ -2\dfrac{\sigma^{\mathbf{zz}\ \ I}_{\mathbf{i,k+1}} - \sigma^{\mathbf{zz}\ I}_{\mathbf{i,k}}}{\Delta z_{k+1}+\Delta z_k} \end{bmatrix} \end{bmatrix} \tag{D.37}$$

D.4 Boundary Conditions for Strain Rate Velocities from Discrete Tensor Operators

Like Section C.3, the discrete tensor operators are calculated for infinite domains. Adjustments have to be made for the discrete locations along or near the boundaries to prevent the discrete operators from requiring information that does not exist in the domain. The strain rate operators in the trace do not require any velocity information from beyond the existing domain and ghost points that have been defined in previous sections. The symmetric off-diagonal terms are summed using the $\mathbf{EC}$ inner product and have circumferential derivatives that use an expanded central difference requiring points above and below the local value. The discrete tensor divergence operator requires i=1 to i=$N_{\chi-1}$ and k=1 to i=N_z for the radial terms, where $\sigma^{\chi\theta}_{\ell,k}$ needs radial ghost velocity values for the radial velocity on the rotor and stator. As before, the second layer ghost cell values for

radial velocity is equivalent to the negative of the first cell inside the domain because it is zero on the boundary with a constant gradient on the boundary, creating a standard mirror condition across the physical boundary $u_{-1,k} = -u_{1,k}$ and $u_{0,k} = u_{S,k} = 0$. The circumferential terms are calculated at i=1 to i=N_χ and k=1 to i=N_z and require second layer ghost cell values for both radial and circumferential velocity. The axial terms require second layer ghost cell values for axial velocity when calculated at i=1 to i=N_χ and k=1 to i=$N_z - 1$ for $\sigma^{\theta z}_{i,n}$. These second layer ghost cell values for circumferential and axial velocity are more complicated because there is already a mirror condition at the first ghost layer. Instead, the second layer value is equal to the first ghost layer weighted by distance from the physical boundary $v_{-1,k} = 3v_{0,k} = -3v_{1,k}$ and $w_{-1,n} = 3w_{0,n} = -3w_{1,n}$.

Bibliography

[1] Dara Childs. *Turbomachinery Rotordynamics*. John Wiley & Sons, Inc, New York, NY, 1993.

[2] HF Black. Effects of hydraulic forces in annular pressure seals on the vibrations of centrifugal pump rotors. *Journal of Mechanical Engineering Science*, 11(2):206–213, 1969.

[3] Dara W Childs, Luis E Rodriguez, Vito Cullotta, Adnan Al-Ghasem, and Matthew Graviss. Rotordynamic-coefficients and static (equilibrium loci and leakage) characteristics for short, laminar-flow annular seals. 2006.

[4] F. Simon and J. Frene. Analysis for Incompressible Flow in Annular Pressure Seals. *Journal of Tribology*, 114(3):431–438, July 1992.

[5] K. M. Becker and Joseph Kaye. Measurements of Diabatic Flow in an Annulus With an Inner Rotating Cylinder. *Journal of Heat Transfer*, 84(2):97–104, May 1962.

[6] FM White. Fluid mechanics (mechanical engineering). 2015.

[7] Joseph Kaye and E.C. Elgar. Modes of adiabatic and diabatic fluid flow in an annulus with an inner rotating cylinder. *Trans ASME*, 80:753–765, 1958.

[8] Julius Weisbach and Gustav Herrmann. Lehrbuch der ingenieur- und maschinen mechanik. Erster theil: Theoretische mechanik. [Textbook of engineering and machine mechanics]. 1875.

[9] Henry Darcy. Recherches expérimentales relatives au mouvement de l'eau dans les tuyaux. 1857.

[10] Sydney Goldstein. The similarity theory of turbulence, and flow between parallel planes and through pipes. *Proceedings of the Royal Society of London. Series A-Mathematical and Physical Sciences*, 159(899):473–496, 1937.

[11] S Suzuki. On the leakage of water through clearance space. *Journal of Fac. of Eno., Univ. of Tokyo*, 18(2):71, 1929.

[12] Yutaka Yamada. Resistance of flow through an annulus with an inner rotating cylinder. *Journal of JSME*, 27(180):1267–1276, 1961.

[13] Yutaka Yamada. On the pressure loss of flow between rotating co-axial cylinders with rectangular grooves. *Bulletin of JSME*, 5(20):642–651, 1962.

[14] Yutaka Yamada. Torque resistance of a flow between rotating co-axial cylinders having axial flow. *Bulletin of JSME*, 5(20):634–642, 1962.

[15] Yutaka Yamada, Koichi NAKABAYASHI, and Kozo Maeda. Pressure drop measurements of the flow through eccentric cylinders with rotating inner cylinders. *Bulletin of JSME*, 12(53):1032–1040, 1969.

[16] Yutaka Yamada and Satoru Watanabe. Frictional moment and pressure drop of the flow through co-axial cylinders with an outer rotating cylinder. *Bulletin of JSME*, 16(93):551–559, 1973.

[17] Gilles Gerardus Hirs. Fundamentals of a bulk-flow theory for turbulent lubricant films. 1970.

[18] John Zuk. Fundamentals of fluid sealing. 1976.

[19] Joseph K Scharrer. Theory versus experiment for the rotordynamic coefficients of labyrinth gas seals: Part I—a two control volume model. *Journal of Vibration and Acoustics*, 110(3):270–280, 1988.

[20] Patrick J Migliorini, Alexandrina Untaroiu, Houston G Wood, and Paul E Allaire. A computational fluid dynamics/bulk-flow hybrid method for determining rotordynamic coefficients of annular gas seals. *Journal of tribology*, 134(2), 2012.

[21] X. Yan, Jun Li, and Zhenping Feng. Validation of two-control-volume bulk flow method for rotordynamic characteristics of hole-pattern seals. *Hsi-An Chiao Tung Ta Hsueh/Journal of Xi'an Jiaotong University*, 43:24–28, 2009.

[22] G.F. Kleynhans. *A Two-Control-Volume Bulk-Flow Rotordynamic Analysis for Smooth-Rotor/Honeycomb-Stator Gas Annular Seals*. Texas A & M University, 1996.

[23] Rohan J. D'Souza and Dara W. Childs. A Comparison of Rotordynamic-Coefficient Predictions for Annular Honeycomb Gas Seals Using Three Different Friction-Factor Models. *Journal of Tribology*, 124(3):524–529, July 2002.

[24] Tae Woong Ha and An Sung Lee. A rotordynamic analysis of circumferentially-grooved pump seals based on a three-control-volume theory. *KSME international journal*, 14(3):261–271, 2000.

[25] Cori Watson. *Computational Modeling of Helical Groove Seals*. PhD thesis, University of Virginia, Charlottesville, VA, April 2018.

[26] L Prandtl. Uber ein neues Formelsystem fur die ausgebildete Turbulenz, Nachrichten von der Akad. der Wissenschaft in Gottingen, Math. 1945.

[27] DL Rhode and SR Sobolik. Simulation of subsonic flow through a generic labyrinth seal cavity. In *Turbo Expo: Power for Land, Sea, and Air*, volume 79382, page V001T03A024. American Society of Mechanical Engineers, 1985.

[28] R Nordmann and P Weiser. Evaluation of rotordynamic coefficients of look-through labyrinths by means of a three volume bulk flow model. Technical report, NASA, 1991.

[29] JT Han. Fluid mechanics model to estimate the leakage of incompressible fluids through labyrinth seals. Technical report, Oak Ridge National Lab., TN (USA), 1978.

[30] Neal R Morgan, Alexandrina Untaroiu, Patrick J Migliorini, and Houston G Wood. Design of experiments to investigate geometric effects on fluid leakage rate in a balance drum seal. *Journal of Engineering for Gas Turbines and Power*, 137(3), 2015.

[31] Neal R Morgan, Houston G Wood, and Alexandrina Untaroiu. Numerical optimization of leakage by multifactor regression of trapezoidal groove geometries for a balance drum labyrinth seal. In *Turbo Expo: Power for Land, Sea, and Air*, volume 56659, page V02CT45A021. American Society of Mechanical Engineers, 2015.

[32] NR Morgan, HG Wood, PJ Migliorini, and A Untaroiu. Groove geometry optimization of balance drum labyrinth seal to minimize leakage rate by experimental design. In *13th EDF/Pprime Workshop: Energy Saving in Seals, Poitier, France, Oct*, volume 2, 2014.

[33] Alexandrina Untaroiu, Neal Morgan, Vahe Hayrapetian, and Bruno Schiavello. Dynamic response analysis of balance drum labyrinth seal groove geometries optimized for minimum leakage. *Journal of Vibration and Acoustics*, 139(2), 2017.

[34] JA Brighton and JB Jones. Fully developed turbulent flow in annuli. *Journal of Fluids Engineering*, 86(4), 1964.

[35] D. Elrod, C. Nelson, and D. Childs. An Entrance Region Friction Factor Model Applied to Annular Seal Analysis: Theory Versus Experiment for Smooth and Honeycomb Seals. *Journal of Tribology*, 111(2):337–343, April 1989.

[36] F. J. Dietzen and R. Nordmann. Calculating Rotordynamic Coefficients of Seals by Finite-Difference Techniques. *Journal of Tribology*, 109(3):388–394, July 1987.

[37] R. Nordmann, F. J. Dietzen, and H. P. Weiser. Calculation of Rotordynamic Coefficients and Leakage for Annular Gas Seals by Means of Finite Difference Techniques. *Journal of Tribology*, 111(3):545–552, July 1989.

[38] FJ Dietzen and R Nordmann. A 3-dimensional finite-difference method for calculating the dynamic coefficients of seals. Technical report, NASA, 1989.

[39] M. Athavale, A. Przekwas, and R. Hendricks. A finite-volume numerical method to calculate fluid forces and rotordynamic coefficients in seals. In *28th Joint Propulsion Conference and Exhibit*, Nashville,TN,U.S.A., July 1992. American Institute of Aeronautics and Astronautics.

[40] MM Athavale, Robert C Hendricks, and Bruce M Steinetz. Numerical simulation of flow in a whirling annular seal and comparison with experiments. 1995.

[41] M. M. Athavale and R. C. Hendricks. A Small Perturbation CFD Method for Calculation of Seal Rotordynamic Coefficients. *International Journal of Rotating Machinery*, 2(3):167–177, 1996.

[42] Tomohiko Tsukuda, Toshio Hirano, Cori Watson, Neal R Morgan, Brian K Weaver, and Houston G Wood. A numerical investigation of the effect of inlet preswirl ratio on rotordynamic characteristics of labyrinth seal. *Journal of Engineering for Gas Turbines and Power*, 140(8), 2018.

[43] Cori Watson and Houston Wood. Evaluating configurations of double surface helical groove seals using computational fluid dynamics. In *Turbo Expo: Power for Land, Sea, and Air*, volume 51012, page V02CT42A053. American Society of Mechanical Engineers, 2018.

[44] Cori Watson and Houston Wood. Second stage optimization of helical groove seals using computational fluid dynamics to evaluate the dependency of optimized design on preswirl. In *Fluids Engineering Division Summer Meeting*, volume 51579, page V003T12A028. American Society of Mechanical Engineers, 2018.

[45] Wisher Paudel, Cori Watson, and Houston G Wood. The impact of adding a labyrinth surface to an optimal helical seal design. In *ASME International Mechanical Engineering Congress and Exposition*, volume 52101, page V007T09A092. American Society of Mechanical Engineers, 2018.

[46] Wisher Paudel, Cori Watson, and Houston G Wood. Mixed helical labyrinth groove seal optimization using computational fluid dynamics. In *Turbo Expo: Power for Land, Sea, and Air*, volume 50794, page V02BT41A004. American Society of Mechanical Engineers, 2017.

[47] Cori Watson and Houston G Wood. Developing an optimal helix angle as a function of pressure for helical Groove seals. In *Fluids Engineering Division Summer Meeting*, volume 58042, page V01AT05A020. American Society of Mechanical Engineers, 2017.

[48] Cori Watson and Houston G Wood. Optimizing a helical groove seal with grooves on both the rotor and stator surfaces. In *Turbo Expo: Power for Land, Sea, and Air*, volume 50794, page V02BT41A044. American Society of Mechanical Engineers, 2017.

[49] Cori Watson, Wisher Paudel, Houston G Wood, and Brian K Weaver. Quantifying the linearity of the fluid dynamics for noncontacting annular seals. In *ASME International Mechanical Engineering Congress and Exposition*, volume 50541, page V04AT05A041. American Society of Mechanical Engineers, 2016.

[50] Cori Watson, Alexandrina Untaroiu, Houston G Wood, Brian K Weaver, Neal Morgan, and Hanxiang Jin. Response surface mapping of performance for helical groove seals with incompressible flow. In *Turbo Expo: Power for Land, Sea, and Air*, volume 49842, page V07BT31A036. American Society of Mechanical Engineers, 2016.

[51] DL Rhode, SH Ko, and GL Morrison. Leakage optimization of labyrinth seals using a Navier-Stokes code. *Tribology transactions*, 37(1):105–110, 1994.

[52] Volker Schramm, Jens Denecke, Siegfried Kim, and Sigmar Wittig. Shape optimization of a labyrinth seal applying the simulated annealing method. *International Journal of Rotating Machinery*, 10, 2004.

[53] SP Asok, K Sankaranarayanasamy, T Sundararajan, K Rajesh, and G Sankar Ganeshan. Neural network and CFD-based optimisation of square cavity and curved cavity static labyrinth seals. *Tribology International*, 40(7):1204–1216, 2007.

[54] Alexandrina Untaroiu, Houston G Wood, Paul E Allaire, and Timothy W Dimond. Calculation of dynamic coefficients for a magnetically levitated artificial heart pump using a CFD approach. In *ASME International Mechanical Engineering Congress and Exposition*, volume 48630, pages 537–543, 2008.

[55] A Bellaouar, BV Kopey, and N Abdelbaki. Methods of the rational choice of a labyrinth seal design for gas pumping units. *MECHANIKA*, 19(1):81–86, 2013.

[56] KM Becker and Joseph Kaye. Closure to "Discussion of 'Measurements of diabatic flow in an annulus with an inner rotating cylinder'"(1962, ASME j. Heat transfer, 84, pp. 104–105). 1962.

[57] Pijush K Kundu and Ira M Cohen. *Fluid Mechanics*. Academic Press, 3rd edition, 2004.

[58] Kuei-Yuan Chien. Predictions of Channel and Boundary-Layer Flows with a Low-Reynolds-Number Turbulence Model. *AIAA Journal*, 20(1):33–38, January 1982.

[59] G. Chochua, W. Shyy, and J. Moore. Thermophysical modeling for honeycomb-stator gas annular seal. In *35th AIAA Thermophysics Conference*, Anaheim,CA,U.S.A., June 2001. American Institute of Aeronautics and Astronautics.

[60] Rui Xu, Yaoyu Hu, Junlian Yin, Jiangtao Zhang, and Dezhong Wang. A transient CFD research on the dynamic characteristics of liquid annular seals. *Annals of Nuclear Energy*, 120:528–533, 2018.

[61] Yahya Doğu, Mustafa C Sertçakan, Ahmet S Bahar, Altuğ Pişkin, Ercan Arıcan, and Mustafa Kocagül. CFD investigation of labyrinth seal leakage performance depending on mush-room shaped tooth wear. In *Turbo Expo: Power for Land, Sea, and Air*, volume 56734, page V05CT15A034. American Society of Mechanical Engineers, 2015.

[62] Alexandrina Untaroiu, Cheng Liu, Patrick J Migliorini, Houston G Wood, and Costin D Untaroiu. Hole-pattern seals performance evaluation using computational fluid dynamics and design of experiment techniques. *Journal of Engineering for Gas Turbines and Power*, 136(10), 2014.

[63] J. Jeffrey Moore. Three-dimensional CFD rotordynamic analysis of gas labyrinth seals. *Journal of Vibration and Acoustics*, 125(4):427–433, 2003.

[64] V Schramm, K Willenborg, S Kim, and S Wittig. Influence of a honeycomb facing on the flow through a stepped labyrinth seal. *J. Eng. Gas Turbines Power*, 124(1):140–146, 2002.

[65] K. Willenborg, V. Schramm, S. Kim, and S. Wittig. Influence of a honeycomb facing on the heat transfer in a stepped labyrinth seal. *Journal of Engineering for Gas Turbines and Power-transactions of The Asme*, 124(1):133–139, 2002.

[66] Sivakumar Subramanian, A.S. Sekhar, and B.V.S.S.S. Prasad. Rotordynamic characterization of rotating labyrinth gas turbine seals with radial growth: Combined centrifugal and thermal effects. *International Journal of Mechanical Sciences*, 123:1–19, 2017.

[67] CJ Chen and SY Jaw. Reviews-Fundamentals of turbulence modeling. *Journal of Fluid Mechanics*, 371:379–379, 1998.

[68] Virendra C. Patel, Wolfgang Rodi, and Georg Scheuerer. Turbulence models for near-wall and low Reynolds number flows - A review. *AIAA Journal*, 23(9):1308–1319, September 1985.

[69] V. C. Patel and H. C. Chen. Turbulent wake of a flat plate. *AIAA Journal*, 25(8):1078–1085, August 1987.

[70] H. C. Chen and V. C. Patel. Near-wall turbulence models for complex flows including separation. *AIAA Journal*, 26(6):641–648, June 1988.

[71] M. Wolfshtein. The velocity and temperature distribution in one-dimensional flow with turbulence augmentation and pressure gradient. *International Journal of Heat and Mass Transfer*, 12(3):301–318, 1969.

[72] Larry A. Villasmil, Dara W. Childs, and Hamn-Ching Chen. Understanding friction factor behavior in liquid annular seals with deliberately roughened surfaces. *Journal of Tribology-transactions of The Asme*, 127(1):213–222, 2005.

[73] Włodzimierz Wroblewski, Daniel Fraczek, and Krzysztof Marugi. Leakage reduction by optimisation of the straight–through labyrinth seal with a honeycomb and alternative land configurations. *International Journal of Heat and Mass Transfer*, 126:725–739, 2018.

[74] Andrei V Ivanov and Aleksandr V Moskvicev. Influence of geometry on vortex configuration and dimension in LRE turbopump labyrinth seal. *Procedia Engineering*, 106:126–131, 2015.

[75] Hasham H Chougule, Douglas Ramerth, and Dhinagaran Ramachandran. Low leakage designs for rotor teeth and honeycomb lands in labyrinth seals. In *Turbo Expo: Power for Land, Sea, and Air*, volume 43147, pages 1613–1620, 2008.

[76] Tuncer Cebeci. *Turbulence Models and Their Application: Efficient Numerical Methods with Computer Programs*. Horizons Pub, Long Beach, Calif, 2004.

[77] William T Snyder and Gerald A Goldstein. An analysis of fully developed laminar flow in an eccentric annulus. *AIChE Journal*, 11(3):462–467, 1965.

[78] Noriyasu Mori, Mitsuhiro Yagami, Takaaki Eguchi, Kiyoji Nakamura, and Akira Horikawa. Pressure flow of Non-Newtonian fluids between eccentric double cylinders with the inner cylinder rotating. *Journal of the Textile Machinery Society of Japan*, 33(3):73–77, 1987.

[79] Edoardo Alinovi and Alessandro Bottaro. A boundary element method for Stokes flows with interfaces. *Journal of Computational Physics*, 356:261–281, March 2018.

[80] Chang-Yong Choi and Elias Balaras. A dual reciprocity boundary element formulation using the fractional step method for the incompressible Navier–Stokes equations. *Engineering Analysis with Boundary Elements*, 33(6):741–749, June 2009.

[81] Keng-Cheng Ang. Introducing the boundary element method with MATLAB. *International Journal of Mathematical Education in Science and Technology*, 39(4):505–519, June 2008.

[82] OP Gupta. *Finite and Boundary Element Methods in Engineering*. CRC Press, 1999.

[83] Jichun Li and Yi-Tung Chen. *Computational Partial Differential Equations Using MATLAB®*. Crc Press, 2019.

[84] Randall J LeVeque. *Finite Difference Methods for Ordinary and Partial Differential Equations: Steady-State and Time-Dependent Problems*. SIAM, 2007.

[85] S Gerace, K Erhart, E Divo, and A Kassab. Adaptively refined hybrid FDM-RBF meshless scheme with applications to laminar and turbulent viscous fluid flows. *Computer Modeling in Engineering & Sciences(CMES)*, 81(1):35–67, 2011.

[86] MA Buès and C Oltean. Numerical simulations for saltwater intrusion by the mixed hybrid finite element method and discontinuous finite element method. *Transport in Porous Media*, 40(2):171–200, 2000.

[87] TJ Chung. *Computational Fluid Dynamics*. Cambridge university press, 2010.

[88] Konstantin Lipnikov, Gianmarco Manzini, and Mikhail Shashkov. Mimetic finite difference method. *Journal of Computational Physics*, 257:1163–1227, January 2014.

[89] José E Castillo and Guillermo F Miranda. *Mimetic Discretization Methods*. CRC Press, 2013.

[90] Lourenço Beirao da Veiga, Konstantin Lipnikov, and Gianmarco Manzini. *The Mimetic Finite Difference Method for Elliptic Problems*, volume 11. Springer, 2014.

[91] G.T. Oud, D.R. van der Heul, C. Vuik, and R.A.W.M. Henkes. A fully conservative mimetic discretization of the Navier–Stokes equations in cylindrical coordinates with associated singularity treatment. *Journal of Computational Physics*, 325:314–337, November 2016.

[92] G.T. Oud. *A Dual Interface Method in Cylindrical Coordinates for Two-Phase Pipe Flows*. PhD thesis, Delft University of Technology, 2017.

[93] Dejan Brkić. Review of explicit approximations to the Colebrook relation for flow friction. *Journal of Petroleum Science and Engineering*, 77(1):34–48, April 2011.

[94] Cyril Frank Colebrook, T Blench, H Chatley, EH Essex, JR Finniecome, G Lacey, J Williamson, and GG Macdonald. Correspondence. turbulent flow in pipes, with particular reference to the transition region between the smooth and rough pipe laws. *Journal of the Institution of Civil engineers*, 12(8):393–422, 1939.

[95] Heinrich Blasius. Grenzschichten in flüssigkeiten mit kleiner reibung. 1907.

[96] SJ Davies and CM White. A review of flow in pipes and channels. *Engineering*, 128:69–72, 1929.

[97] Re Jo Cornish. Flow of water through fine clearances with relative motion of the boundaries. *Proceedings of the Royal Society of London. Series A, Containing Papers of a Mathematical and Physical Character*, 140(840):227–240, 1933.

[98] Ludwig Prandtl. über Flussigkeitsbewegung bei sehr kleiner Reibung. *Verhandl. III, Internat. Math.-Kong., Heidelberg, Teubner, Leipzig, 1904*, pages 484–491, 1904.

[99] Dara W Childs and John B Dressman. Testing of turbulent seals for rotordynamic coefficients. Technical report, NASA, 1982.

[100] JRMCRHS Fenwick, R DiJulio, MC Ek, and R Ehrgott. Linear force and moment equations for an annular smooth shaft seal perturbed both angularly and laterally. 1982.

[101] JW Polkowski. Turbulent flow between coaxial cylinders with the inner cylinder rotating. 1984.

[102] C. Gazely. Heat Transfer Characteristics of the Rotating and Axial Flow Between Concentric Cylinders. *ASME Transactions*, 80:79–89, 1958.

[103] H. F. Black and D. N. Jenssen. Paper 9: Dynamic Hybrid Bearing Characteristics of Annular Controlled Leakage Seals. *Proceedings of the Institution of Mechanical Engineers, Conference Proceedings*, 184(14):92–100, September 1969.

[104] GG Hirs. A systematic study of turbulent film flow. 1974.

[105] D. W. Childs. Dynamic Analysis of Turbulent Annular Seals Based On Hirs' Lubrication Equation. *Journal of Lubrication Technology*, 105(3):429–436, July 1983.

[106] HF Black, PE Allaire, and LE Barrett. The effect of inlet flow swirl on the dynamic coefficients of high-pressure annular clearance seals. In *Ninth International Conference in Fluid Sealing, BHRA Fluid Engineering, Leeuwenhorst, the Netherlands*, 1981.

[107] Lewis F Moody. Friction factors for pipe flow. *Trans. Asme*, 66:671–684, 1944.

[108] C. C. Nelson and D. T. Nguyen. Comparison of Hirs' Equation With Moody's Equation for Determining Rotordynamic Coefficients of Annular Pressure Seals. *Journal of Tribology*, 109(1):144–148, January 1987.

[109] Zhou Yang, Luis San Andres, and Dara W. Childs. Thermal Effects in Cryogenic Liquid Annular Seals—Part I: Theory and Approximate Solution. *Journal of Tribology*, 115(2):267–276, April 1993.

[110] Luis San Andres, Zhou Yang, and Dara W Childs. Thermal effects in cryogenic liquid annular seals—Part II: Numerical solution and results. 1993.

[111] Dara W Childs and Patrice Fayolle. Test results for liquid "damper" seals using a round-hole roughness pattern for the stators. 1999.

[112] F. Simon and J. Frene. Static and Dynamic Characteristics of Turbulent Annular Eccentric Seals: Effect of Convergent-Tapered Geometry and Variable Fluid Properties. *Journal of Tribology*, 111(2):378–384, April 1989.

[113] HG Elrod Jr and CW Ng. A theory for turbulent fluid films and its application to bearings. 1967.

[114] C. C. Nelson. Rotordynamic Coefficients for Compressible Flow in Tapered Annular Seals. *Journal of Tribology*, 107(3):318–325, July 1985.

[115] J.M. Hyman and M. Shashkov. Natural discretizations for the divergence, gradient, and curl on logically rectangular grids. *Computers & Mathematics with Applications*, 33(4):81–104, February 1997.

[116] Mikhail Shashkov and Stanly Steinberg. Support-Operator Finite-Difference Algorithms for General Elliptic Problems. *Journal of Computational Physics*, 118(1):131–151, April 1995.

[117] James M. Hyman and Mikhail Shashkov. Adjoint operators for the natural discretizations of the divergence, gradient and curl on logically rectangular grids. *Applied Numerical Mathematics*, 25(4):413–442, December 1997.

[118] Francois Treves. *Topological Vector Spaces Distributionsand Kernels*. Pergamon Press, 1967.

[119] HH Schaefer-MP Wolff and HH Schaefer. Topological vector spaces. *Graduate Texts in Mathematics*, 3, 1999.

[120] J. Hyman, M. Shashkov, and S. Steinberg. The effect of inner products for discrete vector fields on the accuracy of mimetic finite difference methods. *Computers & Mathematics with Applications*, 42(12):1527–1547, December 2001.

[121] J.M. Hyman and S. Steinberg. The convergence of mimetic discretization for rough grids. *Computers & Mathematics with Applications*, 47(10-11):1565–1610, May 2004.

[122] Osborne Reynolds. IV. On the dynamical theory of incompressible viscous fluids and the determination of the criterion. *Philosophical transactions of the royal society of london.(a.)*, (186):123–164, 1895.

[123] David C Wilcox et al. *Turbulence Modeling for CFD*, volume 2. DCW industries La Canada, CA, 1998.

[124] Andrey Nikolaevich Kolmogorov. The local structure of turbulence in incompressible viscous fluid for very large Reynolds numbers. *Cr Acad. Sci. URSS*, 30:301–305, 1941.

[125] Andrej Nikolaevich Kolmogorov. On degeneration (decay) of isotropic turbulence in an incompressible viscous liquid. In *Dokl. Akad. Nauk SSSR*, volume 31, pages 538–540, 1941.

[126] Peter Bradshaw and J Blair Perot. A note on turbulent energy dissipation in the viscous wall region. *Physics of Fluids A: Fluid Dynamics*, 5(12):3305–3306, 1993.

[127] J. Boussinesq. *Thorie Analytique de La Chaleur Mise En Harmonie Avec La Thermodynamique et Avec La Thorie Mcanique de La Lumi_re: Refroidissement et Chauffement Par Rayonnement, Conductibilit'des Tiges, Lames et Masses Cristallines, Courants de Convection, Thorie Mcanique de La Lumi_re. 1903. Xxxii, 625,[1] p.* Cours de Physique Mathm̄atique de La Facult Des Sciences. Gauthier-Villars, 1903.

[128] N Nd Mansour, John Kim, and Parviz Moin. Reynolds-stress and dissipation rate budgets in a turbulent channel flow. 1987.

[129] Geoffrey Ingram Taylor. Statistical theory of turbulence-II. *Proceedings of the Royal Society of London. Series A-Mathematical and Physical Sciences*, 151(873):444–454, 1935.

[130] Amgad Salama, Shuyu Sun, and Mohamed F El Amin. A novel numerical approach for the solution of the problem of two-phase, immiscible flow in porous media: Application to LNAPL and DNAPL. In *AIP Conference Proceedings 4*, volume 1453, pages 135–140. American Institute of Physics, 2012.

[131] Shuyu Sun, Amgad Salama, and MF El Amin. Matrix-oriented implementation for the numerical solution of the partial differential equations governing flows and transport in porous media. *Computers & Fluids*, 68:38–46, 2012.

[132] Qiang Sun, Evert Klaseboer, Boo Cheong Khoo, and Derek Y.C. Chan. A robust and non-singular formulation of the boundary integral method for the potential problem. *Engineering Analysis with Boundary Elements*, 43:117–123, June 2014.

[133] Tao Zhang, Amgad Salama, Shuyu Sun, and Hua Zhong. A Compact Numerical Implementation for Solving Stokes Equations Using Matrix-vector Operations. *Procedia Computer Science*, 51:1208–1218, 2015.

[134] Michael Lee Scott. *Programming Language Pragmatics*. Morgan Kaufmann, 2000.

[135] Benjamin C Pierce and C Benjamin. *Types and Programming Languages*. MIT press, 2002.

[136] Uwe Kastens. Programming languages and compilers. 2006.

[137] Edward B Magrab, Shapour Azarm, Balakumar Balachandran, James Duncan, Keith Herold, and Gregory Walsh. *Engineers Guide to MATLAB*. Prentice Hall Press, 2007.

[138] ANSYS CFX-Solver Theory Guide. Technical report, ANSYS, Inc., Canonsburg, PA, 2019.

[139] ANSYS CFX Reference Guide. Technical report, ANSYS, Inc., Canonsburg, PA, 2019.

[140] ANSYS CFX Introduction. Technical report, ANSYS, Inc., Canonsburg, PA, 2019.

[141] BG Galerkin. Rods and plates. Series occurring in various questions concerning the elastic equilibrium of rods and plates. Eng. *Bull.(Vestnik Inzhenerov)*, 19:897–908, 1915.

[142] A.R. Mitchel and R. Wait. *The Finite Element Method in Partial Differential Equations*. Wiley, New York, NY, 1977.

[143] Carl Friedrich Gauss. *Methodus Nova Integralium Valores per Approximationem Inveniendi*. apvd Henricvm Dieterich, 1815.

[144] Kenneth Arthur Stroud and Dexter J Booth. *Advanced Engineering Mathematics*. Palgrave, 2003.

[145] Wolfgang Hackbusch. *Multi-Grid Methods and Applications*, volume 4. Springer Science & Business Media, 2013.

[146] J.M. Hyman and M. Shashkov. Approximation of boundary conditions for mimetic finite-difference methods. *Computers & Mathematics with Applications*, 36(5):79–99, September 1998.

[147] J. Hyman, J. Morel, M. Shashkov, and S. Steinberg. Mimetic Finite Difference Methods for Diffusion Equations. *Computational Geosciences*, 6(3):333–352, 2002.

[148] Ali H Nayfeh. *Perturbation Methods*. John Wiley & Sons, 2008.

[149] TJ Dekker. Finding a zero by means of successive linear interpolation. *Constructive aspects of the fundamental theorem of algebra*, pages 37–51, 1969.

[150] Richard P. Brent. An algorithm with guaranteed convergence for finding a zero of a function. *The Computer Journal*, 14(4):422–425, 1971.

[151] CH Edwards. The calculus according to cauchy, riemann, and weierstrass. In *The Historical Development of the Calculus*, pages 301–334. Springer, 1979.

[152] Joanna Maria Papakonstantinou. Historical development of the BFGS secant method and its characterization properties. Technical report, 2010.

[153] Germund Dahlquist, Åke Björck, et al. *Numerical Methods*. Prentice Hall, 1974.

[154] Norman R Draper and Harry Smith. *Applied Regression Analysis*, volume 326. John Wiley & Sons, 1998.

[155] P. M. Gresho, Robert L. Sani, and M. S. Engelman. *Incompressible Flow and the Finite Element Method : Advection-diffusion and Isothermal Laminar Flow.* John Wiley and Sons, Inc, 1999.

[156] Richard Courant, Kurt Friedrichs, and Hans Lewy. ”U on the partial difference equations of mathematical physics. *mathematical annals*, 100(1):32–74, 1928.

[157] D John and JR Anderson. Computational fluid dynamics: The basics with applications. *P. Perback, International ed., Published*, pages 4–30, 1995.

[158] Yu Pan, Zhen-Guo Yan, Joaquim Peiró, and Spencer J Sherwin. Development of a balanced adaptive time-stepping strategy based on an implicit JFNK-DG compressible flow solver. *Communications on Applied Mathematics and Computation*, pages 1–30, 2021.

[159] Luis San Andrés and Xueliang Lu. Leakage, drag power, and rotordynamic force coefficients of an air in oil (wet) annular seal. *Journal of Engineering for Gas Turbines and Power*, 140(1), 2018.

[160] Ludwig Prandtl. 7. Bericht über untersuchungen zur ausgebildeten turbulenz. *ZAMM-Journal of Applied Mathematics and Mechanics/Zeitschrift für Angewandte Mathematik und Mechanik*, 5(2):136–139, 1925.

[161] Edward R Van Driest. On turbulent flow near a wall. *Journal of the aeronautical sciences*, 23(11):1007–1011, 1956.

[162] Z-Y Li, T-C Hung, and W-Q Tao. Numerical simulation of fully developed turbulent flow and heat transfer in annular-sector ducts. *Heat and mass transfer*, 38(4):369–377, 2002.

[163] Johann Nikuradse et al. Laws of flow in rough pipes. 1950.

[164] Brian Edward Launder and Dudley Brian Spalding. The numerical computation of turbulent flows. In *Numerical Prediction of Flow, Heat Transfer, Turbulence and Combustion*, pages 96–116. Elsevier, 1983.

[165] Examining Spatial (Grid) Convergence. https://www.grc.nasa.gov/www/wind/valid/tutorial/spatconv.html, 2022.

[166] Fuchang Gao and Lixing Han. Implementing the Nelder-Mead simplex algorithm with adaptive parameters. *Comput Optim Appl*, 51(1):259–277, January 2012.

[167] Mohsen Jalaeian-F. Augmented Downhill Simplex a Modified Heuristic Optimization Method. page 6, 2012.

[168] Iztok Fajfar, Árpád Bűrmen, and Janez Puhan. The Nelder–Mead simplex algorithm with perturbed centroid for high-dimensional function optimization. *Optim Lett*, 13(5):1011–1025, July 2019.

[169] Luis San Andrés and Xueliang Lu. Leakage, Drag Power, and Rotordynamic Force Coefficients of an Air in Oil (Wet) Annular Seal. *Journal of Engineering for Gas Turbines and Power*, 140(1):012505, January 2018.

[170] Pascal Jolly, Mihaï Arghir, Olivier Bonneau, and Mohamed-Amine Hassini. Experimental and Theoretical Rotordynamic Coefficients of Smooth and Round-Hole Pattern Water-Fed Annular Seals. *Journal of Engineering for Gas Turbines and Power*, 140(11):112501, November 2018.

[171] R Schaback. A Practical Guide to Radial Basis Functions. page 58.

[172] Satoru Kaneko, Takashi Ikeda, Takuro Saito, and Shin Ito. Experimental Study on Static and Dynamic Characteristics of Liquid Annular Convergent-Tapered Damper Seals With Honeycomb Roughness Pattern. *Journal of Tribology*, 125(3):592–599, July 2003.

[173] Rajat Mittal and Gianluca Iaccarino. Immersed boundary methods. *Annu. Rev. Fluid Mech.*, 37:239–261, 2005.

[174] James M. Hyman and Mikhail Shashkov. The Orthogonal Decomposition Theorems for Mimetic Finite Difference Methods. *SIAM J. Numer. Anal.*, 36(3):788–818, January 1999.